NUMERICAL ANALYSIS OF ROCK FAILURE AND LABORATORY STUDY OF THE RELATED ACOUSTIC EMISSION

by

DAIHUA ZOU

B.Sc., China Mining Institute, 1982

A THESIS SUBMITTED IN PARTIAL FULFILMENT OF

THE REQUIREMENTS FOR THE DEGREE OF

DOCTOR OF PHILOSOPHY

in

Mining Engineering

THE FACULTY OF GRADUATE STUDIES

Department of Mining and Mineral Process Engineering

We accept this thesis as conforming

to the required standard

THE UNIVERSITY OF BRITISH COLUMBIA

January 1988

In presenting this thesis in partial fulfilment of the requirements for an advanced degree at the University of British Columbia, I agree that the Library shall make it freely available for reference and study. I further agree that permission for extensive copying of this thesis for scholarly purposes may be granted by the head of my department or by his or her representatives. It is understood that copying or publication of this thesis for financial gain shall not be allowed without my written permission.

Department of MINING AND MINERAL PROCESS ENGINEERING

The University of British Columbia
1956 Main Mall
Vancouver, Canada
V6T 1Y3

Date JANUARY 1988

ABSTRACT

Sudden rock failure in the form of rockbursting has long been a problem in underground mines. The basic mechanism of this phenomenon is still unresolved. This thesis describes the research work on this problem conducted by the doctoral candidate Daihua Zou in the Department of Mining and Mineral Process Engineering at The University of British Columbia, under the supervision of Professor Hamish D.S. Miller.

This research project was undertaken in order to investigate the process of violent rock failure and was achieved by examining various aspects of the rock failure mechanism.

The assumption that acoustic emission can be used as a reliable means of predicting rock failure was investigated, as well as the possibility that violent rock failure could occur in any mine rock.

As part of the research, a rock failure mechanism was postulated. A process analogous to shearing is postulated to be important at the post-failure stage. The stick-slip phenomenon has been analyzed using a numerical model under a variety of conditions. The conditions which could give rise to possible violent rock failure were determined. At the same time, acoustic emissions were tested from rock specimens under different loading conditions. The experimental results obtained show a correlation with field measurements made in a mine. In order to verify the testing results from limited experiments, a numerical acoustic

model was developed, which is unique in that it is entirely based on the stick-slip process not on any acoustic theory. This model allows rock tests and their associated acoustic emission to be realistically simulated. With this model, acoustic emissions were simulated under various loading conditions for different kinds of rocks. The case of a hard or a soft intercalation was also modelled.

TABLE OF CONTENTS

LIST OF TABLES

LIST OF FIGURES

ACKNOWLEDGEMENT

The author would like to thank:

- The Chinese Government for funding this project during the first two years.
- Dr. Hamish D. S. Miller for his continuous supervision, great help during this research and funding the rest of this project.
- Professor C. O. Brawner, Dr. Ross Hammett and Professor A. Reed for their helpful advice and comments throughout this program.
- Dr. A. Hall and other Faculty members and Graduate students in the Department of Mining Engineering for their valuable discussion and encouragement.
- Professor J. S. Nadeau in the Department of Metallurgy for lending us the acoustic emission equipment and technians Mr. Frank Schmidiger and Mr. R. Gutenberg for their help during the laboratory tests.
- Ms. Sylvia Paulin for proof reading the thesis.

To MY PARENTS

CHAPTER 1. INTRODUCTION

1.1. INTRODUCTION

Rock failure can take place gradually or suddenly. When it occurs suddenly, unexpected and severe problems can result. This research therefore concentrates on aspects of sudden rock failure. Large sudden rock failures in a mine are referred to as rockbursts and these have long been a serious problem in underground mines, dating back to the beginning of this century. As mining depth has continued to increase in recent years, the problem is becoming critical. More and more mines with no previous history of bursting are being affected.

Sudden rock failure is usually characterized by the way in which energy is released and by the damage that results. Rockbursting is generally defined as the violent failure of a rock mass under a high stress field, accompanied by sudden release of a large amount of strain energy stored in the rock mass and characterized by expulsion of rock in varying quantities from the surface of an opening [1,2,3]. Therefore, this type of failure is distinguished from normal non-violent rock failure by its suddenness, the absence of warning and the intensity of the resulting damage.

Once violent rock failure occurs, it can give rise to various problems in a mine, depending on the energy released and the distance of the mine opening from the focus of the event. If a large amount of energy is released by a mining induced seismic event, with a magnitude possibly reaching 5.5 on the Richter scale [1], the effect could be similar to that of a small earthquake. The

result can be, and frequently is, catastrophic failure and damage to mine structures and facilities. Millions of dollars are lost annually due to this kind of rock failure. The most dangerous aspect of violent rock failure is its threat to miners' lives, and casualties are often a direct result. For example, one rockburst that occurred in a South African mine this year killed nine people and injured many more. In fact, since the earliest days of gold mining in South Africa, this kind of rock failure has been a major cause of fatalities, damage and loss of production[4]. During 1975 alone, more than 680 cases of violent rock failure were reported in these mines, causing 73 fatalities and the loss of more than 48,000 man-shifts [5]. A rockburst occurred in a mine in Ontario two years ago claimed the lives of four miners.

Although research initiated in the last few decades has achieved some progress, the results have not been satisfactory, and the problem of violent rock failure in mines is still unresolved. This is because first of all, the mechanism of violent rock failure is not well understood and as a result the conditions which cause this kind of rock failure are unknown.

Because there is virtually never any physical visual evidence prior to violent rock failure in underground openings, it is extremely difficult in practice to predict or to give any warning to such an event. Each year, millions of dollars has been spent on field research of rockburst prediction and control, but the progress is very slow. The Government of Ontario spent 4.2 million dollars for rockburst research in 1986/87 but little progress has been reported. The South African Chamber of Mines which is the earliest and still the leading

rockburst research group in the world, has spent more than an estimated 50 million dollars since its establishment in 1964 and only recently has it had some measure of success in predicting violent rock failure in a mine. All research groups throughout the world have faced the same difficulty in predicting rockbursts that arise as a result of not having reliable precursors.

Because field research of violent rock failure in operating mines is a very expensive and difficult exercise, this research attempts to study the problem by applying numerical analysis and laboratory experiments in an attempt to derive a method or to provide a guideline for subsequent field work. The major objectives are:

I. to investigate the conditions which may give rise to violent rock failure, discussed in chapters 3 through 9, and

II. to find precursive signals for such an event, given in chapters 10 to 13.

In order to find the conditions causing violence, the mechanism of rock failure will be studied first. Violent failure can occur in massive rock as well as on a fault or joint plane. Failure in both cases should be examined and a qualitative assessment made of any common factors. In mining, stress induced fracturing is intrinsic to the failure of massive rock and is considered by some researchers to be the basic mechanism of violent rock failure [2]. Others [6] explain violent rock failures as a result of sudden slips along geological discontinuities, such as faults or bedding planes. Whether violent failure occurring in these two conditions is independent or related needs studying.

The emission of acoustic noise from material undergoing stress loading would appear to have the greatest potential for giving warning of impending failure. It is for this reason therefore that acoustic emissions from rock specimens will be monitored in laboratory conditions and modelled using numerical techniques.

CHAPTER 2. BASIC CONCEPTS OF ROCKBURSTING AND ITS CONTROL

In order to provide some background for study of violent rock failure, results from previous research on rockbursts are investigated in this chapter. More than ninety published papers have been reviewed but only the more relevant ones are referred to here. The results of this survey are summarized in the following and major problems existing in practice are also listed.

2.1. HISTORY

Rockbursting in underground mines was reported as early as at the beginning of the 20th century. The earliest report in India was in 1898 [1], in South Africa was in 1908 [5] and in Ontario mines was in 1929 [7]. Rockbursting is generally not a problem in shallow mines because the gravitational load on the rock structure is not very high unless high tectonic stresses exist. However, the problem becomes greater as mining depth increases, particularly in a mine where natural faults exist or a vein of dyke material or competent orebody is intercalated in a moderate to hard rock matrix.

Much research into rockbursting has been carried out in an attempt to understand and to prevent what were initially called "earth tremors". From the results achieved, we are getting better in understanding this problem. With the improvement of monitoring techniques, the monitored rock mass shows some precursory signals in seismicity before violent rock failure occurs. By using control methods, such as avoiding high stress concentration, destressing, etc., the incidence of rockbursting can be reduced.

2.2. CHARACTERISTICS OF ROCKS

Various properties of rocks are considered because they are important inherent factors in violent failure. It is well known that geological materials, such as rock, have little tensile strength but have relatively high compressive strength. Most rocks exhibit brittle characteristics under compression, although some like potash behave plastically, particularly when under high confinement and low loading speed.

Generally, a rock will behave elastically when the stress is less than its strength as illustrated in figure 2.1. Beyond the peak strength, point A, the capacity of rock to support external load will decrease dramatically. Eventually, rock will deform continuously even when the load is held constant or complete failure takes place. The elastic modulus, or the slope of the OA part of the curve varies widely with different types of rock. Pre-failure behavior is similar for all kinds of rock when loaded in uniaxial compression. However, the post failure behavior varies greatly. Even for the same rock, this behavior will be either brittle or plastic when under different confinements as shown in figure 2.2 [8]. It can be seen from this figure that the elastic modulus does not change with the confining pressure, but the strength does. Furthermore, at the post failure stage, rock will "flow" when the confining pressure reaches a certain level, where the deformation continues at a constant load. In the case of brittle behavior, upon rupture the accumulated strain energy is fully released, while in the case of plastic behavior, to the extent that energy is dissipated in the flow process, there is no energy accumulation.

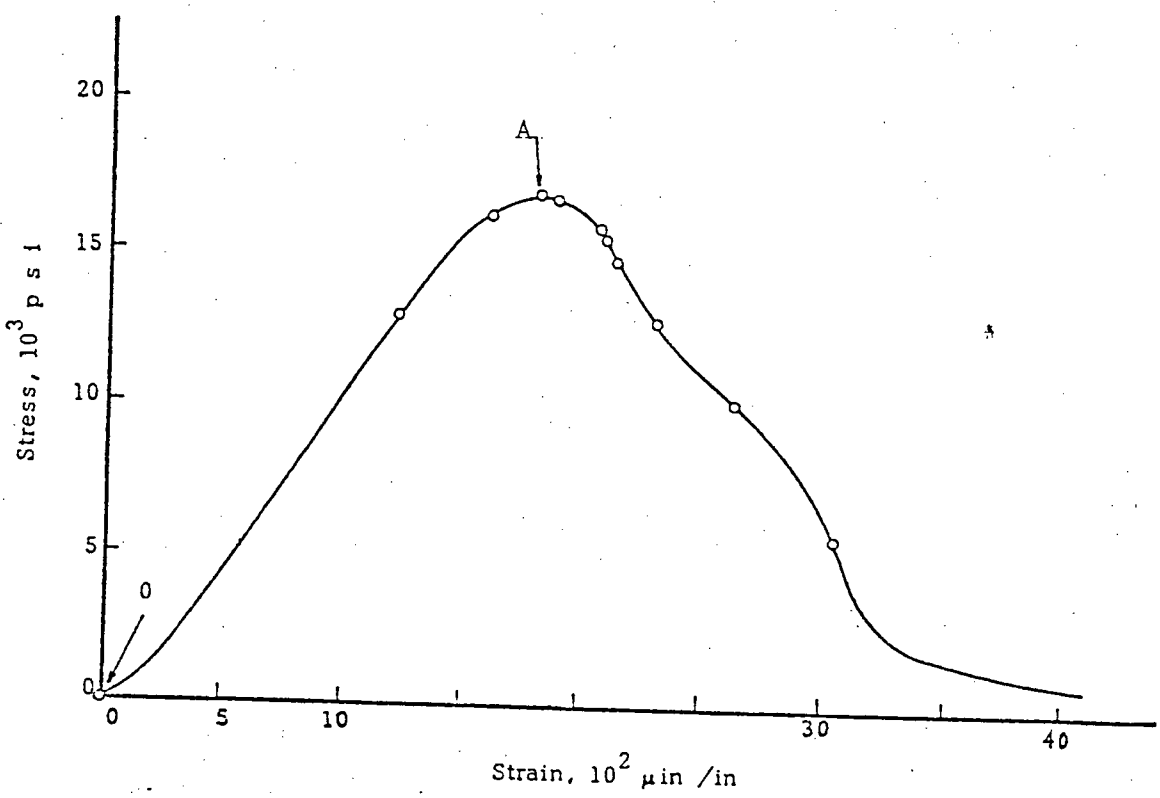

Fig. 2.1 Complete stress-strain curve for unconfined rock specimen (from Starfield et al, [56])

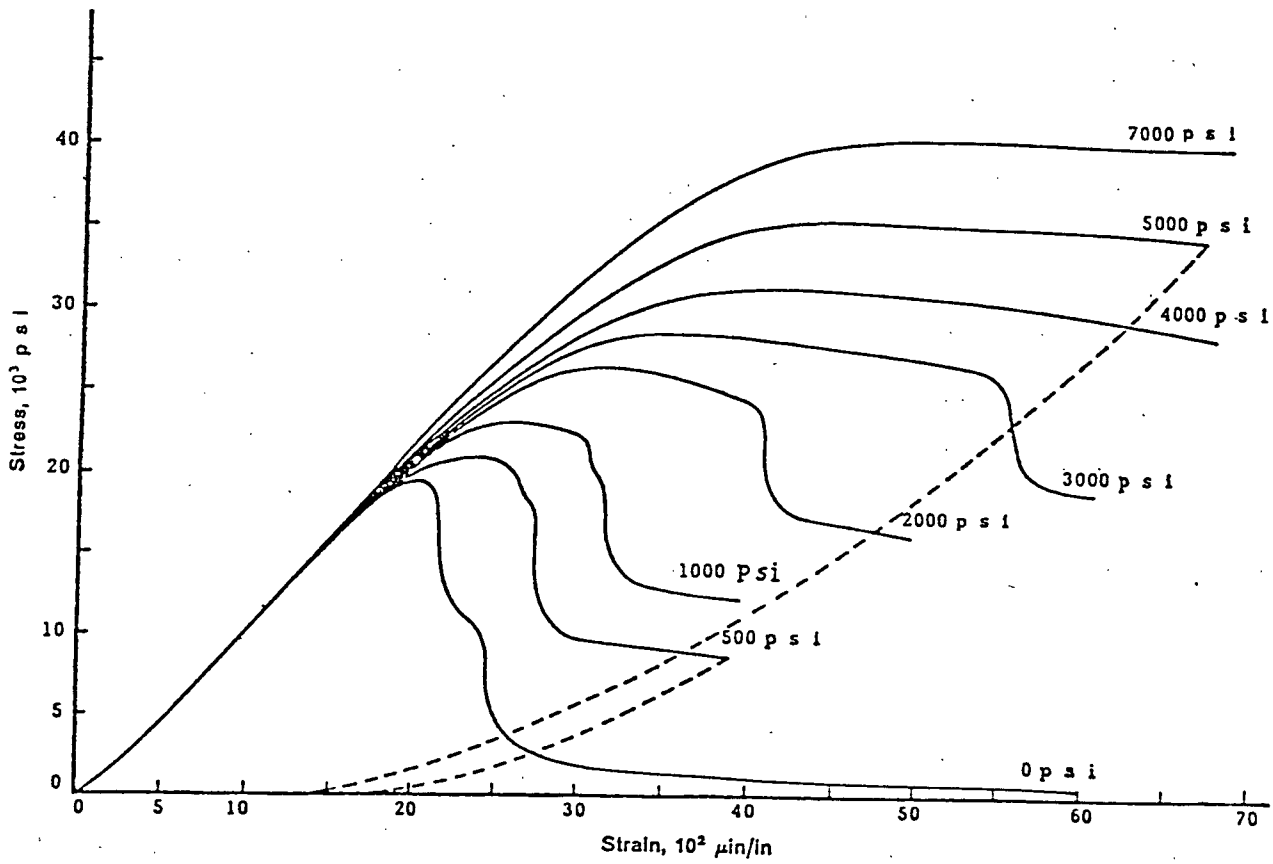

Fig. 2.2 Complete stress-strain curves for unconfined and confined Tennessee marble (after Wawersik et al, [8])

Therefore, a rock mass may fail gradually under high confinement and probably violently under low confinement if the energy is released suddenly. This may suggest that rockbursting or violent rock failure will never take place in a deep confined zone, but possibly at or near the surface of an opening or where relaxation has taken place.

Laboratory work has also shown [9,10] that the rock failure process is dependent upon the testing machine. Rocks which fail abruptly when tested in a conventional or "soft" testing machine will fail gradually, with a complete stress-strain curve being obtained when tested in a stiff testing machine. This implies that the rock failure process depends not only on the rock properties but also on the loading system. However, for some kinds of rock, the violent failure of a rock specimen cannot be completely controlled only by stiffening the testing machine [8] because of the inherent characteristics of the rock. In addition, the behavior of a rock mass is related to other environmental variables, such as temperature, time and pore pressure.

2.3. FIELD INVESTIGATIONS OF ROCKBURSTS

It is observed from field investigations that rockbursts usually occur in high stress zones or in areas near geological structures and are also closely associated with mining activities. Many other factors, such as mining depth, geological conditions, rock properties, geometry of openings, etc. contribute to rockbursting as well.

2.3.1. Mining Activity

More rockbursts occur during and immediately after excavation are created than non-extraction periods. Mining disturbs the stress equilibrium in the rock mass and results in a redistribution of stresses. The rapidity of stress change is very important to rock failure. A sudden change of stress brought about, for example, by blasting may be the immediate cause of violent failure [6]. Therefore the high speed of stress change induced by blasting may have higher risk of causing rockbursts than that by relatively low speed, continuous excavation.

2.3.2. Mining Depth

Rockbursts are usually experienced at depth starting at around 600 - 1000 meters but can occur at shallower depth. In some cases, rockbursts have occurred within a depth of less than 300 meters, as well as in surface excavations and quarries. This can be accounted for by the high horizontal components of the existing tectonic stress field. The general tendency is that the severity and the frequency of bursts are expected to increase with mining depth because of the increase of the gravity stress. As mining goes deeper, confinement increases and the rock away from the mine openings may behave quite differently in the post-failure stage as shown in figure 2.2. In addition, the stress field might become hydrostatic at great depth, thus reducing the shear stress on a failure surface. However, as the excavation process disturbs the in-situ stress field and relaxation occurs in and around the mining openings, the potential for rockbursting will be enchanced. This is because of the greater stress differentials created with an increase in depth.

2.3.3. Geological Conditions

Rockbursts are usually associated with geological structures, such as a fault, or a hard intrusion. In-situ stress fields can arise from three different sources: the gravitational stress field, tectonic stress field and the stress concentrations in the vicinity of these geological structures. The presence of geological structures will introduce uneven distributions within the stress field, resulting in some parts of the rock mass being more highly stressed than others. These local stress concentrations will certainly increase the risk of violent failure because of larger amount of strain energy present. In the case of a fault, a sudden slip along the fault caused by rapid stress change may cause violent failure. In fact, this is considered to be the cause of many shallow earthquakes [11].

2.3.4. Properties of a Rock Mass

The properties of a rock mass are important factors in rock failure. For, while rockbursts are usually more related to strong and brittle rocks than to soft rocks, they tend to occur more often in igneous and metamorphic rocks than in sedimentary rocks. This, however, does not imply that rockbursts will not occur in soft, sedimentary rocks. Strain energy, which is proportional to the square of the compressive strength and inversely proportional to the elastic modulus, is commonly considered as a measure of the tendency of a rock mass to burst. The more energy stored, the higher the risk of bursting exists. Therefore, in the same stress field, the rock mass with higher compressive strength and hence higher capacity of energy storage is more likely to burst.

2.3.5. Geometry of Openings

The geometries of underground openings are also closely related to rockbursts. This is not to say that a smaller or a bigger opening will be more likely to burst, but the relative positions of openings and the pillar shapes between openings can be significant, and the irregularities of mining structures are usually more burst prone because of uneven stress concentrations. According to experience in the field, all openings and stopes must be carefully planned to avoid irregularities and hence abnormal stress concentrations. The orientation of an opening or a stope should be such that it will not make an acute angle with another opening or with any geological weakness, such as a fault. The axis of the opening should be parallel to the direction of the major principal stress in order to minimize the stress concentration.

2.4. DEVELOPMENT OF ROCKBURST THEORY

Since the earliest stage in rockburst research, vavious theories have been used to interpret the phenomenon of rockbursting [1]. Early in 1915, in South Africa a committee was formed to investigate the problem. Committee members suggested the concept of domes, zones of fractured rock around stopes and concluded that the domes supported load and also transferred load to pillars. The removal and failure of pillars may cause a dome to fail, giving bursts. During the late 1920, by the theory of elasticity, the concept of fracture development around excavations due to stress concentration was used and the sufficiently violent fracturing could result in bursts.

Prior to 1930, all hypotheses were based primarily on observation. Little

effort was made to understand the mechanism causing a burst. During this time, the number and severity of bursting increased. By the end of 1930s, two main causes of rockbursts were accepted: (1) the pressure-dome theory using stress concentration around mine openings to account for rockbursts in mines where the veins dipped steeply, and (2) the cantilever theory used in mines where the veins were mostly flat-lying. Both theories were based primarily on observed and measured behavior of stope walls and suited to a particular geometry. Despite the application of various control methods as a result of these theories, bursting continued and became more severe as mines went deeper.

In 1938, the first mathematic model based on elastic theory and experimental results was proposed to explain rockbursting but it was never accepted by mine operators because at that time, it was felt that mathematics could not be used to predict mine behavior. During the 1950s, mathematics was paid more attention and the theory of elasticity was used to a greater extent.

In 1963, Cook [12] proposed that the mechanics of rockbursts could best be analyzed by an energy approach. To control bursting, the energy release at excavation must be in small amounts that it could be dissipated nonviolently. Later he further suggested [13] that rockbursts might be considered as a stability problem in the same way as a specimen behaves in laboratory tests. If the specimen is stiffer than the loading system, excessive strain energy stored in the loading system instantaneously loads the rock structure further when failure is initiated, causing violence [10]. In other words, depending on the relative stiffness, the specimen will fail violently or nonviolently if energy can or can not

be extracted from the loading system at failure. It was concluded in 1966 that rockbursts are controlled by the rate at which energy is released as an excavation is made.

The stiffness approach is certainly valid in explaining rockbursts in a massive rock. However, there has been no further work published on this topic and this approach can not explain rockbursting along natural faults, because in this case, the failure takes place as shearing. In addition, this approach can not correlate the violence to the acoustic activity preceding the violent failure.

In summary, rockbursts have been adequately described. Yet the basic mechanics of rockbursting are still unclear because little research has been directed towards how a burst occurs.

2.5. WARNING METHODS

During the past study of rockbursting, major efforts have been made to provide warnings of impending rockbursts. Methods such as closure measurement, stress measurement and microseismic monitoring have been used to monitor the pre-failure behavior of the rock mass, with the last one having the most potential.

2.5.1. Closure Measurement

This is a primitive method used to pinpoint the areas of large deformation and the possible locations for rockbursts. It is found that large ground movements, such as closure of a tunnel or a stope, between roof and floor, sometimes

precede a burst [14], in the order of 10 times as rapid as normal movement occurring over a long period. While the abnormal rate of displacement gives a warning of impending failure, this method cannot reliably predict and locate rockbursts.

2.5.2. Stress Measurement

Stress measurement at various points in a mine made over a long period will show the change of the stress field as mining proceeds. The areas of high stress concentration which usually precede the potential burst zones can then be located. While this should be possible analytically since high stress is necessary for a burst, because of the wide variation of geological conditions and the changing nature of the stress field at different regions throughout the mine, the accuracy of this method is not sufficient either.

2.5.3. Microseismic Monitoring

Microseismic monitoring is the use of a geophysical technique which has had a long history in oil and mineral exploration fields, but its use in mining is fairly recent. Experience has proven the microseismic technique to be quite successful and encouraging, especially since the introduction of the electronic computer, which makes possible online data processing. This technique promises to provide warning of impending violent rock failure, and is therefore described in more detail.

The principle of this method is based on the fact that during the stress redistribution induced by mining, self-adjustment takes place in the rock mass by fracturing which is accompanied by acoustic emission, or rock noise which is

audible or subaudible and will be discussed in detail in the next chapter and later. By recording the acoustic signals with a transducer, the microseismic event can be detected and the energy released estimated. The term microseismic event here is synonymous with acoustic emission of rock. Then a relationship between the acoustic activity and the final failure may possibly be established from continuously monitored data.

The recording system used for microseismic monitoring include geophones, amplifiers, cable and a central processor. The signal of a microseismic event is recorded and transformed into an electrical signal by a geophone, passed through an amplifier, the amplified signal then being transmitted by cable to a central processor, which analyses the signal and gives final results in the form of event rate, seismic energy rate, energy ratio or whatever is needed [15]. It has been found in laboratory studies and in field monitoring that the impending rock failure is usually preceded by a sharp increase in acoustic emission. Therefore, by monitoring acoustic emission from the rock mass in a successive monitoring period, it is theoretically possible to predict a coming failure and to give warning in advance if an abnormal pattern of acoustic emission occurs.

If the velocity with which the shock wave propagates in the rock mass is known, it is possible to locate the seismic event, provided the travel time of the shock wave from the source to the detecting point is measured and the co-ordinates of the detecting stations are known [16]. Usually, the time differences of the first arrival of the shock wave, usually P-wave, at several detecting points in the rock mass are measured by setting up an array of

sensors at different locations. The wave velocity can be determined by a calibration test with a man-made signal as a source event.

There are three major types of monitoring systems in use in the field. One is the single channel system, which is portable and consists of a single sensor and a simple processor. It is effective over a radius of about 20 meters and gives warning signals within its coverage when an unstable condition occurs and a failure is pending. It cannot give the exact location of the unstable area, and an improvement on this is the system consisting of several single channel systems, which can monitor a wider region and give similar but better results than the first system. Finally, the most commonly used is the source location system, which has an array of from 7 to up to 32 geophones installed at different locations in the rock mass to be monitored. It has a more sophisticated signal processing system consisting of a minicomputer, a recorder, visual monitor and hard copy printer, etc. This system is able to accurately locate the seismic events within ± 10 feet or even better and pinpoint any unstable area whenever it occurs.

The major problem of the microseismic technique is its low reliability in rockburst prediction. Few rockbursts have been successfully predicted in the past, nor has a reliable key precursor yet been found. In fact, the evidence of potentially successful prediction of rockburst is only reported on from South Africa [17]. Nevertheless, this method still has a bright future and its use is becoming wide spread. Moreover, the final goal of a monitoring system is not just to predict a burst, but more importantly, to locate seismic "hot spot" in a mine and so provide an early warning so that measures can be taken to avoid

the coming problem.

2.6. ROCKBURST CONTROL

Rockbursting seems to be inevitable in some cases particularly when mining reaches great depths, and every effort should be taken to control it. So the objective of rockburst control is to eliminate or at least to reduce the bursting incidence and consequently to minimize the damage from the burst. The major measures in use today are these:

- the optimization of mining layouts to prevent unnecessary high stress concentrations,
- the destressing of an area concerned to avoid the burst or to reduce the incidence of bursting when high stress builds up, and
- the introduction of rock support system that can handle the results of rockbursts.

Usually these three methods are used in combination so as to get better results.

2.6.1. Optimization of Mining Layout

The optimized mining layout offers the most effective measure of rockburst control, and at the stage of designing the mining system, unnecessary high stress concentrations should be avoided. There is no general rule for the optimum design for it varies with the geological conditions, mining method and rock properties in a particular mine, and the general principle is to reduce stress concentrations as much as possible. For instance:

1. In pillar operation, ore should be recovered as much as possible. If sprags,

pillar remnants, or complete pillars have to be left in the mined-out areas, they should be evenly distributed for best stress distribution.

2. Pillars should be approximately the same size and shape, and large enough to support the overburden.
3. Roof spans projecting over the mined-out areas should be kept as short as possible or else provided with support that ensures that the roof beds do not fracture.
4. The axes of the workings should be parallel to the direction of the major principal stress in order to minimize the stress concentration.
5. Sequential extraction from strata or from stages and horizons should be adopted for multi-layer mining.

2.6.2. Destressing

A high stress field giving rise to large stress differences and gradients is a necessary condition for rockbursting to occur in a massive rock. Therefore if stress concentrations can be avoided, or if a high stress can be lowered, the incidence of rockbursting will decrease greatly. The purpose of destressing is to extend the fractured zone ahead of the working face over the normal fracturing depth, thus reducing the stress concentration, or at least moving the trouble source further away from the working areas and cushioning the effects of bursting with a deeper zone of broken rock. Destressing can be used either before excavation of openings---the rock preconditioning [18], to prevent high stress build-up, or at the stress concentration zone [19] to reduce the high stress

or to shift it further into the rock mass.

The destressing process usually consists of drilling deep holes into the rock mass in the area to be destressed, then either injecting high pressure water into these holes---the infusion method [19,20], or loading these holes with explosives and blasting them---the blasting method [18,19]. The basic principle of this method is to "soften" the rock mass within the area to be destressed by fracturing the rock mass, thus decreasing the stress gradients and therefore its capacity of storing energy and reducing the potential for rockbursting.

It should always be kept in mind that the extent of rock fracturing is such that the rock mass will not lose its ability to sustain the external load, otherwise, unexpected results and damage will occur due to over-deformation of the rock mass.

2.6.3. Rock Support

Suitable rock supports which can handle the results of rockbursting are important in reducing the damage to mining openings. Because rockbursting generates strong shock waves, as the compressive wave reaches the interface between air and rock surface, a reflection tensile wave is induced which propagates backwards to the source. As such, the rock mass will fail in tension at the surface. At the sametime, rockbursting is a rapid action and the deformation rate is very high. If the rock supporting system can reduce the effect of the tensile wave and tolerate the rapid deformation, the damage can be reduced to minimum. Usually the rapid yielding hydraulic prop is used in stopes and the grouted steel cable is

used in tunnels [58].

2.7. SUMMARY

Despite extensive research over many years, the actual mechanism of rockbursting is not yet properly understood and therefore the conditions which give rise to violent failure are not clear. The latest theory of rockbursting is the energy and stiffness approach proposed in 1965 [13] but since then little work has been reported. This approach seems to explain rockbursting well in a massive rock, but it has difficulties in:

- explaining the rockbursts occurring along natural faults,
- determining the stiffnesses around an underground opening and the loading system of a mine,
- correlating the rockburst with the acoustic activity that preceds the bursting.

Therefore this theory needs improving or another hypothesis should be postulated to explain rockbursting.

While the use of microseismic monitoring has improved the technique of locating potential rockburst sites, the reliability of predicting the precise time of a rockburst is still low. Sometimes failures occur with a recognizable pattern of pre-failure acoustic emission, but often this pattern is absent [21]. The difficulty of predicting rockbursts is faced worldwide and little progress has been reported after many years research. This makes it doubtful that as used at present microseismic activity or acoustic emission can serve as a reliable precursive signal for violent rock failure.

In summary, rockbursting has had a long history and has become a serious problem as the mining depth continues to increase. It is usually related to rock properties, mining conditions, geological environment and rapidity of stress change. While progress has been achieved as a result of past research, the problem is still far from being solved.

CHAPTER 3. FAILURE OF A MASSIVE ROCK

3.1. GENERAL CONCEPTS

To study the mechanism of violent rock failure, it is important to understand the failure of a mssive rock. Violent rock failure is different from normal rock failure by its suddenness and the severity of damage. In mining excavations, rock usually fails in the form of spalling, breaking, roof sag, collapse of a pillar, or closure of an opening, etc. These normal failures have a relatively slow long term action and usually have some visual evidence prior to final failure. They can be controlled and the damages they cause can be reduced to minimum by installing proper supports at the right time. However, rockbursting Violent rock failure, as described before is an instant action, accompanied by the release of a tremendous amount of strain energy. There is usually no visual evidence in advance.

It is therefore important to understand the conditions which give rise to violence. The rock mass is an anistropic, nonhomogeneous geological material. Because it contains many weaknesses, such as joints, beddings, foliations, etc., its mechanical properties are not solely dependent on the material itself but also on these weaknesses. Most kinds of rocks are characterized by brittle behavior, especially on a short term base, for they have little plasticity and tensile strength. The development of fractures in intact rock is an important process that should be taken into account when considering violent rock failure.

3.2. FRACTURING PROCESS

The development of rock fractures has been studied by many researchers, and the generally accepted theory of brittle fracture of rock is the one developed by Bieniawaski (1967) [22] and is used in this research. From his research and experimental results, Bieniawaski postulated the five stages of brittle fracture of rock in multiaxial compression, figure 3.1:

1. closing cracks, O-I
2. linear elastic deformation, I-II
3. stable fracture propagation, II-III
4. unstable fracture propagation, III-IV
5. forking and coalescence of cracks, IV-V.

The behavior of rock fracturing is mainly described by the curve of linear stress versus linear axial strain. These stages of brittle fracture of rock generally apply for tension. In tension, however, crack closure will, of course, be absent and processes of stable and unstable fracture propagation will be of very small duration due to the fact that, in tension, a crack will propagate in its own plane compared with in compression where a crack does not propagate in its own plane but in the weak direction.

By this theory, before failure takes place, the whole process is a matter of fracture development. As a compressive stress is induced in the rock under load, the pre-existing small cracks or Griffith cracks close first up to stress level corresponding to point I in figure 3.1. Then the rock shows a perfect elastic deformation under further loading. After stress has reached point II where

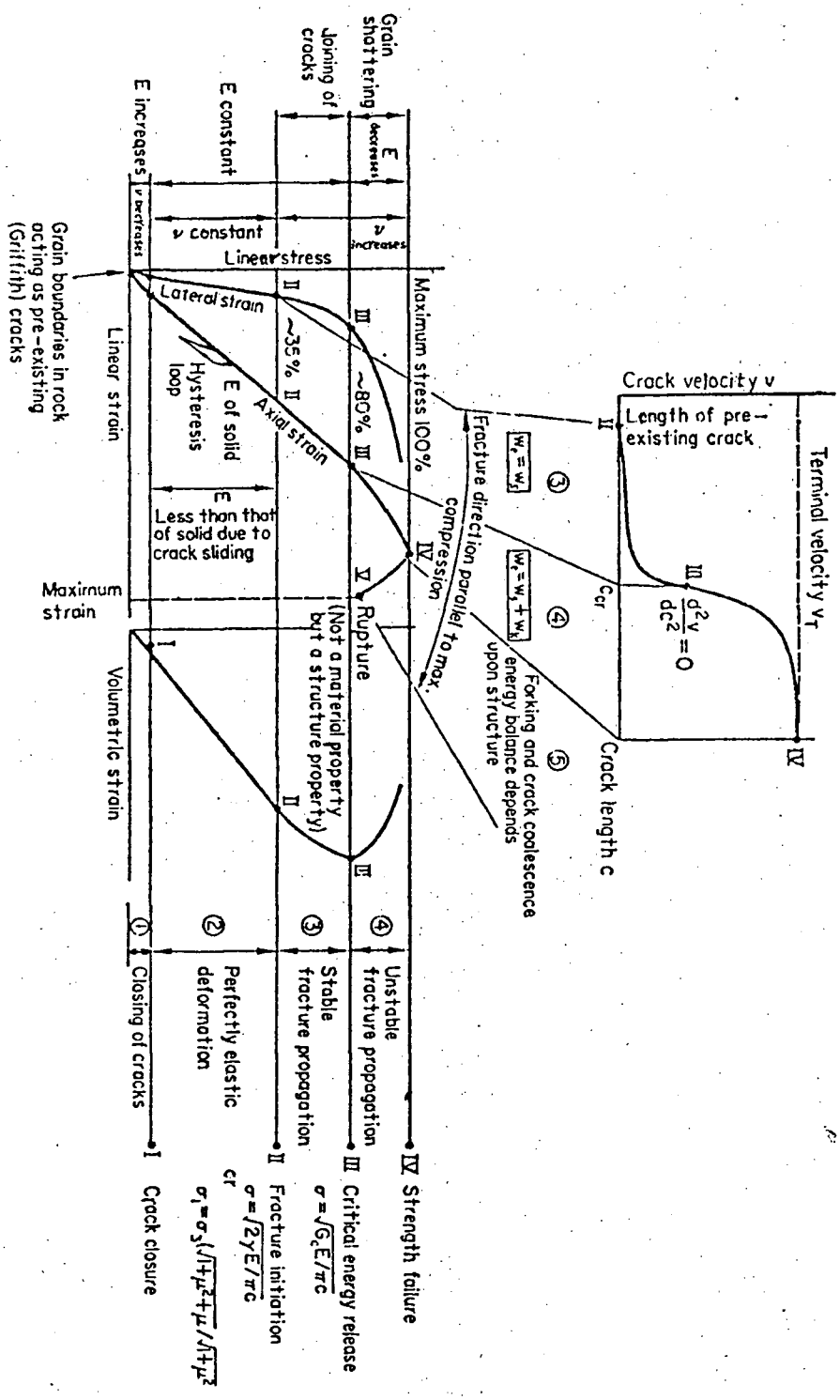

Fig.3.1 Mechanism of brittle fracture of rock in multiaxial compression (from Bieniawaski, [22])

fracture initiation begins or the preexisting cracks begin to extend, microfracturing propagates forward in the material. The fracture propagation continues until the strength failure at point IV. However, between points II and IV, the fracturing process is somewhat different and can be divided into two stages. During the first stage, between points II-III, fracture propagation is stable, which means the fracturing can be stopped by stopping loading because at this stage, the elastic energy released by crack extension is not sufficient to maintain the fracture development and the fracturing is directly controlled by stress. However during the second stage, between points III-IV, fracture propagation is unstable and becomes self-maintained, which means the fracturing cannot be stopped by maitaining the load constant. Because the energy required to maintain crack propagation decreases with the crack velocity which quickly reaches the terminal value after point III, this required energy is lowered at some stress level. On the other hand, the elastic energy released from crack extension increases with the crack length. Therefore at the second stage, even if the load is held constant, a fracture will continue to extend. Any increase of load will accelerate the fracture propagation.

Obviously, during unstable fracture propagation, the elastic energy released from crack extension can not be completely consumed in maintaining fracturing to create new crack surfaces. This released energy can also be possibly converted into several other forms of energy losses in addition to the crack surface energy:

- kinetic energy,
- plastic energy,
- energy dissipated on the breakdown of atomic bonds at the tips of

extending cracks.

- energy changes due to mining such as caused by artificial rock breaking, heat removed due to ventilation, etc.

From Bieniawaski's study [22], all other energy losses can be neglected in the present discussion, except the kinetic energy, which is associated with the movement of the faces of the extending crack. However, this kinetic energy is also found to approach a constant value once the crack velocity quickly approaches its terminal velocity during unstable fracture propagation. In order to dissipate the additional energy, the crack tends to increase its surface area and hence its surface energy by forking in the weak direction to form additional cracks.

The onset of forking represents a transition within the process of unstable fracture propagation. This transition coincides with the failure strength of the material, point IV in figure 3.1. Once this transition has taken place, successive forking will lead to coalescence of many microfractures, consequently forming macrofractures. These macrofractures will eventually join together within the fractured zone, to form a new surface on which the final failure takes place. The proof of this suggestion will be provided later.

3.3. DETECTION OF FRACTURING

Fracturing is an important characteristic mechanism within of a rock mass. But the process of fracturing is not visible and most of the acoustic emission accompanying these microfractures are not audible to human ears because of the

tiny amount of energy released or their high frequencies [15,23,24]. However, as noted previously, part of the elastic energy released from crack extension accompanying the microfracturing is converted into kinetic energy which is associated with the movement of the crack surfaces. This portion of the energy will propagate spherically outwards through the movement or vibration of particles of rock until it is completely dissipated. Although the vibration is extremely weak, it can be detected by suitable instrumentation and after amplification can be converted into audible sound.

By detecting the released acoustic energy, it is possible to study the development of the fracture process and hence the potential failure of the material. In fact, acoustic emission testing has been widely used in material and structural engineering. Results from previous studies [23,24] have showed that micro-fractures prior to failure result in small events, which have higher frequencies whereas large events are preceded by macro-fractures, which have lower frequencies. In laboratory tests, acoustic activity generally increases sharply prior to the failure of a rock specimen.

One question emerges: what is the relationship between the acoustic emission from rock specimens in laboratory tests and the seismic events generated from a rockburst or a natural earthquake? Theoretically, the acoustic emission should be similar for these two cases because the fracture process itself should be similar if the materials and loading conditions are the same. The only difference will be a matter of scale. Many seismologists agree with this. Mogi [25] compared his laboratory results of microfracturing behavior of rock with

earthquakes and concluded that the statistical behavior of microfractures is very similar to observed behavior of earthquakes, and he suggested that laboratory fracture experiments might be a scale model of crustal deformation. Mogi also observed that the buildup of microfracturing before failure is similar to foreshock sequences and that the specimen failure may correspond to the main shock. Scholz [23] also found that the microfractures radiate elastic energy in a manner analogous to earthquakes.

Rockbursting can be regarded as similar to earthquakes either in their occurrence or in their damage. From the point of view of a seismologist, a natural earthquake and a rockburst are extremely similar in terms of seismic emission. Therefore, by comparison, acoustic emission can be used to monitor rockbursts and the above observations should apply for rockbursting as well. The microseismic monitoring of rockbursts is actually based upon this principle. Then the microfracturing process prior to the specimen failure can be considered similar to that prior to a rockburst. In other words, the acoustic emissions should follow similar patterns for these two cases.

3.4. FAILURE DEVELOPMENT AND THE SHEARING PROCESS

As discussed before, the failure process of a rock mass is a matter of fracture development up to the failure strength. However, the previous discussion was concentrated on the fracture itself. On a macro scale, fracturing seems to initiate randomly in the rock mass at first. As loading continues, these fractures tend to develop in the direction which usually coincides with the planes of maximum shear stress, gradually forming a zone of fracturing. This zone usually has the

highest stress concentration and is where final failure occurs. As loading reaches the strength point, cracks start to fork in the weak direction when enough additional energy is available from crack extension. The forking process will develop as a result of the available internal energy. Because the ability of the rock mass to sustain external load decreases after the strength point, further loading will speed up the failure process. This forking process quickly joins the existing fractures, forming a macro-fracture surface within the fracturing zone.

From this moment, the failure is similar to a shearing process. In other words, the shear stress and shear strength control the stability. At this moment, if the external load is removed, the failure may not develop further. If the external load is lowered and remains in balance with the supporting ability of the rock mass, or if the shear stress and shear strength are in equilibrium, the failure will develop gradually. If the external load remains at the strength level or increases further, the failure will develop quickly and even violently if the resultant shear stress is too high.

Take the failure of a rock specimen in compression as an example. It is known that the same rock which failed violently during a conventional compressive test may fail gradually when tested on a servo-controlled testing machine. This is because the servo-controlled machine receives a feed-back signal from the deformation of the rock specimen and the load on the specimen is adjusted to prevent excessive deformation. When the failure strength is approached, or when a failure surface is initiated, the failure process becomes a shearing process. At this stage, the supporting ability of the specimen decreases

rapidly to the shear strength on the failure surface. This ability is usually viewed as the residual strength of that rock at the post failure stage. If the load is reduced quickly enough to meet the decreasing speed of the supporting ability of the rock specimen, the failure occurs gradually and non-violently and a complete stress-strain curve can usually be obtained. On the other hand, the conventional testing machine has no ability to lower the load and can not prevent the specimen failure. Therefore, after the strength point, the decrease of supporting ability of the specimen together with the release onto the specimen of the strain energy stored in the testing machine make the failure happen extremely rapidly. Usually violence is observed because of the high speed release of strain energy. A typical example of this will be given in the chapter on sudden loading.

The formation of the failure surface within the fracturing zone can be demonstrated by experiments. A few years ago, Scholz [23] conducted an experimental study and traced the fracturing process by locating acoustic emission. He observed that events below some stress level which may correspond to the beginning of the unstable fracture propagation, appear to be scattered throughout the specimen. However, events above that stress level group tightly on a plane which corresponds closely with the observed failure surface, such as in figure 3.2. This means that the fracturing process will eventually lead to the formation of a failure surface.

This failure surface can also be observed from damage occurring in underground structures and rock failures. Underground investigations of rockbursts

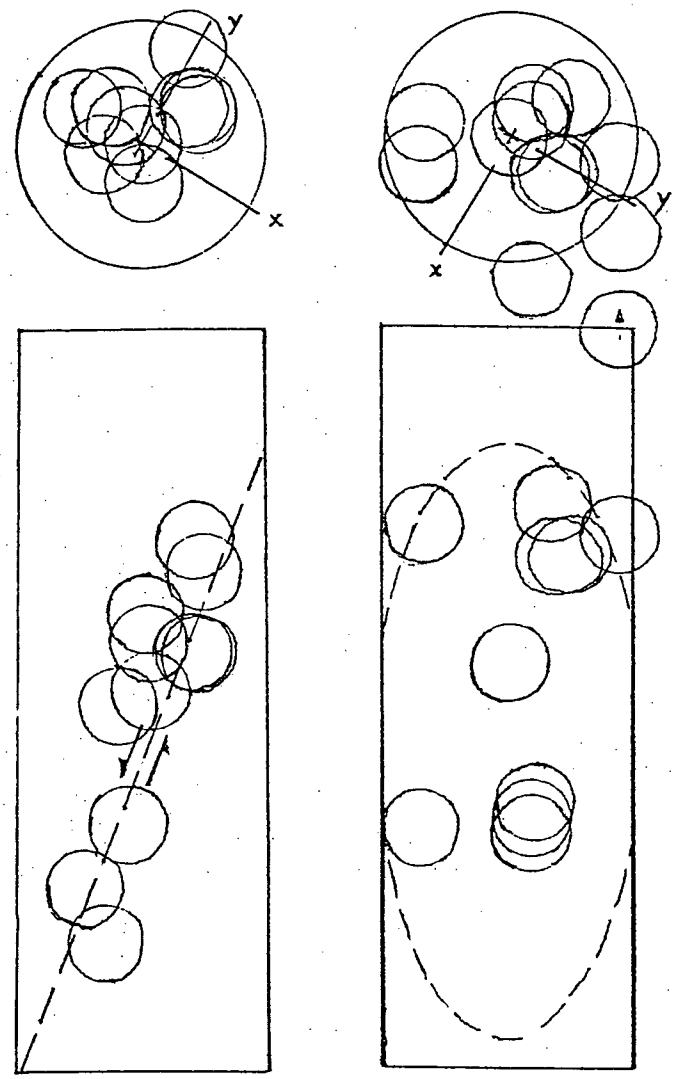

Fig. 3.2 Front, top and side views of the central section of the sample showing locations of events occurring in the dynamic cracking region (from Scholz, [23])

indicate that failure usually takes place along failure planes or surfaces. A particular example is the case of the failure of a rock pillar, where the failure plane has a conical shape and is very similar to the failure of rock specimen in compression. Figure 3.3 shows an unconfined rock specimen in an advanced stage of failure, where the macro-failure surface has been well developed. The final failure occurred along this surface, which made an acute angle to the direction of maximum compression. In field study of rockbursts, observations and measurements of fractures induced in the stope roof during excavation indicate that fractures dipping outwards from the face are likely to cause burst [2].

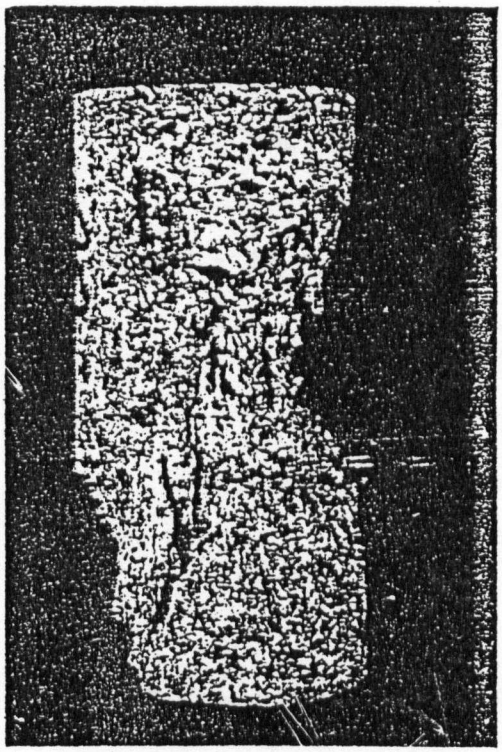

Fig.3.3 Unconfined Charcoal Gray granite I in advanced stage of failure (after Wawersik et at, [8])

3.5. DETERMINATION OF A FAILURE PLANE

As can be seen from previous discussion, the fracture development will lead to the formation of a failure surface on which the failure is eventually completed by shearing. This surface may or may not be a plane. For an intact rock, it will be a fracturing surface, which is not necessarily the plane where maximum shear stress exists and can be determined as following.

In underground mines, the mining structures are usually in a three dimensional compressive stress field. Typically there are one vertical and two horizontal compressive stresses, together with three shear stresses, with a total of six independent components. However, from elasticity theory [26], it is always possible to define a stress field only with three components to represent the original stress field. The three orthognal components are the principal stresses, $\sigma_1 \geq \sigma_2 \geq \sigma_3$. They are the normal stresses to the three principal planes respectively, on which there is no shear stress.

For a structure of isotropic and homogeneous material, its strength is the same in all directions. Its stability can then be determined by shear stress τ on the bigger half circle defined by σ_1 and σ_3 on Mohr's diagram. Thus the stress field has only two normal components σ_1 and σ_3 correspondingly, and can be treated as in two dimensions, figure 3.4. If the line OP, which represents the shear strength, is above the circle, it is stable. Otherwise failure takes place. In the latter case, the normal to the failure plane makes an angle of $\alpha = 45^\circ + \phi/2$ with the major principal stress σ_1, or the failure plane makes an angle of β with σ_1.

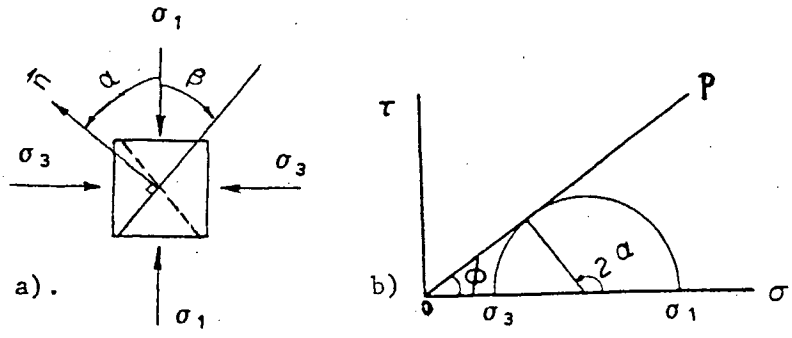

Fig.3.4 Schematic showing shear failure plane.

Because shear stresses are conjugate and $\beta+\alpha=90°$, the failure planes make angles of

$$\beta = \pm(45° - \phi/2) \quad \text{..... (3.1)}$$

with the major principal stress. This explains the phenomenon that the failure plane of rock specimens usually makes an angle of about 45° with the axial load.

However, in nature, perfect intact material is rare. Rock mass usually contains more or less joints or weaknesses of lower strength. Therefore failure would possibly take place along these weaknesses. Obviously, the failure plane can be either a pre-existing weakness or a fractured surface, depending upon the orientation of the weakness and its strength with respect to the rock mass. More often, rock failure takes place along some weakness.

3.6. SUMMARY

The results from analysis in this chapter can be summarized as follows:

1. A rock mass is a kind of anistropic, nonhomogeneous material, which is brittle, especially on a short term base.
2. As stress reaches some level, the process of rock failure is a matter of fracture development until the strength point is reached. The development of fractures can be divided into two stages: stable fracture propagation, which can be stopped by stopping loading and unstable fracture propagation, which is self-maintained and cannot be stopped by stopping loading only.
3. These micro-fractures initiate randomly throughout the body of the rock when load is low and concentrate in a zone which has the highest stress as load increases.
4. As unstable fracture propagation is approached, the extra energy available from fracture development makes the existing fractures fork in the weak direction. The forking process will eventually lead to the formation of a macro-fracture surface on which the final failure takes place.
5. After the formation of the macro-fracture surface, the failure process is similar to shear, so any sudden increase of shear force or any sudden decrease of shear resistance can cause violent failure.
6. Accompanying the fracture development, acoustic emission occurs, which is characterized by higher frequency for smaller events and by lower frequency for larger events.
7. Results from studies by Mogi and Scholts have shown that the process of fracture development and the associated acoustic emission are similar both in laboratory tests and in the field.

CHAPTER 4. FAILURE BY A PROCESS OF SHEARING

4.1. GENERAL

The failure behavior on surfaces will be an important aspect to be analyzed in studying violent failure because rockbursting can originate as shear failure of previous intact rock in the vicinity of the face (Spottiswood 1984) and can occur along a geological weakness, such as a fault. For the case of a fault, the failure is obviously a process of shearing. For the case of a massive rock, as discussed previously, the fracture development will eventually lead to the formation of the final failure surface.

Shear failure has been considered by seismologists to be the mechanism of shallow earthquakes along geological faults. This kind of earthquake is thought to be the result of shear failure on a fault because a sudden slip can release a large amount of energy. Because of the similarity of rockbursts and earthquakes in terms of seismic emissions and the manner in which they occur, this mechanism is assumed to apply for rockbursts as well. Therefore, it may be possible to describe rockbursts occurring on a fault as well as in a massive rock mass by shear failure and consequently to derive the conditions which may give rise to violence. As such it is worthwhile to study the characteristics of rock during shearing.

Shearing usually implies that two contacting surfaces tend to move with respect to each other under a pair of forces parallel to these surfaces. It is a universal phenomenon in earth engineering, such as landsliding, slope sliding and

wedge failure of a slope. In order to study the shear failure, first the friction on rock surfaces, shear strength and slip behavior should be examined.

4.2. THE LAW OF FRICTION

During shearing process, the friction on the contacting surfaces is the major resistance. Therefore, the study of friction is of greatest importance. The effects of friction arise on all scales: from microscopic scale in which friction is postulated between opposing surfaces of minute Griffith cracks to macroscopic scale of friction on joint or fault surfaces [26].

The simplest model for study of friction is the one in which two bodies with an approximate plane surface of contact are pressed together by a normal force P and pulled by a shear force F, figure 4.1. Obviously, the upper body will never move until F reaches some critical value. However, by Newton's law of motion: $F=M\ddot{X}$, the body should move once $F>0$. This means that there must be some resistance between the contact surfaces in the direction opposite to F. This resistance is called frictional force and is denoted by f here.

This frictional force depends upon many factors, such as properties of the material, roughness of the shear surface, normal stress, etc. The time effect of viscosity of rock, which is important in the long term period, is ignored in this research, because from field observations, it was seen that rockbursts usually occurred at the time of rapid stress change, such as during blasting. The simplest and widely used form for the maximum frictional force is the Coulomb relation:

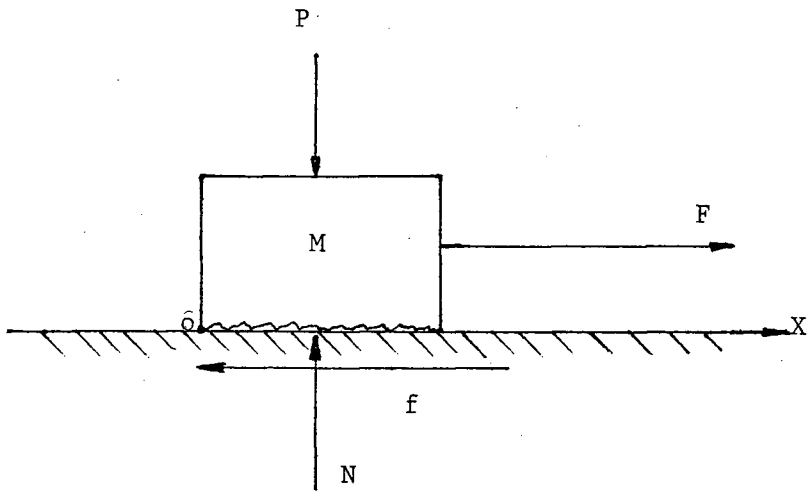

Fig.4.1 Simple model for shearing

$$f = C + \mu\sigma \quad \text{..... (4.1)}$$

where C is the cohesion, material property

σ is the normal stress

μ is the frictional coefficient, constant.

Obviously, when F is less than this maximum frictional force, by Newton's law of action and reaction, the frictional force will be equal to F acting in the opposite direction.

It has been observed in many laboratory experiments that once shear movement begins, the frictional force drops and crucially controls the nature of motion. The simplest way to consider this effect is to replace the constant μ in equation (4.1) with a lower value μ'---the dynamic coefficient of friction. The value of μ' is expected to be less than μ and to vary with the slip velocity $\dot{X}$, i.e. $\mu' = \mu'(\dot{X})$.

Unfortunately, this dynamic coefficient μ' is little understood and its relationship with the slip velocity is not well known to date. In order to consider this dynamic effect, a slip-velocity dependent coefficient of friction is derived here based on the laboratory data of Scholz and Engelder (1976) [27]. The dots in figure 4.2 are the original data. Based on the appearance of these, an empirical formula is postulated as

$$\mu = a + b/[7 + \log(\dot{X}+10^{-6})] \quad \text{..... (4.2)}$$

where a and b are constants to be determined.

These data were read off by digitizer and are listed in table 4.1. Constants a and b are obtained by nonlinear regression analysis for data in column (u,#1), with static coefficient of friction $\mu_s=0.805$. For comparison, another formula

$$\mu = a + b/[6 + \log(\dot{X}+10^{-5})]$$

was analyzed with the same data. It came up with correlation coefficient $r=0.9157$ and standard deviation Sd_{n-1}: ($\dot{X}\pm0.148$, $\mu\pm0.0105$). Finally, equation (4.2) is chosen, for its lower standard deviation, as the best fit represented by the curve in figure 4.2.

Through linear scaling in figure 4.2, another group of data for a typical case of $\mu_s=0.55$ were estimated and listed in column (u,#2) of table 4.1. The constants a and b were also obtained.

It can be seen that the correlation coefficient r is above 0.9, which means the formula represents the laboratory data very well. However, because

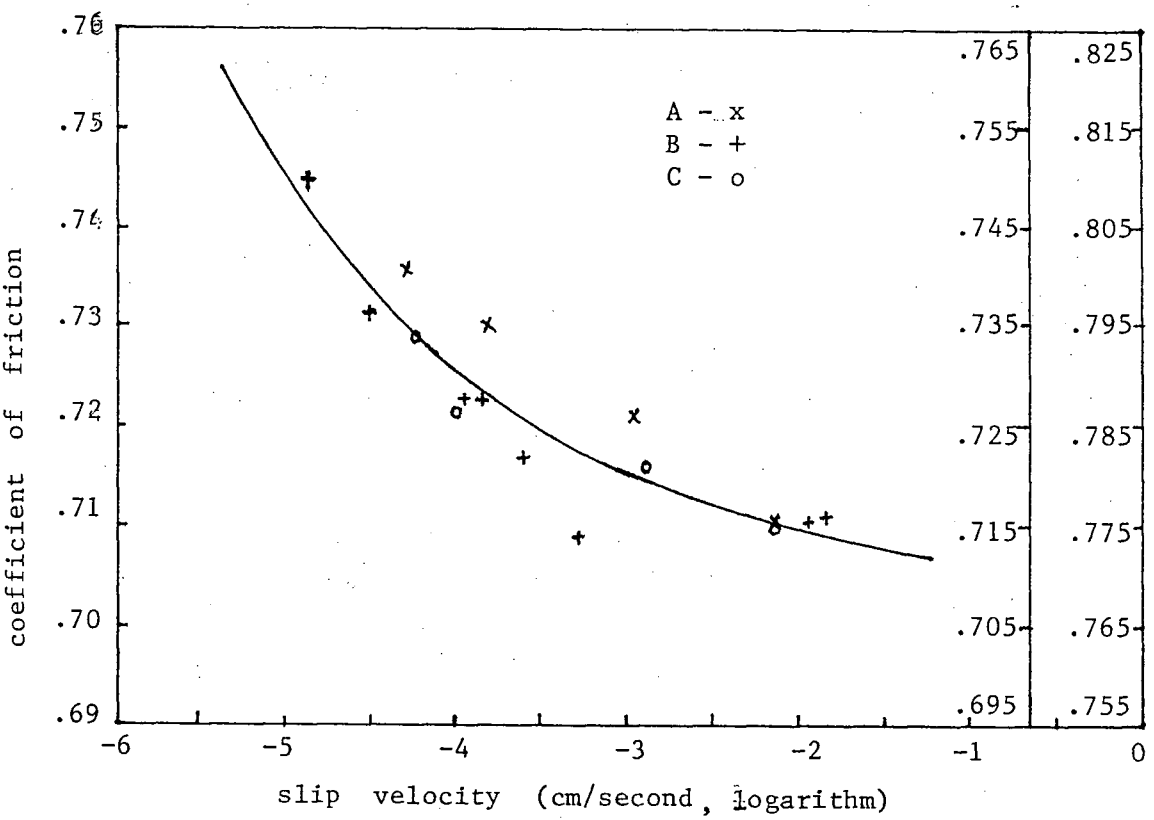

Fig.4.2 Velocity dependent friction. A, B and C refer to different experimental runs (data from Scholz et al, [23])

this formula is derived based on limited data with sampling points $n=16$, the value of ρ, or the population correlation coefficient is not necessarily so high as r, the sample correlation coefficient. In order to verify this formula, r is tested on significance level $\alpha=0.05$. According to the testing theory in statistics, for a given null hypothesis:

$$H_0: \rho=0,$$

Table 4.1 regression analysis of velocity-dependent coefficient of friction

#	$\log\dot{X}$	$\dot{X}\times10^{-5}$	$7+\log(\dot{X}+10^{-6})$	$1/[7+\log(\dot{X}+10^{-6})]$	u,#1	u,#2
1	-4.9359	1.159	2.100	.47618	.7445	.485
2	-4.5	3.1624	2.5135	.39785	.7312	.4712
3	-4.2813	5.2324	2.7269	.36671	.7347	.4753
4	-3.7813	16.5463	3.2213	.31043	.7300	.4700
5	-4.2188	6.0423	2.7883	.35864	.7279	.4682
6	-3.8397	14.4644	3.1633	.31613	.7226	.4623
7	-3.9359	11.5904	3.6783	.32596	.7224	.4623
8	-4.0064	9.8557	2.9980	.33356	.7212	.4612
9	-3.5513	28.0996	3.4502	.28984	.7165	.4565
10	-2.9038	124.7958	4.0966	.24411	.7209	.4609
11	-2.8077	155.7041	4.1926	.23852	.7159	.4556
12	-3.2308	58.7760	3.7699	.26526	.7087	.4488
13	-1.7756	1676.486	5.2244	.19141	.7118	.4517
14	-2.0641	862.7799	4.9359	.20259	.7088	.4476
15	-1.8718	1343.383	5.1282	.19500	.7089	.4477
16	-2.0820	827.9422	4.9181	.20333	.7100	.4476

nonlinear regression for u,#1

$\mu=0.6859+0.1192/[7+\log(\dot{X}+10^{-6})]$
with $\mu_s=\mu(0)=0.805$
correlation coefficient $r=0.9214$
standard deviation Sd_{n-1}: $\dot{X}\pm0.08168$, $\mu\pm0.01057$

for u,#2

$\mu=0.4245+0.1235/[7+\log(\dot{X}+10^{-6})]$
with $\mu_s=\mu(0)=0.55$
correlation coefficient $r=0.92$
standard deviation Sd_{n-1}: $\dot{X}\pm0.07797$, $\mu\pm0.01050$

if $|r|\leq r_a$, H_0 is accepted. Otherwise, H_0 is rejected. In our case, $n=16$, from the table of critical correlation coefficient [28], $r_a=0.4973$. Obviously, $|r|>r_a$. Therefore, H_0 is rejected. This means $\rho\neq0$ and appears greater than zero. If we wish to set a confidence interval on ρ, the Fisher's testing method should be used, which requires $n\geq50$. Therefore the empirical formula (4.2) is a reasonable representation of these data.

Equation (4.2) will be used later as the law of friction. To consider the variation of static coefficient of friction, constants a's and b's are estimated for other possible μ_s by linear interpolation and listed in table 4.2.

4.3. SHEAR STRENGTH

The shear strength is the maximum shear stress required to cause slip on a rock surface. It varies with rock type, surface roughness, confining pressure and conditions of temperature, pore pressure, loading rate, etc. For rock, the shear surfaces vary from the roughest rock joints formed in intrusive rocks to the smoothest planar cleavage surface found in slates. The simplest and most widely used shear failure criterion is the Coulomb criterion where the strength envelope is a straight line. However, it has been commonly accepted that the envelope of shear strength of rock surface is not a straight line but curvilinear. At low normal pressure, this strength decreases to zero. At high normal pressure, this envelope curves downwards. It is not impossible but difficult and unnecessary to describe this envelope with an exact formula. From laboratory results, such as in figure 4.3 [29], it is found that this envelope can be represented very well by a multilinear line. The common practice is to use a bilinear envelope with the first part for low normal pressure passing through the origin of the τ-σ coordinate system.

At low normal pressure, many authors [29] suggested the following equation for the peak shear strength for non-planar shear surface:

$$\tau = \sigma \mathrm{tg}(\phi + \mathrm{i}) \quad \text{..... (4.3)}$$

where ϕ is the basic angle of friction,

i is the dilation angle, or the effective roughness.

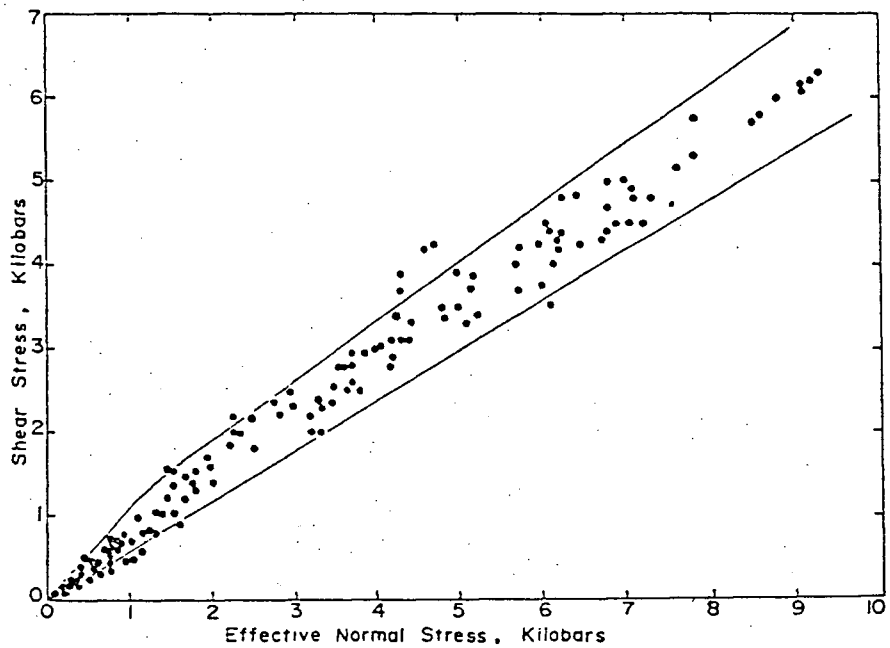

Fig.4.3 Friction strength of sawcut and fault surfaces of variety of rock types under different conditions of temperature(to 400 degree celsius), rate and amount of water (after Stesky, [29])

Table 4.2 Constants for empirical formula of slip-velocity dependent friction

#	1	2	3	4	5	6	7
μ_s	.35	.505	.55	.65	.75	.805	.95
a	.2235	.381	.4245	.528	.63	.6859	.8333
b	.1265	.1241	.1235	.1218	.12	.1192	.1166

Many experimental data reported in literature for blasted and sawcut surfaces indicate that most rocks have ϕ between 25°~35° [30]. Unfortunately, the data for i value is rather scarce, but can be determined by shearing test. Schneider(1976) [31] gave an empirical formula as

$$i = i_0 \exp(-k\sigma), \text{ or}$$

$$i = R \log(\sigma_c/\sigma)$$

with k, R being the empirical constants. Barton(1973) [30] from information extracted from literature gave some values of i between 6.2°~30.1°.

At high normal pressure, since most of the irregularities would be sheared off and the amount of dilation would decrease, the term of frictional resistance would dominate the shearing characteristics. In this case, the Coulomb relationship

$$\tau = C + \sigma \mathrm{tg}\phi \quad \text{..... (4.4)}$$

would be valid.

Usually, the critical value between the high and low normal pressures is defined as the crushing strength of the asperities. However, due to the variety of irregularities of rock surfaces, there is no general form for it. Barton [32] considered this critical normal pressure to be that at the brittle-ductile transition. But Byerlee(1968) [33] found no dilation during sliding on a sawcut surface in granite at a normal pressure considerably below this transition for that rock. Vesic and Clough [34] found this to be $(5\sim10)\times10^7$ Pa for medium to fine grained sands.

In contrast, another empirical envelope for the shear strength was given by Barton [30] for rough-undulating joints:

$$\begin{cases} \tau = \sigma \mathrm{tg}70°, \text{ if } \sigma_c/\sigma \geq 100 \quad \text{..... (4.5)} \\ \tau = \sigma \mathrm{tg}[\mathrm{JRC} \cdot \log(\mathrm{JCS}/\sigma) + \phi], \text{ if } 100 > \sigma_c/\sigma \geq 1 \end{cases}$$

where 70° is used to replace $(\phi+i)$ in equation (4.3),

σ_c is the unconfined compressive strength,

JCS is the effective joint wall compressive strength. JCS$=\sigma_c$ if the joint is unweathered.

JRC is the joint roughness coefficient, with a value of 20, 10 and 5 for rough-undulating joints, smooth-undulating joints and smooth-nearly planar joints respectively.

For a basic angle of friction $\phi = 28.5° \sim 31.5°$, we have

$\phi + i = 64° \sim 76°$ and consequently,

$\sigma_c/\sigma = 50$ to 200 are suggested.

It should be emphasized here that all the above values are purely empirical and the only thing which is certain is that for rock surfaces, the curvilinear envelope is much safer and more realistic than the simple Coulomb criterion. A bilinear envelope is therefore used and is given by equations (4.3) and (4.4) will be used, because most data available from past shear tests given is (C, ϕ) parameters,

$$\text{ie.} \quad \begin{cases} \tau = \sigma \operatorname{tg}(i + \phi), & \text{if } \sigma_c/\sigma \geq B \\ \tau = C + \sigma \operatorname{tg}\phi, & \text{if } B > \sigma_c/\sigma \geq 1 \end{cases} \quad \text{..... (4.6)}$$

where the constant B should be determined such that the continuation of the strength envelope is maintained at the point $\sigma = \sigma_c/B$. If i is known, then from equation (4.6), B is given by

$$B = [\operatorname{tg}(i + \phi) - \operatorname{tg}\phi]\sigma_c/C \quad \text{..... (4.7)}$$

or if B is given, then

$$i = \operatorname{tg}^{-1}[C \cdot B/\sigma_c + \operatorname{tg}\phi] - \phi \quad \text{..... (4.8)}$$

If data from shear tests were given as (C, μ_s) parameters, equations (4.6)-(4.8)

become

$$\tau = \sigma\mu_s', \text{ if } \sigma_c/\sigma \geq B \quad \text{..... (4.6a)}$$

$$\{$$

$$\tau = C + \sigma\mu_s, \text{ if } B > \sigma_c/\sigma \geq 1$$

$$B = [\mu_s' - \mu_s]\sigma_c/C \quad \text{..... (4.7a)}$$

$$\mu_s' = B \cdot C/\sigma_c + \mu_s \quad \text{..... (4.8a)}$$

Then the shear strength of rock joints will appear as shown in figure 4.4a). When slip begins, for a given normal stress σ, the shear strength will vary along a vertical line within the shadowed area of figure 4.4b).

4.4. EFFECTS OF ENVIRONMENT

As mentioned before, the behavior of the shearing process and the shear strength also depend on conditions of confining pressure, temperature, pore pressure, etc. A brief review and discussion related to mining situations is given below.

4.4.1. Normal Pressure

The normal pressure is obviously dominant during shearing process. It has a bilinear relation with shear strength as discussed in the previous section. At higher normal pressure, the coefficient of friction decreases more or less due to the crushing of asperities on the shear surface.

In laboratory studies, it is commonly found that stick-slip is dominant at high normal pressure, although the sliding is stable at low normal pressure. A typical example of testing results is shown in figure 4.5 [29]. This stick-slip process is considered to be the mechanism of generation of shallow earthquakes on natural faults [11]. This implies that the normal pressure is a significant

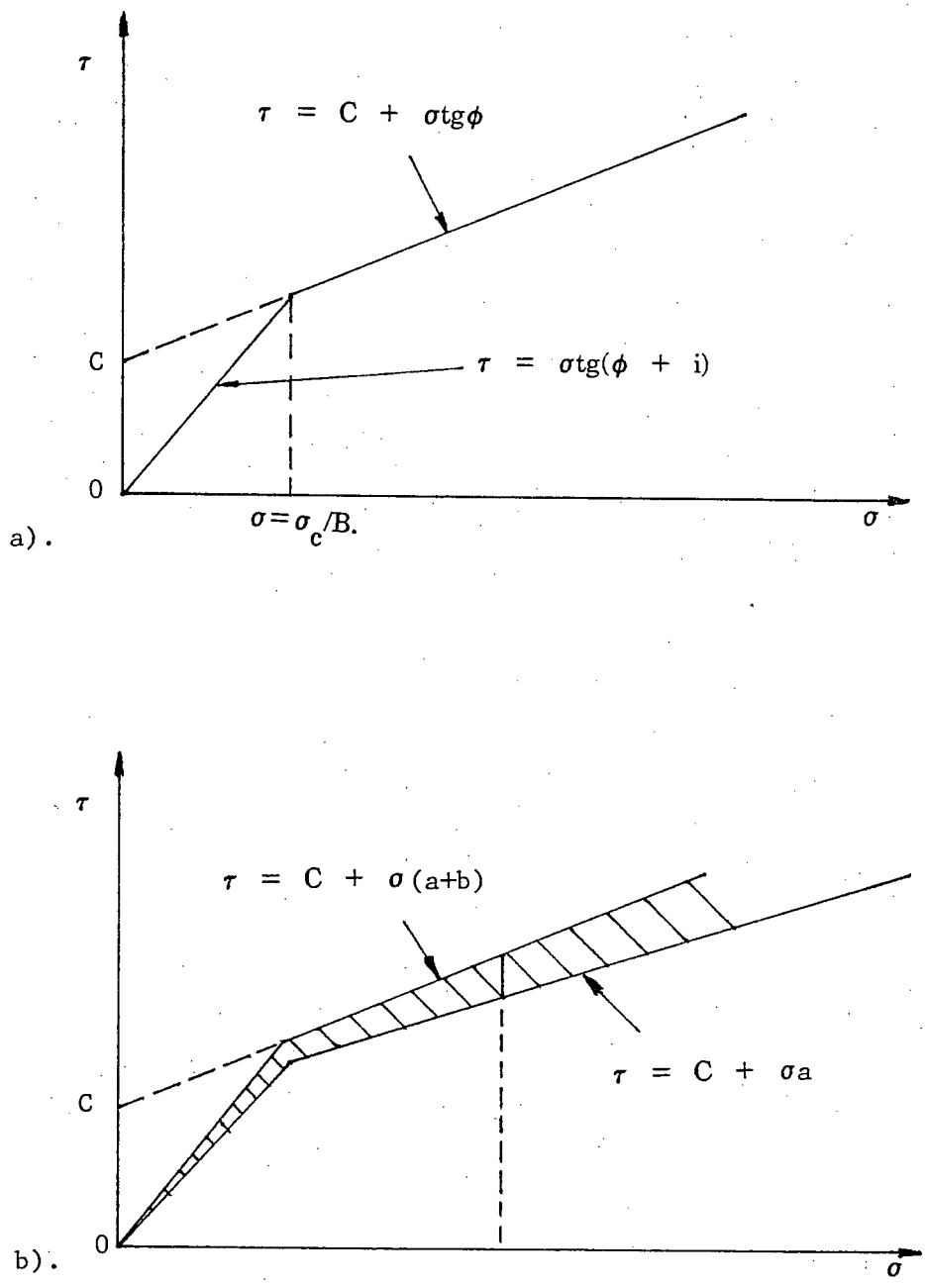

fig.4.4 a) Postulated bilinear shear strength; b) the effect of slip velocity

factor in rockbursting as well.

It should be noted that all the above arguments and the strength envelope developed are only good for normal pressures up to the unconfined compressive strength of the rock in question. At pressure above 10 Kbars (less for certain rocks) or at temperature above 400°C, equation (4.6) no longer holds and the friction strength becomes less dependent on the normal pressure [35]. Under these extreme conditions, the friction strength is supposed to be equal to

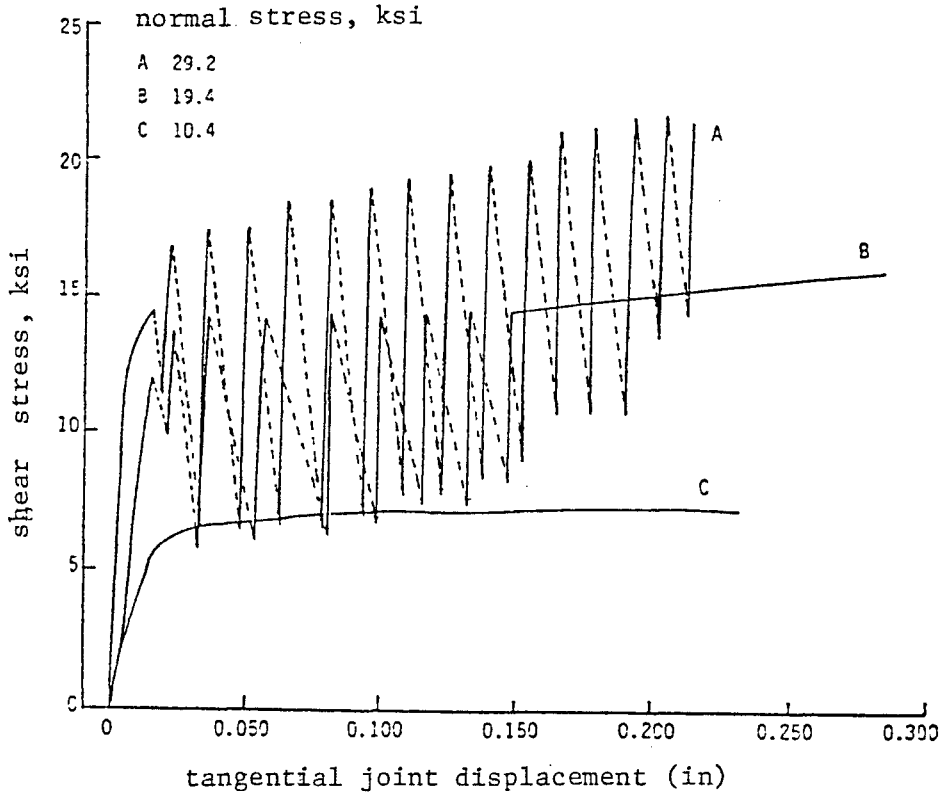

Fig.4.5 Sliding characteristics of stick-slip (curve A) and stable sliding (curve C) on sawcut surfaces (after Christensen et al, [57])

the compressive strength of intact rock.

4.4.2. Temperature

The role of temperature seems to be complicated. Under some conditions, the friction strength increases with temperature either due to the removal of absorbed water [36] or due to the formation of glass [37]. Under other conditions, this shear strength either is unchanged or decreases with increasing temperature [35]. In general, the strength envelope is valid at temperatures up to 400°C as shown in figure 4.6. The friction behavior seems also to change with temperature. The stick-slip phenomenon is enhanced by low temperature [35].

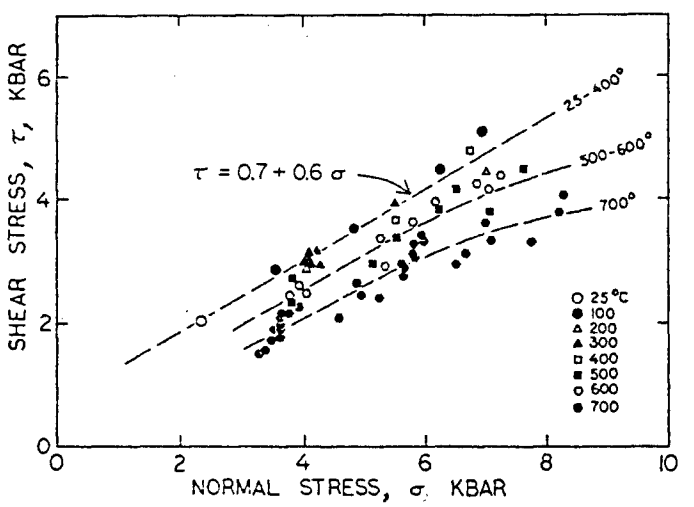

Fig.4.6 The effect of temperature on the friction strength of dry gabbro (after Stesky, [29])

4.4.3. Pore Pressure

The presence of water in a rock joint leads to several mechanical and chemical effects. The most important of them probably is the reduction of effective normal pressure. This certainly leads to the reduction of shear strength.

The effect of water pressure on shear strength seems to depend upon mineralogy of the rock and the surface roughness. In some cases, the frictional coefficient of massive crystal structures such as quartz and calcite increases in the presence of water. In the other cases, the frictional coefficient for larger lattice structures such as mica and chlorite decreases when wet. However, these effects diminish as the surface roughness increases.

In addition to the effect of reduction of effective normal stress, the shear strength increases or remains unchanged for smooth, polished surfaces when wet, and decreases for non-planar rough surfaces due to the adverse effect of moisture on the tensile and compressive strength of rock [30]. The presence of water on shear surface tends to enhance the stick-slip stress drop [38], but does not change the effective normal stress at which the transition between stick-slip and stable sliding takes place.

4.4.4. Time Dependency

The effect of time includes two aspects: the time of loading to failure or loading rate and the time duration in which stationary contact remains.

It was found that there is some strength reduction in both tension and

compression, when comparing the high "instantaneous loading" strength with the long term strength (2~4 weeks). This is thought to be from the creep effect. By extending this result, it is probable that normal laboratory shear tests might give an over-estimate of strength [30].

Another aspect of time dependency is from the stationary contact. In those experiments by Dieterich(1978) [39], the stresses τ and σ were held constant for some time and then the shear stress τ was increased rapidly to the critical level required to cause slip. It was found that the static coefficient of friction μ_s increases with the logarithm of the time of stationary contact. However, the magnitude of the time-dependency effect was found to be small compared with both the uncontrolled variability of μ between stick-slip events and the often observed overall increase in μ with displacement. Therefore even though the time dependency of μ is a general characteristic of rock friction, this effect may be easily masked by other effects.

The time effect is mainly brought about by the creep of asperities. The asperity creep depends on absorbed water. Therefore it is expected that the time dependency effect would be reduced if experiments were conducted in a water free environment. Besides, because the duration of rock burst process is very small, this time effect can be ignored as being of less important than other factors.

4.5. STICK-SLIP PHENOMENON

It is well known that regular relaxation oscillations frequently occur in experiments of metallic friction. Similarly, these phenomena were also observed during studies of rock friction [29,39,40]. The sliding behavior on a shear surface may occur as either of two types of motion. If the sliding is smooth with only small fluctuations in velocity when the shear stress reaches some critical value, it is called "stable sliding". If the sliding takes place by a series of discrete, rapid slips with a period of little motion in between, the sliding behavior is called "stick-slip". Figure 4.5 gives a typical example of stick-slip phenomenon from laboratory recordings.

The conditions under which either stable sliding or sick-slip occurs are very complex. Experimentally, the sliding behavior depends on normal pressure, presence of water, surface properties and possibly other factors [29]. From laboratory studies, it has been found that the behavior of sliding will change when loading condition varies. For example, stable sliding can become stick-slip with the increase of normal pressure, figure 4.5. This suggests that there may be a critical normal pressure at which the transition would take place given certain other factors. This transition normal pressure is considered by some to be the minimum normal pressure to cause asperity indentation and ploughing [39]. But stick-slip is also observed at normal pressures below that level [29].

The roughness of the shear surface seems also to affect the sliding behavior. On rough surfaces, the sliding is stable. On the contrary, stick-slip was observed with smooth or polished surfaces [40]. By reworking the shear surface

to a different roughness, the stick-slip behavior could be inhibited. However, from the point of view of rock mechanics, this stick-slip due to roughness is not considered to be important since a high degree of surface finish is rare except in some slickensided or natural cleavage surfaces.

Stick-slip is also reported to be dependent on the stiffness of the testing system [39]. The tendency of stick-slip decreases with the increase of the machine stiffness as observed in metal. Similarly, this tendency is enhanced by low machine stiffness. Figure 4.7 shows some typical laboratory results of transition normal stress versus machine stiffness and other factors. In general, stick-slip is enhanced by high normal stress, the absence of gouge, low surface roughness, low stiffness of testing machine and the presence of strong, brittle minerals such as quartz and feldspar.

Among the two types of slip behavior, stable sliding can not cause violent failure because no extra energy can be stored in the system. However, for the case of stick-slip, energy can be accumulated during the stick period and released at slip. A sudden slip will give rise to violence. Therefore, it is important to understand the conditions bringing stick-slip. From the above discussion, this condition may be a combination of many factors not a single factor and will be studied in the following chapter.

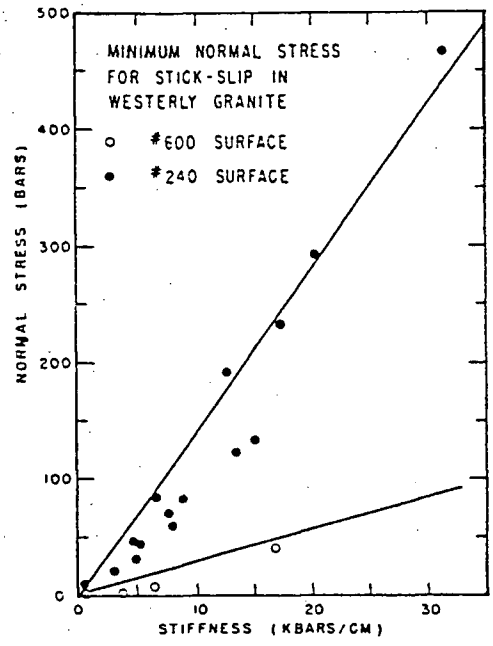

Fig.4.7 Transition from stable sliding to stick-slip as a function of normal stress, stiffness and surface finish. (after Dieterich, [39])

4.6. SUMMARY

Shear behavior on rock surfaces has been investigated and the following results are found:

1. The law of friction is introduced, and the coefficient of friction is found to be slip-velocity dependent, for which an empirical formula is derived based on the previous testing data.
2. A bilinear envelope is used as the most reasonable representation of shear strength of rock surfaces, with the first part passing through the origin and the second part having a nominal value of cohesion.
3. Environmental factors, such as normal pressure, pore pressure and time, have significant effects on shear strength.

4. Stick-slip is an important phenomenon because it can cause violence by a sudden slip due to the release of energy accumulated during the stick period.
5. Stick-slip is usually enhanced by high normal pressure, low surface roughness and low stifffness of the testing machine. The conditions which cause stick-slip appear to be complex and need further study.

CHAPTER 5. THEORETICAL SHEAR MODEL: CONSTANT FRICTION

Because it is impossible both economically and technically to carry out a complete study of shear failure by experiments under a variety of conditions and observation from one situation may be different from another situation [29,39], a model is developed in this research so as to give a full analysis of stick-slip during shearing. In order to study violent rock failure occurring in a massive rock and along a fault, the failure process for both cases is discussed in the previous two chapters and this process seems to be closely associated with the behavior on the failure surface. Sudden loading and stick-slip during shearing may be the causes of violent failure. Sudden loading will be discussed later in chapter 8. Stick-slip from previous discussions seems to be affected by many factors, such as rock type, normal pressure, surface roughness, etc.

5.1. MATHEMATICAL MODEL

A shearing model should be able to simulate the phenomena of both stick-slip and stable sliding. With this intention, a spring-mass system is suggested in figure 5.1 [26]. It consists of a block of mass M which rests on a surface under normal load P and is connected by a spring of stiffness λ to a support, which moves with a speed of V. The spring represents the elasticity of rock mass, the normal force P and the shear force F are self-explained. In the given coordinates, the system is stable in Y direction due to the balance of the normal force (P+Mg) and its reaction force N. In X direction, by Newton's law of motion, we have

$$M\ddot{X} = F + f \qquad (5.1)$$

where F and f are the shear force and the resistance, respectively.

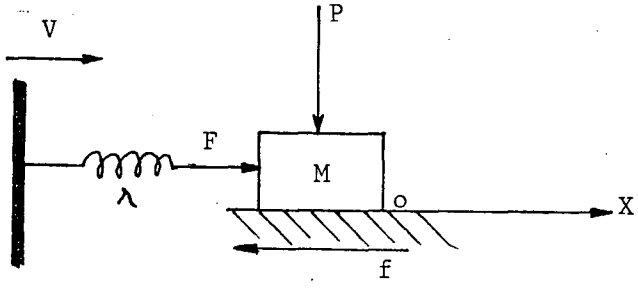

Fig.5.1 Simple shear model

If we begin to count the time at the moment when the mass is just about to move, the driving support would have moved a distance ξ_0 at time $t=0$. Let the contact area between the mass and the surface concerned be unit. Then the shear force and normal force will be equal to the corresponding stresses.

At any moment t, the shear force, which is a function of time t and displacement X of the mass M, is given by

$$F(t,X) = \lambda(\xi_0 + Vt - X) \quad \text{..... (5.2)}$$

where λ is the stiffness of the connecting spring,

X is the displacement of mass M, a function of time,

V is the moving speed of the support.

The resistance includes frictional force, resistance from viscosity and seismic radiation. For simplicity, only the frictional force is considered at the

moment. The viscous effect is ignored because it occurs only in long term failure and the rockbursting is a quick action. The seismic radiation will be introduced in a more sophisticated model in next chapter. Then, the maximum resistance is just the shear strength,

$$f(0) = C + (P + Mg)\mu_s \quad \text{..... (5.3)}$$

where C is the inherent cohesion,

μ_s is the static coefficient of friction, and

P is the normal force acting on the mass M,

f is the frictional resistance, a function of slip velocity: $f(\dot{X})$.

When the shear force F is less than f(0), by the law of action and reaction, the friction f is obviously equal to F in its value, pointing to the opposite direction. If F is bigger than f(0), the mass begins to move. As discussed before, the frictional resistance varies with the slip velocity of the mass M. To further simplify this model, we assume a constant friction during the moving process by introducing a dynamic coefficient of friction μ', which is less than the static coefficient, $\mu' < \mu_s$. The complete function of the friction would thus look like

$$f = \begin{cases} -C - \mu'(P + Mg), & \text{if } \dot{X} > 0, \\ C + \mu'(P + Mg), & \text{if } \dot{X} < 0, \\ -\lambda(\xi_0 + Vt - X), & \text{if } \dot{X} = 0 \text{ and } |F(t,X)| < f(0), \\ C + \mu_s(P + Mg), & \text{opposite to F in direction, if } \dot{X} = 0 \text{ and } |F(t,X)| \geq f(0). \end{cases} \quad \text{..... (5.4)}$$

where μ_s, μ' are the static and dynamic coefficients of friction, respectively,

ξ_0 is the initial value of compression in the spring, and

$\xi_0 = f(0)/\lambda = [C+\mu_s(P+Mg)]/\lambda$.

To study the slip behavior, only the condition of $\dot{X}\neq 0$ needs considering. With equation (5.2) and the upper two parts of (5.4), (5.1) becomes

$$M\ddot{X} = \lambda(\xi_0+Vt-X) \mp [C+\mu'(P+Mg)] \ ^{*}$$

$$= [C+\mu_s(P+Mg)] \mp [C+\mu'(P+Mg)] + \lambda(Vt-X),\ \dot{X}>\text{or}<0, \text{ or}$$

$$\ddot{X}+\lambda X/M = [C+\mu_s(P+Mg)]/M \mp [C+\mu'(P+Mg)]/M + \lambda Vt/M,\ \dot{X}>\text{or}<0$$

$$\ddot{X} + a^2X = b + a^2Vt \quad \text{.......} \quad (5.5)$$

where a and b are constants, given by

$a^2 = \lambda/M$, and

$b = [C+\mu_s(P+Mg)]/M \mp [C+\mu'(P+Mg)]/M$, $\dot{X}>$ or <0.

The ordinary second order differential equation (5.5) is a non-homogeneous vibration equation with an inciting force of $(b+a^2Vt)$.

The initial conditions for equation (5.5) is that both the displacement and the slip velocity of the mass are zero at t=0, ie.

$$\dot{X}(0) = X(0) = 0 \quad \text{.......} \quad (5.6)$$

5.2. SOLUTIONS TO THE DIFFERENTIAL EQUATION

The differential equation in (5.5) can be solved exactly, if V is known. The speed V of the moving support should be a function of time, because in the situation of mining, the rate of stress change varies during redistribution. At and right after excavation, the resembling speed V should increase. A while later after excavation when a new state of stress equilibrium is about to be reached,

*note: the sign $\mp$ is $-$ when $\dot{X}>0$ and is $+$ when $\dot{X}<0$.

V should decrease. However, it is difficult to simulate this rate of stress change exactly. A binomial function is introduced here:

$$V = V_0 + \omega t \geq 0 \quad \text{..... (5.7)}$$

where V_0 is a constant,

ω is the rate of speed change, a constant. $\omega>0$ means acceleration, for stress increasing; $\omega<0$ means deceleration, for stress relaxing.

Substitute (5.7) into (5.5), we have

$$\ddot{X} + a^2X = b + a^2V_0t + a^2\omega t^2 \quad \text{..... (5.8)}$$

The general solution to the homogeneous equation corresponding to (5.8) is a trigonometric function, given by

$$X^{*} = A\cos(at + \psi) \quad \text{..... (5.9)}$$

where A and ψ are constants to be determined from the initial conditions. A specific solution to (5.8) has the same form as the right hand side of (5.8), i.e.

$$X^{**} = B + Gt + Dt^2 \quad \text{..... (5.10)}$$

where B, G and D are constants, determined as followings. Because

$$\ddot{X}^{**} = 2D \quad \text{..... (5.11)}$$

by substituting (5.10) and (5.11) into (5.8), we have

$$2D + a^2(B+Gt+Dt^2) = b + a^2V_0t + a^2\omega t^2, \text{ or}$$

$$(2D+a^2B) + a^2Gt + a^2Dt^2 = b + a^2V_0t + a^2\omega t^2$$

Comparing the coefficients of each term on both sides of above equation, we obtain

$$a^2D=a^2\omega,\ a^2G=a^2V_0,\ 2D+a^2B=b, \text{ or}$$

$$D=\omega,\ G=V_0,\ B=(b-2D)/a^2=(b-2\omega)/a^2 \quad \text{..... (5.12)}$$

The real solution to equation (5.8) is the sum of the specific solution and the general solution corresponding to its homogeneous equation, i.e.

$$X = X^{*} + X^{**}$$

Considering equations (5.9), (5.10) and (5.12), we have

$$X = A\cos(at + \psi) + \omega t^2 + V_0 t + B \quad \text{..... (5.13)}$$

The first order differentiation of (5.13) gives

$$\dot{X} = -aA\sin(at + \psi) + 2\omega t + V_0 \quad \text{..... (5.14)}$$

Taking the initial conditions (5.6) into consideration, we can obtain the constants A and ψ.

$$\begin{cases} X(0) = A\cos\psi + B = 0 \\ \dot{X}(0) = -aA\sin\psi + V_0 = 0, \end{cases}$$

$$\begin{cases} \cos\psi = -B/A \\ \sin\psi = V_0/aA, \text{ or} \\ \psi = tg^{-1}(-V_0/aB) = tg^{-1}[-aV_0/(b-2\omega)] \end{cases}$$

$$\begin{cases} A = V_0/\sin\psi \end{cases} \quad \text{..... (5.15)}$$

(5.13) and (5.15) are the solutions to the differential equation (5.8) of our model.

5.3. MODEL RESULTS

With above solution, the slip behavior of this model can be described. In the following, a few commonly used parameters are discussed.

5.3.1. Slip Time

Slip time is the duration of a slip. Once the shear stress F(t,X) reaches the maximum resistance f(0), the mass begins to move. Its slip velocity varies according to equation (5.14). Due to the movement of the mass, the stress in

the spring is relaxed in turn. After time T_1, the mass stops moving, i.e.

$$\dot{X}(T_1) = -aA\sin(aT_1+\psi)+2\omega T_1+V_0=0 \quad \text{..... (5.16)}$$

The explicit solution of T_1 is not obtainable here, although it can be obtained numerically. For the simple case of uniform rate of stress redistribution, the moving speed of the support is constant, i.e. $\omega=0$. Then (5.16) becomes

$$-aA\sin(aT_1+\psi) + V_0 = 0$$

$$\sin(aT_1+\psi) = V_0/aA$$

$$= \frac{V_0}{a}/(\frac{V_0}{a}/\sin\psi) = \sin\psi \quad \text{..... (5.17)}$$

Note $\sin(aT_1+\psi)=\sin(aT_1)\cos\psi+\cos(aT_1)\sin\psi$, therefore, above equation becomes

$$\sin(aT_1)\mathrm{ctg}\psi = 1 - \cos(aT_1) \quad \text{..... (5.18)}$$

In the above equation, left side $= 2\sin(aT_1/2)\cos(aT_1/2)\mathrm{ctg}\psi$

right side $= 2\sin^2(aT_1/2)$

Substituting them back into (5.18), we have

$$\mathrm{tg}(aT_1/2) = \mathrm{ctg}\psi = -aB/V_0 \quad \text{..... (5.19)}$$

The solutions to (5.19) are infinitive and are given as

$$\tfrac{1}{2}aT_1 = k\pi + \mathrm{tg}^{-1}(-aB/V_0), \text{ or}$$

$$T_1 = \frac{2}{a}k\pi - \frac{2}{a}\mathrm{tg}^{-1}(aB/V_0)$$

where $k=1, 2, 3, \ldots$, all positive integers.

From the physical meaning of our model, it is known that only the first solution is valid, i.e. $k=1$ and $\dot{X}>0$. Considering (5.12) and (5.5)

$$T_1 = \frac{2}{a}\pi - \frac{2}{a}\mathrm{tg}^{-1}[(\mu_s-\mu')\ (P+Mg)/(V_0\sqrt{\lambda M})],\ \dot{X}>0 \quad \text{..... (5.20)}$$

The value of T_1 for $k=1$ and $\dot{X}<0$ is the time the mass takes to slip forward and to slip back.

5.3.2. Slip Distance

By the time T_1 when moving is ceased, the mass would have moved a maximum distance X_1, which can be determined from equation (5.13)

$$X_1 = X(T_1) = A\cos(aT_1+\psi) + V_0T_1 + B$$

Note $\cos(aT_1+\psi) = \pm\sqrt{1-\sin^2(aT_1+\psi)}$

$= \pm\sqrt{1-\sin^2\psi}$, (see eqn. (5.17))

$= \pm\cos\psi$.

First, consider $\cos(aT_1+\psi)=-\cos\psi$ and equation (5.15),

$$X_1 = -(V_0/a\ \sin\psi)\cos\psi + V_0T_1 + B$$

$$= -\frac{V_0}{a}\mathrm{ctg}\psi + V_0T_1 + B$$

$$= V_0T_1 - \frac{V_0}{a}(-\frac{a}{V_0}B) + B$$

$$= V_0T_1 + 2B$$

$$= V_0T_1 + 2[(\mu_s-\mu')(P+Mg)]/\lambda,\ \dot{X}>0 \quad \text{..... (5.21)}$$

Similarly, $\cos(aT_1+\psi)=\cos\psi$ gives rise to $X_1=V_0T_1$, which is invalid and ignored because at time T_1, the mass must have moved a distance $X_1>V_0T_1$, the displacement of the support during time T_1, so that the stress in the spring can be released.

5.3.3. Stick Time

After the mass has moved a distance X_1, the total potential energy in the mass-spring system is lowered. This drop of energy was consumed against the resistance. Because the support still moves with a speed V, the force and potential energy in the connecting spring begins to build up again until they reach the maximum values the mass-spring system can hold. During this period,

the whole system is stable and the duration of this period T_2 is called stick time and can be determined as following:

At the moment the mass is about to move, or at $t=0$, the total potential energy is the energy stored in the spring,

$$E_{po} = \tfrac{1}{2}\lambda\xi_0^2$$

suppose the mass were to stay at the maximum distance after each slip. Then at the time $t=T_1+T_2$ when the mass is about to move again, the potential energy reaches

$$E_{p2} = \tfrac{1}{2}\lambda(\xi_0 + Vt - X_1)^2$$

Obviously, at the two moments, $t=T_1$ and $t=T_1+T_2$, the energy should be the same, i.e.

$$E_{po} = E_{p2}$$

$$\tfrac{1}{2}\lambda\xi_0^2 = \tfrac{1}{2}\lambda(\xi_0 + Vt - X_1)^2$$

$$\xi_0^2 = (\xi_0 + Vt - X_1)^2, \text{ or}$$

$$\xi_0 + Vt - X_1 = \pm\xi_0$$

Remember that ξ_0 is the initial compression and is positive. So $-\xi_0$ is neglected. Then,

$$Vt - X_1 = V_0t + \omega t^2 - X_1 = 0 \quad \text{..... (5.22a)}$$

$$t = (-V_0 + \sqrt{V_0^2 + 4\omega X_1})/2\omega \quad \text{..... (5.22b)}$$

If $\omega=0$, from (5.22a), $t=X_1/V_0$, then

$$T_2 = X_1/V_0 - T_1 \quad \text{..... (5.22)}$$

Alternatively, because in this simple model, the only external force is from

the support, the stick time T_2 can also be obtained from force accumulation in the spring. At time T_1, the shear force is, from (5.2)

$$F(T_1,X_1) = \lambda(\xi_0 + VT_1 - X_1)$$

After time T_2, the shear force reaches the maximum resistance f(0)

$$F(T_1+T_2,X_1) = \lambda[\xi_0+V(T_1+T_2)-X_1] = f(0) = \lambda\xi_0,$$ (see eqn. (5.4)), or

$$V(T_1+T_2) - X_1 = 0,$$

the same as (5.22a). However, the energy method can be used in any conditions.

In the case that the mass may slip back due to the elasticity and finally stay at a distance less than X_1, the stick time will be less than the value given by equation (5.22). This situation may not exist in the highly restricted rock mass. The high restriction may stop the motion in less than one cycle, although it may slip back a bit.

5.3.4. Comparison with Laboratory Results

In order to verify the validity of this model in simulating the slip behavior, the modelling results are compared with laboratory tests. Figure 5.2 shows [40] some typical laboratory recordings from shear tests. The stick-slip phenomenon is characterized by the oscillation as shown in figure 5.2b) in comparison with the stable sliding of figure 5.2a). For a close up, one cycle of the stick-slip is enlarged in figure 5.3a), which clearly indicates the force buildup during the stick time and the force drop at slip. Correspondingly, the slip distance and the stick time are illustrated in figure 5.3b), where the displacement is unchanged during stick time and increases suddenly at slip.

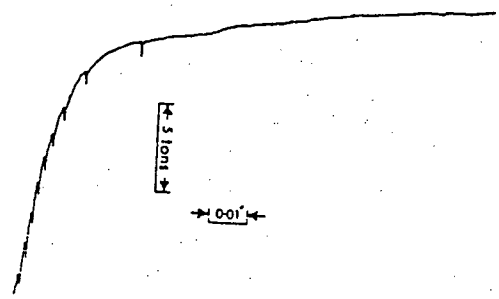

a).

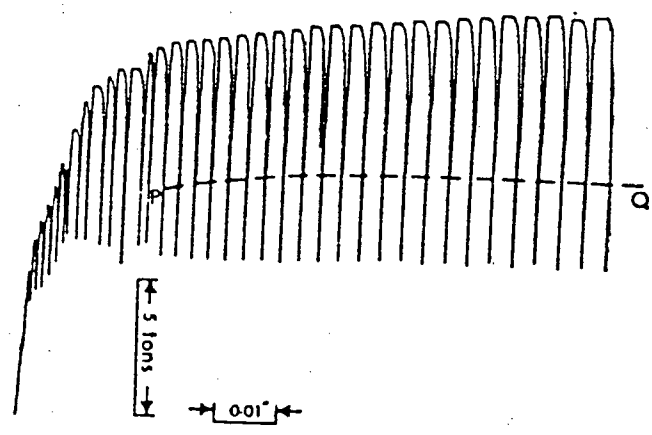

b).

Fig.5.2 a) Load-displacement for a shearing test, surface roughness 180 micro in; b) the oscillation of load with displacement on a magnified scale, surface roughness 35 micro in (after Hoskins et al, [40])

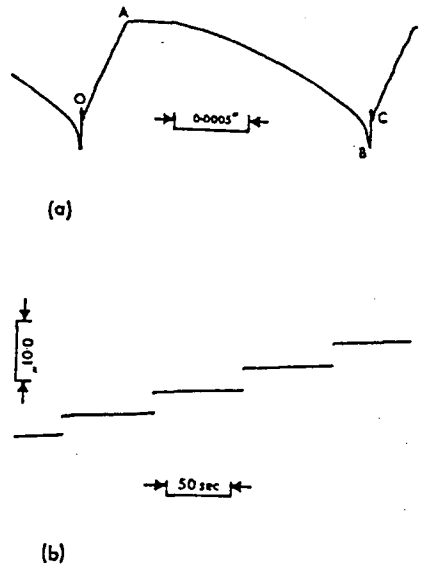

Fig.5.3 a) One cycle of the oscillation of Figure 5.2b) on an enlarged scale; b) the same showing displacement against time (from Hoskins et al, [40])

For comparison, the results of this model are plotted in figures 5.4 and 5.5. The detail of shear force, resistance, slip distance and slip velocity for a typical slip are illustrated in figure 5.4, where the shear force drop and resistance varies with slip velocity. In figure 5.5, the overall picture of the change of the shear force with slip distances and of the slip distance with testing time, are plotted. Obviously, they have similar patterns as the laboratory results, figure 5.3.

It can be seen that this shear model can reproduce the laboratory results and simulate the stick-slip well. Therefore, it can be used to further study the

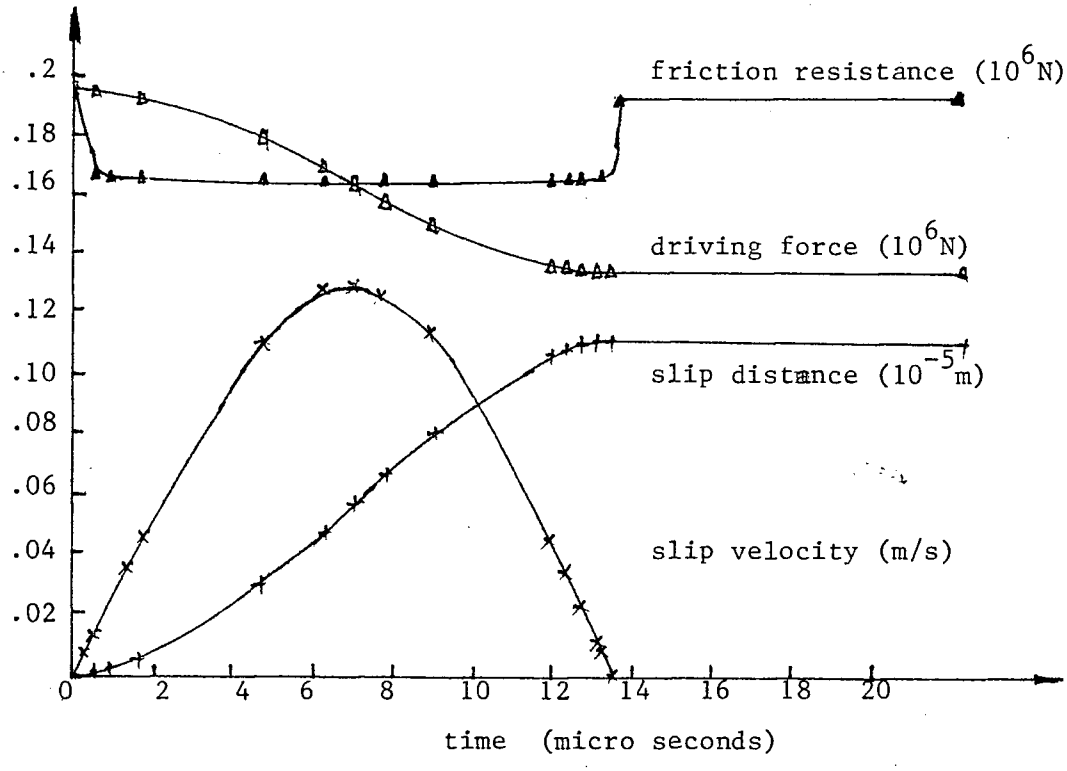

Fig.5.4 Model results showing changes of slip parameters with time

shearing process under various conditions of normal load P, surface roughness μ_s, driving speed V and stiffness λ and to search for the transition conditions between stick-slip and stable sliding. This will be discussed in next chapter.

5.4. DISCUSSIONS

In the previous chapter, the stable sliding is described as the smooth slip with only small fluctuation in velocity. Therefore it is important to examine the slip velocity. For stable sliding, slip will not change direction. For stick-slip however, slip may do. From (5.14), we know

$$\dot{X}_{min} = 2\omega t + V_0 - |Aa| \leq \dot{X} \leq 2\omega t + V_0 + |aA| = \dot{X}_{max}, \text{ or}$$

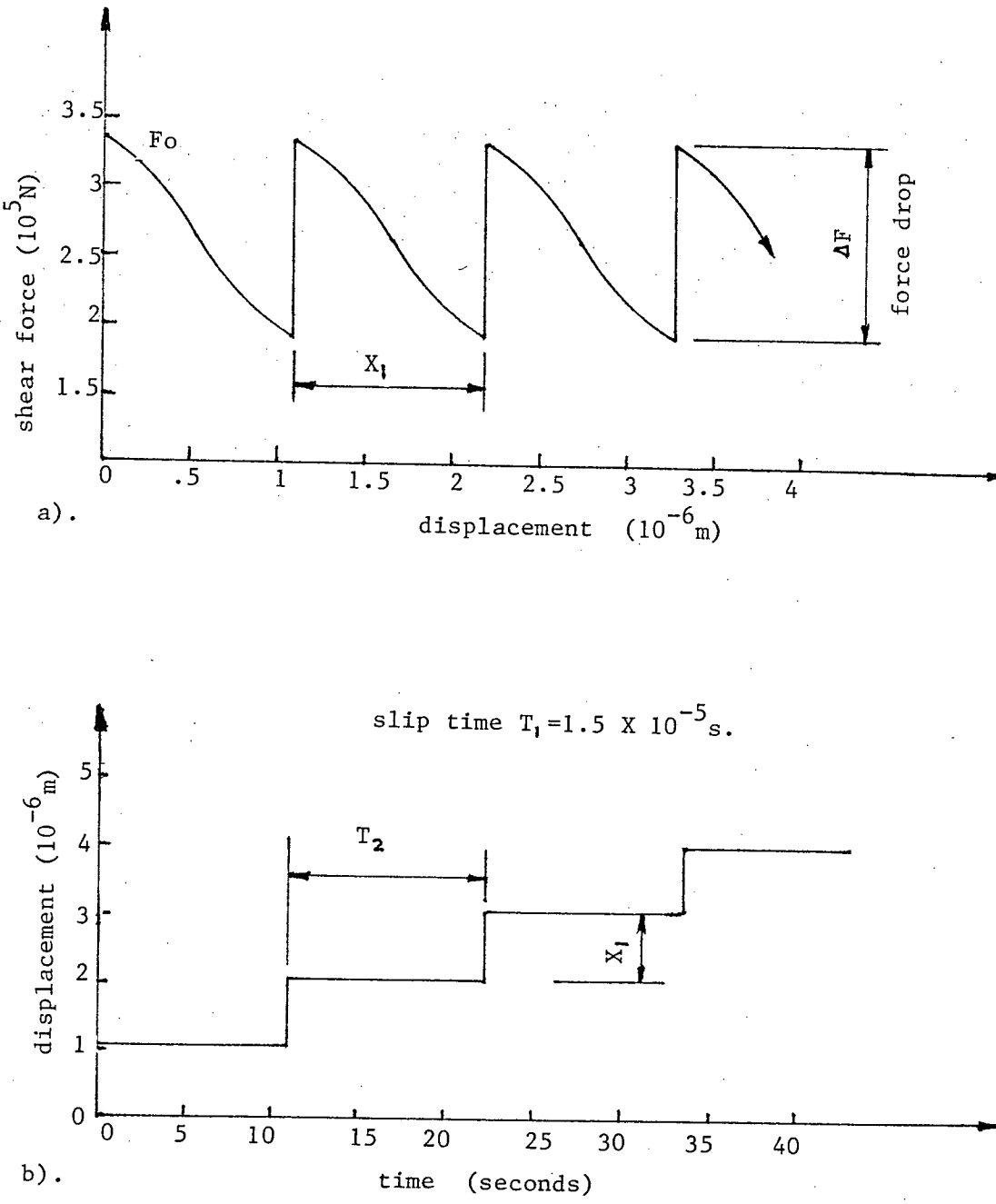

Fig.5.5 Model results: a) force-displacement curve; b) displacement-time curve

$$\dot{X}_{min} = 2\omega t + V_0 - V_0/|\sin\psi| \leq \dot{X} \leq 2\omega t + V_0 + V_0/|\sin\psi| = \dot{X}_{max} \quad \text{..... (5.23).}$$

If $\dot{X}_{min}$ and $\dot{X}_{max}$ have the same signs simultaneously, the sliding occurs. If one of them is zero, stick-slip occurs. If they have opposite signs, vibration occurs. However, this is not free vibration. As time continues, the vibration will damp off very quickly for low driving speed before the next slip begins.

For the case of $\omega > 0$, (5.23) gives $\dot{X}_{max} \geq 0$; note $|\sin\psi| \leq 1$, $V_0/|\sin\psi| - V_0 \geq 0$. In this case,

vibration occurs if $\dot{X}_{min} < 0$, or $2\omega t < V_0(1/|\sin\psi| - 1) \geq 0$ ..... (5.24a)

stick-slip occurs if $\dot{X}_{min} = 0$, or $2\omega t = V_0(1/|\sin\psi| - 1) \geq 0$ ..... (5.24b)

stable sliding occurs if $\dot{X}_{min} > 0$, or $2\omega t > V_0(1/|\sin\psi| - 1) \geq 0$ ..... (5.24c)

Obviously, equations (5.24a) and (5.24b) only exist temporarily. As the time continues, (5.24c) always exists. In other words, as long as $\omega > 0$, stable sliding is always possible.

For the case of $\omega = 0$, (5.23) becomes

$$\dot{X}_{min} = V_0(1 - 1/|\sin\psi|) \leq \dot{X} \leq V_0(1 + 1/|\sin\psi|) = \dot{X}_{max}.$$

Obviously, $\dot{X}_{max} \geq 0$, and $1 - 1/|\sin\psi| \leq 0$, or $\dot{X}_{min} \leq 0$. Therefore, stick-slip happens when $\dot{X}_{min} = 0$. Otherwise damping vibration occurs.

For the case of $\omega < 0$, (5.23) gives $\dot{X}_{min} \leq 0$. By (5.7), the lower limit for ωt is: $\omega t \geq -V_0$. Therefore,

$$\begin{aligned} \dot{X}_{max} &= V_0(1 + 1/|\sin\psi|) + 2\omega t \\ &\geq V_0(1 + 1/|\sin\psi|) - 2V_0 \\ &= V_0(1/|\sin\psi| - 1) \geq 0 \end{aligned}$$

the same happens as when $\omega=0$.

Therefore, when $\omega>0$, as time continues, stable sliding is always possible. When $\omega\leq 0$, stick-slip occurs if V_0 is small enough for the vibration to damp off before the next slip. Because of the high restrictions in the rock mass, the vibration can last very little time and the mass of this model can be suggested to stay at the maximum displacement. Therefore only stick-slip exists when $\omega\leq 0$.

In conclusion, if the driving speed which resembles the rate of stress change in the rock mass is zero, the system is stable if there was no potential problem before. On the other hand, for the case of nonzero driving speed, if the rate of stress change is decreasing, the slip behavior will eventually be stick-slip and the system will also become stable after the rate reaches zero. If the rate is constant, the process will probably be stick-slip, depending on other conditions. If the rate is increasing, the system will be unstable and stable sliding occurs eventually.

It can be seen that the driving speed is very important to the behavior of shearing. This means the importance of the stress change rate to rockburst. It should be pointed out however that in the above discussion, only driving speed is analyzed, and there are some other factors influencing the behavior. Besides only the static loading is considered here and the dynamic effect is not taken into consideration. All these will be discussed in the following chapters.

5.5. SUMMARY

1. A mathematical model of shearing, which can show phenomena of both stick-slip and stable sliding, is developed using constant static and dynamic coefficients of friction in order to analyze the slip behavior.
2. Using this model, the slip parameters, such slip distance, slip time and stick time are obtained theoretically, and their results are compared with laboratory recordings and similar patterns are found between them.
3. By comparison, this model is reasonable to simulate the shearing process.

CHAPTER 6. SLIP BEHAVIOR UNDER VARIOUS CONDITIONS

The slip behaviour of stick-slip in terms of slip distance, force and energy drops in each slip, stick time in between, etc., is very important in studying violent failure and determining the conditions which may give rise to violence. The model developed in the previous chapter where a constant friction was assumed will be used to analyze the slip behavior under various conditions. Here the variation of friction with the slip velocity and the seismic radiation, which is the signal detected directly by a seismic monitoring system, will be taken into consideration.

6.1. SUMMARY OF ROCK PROPERTIES

In order to take into account as many practical situations as possible, a few important parameters representing the rock properties are compiled here from publications. The data listed in table 6.1 are the results of laboratory tests and field measurements, most of them are from Jaeger and Cook [26].

6.1.1. Frictional Coefficient

The static friction of rock surface is the maximum resistance when the block is at rest and varies with the rock type and surface roughness. In general, harder rock and rougher surface have higher friction than softer rock and smoother surface. For instance, sandstone has a value of as low as 0.51, marble between 0.62~0.75, dolerite as high as 0.95. The coefficient μ_s in table 6.1 corresponds to the maximum friction resistance or the shear strength.

Table 6.1 summary of rock properties

index	general range	most of rocks	representative rock types
static frictional coefficient μ_s	0.45~0.95	0.5~0.8	sandstone, quartz, ~ marble, dolerite
cohesion C	0.3~1.1 MPa*	0.3~0.45 MPa	granite, trahyte ~ marble
elastic modulus E	7~100 GPa	40~100 GPa	sandstone, granite ~ diabase
uniaxial compressive strength σ_c	35~570 MPa	70~570 MPa	sandstone, marble ~ granite

* note: 1 KPa=10^3Pa, 1 MPa=10^6Pa, 1 GPa=10^9Pa

6.1.2. Cohesion

Cohesion is defined as the maximum frictional resistance when normal load is zero. In the case of rock, this resistance is usually nearly zero at null normal load. However, as discussed before, the strength envelope for rock can be represented by a bilinear curve passing through the origin of the τ-σ coordinate system. When normal load becomes higher, this curve is characterized by a lower slope and a nominal value of cohesion. The corresponding data is given in table 6.1

The cohesion also comes from the viscosity between the grain particles and therefore varies with the rock type. Again, harder rock has higher value, such as granite of 0.3 MPa, marble of 1.1 MPa.

6.1.3. Elastic Modulus

Elastic modulus, a measurement of the elasticity of a material, varies with rock type and is defined as the slope of the stress-strain curve of uniaxial compression before the strength point. It actually indicates the ability of rock to stand stress per unit change of strain. Usually, the higher its value, the harder the rock. A typical value of sandstone is 9.5 GPa, granite is 55 to 83 GPa and diabase up to 99 GPa. More is listed in table 6.1.

6.1.4. Uniaxial Compressive Strength

This is one of the most important indices of rock property. It is defined as the maximum ability of rock to sustain external stress without failure under one dimension load. Due to different minerals contained in a rock, this value σ_c varies widely, ranging from 34~586 MPa. Generally, soft rock has lower value. For example, a typical value for sandstone is 37 MPa, marble is 76~150 MPa and granite up to 586 MPa.

Under the condition of multiaxial loading, the compressive strength varies not only with the rock type, but also with the confining pressure. This relation is defined as the difference between the major and minor principal stresses by Hoek's empirical formula [42],

$$\sigma_1 = \sigma_3 + \sqrt{m\sigma_c\sigma_3 + s\sigma_c^2} \quad \text{..... (6.1)}$$

where σ_1, σ_3 are major and minor principal stresses

σ_c is th uniaxial compressive strength

m, s are empirical constants, given in reference [42]

This relation is valid only if the maximum effective normal stress satisfies the

condition: $\sigma \leq \sigma_c$.

6.2. SEISMIC EFFECT

In the study of rockbursting, seismic radiation is a very important factor to be considered. It is a mechanism in nature whereby energy released during a burst can be removed from the neighborhood of the bursting. As a burst occurs, tremendous energy is released, part of which is radiated out from the bursting center in a form of seismic energy, which is the source to be detected by a seismic monitoring system. The radiation of seismic energy is a process of chain reaction among the grain particles of rock mass. It starts at the energy release centre and propagates out spherically. When the seismic waves reach a point around this centre, the particles of rock mass begin to vibrate. This vibration in turn motivates particles adjacent to them. In this process, part of the seismic energy is consumed against the resistance of vibration and part of it is transmitted to adjacent particles. This process continues until the seismic energy is over or until the seismic waves reach some boundary between the rock mass and other medium, such as air. In the latter case, a reflection of the shock wave occurs as a tensile wave with disastrous effects on the free surface of the mine excavation. Intense slabbing and spalling occurs within milliseconds filling the opening virtually instantaneously with broken rock.

6.2.1. Formulation of Seismic Radiation

The process of seismic radiation itself is very complicated. No attempt is made in this research to study this process in detail. Here we are trying to use some simple way by which this process can be introduced into the shearing model.

One way [43] in which radiation effects can be simulated without making the model unduly complicated is to attach a semi-infinite string to each particle of the rock mass in such a way that motion of the particle excites an elastic wave which propagates along the string.

This idea is diagrammatically shown in figure 6.1. A string is attached to the particle M at X=0, and is fixed at X=∞. Any motion of the particle can induce a longitudinal wave in the string.

Suppose this string has an area A and elastic modulus E in certain length. Consider an infinitesimal element of dX between sections X and X+dX, figure 6.2. Obviously, the stress at any point is a function of its position on the string, i.e. σ(X). If the stress is σ_1 at section X and σ_2 at section X+dX, this element will be moved to the position bounded by the dashed lines under

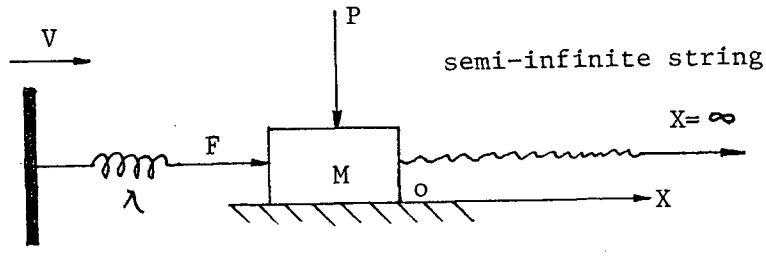

Fig.6.1 Simulating the effect of seismic radiation

the differential force $(\sigma_1 - \sigma_2)A$. By Newton's motion law, the force and the instantaneous movement u would be related in the following way,

$$(\sigma_1 - \sigma_2)A = A\rho\frac{d^2u}{dt^2}dX \quad \text{..... (6.2)}$$

where A is the section area of the element

ρ is the density of the string

ρAdX is the mass of the element dX.

From the definition of first derivative, we have

$$\frac{d\sigma}{dX} = \frac{\sigma(X+\Delta X) - \sigma(X)}{dX}$$

$$= \frac{-\sigma_2 - (-\sigma_1)}{dX} = \frac{\sigma_1 - \sigma_2}{dX} \quad \text{..... (6.3)}$$

From elasticity theory,

$$\sigma = E\epsilon = E\frac{du}{dX} \quad \text{..... (6.4)}$$

Differentiating equation (6.4) with respect to X leads to

$$\frac{d\sigma}{dX} = E\frac{d^2u}{dX^2} \quad \text{..... (6.5)}$$

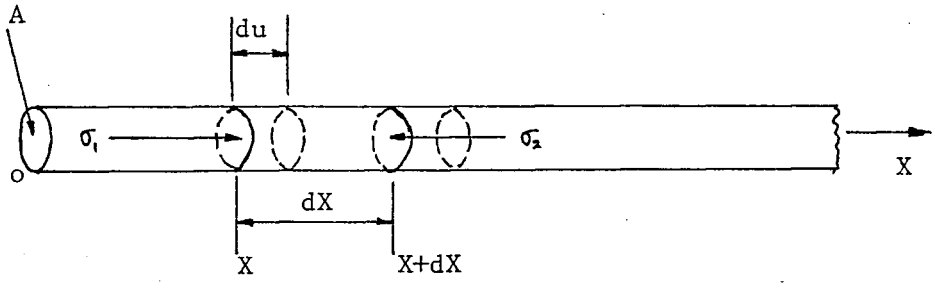

Fig.6.2 An element of the semi-infinite string

Substitute equations (6.3) and (6.5) into (6.2), we have

$$\frac{\partial^2 u}{\partial X^2} = (\rho/E)\frac{\partial^2 u}{\partial t^2}, \text{ or}$$

$$\frac{\partial^2 u}{\partial t^2} - V_p^2 \frac{\partial^2 u}{\partial X^2} = 0 \quad \text{..... (6.6)}$$

where $V_p^2 = E/\rho$, the p-wave velocity.

Equation (6.6) is the classic one-dimensional wave equation without exciting force. If an exciting force is applied at the centre where the wave originates, such as at X=0 in figure 6.1, another term should be added to the right hand side of (6.6)

$$\frac{\partial^2 u}{\partial t^2} - V_p^2 \frac{\partial^2 u}{\partial X^2} = \Phi(t) \quad \text{..... (6.7)}$$

where $\Phi(t)$ is the exciting force, a function of time.

Any function u(X,t) satisfying the above equation will be a solution to it. One such solution to the homogeneous equation of (6.7) has the general form [44] as

$$u(X,t) = u(t - X/Vp) \quad \text{..... (6.8)}$$

To consider the exciting force $\Phi(t)$ in (6.7), another function should be included in (6.8), which would have the same form as $\Phi(t)$. Let $u(t)^*$ be a particular solution to (6.7). Then the complete solution to (6.7) would be the sum of (6.8) and $u(t)^*$:

$$u(X,t) = u(t - X/Vp) + u(t)^* \quad \text{..... (6.9)}$$

This solution can be verified by differentiating (6.9) with respect to time and substitute it into (6.7), which leads to

$$[u(t)^*]''_{tt} = \Phi(t) \quad \text{..... (6.10)}$$

Equation (6.10) is the requirement for $u(t)^*$ to be the particular solution, which

can be obtained by solving the differential equation (6.10) if $\Phi(t)$ is known. The force p in the string at section X will be the corresponding stress times the area A. From (6.4) and (6.9), we have

$$\begin{aligned} p(X,t) &= AE\frac{du}{dX} \\ &= AE\{[u(t - X/Vp)]'_x + [u(t)^*]'_x\} \\ &= AE\{u'(t - X/Vp)\frac{-1}{Vp} + 0\} \\ &= -\frac{AE}{Vp}u'(t - X/Vp) \end{aligned} \quad \text{..... (6.11)}$$

Obviously, the force is a function of time and the position on the string. Even at the same time, this force could be a tension at some sections and compression at other sections, depending on the deformation. However, for this model of shearing process, only the force at the end of the string, i.e. at $X=0$, is important. From figure 6.1, it can be seen that the displacement of the particle M is the same as that of the string end, or $X=u(0,t)$, and so is the slip velocity of the particle, $\dot{X}=\dot{u}(0,t)$.

The force at any moment exerting on the particle by the string is the force at the end of the string, which can be obtained by setting $X=0$ in equation (6.11),

$$p(0,t) = -\frac{AE}{Vp}\dot{u}(0,t) = -Eo\ \dot{u}(0,t) \quad \text{..... (6.12)}$$

where $Eo = AE/Vp$. This means that the force exerted by the semi-infinite string is proportional to but in the opposite direction of the slip velocity $\dot{X}$ of the particle M.

Thus, the seismic radiation effects can be easily taken into account by

adding one term as $(-Eo\dot{X})$ to the resistance equation discussed in chapter 4, ie.

$$f(\dot{X})^{*} = \mp f(\dot{X}) - Eo\dot{X}, \ \dot{X} > \text{ or } < 0 \quad \text{..... (6.13)}$$

where $f(\dot{X})$ is the frictional resistance

Eo is the coefficient of seismic radiation

$\dot{X}$ is the slip velocity of particle M.

The general picture of $f(\dot{X})$ for $\dot{X} > 0$ is shown in figure 6.3.

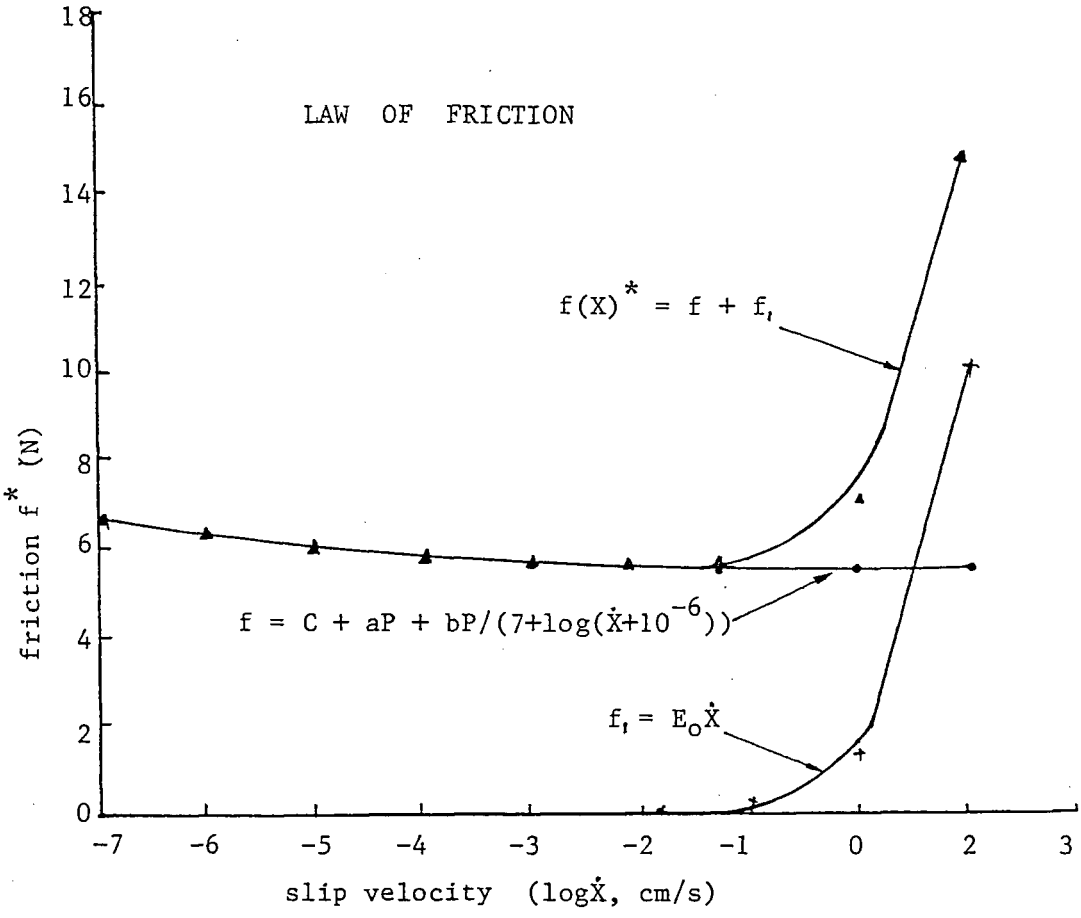

Fig.6.3 Shearing resistance as a function of slip velocity and seismic radiation

6.2.2. Characteristics of Seismic Radiation Coefficient

The coefficient of seismic radiation Eo is defined in equation (6.12) as

$$Eo = AE/Vp.$$

By (6.6), $V_p^2 = E/\rho$, we have

$$Eo = A\sqrt{E\rho}$$

where ρ is the material density

A is the cross section area of the semi-infinite spring.

In general, the variation of density ρ of rock is negligible compared with that of elastic modulus E. Therefore the coefficient Eo is proportional to the square root of elastic modulus E,

$$Eo = k\sqrt{E} \quad \text{..... (6.13a)}$$

where k is a constant.

6.3. MATHEMATICAL MODEL

The model postulated in chapter 5 will be completed here by introducing the slip-velocity dependent friction and the effect of seismic radiation. For the model shown in figure 5.1, the motion equation and other relevant expressions are rewritten here again for convenience.

$$M\ddot{X} = F + f^* \quad \text{..... (6.14)}$$

$$F(X,t) = \lambda(\xi_0 + Vt - X) \quad \text{..... (6.15)}$$

where λ is the stiffness of the connecting spring,

X is the displacement of the mass M,

V is the moving speed of the support,

$\xi_0 = f(0)/\lambda$, the initial compression in the spring,

f(0) is the shear strength.

The resistance force will be as described by (6.13)

$$f^{*} = \begin{cases} -f - Eo\dot{X}, & \text{if } \dot{X}>0 \\ f - Eo\dot{X}, & \text{if } \dot{X}<0 \\ -F(X,t), & \text{if } \dot{X}=0 \text{ and } |F|<f(0) \\ f(0)\,\mathrm{sign}(F), & \text{if } \dot{X}=0 \text{ and } |F|\geq f(0) \end{cases} \quad \cdots\cdots (6.16)$$

where $\mathrm{sign}(F)=-1$ if $F<0$, $\mathrm{sign}(F)=+1$ if $F>0$

$$f = \begin{cases} \sigma\mu', & \text{if } \sigma_c/\sigma \geq B \\ C + \sigma\mu, & \text{if } B>\sigma_c/\sigma \geq 1 \end{cases} \quad \cdots\cdots (6.17)$$

σ_c is the uniaxial compressive strength

C is the cohesion

σ is the normal pressure

μ is the coefficient of friction and is given by equation (4.2):

$$\mu = a + b/[7 + \log(\mp\dot{X}+10^{-6})], \quad \dot{X}< \text{ or } >0 \quad \cdots\cdots (6.18)$$

a, b are constants, given in table 4.2

For a given B,

$$\mu' = BC/\sigma_c + \mu \quad \cdots\cdots (6.19)$$

where B is an empirical constant and is given, or calculated by

$$B = \sigma_c(\mu' - \mu)/C \quad \cdots\cdots (6.20)$$

if μ' is known.

Considering equations (6.15) and (6.16), from (6.14) we have the differential equation

$$\ddot{X} = \begin{cases} (F - f - Eo\dot{X})/M, & \dot{X}>0 \\ (F + f - Eo\dot{X})/M, & \dot{X}<0 \\ 0, & \dot{X}=0 \text{ and } |F|<f(0) \\ [f + f(0)\,\mathrm{sign}(F)]/M, & \dot{X}=0 \text{ and } |F|\geq f(0) \end{cases} \quad \cdots\cdots (6.21)$$

The initial conditions are

$$\dot{X}(0) = X(0) = 0 \quad \text{..... (6.21a)}$$

Considering equation (6.18) where the logarithm of $\dot{X}$ occurs in the denominator, it is obviously impossible to solve equation (6.21) exactly. The only way to do it is to find an approximate solution numerically. This will be discussed later in this chapter. Therefore (6.21) will be left as it is for the convenience in programming.

6.4. ENERGY

In the introductory chapter, rockbursting was defined as a phenomenon of violent energy release. Part of this energy is radiated out as seismic energy. Therefore it is very important to look at the behavior of the shear model in terms of energy change.

It is known that, in a force system, the work done by external forces on the system is equal to the increase of the total energy within this system. This can be expressed as:

$$dE = FdS \quad \text{..... (6.22)}$$

where dE is the total energy increase

F is the total external force

dS is the distance increase over which work is done by F and along F.

For the model shown in figure 5.1, external forces which actually do work on the system are the resistance of equation (6.16) and the driving force F of

(6.15) from the moving support. The total energy includes the kinetic energy of the mass M and the potential energy in the connecting spring. Therefore, by equation (6.22), the energy equation for this system is

$$d[\tfrac{1}{2}M\dot{X}^2 + \tfrac{1}{2}\lambda(\xi_0+Vt-X)^2] = \lambda(\xi_0+Vt-X)Vdt-|f(\dot{X})\dot{X}|dt-Eo\dot{X}\dot{X}dt$$

$$\frac{d}{dt}[\tfrac{1}{2}M\dot{X}^2 + \tfrac{1}{2}\lambda(\xi_0+Vt-X)^2] = V\lambda(\xi_0+Vt-X)-|f(\dot{X})\dot{X}|-Eo\dot{X}^2 \quad \text{..... (6.23)}$$

$$\text{or, } \frac{d}{dt}(E_k + Ep) = \dot{W}e - \dot{W}_f - \dot{W}r \quad \text{..... (6.23a)}$$

The physical significance of each term in above equation is as following:

$E_k = \frac{1}{2}M\dot{X}^2$, the kinetic energy of the system,

$Ep = \frac{1}{2}\lambda(\xi_0 + Vt - X)^2$, the potential energy in the connecting spring,

$\dot{W}e = V\lambda(\xi_0 + Vt - X)$, the rate of doing work in moving the support against the spring and being of order V,

$\dot{W}_f = |f(\dot{X})\dot{X}|$, the rate at which work is done against friction, positive,

$\dot{W}r = Eo\dot{X}^2$, the power radiated along the semiinfinite string, positive.

For a given period $\Delta t=t_2-t_1$, the total work done by external forces should be the integration of the right hand side in equation (6.23) over Δt. Thus, by integration equation (6.23a) becomes

$$\Delta E_k + \Delta Ep = We - W_f - Wr \quad \text{..... (6.24)}$$

In the numerical solution to be described later, the total energy radiated Wr will be computed as

$$Wr = \int_{t_1}^{t_2} \dot{W}r \, dt = \int_{t_1}^{t_2} Eo\dot{X}^2 dt$$

$$\simeq Eo \sum_{j=1}^{n} \dot{X}_j^2 \Delta t_j \quad \text{..... (6.25)}$$

where n is the number of sampling points for the period Δt.

From (6.24), it can be seen that, if we let the loading speed V be sufficiently small, so that $We \simeq 0$ and note $\dot{X} = 0$ at the onset of a slip and at the moment when slipping ceases, so $E_k \simeq 0$. Then the loss of potential energy in the system is approximately equal to the sum of the work done against friction and the energy radiated during the slip, ie

$$\Delta Ep \simeq -W_f - Wr \quad \text{..... (6.24a)}$$

Furthermore, we can see the loss of potential energy is proportional to the energy radiated, ie.

$$\Delta Ep \propto -Wr,$$

this can be seen in the modelling results of chapter 12, figure 12.4b).

6.5. NUMERICAL SOLUTION

For an ordinary differential equation such as (6.21), which is not soluble explicitly, its approximate solution can be found by numerical method. There are a few numerical methods available, such as Euler method, Runge-Kuta method, linear multi-step method and Adams' method. Each of them has its advantages and disadvantages. Due to the accuracy and high speed of convergence, the Runge-Kuta method [45] is chosen here for our particular case.

6.5.1. Introduction to Runge-Kuta Method

6.5.1.1. First Order Differential Equation

Assume that the solution to a first order differential equation

$$Y'(X) = f(X,Y) \quad \text{..... (6.26)}$$

with $Y(Xo) = Yo$

exists and is unique. Based on the value of Y on step n, the approximate value of Y on step n+1 is estimated by Runge-Kuta method as

$$Y_{n+1} = Y_n + [k_1 + 2(k_2+k_3) + k_4]/6 \quad \text{..... (6.27)}$$

where $k_1 = h \cdot f(X_n, Y_n)$

$k_2 = h \cdot f(X_n + h/2,\ Y_n + k_1/2)$

$k_3 = h \cdot f(X_n + h/2,\ Y_n + k_2/2)$

$k_4 = h \cdot f(X_n + h,\ Y_n + k_3)$

h is the increment of X between step n and step n+1.

We can consider this approximate value Y_{n+1} as a substitute of the exact value $Y(X_{n+1})$, ie.

$$Y(X_{n+1}) \simeq Y_{n+1},\ (n=0,\ 1,\ 2,\ \ldots)$$

By doing this, the error introduced is of the order of h^5 and is expressed as

$$\text{error} = O(h^5)$$

6.5.1.2. Simultaneous Differential Equations

Again, if solutions to a set of first order differential equations

$$\begin{cases} Y'(X) = f(X,Y,Z) \\ Z'(X) = g(X,Y,Z) \end{cases} \quad \text{..... (6.28)}$$

with $Y(Xo) = Yo$, and $Z(Xo) = Zo$

exit and are unique, the approximate values of $Y(X_{n+1})$ and $Z(X_{n+1})$ are given by

$$\begin{cases} Y_{n+1} = Y_n + [k_1 + 2(k_2+k_3) + k_4]/6 \\ Z_{n+1} = Z_n + [m_1 + 2(m_2+m_3) + m_4]/6 \end{cases} \quad \cdots\cdots\cdots\cdots \quad (6.29)$$

where $k_1 = h \cdot f(X_n, Y_n, Z_n)$

$m_1 = h \cdot g(X_n, Y_n, Z_n)$

$k_2 = h \cdot f(X_n + h/2, Y_n + k_1/2, Z_n + m_1/2)$

$m_2 = h \cdot g(X_n + h/2, Y_n + k_1/2, Z_n + m_1/2)$

$k_3 = h \cdot f(X_n + h/2, Y_n + k_2/2, Z_n + m_2/2)$

$m_3 = h \cdot g(X_n + h/2, Y_n + k_2/2, Z_n + m_2/2)$

$k_4 = h \cdot f(X_n + h, Y_n + k_3, Z_n + m_3)$

$m_4 = h \cdot g(X_n + h, Y_n + k_3, Z_n + m_3)$

with $n=0, 1, 2, \ldots$. The error resulted from the approximation is also $O(h^5)$.

6.5.2. Application to the Numerical Model

The differential equation given in (6.21) is of second order and nonlinear. It is obvious from its physical meaning that the solution to (6.21) exists and is unique. To apply the Runge-Kuta method, we first introduce a new function Z in such a way that the second order differential equation can be reduced to a first order equation.

Let $\dot{X}(t) = Z(t)$, then $\ddot{X}(t) = \dot{Z}(t)$. (6.21) becomes

$$\begin{cases} \dot{X}(t) = Z(t) \\ \dot{Z}(t) = \begin{cases} (F - f - Eo\dot{X})/M, & \dot{X}>0 \\ (F + f - Eo\dot{X})/M, & \dot{X}<0 \\ 0, & \dot{X}=0 \text{ and } |F|<f(0) \\ [F + f(0)\text{sign}(F)]/M, & \dot{X}=0 \text{ and } |F|\geq f(0) \end{cases} \end{cases} \quad \text{..... (6.30)}$$

and from (6.21a), the initial conditions are: $X(0) = Z(0) = 0$ ..... (6.30a)

Equations (6.30) and (6.30a) have the same form as those given in (6.28). Therefore, the approximate solutions in (6.29) can be directly applied to (6.30), if one keeps in mind that $f(t,X,Z)=Z$ and $g(t,X,Z)$ is a multi-function $\dot{Z}(t)$.

6.6. PROGRAMMING

The execution of numerical solution to (6.30) can only be accomplished by a computer due to the huge amount of calculation. Computer programs have been written for this purpose. Figure 6.4 and 6.5 are the flow charts of program MODEL1 for typical numerical solution and of program MODEL2 for sensitivity analysis of each parameter, respectively. Programs corresponding to these charts were written in FORTRAN language for running on the MTS computer system at the UBC computing center and are listed in appendices 1 and 2. Some variables used in these programs are specified in the following:

T_i is the instant time

X_i is the slip distance at T_i

$\dot{X}_i$ is the slip velocity at T_i

F_i is the driving force at T_i

F_{ti} is the total force at T_i

F_{fi} is the frictional force at T_i

T_1 is the time length of slip duration

T_2 is the stick time between two adjacent slips

X_1 is the maximum distance of a slip

Ep is the potential energy

Wr is the energy radiated

W_f is the energy consumed against friction

W1 is the total potential energy drop after a slip.

Program MODEL1 calculates the numerical solutions of X_i, $\dot{X}_i$, F_i, F_{ti} at time Ti according to Runge-Kuta method. Then it increases to Ti by Δt and calculates these solutions at $Ti+\Delta T$ and at $Ti+\Delta T/2$. If the difference between these solutions at $Ti+\Delta T$ and $Ti+\Delta T/2$ is more than the pre-specified accuracy ϵ, ΔT is further decreased. The above computing is repeated until the accuracy is satisfied. MODEL1 gives the printout of Xi, $\dot{X}_i$, Fi, F_{ti} at Ti during computation and prints X_1, T_1 and T_2 at the end of running. A typical printout is attached to appendix 1.

Program MODEL2 for sensitivity analysis does the work in the same way as MODEL1. However, it prints out Xi, $\dot{X}_i$, Fi, F_{fi} only at $T=0$, $\dot{X}=$maximum and $\dot{X}=0$ during running. At the end of running, it prints X_1, T_1, T_2 and energy parameters. By changing each of the controlling factors in the model, such as the static coefficient of friction μ_s, elastic modulus E, normal pressure P and driving speed V, and at the same time keeping others unchanged during running, we are able to obtain approximate values of X_1, T_1, T_2 and energy parameters under various conditions. A typical printout is attached to appendix 2.

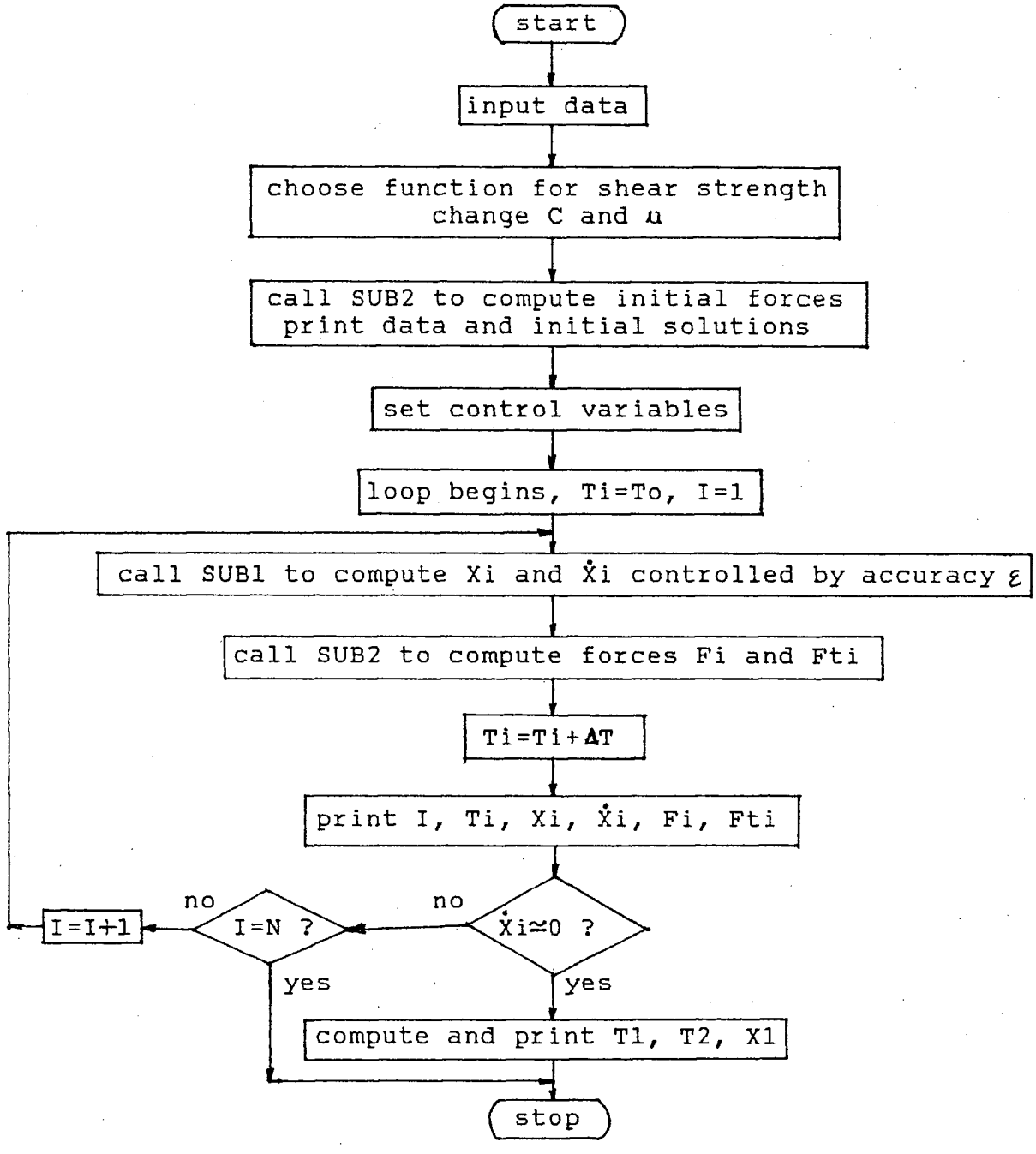

Fig.6.4 Flow chart for program MODEL1: numerical solution to the shearing model

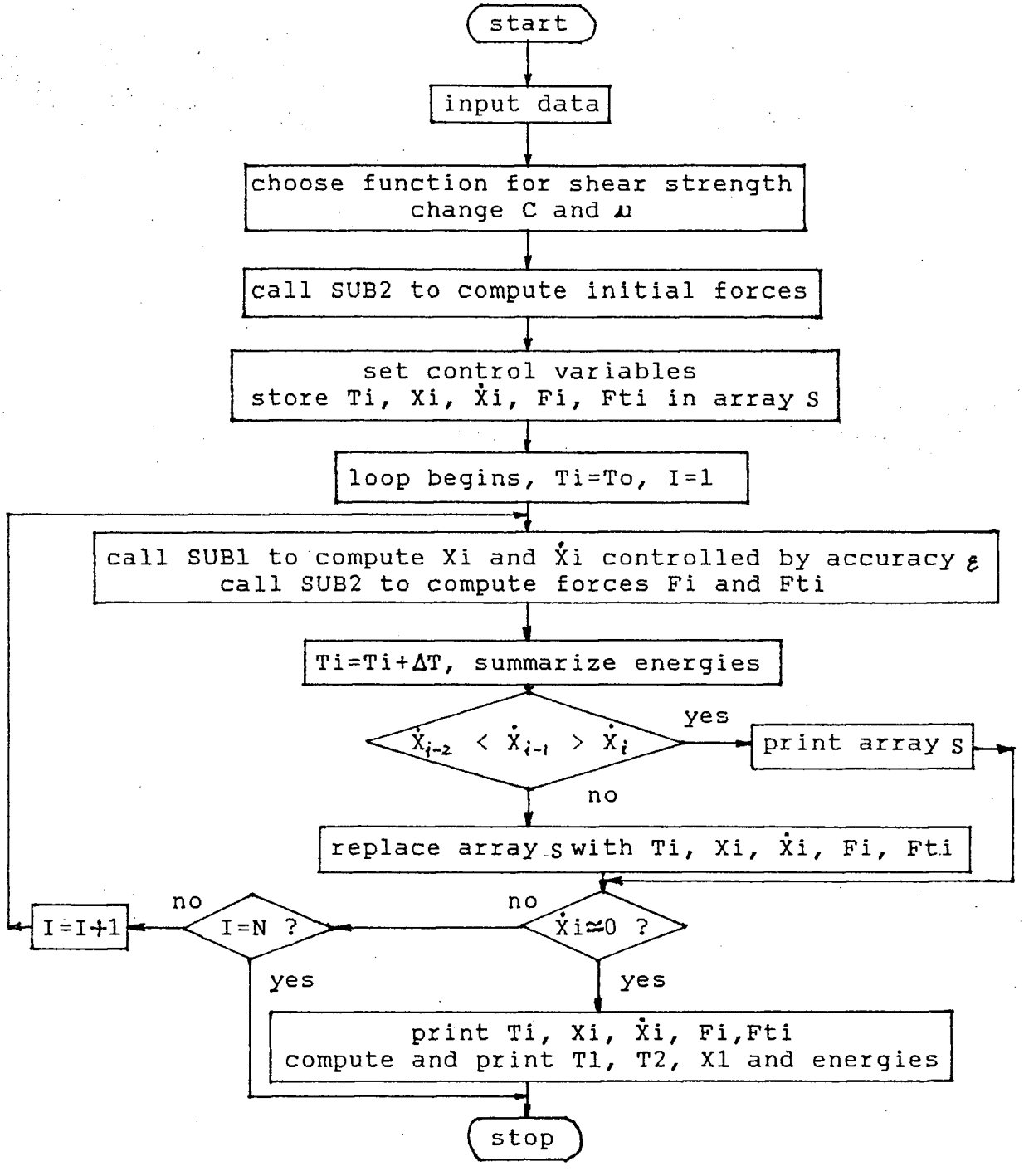

Fig.6.5 Flow chart for program MODEL2: sensitivity analysis

6.7. NUMERICAL RESULTS

By program MODEL2, the sensitivity of this shear model to each factor, such as C, μ_s, λ, P and V is extensively studied under a wide range of possible values listed in table 6.1. The slip behavior is represented by the following parameters:

$\dot{X}_{max}$ --- the maximum slip velocity during a slip

ΔF --- total force drop after a slip

ΔE --- total potential energy drop after a slip

Wr --- energy radiated during a slip

and T_1, X_1, T_2 as described in previous section.

6.7.1. Effects of Major Factors

The effect of each factor on the slip behavior of this shear model can be clearly seen when other factors are kept unchanged. This method of sensitivity analysis is an efficient way to examine how a factor in a system influences the behavior of the system. It is very useful when combined with a numerical method and when it is impossible both economically and technically to study a physical model. The effect of each factor is discussed below.

6.7.1.1. Effect of Cohesion

Cohesion is an inherent property of a rock mass. Its effect on the slip behavior is plotted in figure 6.6. As can be seen, within the range of C=0.1 Pa to 1 MPa, which covers most kinds of rocks, the cohesion has no influence on the slip behavior at all because the slip parameters do not change with it. In table 6.2, the data give some numerical concept of these changes. The last column indicates a value of 1.00 for the ratio of maximum/minimum of each parameter.

This is probably because that cohesion is constant before, during and after slip. Therefore its presence only increases the maximum shear stress required to initiate the slip.

6.7.1.2. Effect of Frictional Coefficient

The coefficient of friction is proportional to the shear strength of a material. This internal characteristic is significant before the initiation of slip. However its effect on the slip behavior after slippage is initiated seems less important. When μ_s increases from 0.35 to 0.95, only the total potential energy drop ΔE increases slightly, figures 6.7. At the same time, the slip time T_1 and the maximum slip velocity $\dot{X}_{max}$ fluctuate a bit. Other parameters, such as the maximum displacement X_1, stick time T_2, total force drop ΔF and energy radiated Wr, are hardly changed with μ_s. This little change of each parameter with μ_s is indicated by a value of near 1.0 in the last column of table 6.3. Generally, rougher surface has higher coefficient of friction. Therefore the slip behavior is hardly affected by the surface roughness within the analyzed range.

Table 6.2 effect of cohesion C on slip behavior

logC (Pa)	-1	0	1	2	3	4	5	6	max/min
T_1 (0.1ms)	.13405	"	"	"	"	"	"	.13405	1
X_1 (mm)	.19473	"	"	"	"	"	"	.19473	1
T_2 (ms)									
$\dot{X}$max(100m/s)	.22822	"	"	"	"	"	"	.22822	1
ΔF (100 MN)	.10710	"	"	"	"	"	"	.10710	1
ΔE (10 KJ)	.52859	"	"	"	"	"	"	.52859	1.037
Wr (J)	.40159	"	"	"	"	"	"	.40159	1

note: the symbol (") means having the same value as the data to the left of it

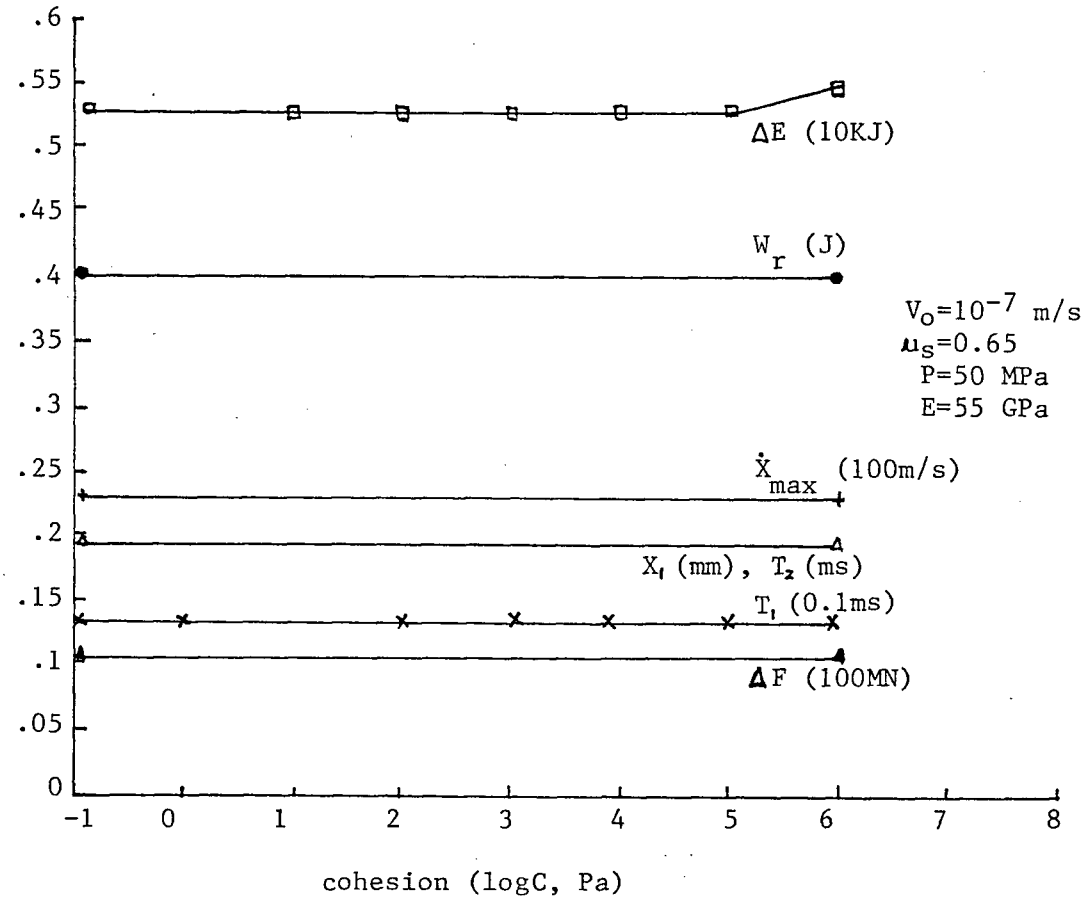

Fig.6.6 Variation in slip behavior parameters with cohesion

6.7.1.3. Effect of Elastic Modulus

The elasticity E of a material is represented by the stiffness, which is proportional to the elastic modulus, of the connecting spring in this shear model. It controls the rate of force transmission and energy buildup. The elastic modulus is constant for a given material but varies with different materials. The value of E ranges from 10 GPa to 100 GPa for various kinds of rocks. For some soft

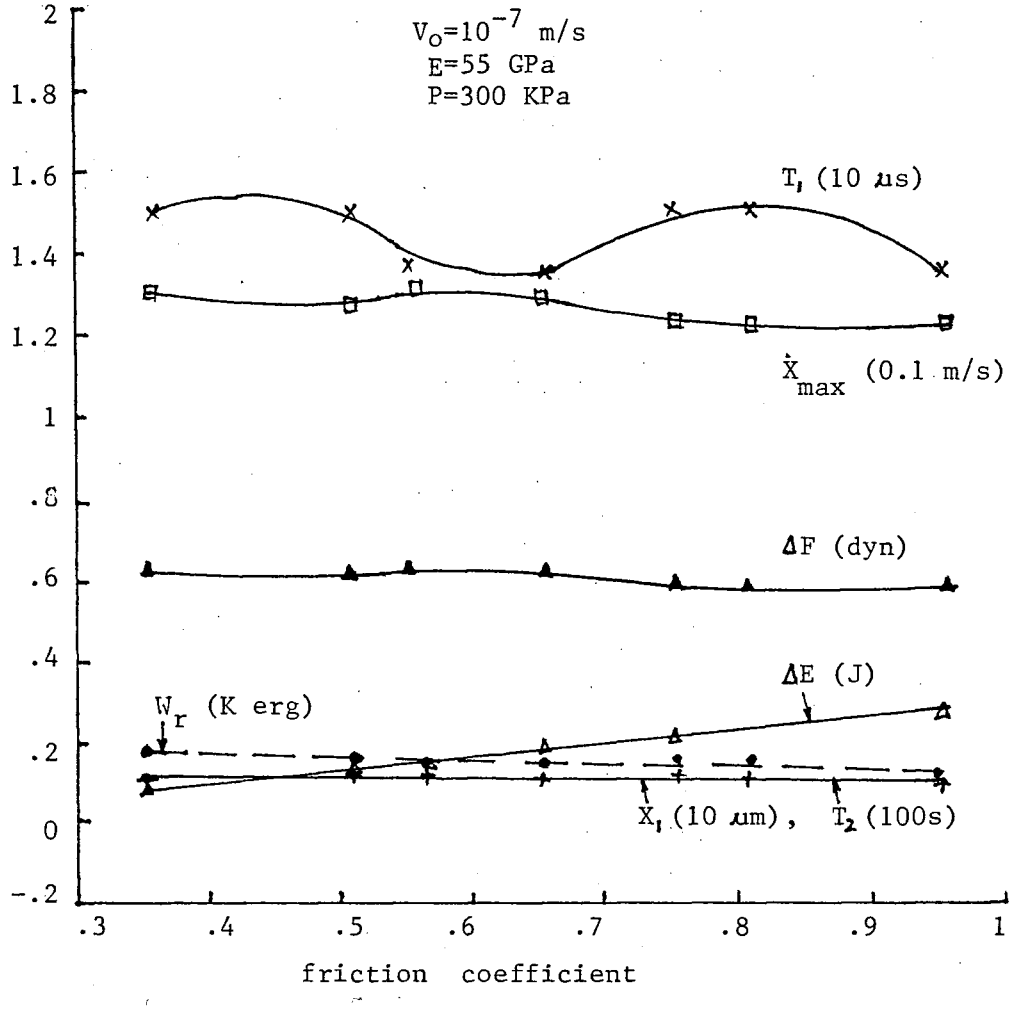

Fig.6.7 Variation in slip behavior parameters with friction coefficient

materials such as coal, this value is even smaller, less than 5 GPa. The effect of E on the slip behavior is significant. The general trend of each parameter is shown in figure 6.8. Except for the total force drop ΔF which is unchanged, all other parameters tend to decrease quickly as E goes up while $E \leq 20$ GPa.

The whole picture of slip behavior can be divided into two parts in this

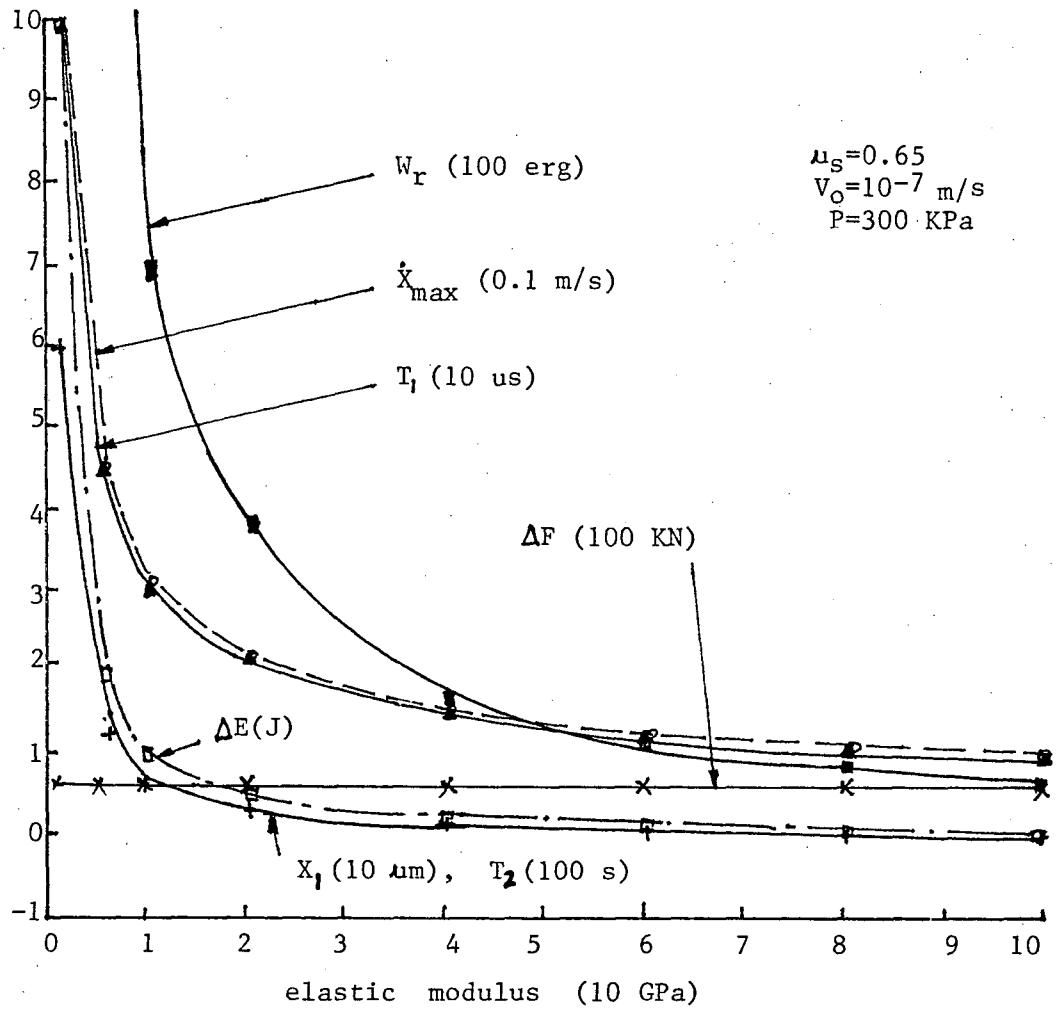

Fig.6.8 Variation in slip behavior parameters with elasticity

graph. In the first part, these parameters decrease as the elasticity increases. In the second part, the slip behavior changes little. For ΔE, X_1 and T_2, the curves can be divided at E=20 GPa, whereas for T_1, $\dot{X}_{max}$ and Wr, at E=40 GPa under the given conditions of modelling. The amplitude of the change varies from 10 to more than 100 as shown in the last column of table 6.4. The effects of the elastic modulus on the energy drop ΔE, the maximum slip distance

Table 6.3 effect of friction coefficient μ_s on slip behavior

μ_s	0.35	0.505	0.55	0.65	0.75	0.805	0.95	max/min
T_1(10μs)	1.4978	1.498	1.348	1.3423	1.4992	1.4994	1.3517	1.12
X_1(10μm)	.11297	.1107	.1143	.1108	.1071	.1063	.1059	1.08
T_2(100 s)								
$\dot{X}$max(0.1m/s)	1.3024	1.276	1.3383	1.298	1.235	1.225	1.2366	1.09
ΔF (dyn)	.6214	.60887	.629	.6095	.5891	.5846	.5824	1.08
ΔE (J)	.08353	.13402	.1527	.18225	.20939	.22557	.27089	3.24
Wr (K erg)	.16861	.16173	.13822	.12968	.15092	.14861	.11791	1.43

Table 6.4 effect of elastic modulus E on slip behavior

E (10 GPa)	0.1	0.5	1	2	4	6	8	10	max/min
T_1(10μs)	9.945	4.451	3.146	2.227	1.574	1.286	1.115	.9965	10
X_1(10μm)	6.193	1.226	.6112	.3038	.1514	.1006	.0752	.0601	103
T_2(100 s)									
$\dot{X}$max(0.1m/s)	9.785	4.33	3.055	2.145	1.512	1.231	1.062	.9507	10
ΔF (100 KN)	.6193	.6132	.6112	.6077	.6054	.6034	.6016	.6013	1
ΔE (J)	10.159	2.016	1.005	.5002	.2493	.1658	.124	.0992	102
Wr (100 erg)	75.63	15.326	6.885	3.762	1.689	1.183	.9208	.6379	118

X_1 and the stick time T_2 are most significant, next to the energy radiated Wr. In general, the value of E is above 40 GPa for most kinds of rocks. In this case, the elastic modulus seems not to affect the slip behavior very much.

6.7.1.4. Effect of Normal Load

The normal load is one of the parameters indicating the state of stress. In the field, it can be determined from the in situ stresses, mining conditions and the orientation of the failure surface. Therefore it varies with conditions. Any change of the above conditions would result in a change in the normal load. This

change could in turn change the slip behavior during shear process, in a way shown in figure 6.9. As can be seen, all parameters, except for the slip time T_1 which is not changed, increase with the increase of the normal load.

Note those graphs are plotted on logarithmic scale. To show a clear relation, empirical formulae of these changes for some typical parameters, ΔF and Wr, are obtained by linear regression based on the numerical data and are given in table 6.5. The force drop ΔF, stick time T_2, peak velocity and maximum slip distance X_1 change in a similar way and have a linear relation with the normal load P. The total energy release ΔE and seismic energy Wr are proportional with each other and increase with P^2. This means that the normal load P is one of the most significant factors in controlling the slip behavior.

6.7.1.5. Effect of Loading Speed

The loading speed V, or the driving speed in this model represents the rate of stress redistribution in the field. This rate can be ignored for virgin stress. When mining activity takes place, the virgin stress field is disturbed and stress changes significantly around the excavation. The maximum rate of stress change occurs right after mining activity. As time continues, this rate decreases and finally ceases. However, the exact process of stress change is not well known.

In this model, constant driving speed Vo was used for simplicity and the slip behavior within the range of $Vo=10^{-10}$ to 10^{-1} m/s is studied. From the numerical results in figure 6.10, it can be seen that only the stick time T_2 is affected by the change of Vo, with

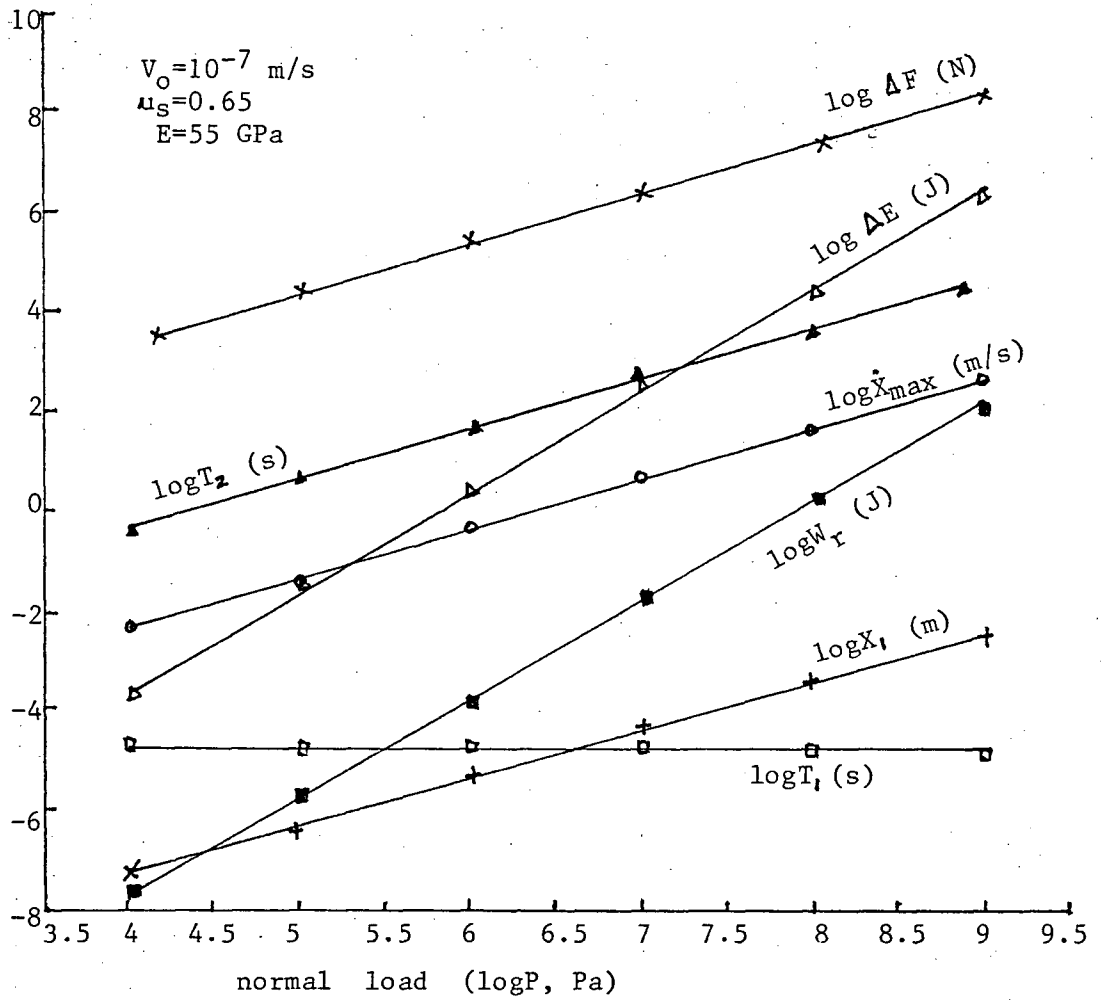

Fig.6.9 Variation in slip behavior parameters with normal load

$T_{2max}/T_{2min}=10^8$, table 6.6. They have a reverse relationship, which can be represented by $T_2=c/Vo$, where c is a constant. All other parameters do not change with Vo if Vo is less than some value. This critical value varies with loading conditions and rock properties and will be discussed in detail in the chapter of transition analysis.

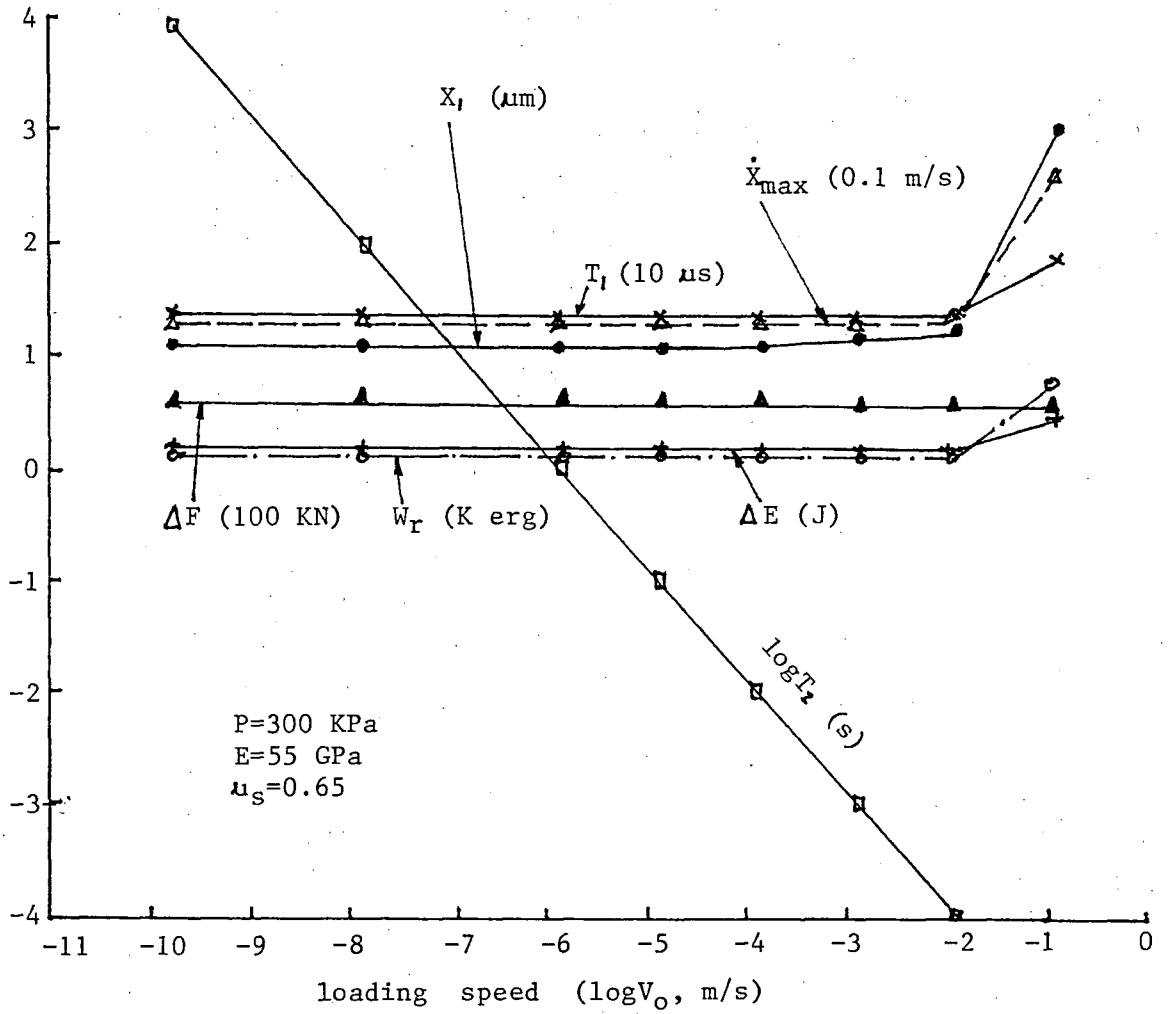

Fig.6.10 Change of slip behavior parameters with loading speed

6.7.2. The Variation of Slip Behavior

The characteristics of the slip behavior, described by parameters: T_1, X_1, $\dot{X}_{max}$, T_2, ΔF, ΔE and Wr, have been explained previously. Among these parameters, the slip time T_1 which is extremely small, in the order of millisecond to microsecond, and the maximum slip velocity $\dot{X}_{max}$ seem to be not significant to the slip behavior and will not be discussed in the following.

Table 6.5 effect of normal load P on slip behavior

logP (Pa)	4	5	6	7	8	9	lg^{-1}max/	lg^{-1}min
$logT_1$ (s)	-4.829	-4.871	-4.873	-4.873	-4.8729	-4.871	1.107	
$logX_1$ (m)	-7.469	-6.44	-5.426	-4.415	-3.4074	-2.4014	1.1684	$\times 10^5$
logẊmax(m/s)	-2.416	-1.372	- .3566	.654	1.6615	2.6676	1.2123	$\times 10^5$
$logT_2$ (s)	- .4692	.5597	1.5745	2.5849	3.5926	4.5986	1.169	$\times 10^5$
logΔF (N)	3.271	4.2999	5.315	6.325	7.333	8.337	1.164	$\times 10^5$
logΔE (J)	-3.7232	-1.6999	.31216	2.3206	4.3269	6.3317	1.135	$\times 10^{10}$
logWr (J)	-7.8374	-5.8664	-3.8273	-1.8056	.21015	2.2223	1.147	$\times 10^{10}$

Empirical formulae for ΔF and Wr

ΔF:	$\log\Delta F = -0.65698 + 0.99673 \log P$, or $\Delta F = C_1 P$ $r = 0.99978$, Sd_{n-1}: $P \pm 2.45$, $\Delta F \pm 2.44$
Wr:	$\log Wr = -15.27 + 1.93 \log P$, or $Wr = C_2 P^2$ $r = 0.99899$, Sd_{n-1}: $P \pm 2.45$, $Wr \pm 4.72$

Table 6.6 effect of loading speed on slip behavior

logVo (m/s)	-10	-8	-6	-5	-4	-3	-2	-1*	max/min
T_1 (10μs)	1.3423	1.3423	1.3423	1.3424	1.343	1.3489	1.4077	1.8917	1.049
X_1 (10μm)	1.108	1.108	1.108	1.1082	1.1094	1.218	1.2511	3.0254	1.129
Ẋmax(0.1m/s)	1.2984	1.2985	1.2985	1.2986	1.2997	1.309	1.4052	2.6648	1.082
$logT_2$ (s)	4.0446	2.0446	.0446	-.9554	-1.955	-2.955	-3.955	-4.955	10^{8}**
ΔF (100 KN)	.60941	.60941	.60941	.60941	.60941	.6096	.6108	.6236	1.002
ΔE (J)	.18225	.18225	.18225	.18227	.18247	.18449	.20563	.50859	1.128
Wr (K erg)	.12968	.12968	.12968	.12970	.12994	.13230	.15742	.84933	1.214

*note: the last column logVo = −1 is not included in computing the ratio max/min for the reason that Vo exceeds the critical value, see chapter 7 for detail.
**: this value is from lg^{-1}max/lg^{-1}min.

6.7.2.1. Maximum Slip Distance

The maximum slip distance X_1 is a measurement of the extent of damage caused by shear failure. The farther the slippage is, the bigger the damage could be. For a given amount of energy released, shorter slip distance means larger energy release rate, then more violence at failure. From the numerical results shown in figures 6.6 through 6.10, the slip distance seems to vary only with the normal load and the elasticity of the material. It has a linear relationship with the former and is approximately in reverse proportion to the latter. When the elasticity is above 20 GPa, or for hard rock, X_1 tends to be constant.

6.7.2.2. Stick Time

The parameter T_2, which is the peace time between two consecutive slips, is a measurement of the slip frequency. For a given condition and given time, shorter peace time means more slips, and then higher slip frequency.

From the numerical results, T_2 seems to be strictly controlled by the loading conditions. It is very sensitive to the change of loading speed and normal load. It has a linear relation to the normal load and a reverse relation to the loading speed. This means that, if other conditions are unchanged, with the decrease of the loading speed, the stick time increases and slip frequency decreases.

As we know, each slip releases some amount of energy, part of which is radiated out as seismic energy, which is called acoustic energy because of its small scale. Therefore, high slip frequency at high driving speed will certainly generate more acoustic activity. This is in perfect agreement with the field

observations, where the rate of rock noise is found to increase sharply right after the mining activity, such as blasting, because of the high rate of stress change. As time continues, the stress changes slowly to reach a new state of equilibrium. The rock noise decreases and eventually dies out. However, low slip frequency does not necessarily mean less acoustic activity, because the source of acoustic emission is not from a single fracture but from many local micro-fractures as observed in laboratory tests, chapter 10.

The change of the normal load on a surface in the rock mass is very complicated during the period of stress redistribution. It may increase in the stress concentration zone and decrease in the relaxing zone. By the linear relationship between T_2 and P, figure 6.9, if the loading speed is the same, lower normal pressure means higher slip frequency because of lower shear strength which requires less time for the shearing force to build up.

The effect of elasticity on the stick time T_2 is impressive, figure 6.8. When the elastic modulus E is below some value, T_2 decreases as the increase of E. When E is above this value, T_2 remains at a low level. In general, hard rock has higher elasticity. This may imply that if all other conditions are the same, the slip frequency is higher for hard rock and probably more acoustic activity too than for soft rock.

6.7.2.3. Force Drop

The force drop ΔF after a slip is a measurement of the change of slip potential and seems to be mainly affected by the normal load. They have a linear relationship, figure 6.9. Obviously, higher normal load requires higher shear force to initiate the slip. Therefore, this could mean that if the driving speed is the same, the time required for the shear force to reach the strength is longer at high normal load than at low normal load, just as indicated by T_2.

6.7.2.4. Energy Release

The energy release is a very important parameter, The more energy is released, the bigger the failure and the damage could be. By equation (6.24a), during each slip, the total energy released is approximately the sum of the energy consumed against friction and the energy radiated, if the small amount of work done by the external force is ignored. In the field monitoring of rockburst, the total energy release and the energy consumed against friction are unknown and it is not possible to estimate them. Only a small portion of total energy released is monitored as seismic energy. Whether the seismic energy Wr can be used to represent the total energy release ΔE depends on the way they change which is not clear.

According to the numerical results, as any of the cohesion, elasticity, normal load or driving speed changes, ΔE and Wr change in the same way, figures 6.6 and 6.8 to 6.10. A slight difference in the way they change occurs as the friction coefficient varies, figure 6.7. In this case, the seismic energy Wr remains nearly the same, whereas the total energy release increases slightly as

the increase of μ_s. However this difference is relatively small. Therefore the seismic energy Wr may represent the total energy release. This will be shown in the energy results generated from an acoustic simulating model in chapter 12.

In figures 6.6 to 6.10, the normal load and elasticity have significant effects on the energy release, whereas other factors have little effect on it. Wr varies proportionally with P^2 and nearly reversely with the elasticity. Apparently, a high normal load represents a high stress field, which causes large amount of energy to be stored in the rock structures. Consequently more energy would be released at failure. When the elastic modulus is low, Wr decreases dramatically with the increase of E. When E is above some value, the change of Wr is very small. This may indicate that the energy released in each slip is nearly the same from hard rocks and is less than from soft rocks. It should be noted that the total amount of energy released in a given period is not necessarily less in hard rock than in soft rock because the slip frequency is higher in hard rock.

6.7.2.5. Average Energy Release Rate and Energy Release Ratio

The total energy release can indicate the possible extent of failure and the damage caused by the failure, whereas the rate of energy release may show the violence of failure. Obviously, for a given time period, the more energy is released, the more violent the failure could be. In practice, it is impossible to estimate the energy released. However, from the above discussion, the seismic energy seems to represent the total energy release quite well. Therefore the rate of seismic energy radiation can be used to estimate the violence of failure.

The instantaneous seismic energy rate is defined in equation (6.25) as

$$\dot{W}r = Eo\dot{X}^2.$$

There will be some difficulty in determining $\dot{W}r$ in practice. Usually, the average rate over a period can be used instead. For a given period Δt, if there are N slips, each of which has released energy W_{ri}, the total energy released in that period will be

$$W_{tr} = \sum_{i=1}^{N} W_{ri} \quad \text{..... (6.31)}$$

Then the average rate of energy release can be estimated as

$$\dot{W}_{avg} = W_{tr}/\Delta t = (1/\Delta t)\sum_{i=1}^{N} W_{ri} \quad \text{..... (6.32)}$$

As can be seen from above numerical results, the slip time T_1 usually is much shorter than the stick time T_2. If T_2 is extremely high compared with T_1, the average energy rate cannot indicate the real rate of energy release well. A better way to do this is to look at the energy during the slip time only. Therefore, the average energy released per event, also called energy release ratio, can be used as an alternative, which can be estimated as

$$W_{avg} = W_{tr}/N = \frac{1}{N}\sum_{i=1}^{N} W_{ri} \quad \text{..... (6.33)}$$

Therefore both $\dot{W}_{avg}$ and W_{avg} should be used together in practice in order to estimate the rate of energy release with a higher confidence.

6.8. SUMMARY

1. In order to take into account all possible conditions in field during analysis of shear behavior, several important parameters of rock properties, such as cohesion, coefficient of friction, elastic modulus and uniaxial compressive

strength, are compiled from the previous publications.

2. The previous model has been completed by introducing slip-velocity dependent friction and seismic effect.
3. The seismic effect is considered by attaching a semi-infinite string to the model and the derived force from seismic radiation is proportional to the slip velocity but pointing to the opposite direction.
4. The energy changes during a slip is calculated.
5. To analyze the sophisticated model, a numerical method, Runge-Kuta Approach is used and computer programs are written specifically for this purpose. By these programs, the sensitivity of this shear model to the environments is extensively analyzed.
6. According to the numerical results, the cohesion C has no effect on the slip behavior, the effect of frictional coefficient μ_s is negligible, the effect of normal load P is most significant, the elastic modulus E and the driving speed Vo rank in between.
7. During each slip, the maximum slip distance X_1 has a linear relation with the normal load, an approximate reverse relation with the elasticity, and does not change with other factors. The stick time T_2, which indicates the frequency of slippage changes linearly with normal load, reversely with the driving speed and elasticity, and is independent from cohesion and frictional coefficient. The total force drop only increases as the increase of the normal load. The seismic energy, which has similar pattern as the total energy release, increases with the square of the normal pressure and reversely with the elasticity.

In summary, this model is useful in studying the slip behaviour of stick-slip under various practical conditions and consequently provides us with a tool to find the conditions which may give rise to violent failure.

CHAPTER 7. TRANSITION CONDITIONS AND VIOLENT FAILURE

7.1. GENERAL

In study of violent rock failure, one of major interests, which is the first objective of this research, is to find the conditions which may give rise to violence. These conditions are associated with stick-slip and the transition between stick-slip and stable sliding. From previous discussion, it is now possible to derive the conditions which cause stick-slip by examining the stick time T_2, which is defined as the time between adjacent slips and indicates the frequency of slippage. Obviously, the smaller T_2 is, the more slips for a given time period. When $T_2 = 0$, the slip number may become infinite. In this case, it does not make much sense to measure the slip behavior by slip number, because the peace period between adjacent slips actually does not exist. The nature of slip has been changed and stable sliding occurs.

7.2. TRANSITION CONDITIONS

From previous chapter, it is known that the stick time T_2 is strictly controlled by the loading conditions. It is very sensitive to the change of loading speed and normal load. The elasticity of rock has a close relation to T_2 as well. The other indices of rock property seem not to have much effect on it, figures 6.6 through 6.10.

Any change of the factors mentioned above will introduce some change to T_2. The condition under which T_2 becomes zero is critical for the transition from stick-slip to stable sliding and vice versa. Because the stick time is affected

by more than one factor, this critical condition is not unique and varies with any of the influencing factors, such as the loading speed V, normal load P, or the elastic modulus E.

To study the possible transition conditions, a computer program called MODEL3, appendix 3, has been written in FORTRAN language for this purpose. Figure 7.1 shows the program flow chart. In this numerical model, the stable sliding is considered to occur when $T_2 < 1\times10^{-5}$ seconds instead of zero, because of the approximation of the numerical solution and the computing cost. During the analysis, only the major influencing factors were included. The principle followed in this modelling is that for any group of data consisting of elastic modulus E, frictional coefficient μ_s and normal load P, the value of T_2 is calculated using a given initial loading speed Vo. If T_2 is too big, Vo is increased and T_2 is calculated again until $T_2 < 1\times10^{-5}$ seconds. If the solution does not converge or the slip velocity $\dot{X}$ never decreases to zero (this value is actually set to 1×10^{-13} m/s in the program instead of zero), Vo is decreased and computation is repeated again. Finally a critical loading speed Voc is obtained corresponding to $T_2 \simeq 0$ for the given condition.

Then one of the factors E, μ_s or P is changed and following the same sequence another Voc is obtained. This process continues until all possible conditions are analyzed. During this analysis, the elastic modulus E is considered in the range between 1 GPa and 100 GPa, the normal load P in the range between 10 Pa and 10^9 Pa, the static coeffecient of friction μ_s in the range between 0.1 and 0.95.

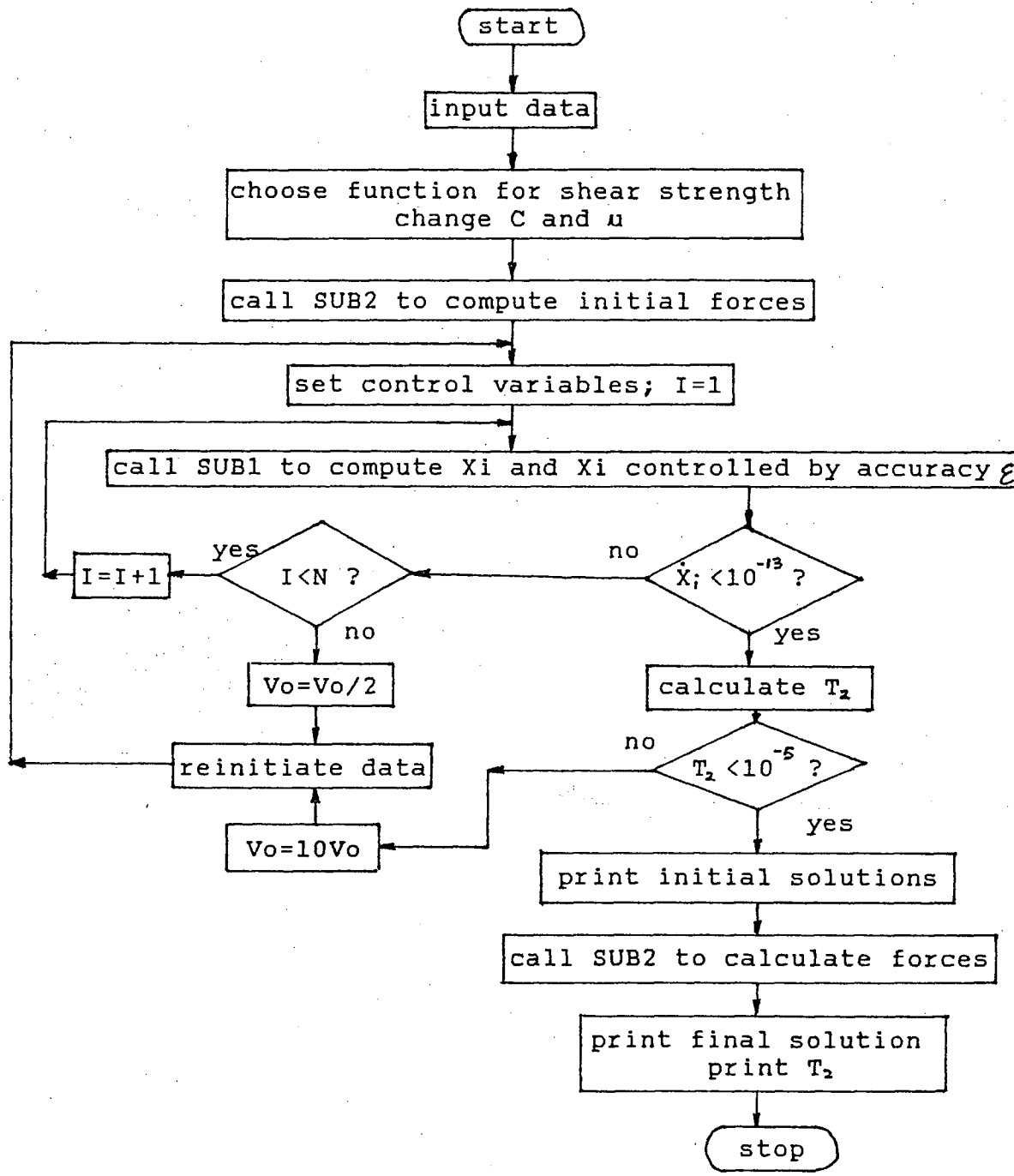

Fig.7.1 Flow chart for program MODEL3: transition analysis

The numerical results from program MODEL3 are given in figure 7.2. It is surprising to note that the frictional coefficient of a shear surface has little effect on the transition condition. This is probably because the effect of surface roughness on the stick time is negligible when compared with the effects from other factors. The effect of surface roughness on stick-slip observed in laboratory may be due to the asperity or unevenness of the surface.

As expected, the loading speed V, the normal load P and the elasticity E have significant effects on the transition. As can be seen from figure 7.2, for a given value of E, the loading speed V and the normal load P have a close linear relationship. In order to give a clear idea, an empirical formula is obtained for this relation by linear regression based on the numerical data.

$$Voc = kP \quad \text{..... (7.1)}$$

with correlation coefficient $r \geq 0.998$ and a constant k:

$k = 4.267 \times 10^{-5}$, when E = 1 GPa,

$k = 0.843 \times 10^{-5}$, when E = 5 GPa,

$k = 0.100 \times 10^{-5}$, when E = 40 ~ 100 GPa.

The upper part in figure 7.2 represents the stable sliding and the lower part the stick-slip. If the conditions of loading speed and normal load fall within the lower part, the slip behavior will show stick-slip, otherwise stable sliding. The maximum value of Vo or the minimum value of P for stick-slip to occur can be read off on this transition chart. For instance, if the elasticity of the material is of E = 10 GPa, under a normal load $P = 10^6$ Pa, the critical loading speed is found from point A in figure 7.2 to be logVoc = 0.78. This means that stick-slip

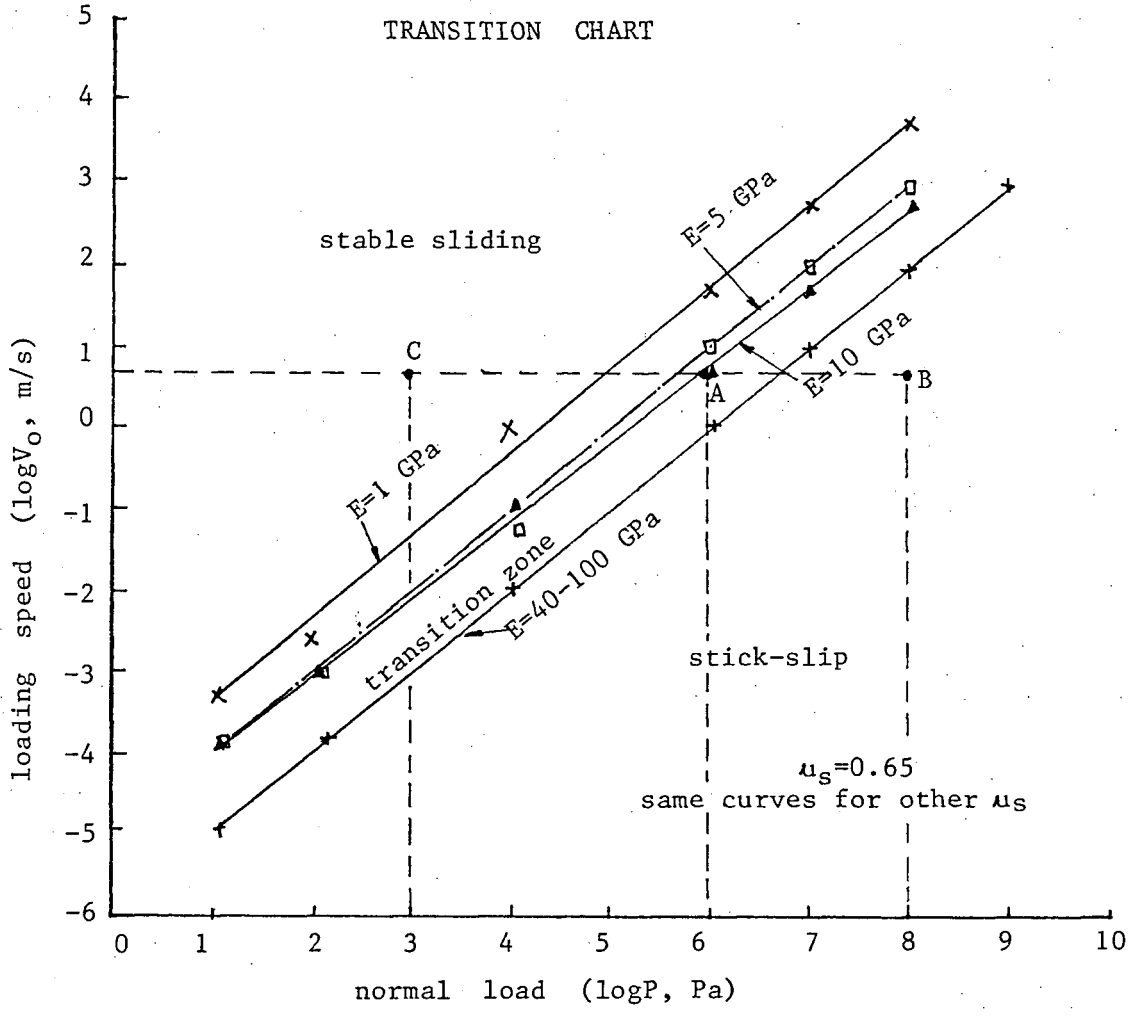

Fig.7.2 Transition conditions for stick-slip and stable sliding

can only happen if $\log V_o \leq 0.78$, or $V_o \leq 6$ m/s. Otherwise, stable sliding would appear.

It should be pointed out that the slip behavior determined from figure 7.2 applies only after slippage is initiated. Before the initiation of slip, the stability of the shear system is still controlled by the shear stress and shear strength.

Besides, this chart is obtained based on general analysis. Therefore it can be used only as a guide line in practice and would apply for a particular case only if it has been calibrated correspondingly.

It is interesting to notice the effect of the elasticity. For a low value of E, say $E \leq 40$ GPa, this effect is apparent and a transition zone is formed in figure 7.2. When E is above 40 GPa, this effect disappears and only a transition line exists. This effect is actually clear in figure 6.8, where E has little effect on T_2 when $E \geq 40$ GPa. In order to show this effect of E more clearly, the data in figure 7.2 is replotted in another way, figure 7.3, where there is no change in the V-E curves when $E \geq 40$ GPa.

7.3. SLIP BEHAVIOR IN SHEAR TEST

Slip behavior in shear tests generally falls into two categories: stable sliding and stick-slip. The characteristic of sliding depends in a complex way on many factors [29], the most important of which are the normal pressure, stiffness of the testing machine and loading speed. The conditions under which stick-slip will occur are complex and are derived in previous section. These conditions are combinations of above factors.

The modelling results given in figure 7.2 show very well the phenomena observed in laboratory tests. In experiment the stick-slip is generally enhanced by higher normal pressure [29], lower surface roughness and lower stiffness of the testing machine [39]. The effect of normal pressure is confirmed in figure 7.2. For instance, at points B and C, the slip behavior is different at two levels of

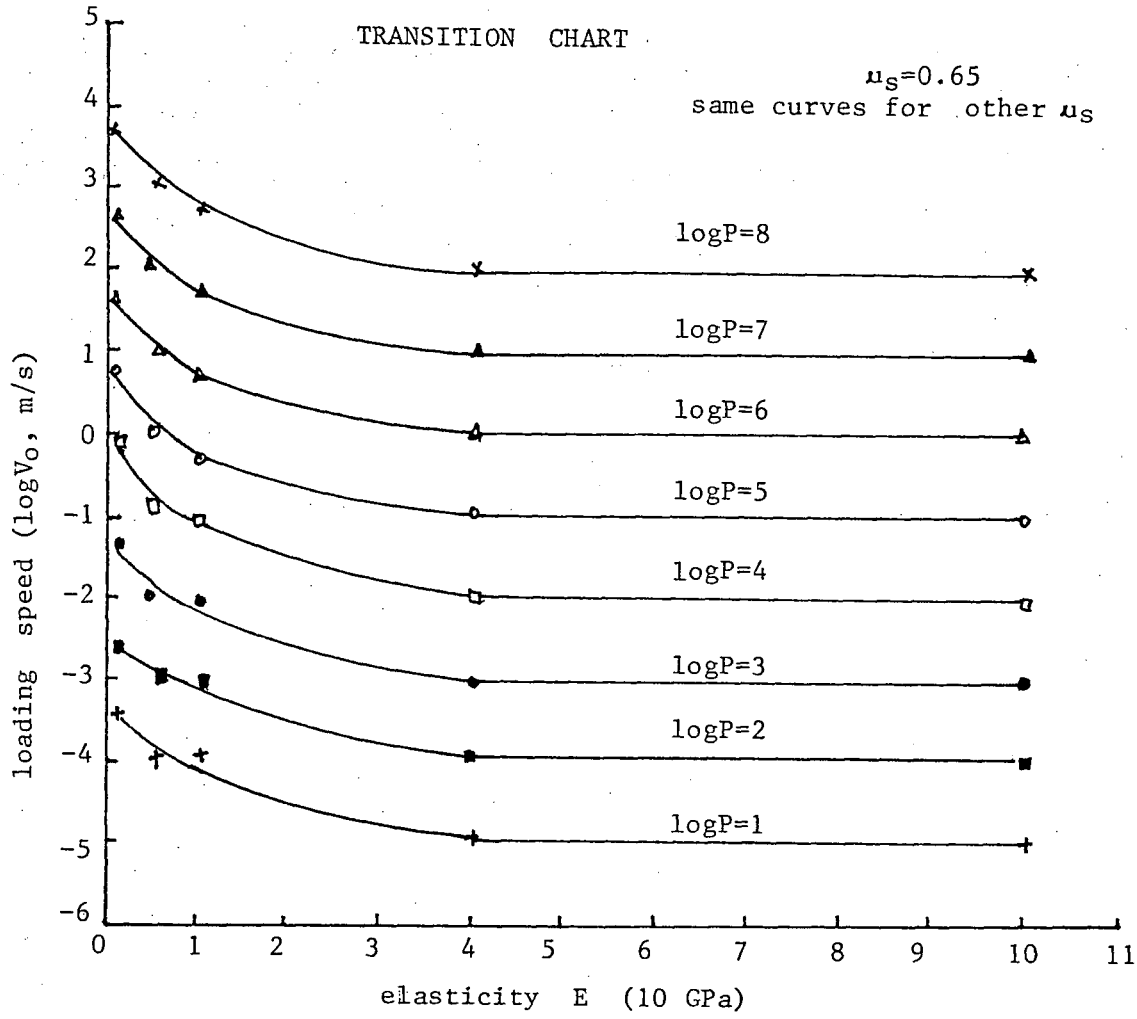

Fig.7.3 Transition conditions showed as loading speed against elasticity

normal pressure when other conditions unchanged. At point B of high normal load, stick-slip occurs. On the contrary, stable sliding takes place at point C of lower normal load.

The fact that lower machine stiffness will enhance the stick-slip can be verified. For a given loading condition and rock specimen, which correspond to a

position in the transition chart, say point A in figure 7.2, if the testing machine is "soft" with stiffness of 1 GPa, apparently point A falls into the lower part of the transition chart. Then stick-slip occurs. On the contrary, if the stiffness is very high, say 50 GPa, point A jumps into the upper part. Therefore stable sliding would happen. However, the effect of stiffness disappears when E is above 40 GPa until 100 GPa, the possible maximum value of elasticity for rock.

The effect of the surface roughness cannot be verified here because no change is found in this model when μ_s varies, as indicated in figure 7.2. This is probably because of the following reasons:

1. The effect of surface roughness is very small within the modelled range when compared with the effects of the normal pressure and the machine stiffness. Therefore, it may be shadowed by the latter.
2. The approximation in the numerical solution may bury this small effect.
3. This effect observed in experiments may be actually from the asperity and unevenness of the surface.

In addition, significant effects from loading speed are observed in this research. As shown in figure 7.2, for a given normal load, the slip behavior will eventually become stable sliding if the loading speed continues to increase. In other words, stick-slip can always occur if the loading speed is sufficiently low.

It is further noticed that the numerical results in figure 7.2 are in conflict with the conclusion by Engelder and Scholz(1976) [46] that the time-dependent stick-slip occurs only if the normal load is sufficiently large to

cause cracking during static contact and that the normal stress at the stable sliding to stick-slip transition corresponds to the minimum normal stress to cause asperity indentation and ploughing. However, these results agree well with Dieterich's (1978) [39] conclusion that the stick-slip can occur at any normal pressure if both the loading speed and the stiffness are sufficiently low. In other words, as long as the combination of the loading conditions and the specimen properties falls in the lower part of figure 7.2, stick-slip is always possible.

7.4. OCCURRENCE OF VIOLENT FAILURE

Violent rock failure occurring either in a massive rock or along a fault is closely related to the energy release at failure and can be associated with stick-slip because even in a massive rock, as discussed before, the fracture development will eventually lead to the formation of a macro-fracture surface on which final failure takes place. Therefore the slip behavior on a surface may be a key to violent failure.

As slip takes place, whether stable sliding or stick-slip will occur can be determined from a chart like figure 7.2. For stable sliding, because the shear stress remains more or less the same as slip continues, figures 4.5 and 5.2, there is no extra energy accumulated during the sliding process. The slip speed is controlled by the loading speed. Therefore, violent failure is not possible unless the loading condition is changed.

For stick-slip, the situation is completely different. The energy accumulated during the quiet period is released at slip. A sudden slip or any change of the

loading conditions can cause violent failure. According to the physical conditions of the shear process and the transition chart, violent failure is expected to occur in the following 3 cases:

Mode I. The violence is from a sudden slip under high normal pressure. The more energy that is released at each slip, the bigger the failure and the damage could be. This energy released increases with the square of normal load P as P increases, figure 6.9. It is also noticed that the higher the rate of energy release, the more violent the failure is. When the loading speed increases, the stick time decreases, or the slip frequency increases, figure 6.10. Then more energy is released during a given time period. By equation (6.32), the average rate of energy release increases correspondingly. Therefore the increase of both the normal load and the loading speed could increase the energy release and release rate and consequently increase the incidence of violent failure. When both the normal load P and the loading speed V are low, the failure may be not violent at stick-slip.

The mode I violence has been used by seismologists to interpret the shallow earthquakes along a natural fault [11]. These quakes are considered to be due to sudden slips in the crust. Because the interior stress field in the earth intends to initiate relative movement in the crust, the strain energy gradually builds up, which may be a result of many decades or even centuries of movement along a fault. When this energy can no longer be held in the crust, it is released by a sudden slip.

Mode II. The violence comes from the transition from stick-slip to stable sliding. For a given situation of stick-slip, if a change of any factor results in a transition suddenly from stick-slip to stable sliding, extra energy will be released. This energy has to be released at the transition point in order to keep up with the sudden change of conditions, consequently resulting in violent failure. This case could happen, as shown in figure 7.2, when either the normal pressure suddenly drops which means the sudden reduction of shear resistance, or the loading speed goes up abruptly. Typical examples will be given in chapter 10, figures 10.6 to 10.17, where this transition effect was observed during the acoustic emission tests of shear experiment and a bang similar to that from a uniaxial compressive test was experienced when the normal pressure was reduced suddenly to zero at the initiation of slippage. The corresponding acoustic emission peaks up sharply at this transition.

In the field of mining, excavation may cause stress increase in some part and stress decrease in other part of the rock mass. If a major discontinuity exists in the vicinity, the mode II violence may occur as a result of this transition. This will be discussed more in chapter 9.

Mode III. The violence occurs under sudden loading. No matter whether the slip behavior is stable sliding or stick-slip, violent failure is bound to happen if a shear force much higher than the shear strength is suddenly applied to the system. Because extra potential energy is always available in this case. Obviously, the higher the extra shear force, the more violent the failure. The example mentioned above of quick reduction of normal pressure at the initiation

of slippage can be considered as a kind of indirect sudden loading. Another example would be the violent failure of rock specimen in uniaxial compression. More about this will be given in next chapter.

It should be noticed that if the shear stress starts from zero, which is usually the case in experiments and in practice, failure happens only when the shear stress has reached or exceeded the shear strength. Under this condition, there are only two possible modes of violence, namely Modes I and II. Mode III only occurs under special conditions, which do exist in mining. A sudden excavation such as blasting can create this kind of situation, especially when the stress state on a fault or a joint plane in the vicinity of excavation changes abruptly.

7.5. SUMMARY

1. Based on the numerical model, the transition conditions between stick-slip and stable sliding are studied by examining the case of zero stick time under a variety of conditions and a transition chart is obtained.
2. Significant effects on the transition are found from the loading speed, normal pressure and elastic modulus of the rock, but little from the coefficient of friction. The condition for stick-slip varies with above factors.
3. From the transition chart and physical conditions, three modes of violence can be defined: Mode I is from the sudden slip under high normal pressure, Mode II comes from the transition from stick-slip to stable sliding and Mode III occurs under sudden loading.
4. According to these modes, the violent failure of rock both in laboratory

tests and in the field can be adequately interpreted regardless of the location and rock type.

CHAPTER 8. EFFECT OF SUDDEN LOADING

8.1. GENERAL

In studying the conditions which may give rise to violent failure, one of the three modes of violence defined in the previous chapter is exclusively from the effect of sudden loading. This effect is examined in detail in this chapter. The term "sudden loading" here refers to the case where a shear force is increased from zero to its maximum value in an extremely short time or this force is applied instantly and the case where a shear force which is much higher than the strength is available. In the following, the effect of sudden loading on the slip behavior is discussed in detail.

In laboratory tests, the shear force is usually applied from zero to the maximum value and can never exceed the shear strength much when sliding is initiated. However, in mining, it may happen that a force is applied very fast, such as at the stress adjustment near an opening right after blasting, and that the shear force is much higher than the strength at the sliding initiation, such as at the stress change on a geological fault due to mining, or at the failure of a rock specimen in compression. In these cases, the effect of a shear force is more than from the static loading and dynamic effect appears. This effect may cause a change of the slip behavior.

8.2. THE EFFECT OF EXCESSIVE LOAD

Suppose the shear strength of a system is f(0). The minimum shear force required to initiate the slip would be $Fo=f(0)$. If the shear force $F \leq Fo=f(0)$, the slip behavior will be the same as discussed previously. If $Fo/f(0) \geq 1$, the slip behavior can be analyzed using the numerical model.

During the numerical analysis, the effects of various ratios of Fo/f(0) were tested using the computer program MODEL2. By changing the initial shear force Fo into various values for a given f(0) during different runs, we can look at the change of all slip parameters. The ratio of Fo/f(0) was set to 1 to 11 respectively. The final results of all slip parameters, such as stick time T_2, seismic energy Wr, etc. are plotted in figure 8.1. The effect of this ratio on each parameter can be clearly seen.

It is interesting to notice that the slip time T_1 does not change with the ratio of Fo/f(0) at all. All other parameters are very sensitive to this ratio and most of them have linear relations with Fo/f(0), whereas the seismic energy release varies approximately with $[Fo/f(0)]^2$. By nonlinear regression of the numerical data, an empirical formula for Wr is derived:

$$Wr \simeq -0.150 + 0.046[Fo/f(0)]^2 \quad \text{..... (8.1)}$$

with correlation coefficient $r = 0.999$, and

standard deviation Sd_{n-1}: $Fo/f(0) \pm 6.73$, $Wr \pm 2.08$.

It is expected that the energy release and the maximum slip distance would increase when the ratio Fo/f(0) goes up. But the speed of increase for

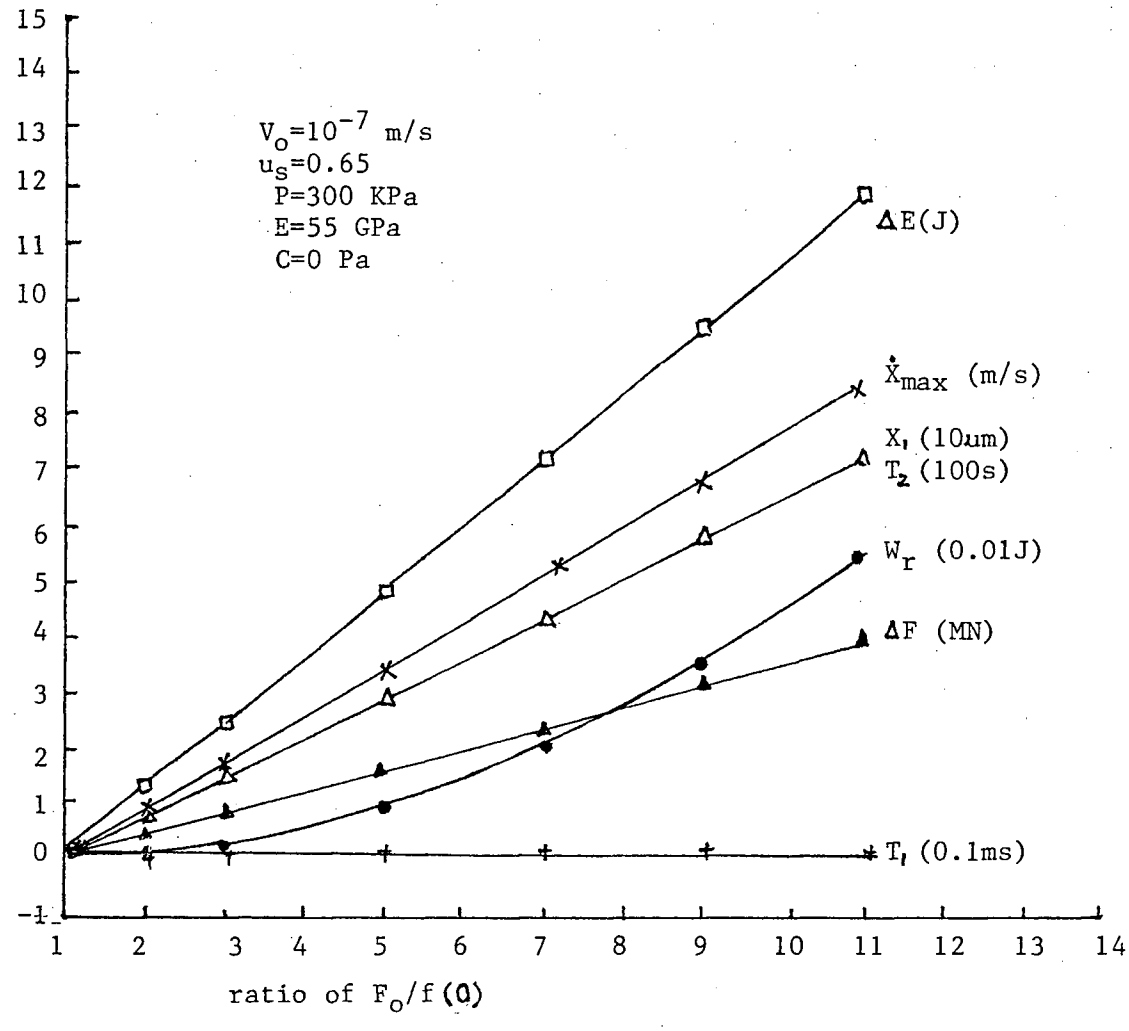

Fig.8.1 Variation of slip parameters with the ratio of initial shear force over the shear strength

each parameter is different. This speed is indicated by the slope of the corresponding curve. The steeper the slope of the curve, the higher the speed. The seismic energy increases with an increasing speed, figure 8.1. The data in the right hand column of table 8.1 shows the actual slope of each parameter.

Therefore when a shear force greater than the shear strength is applied

to a shear system, it can result in tremendous change in the shear behavior. The changes of these slip parameters are much larger than the change of the shear force over the strength, or Fo/f(0). The seismic energy does not change in the same way as the total energy release any more. Instead, it changes at a much higher speed. This means that in the case of excessive loading, a larger portion of the energy released during the shear process has been converted into seismic energy than in the case where $Fo \leq f(0)$. This is probably due to the dynamic effect. It is this dynamic effect which produces vibration in the system. At the same time, the seismic energy is propagated through vibration of particles. Therefore, the higher the sudden loading is, the more intense the vibration will be and consequently the more seismic energy is radiated. In this case, it becomes more conservative to use the seismic energy to estimate the total energy release.

Table 8.1 effect of sudden loading on slip behavior

Fo/f(0)	1	2	3	5	7	9	11	slope*
T_1 (0.1ms)	.13506	.13402	.13402	.13401	.13041	.13401	.13401	0°
X_1 (10μm)	.11076	.82216	1.5315	2.9493	4.3669	5.7843	7.2016	35.34°
T_2 (100s)								
$\dot{X}$max(m/s)	.12969	.96282	1.7947	3.4566	5.1181	6.7795	8.4408	39.73°
ΔF (MN)	.06062	.45219	.84231	1.6221	2.4018	3.1814	3.9609	21.30°
ΔE (J)	.18226	1.3828	2.5095	4.8359	7.1686	9.5083	11.856	49.37°
Wr (0.01J)	.00129	.07152	.24838	.92130	2.0201	3.5444	5.4943	- **

* note: the slope is obtained from linear regression of each curve.
** : Wr varies with the square of $[Fo/f(0)]^2$

8.3. OCCURRENCE OF SUDDEN LOADING

As can be seen from above analysis, sudden loading has significant effect on the slip behavior. Therefore, it is important to understand when sudden loading can occur. In laboratory experiments, sudden loading can be obtained by simply applying a large shear force suddenly to the system, or through some other way, such as releasing the normal pressure quickly when the slip is about to initiate. For the former case, a large force applied suddenly will obviously produce a dynamic effect. For the latter case, the same effect can be achieved. In this research, some shear tests were carried out during the acoustic emission study of rock specimens. The shear tests were done as usual. However when the shear force gradually reached the strength, the normal pressure was released manually as quickly as possible. This experiment was carried out at different levels of normal pressure. In each test, violent failure was observed and a bang the same as from conventional unconfined compressive test was heard. At the same time, a sharp increase of acoustic activity was recorded. These test results will be presented in figures 10.16 and 10.17, where all acoustic emissions occurring at other stages are completely masked by this increase. This means that the violent failure is not unique to the conventional unconfined compressive test and it can also happen in the shear test. Further more, it implies that the violent failure of a rock mass is not only determined by the internal property of the rock mass, but also by the loading conditions.

In mines, sudden loading may happen right after an abrupt excavation, such as blasting. Because in this case the load previously supported by the excavated rock mass has to be undertaken by the rock mass around the opening

before a new equilibrium of stress can be reached. Therefore a high stress is built up instantaneously in some area. If this stress is much higher than the strength of the rock mass and if the loading is finished in a very short time, a dynamic effect appears and violent failure may be caused. This is specially true if a geological weakness , such as a fault exists in the vicinity of excavation, or a newly fractured surface is formed in the highly stressed rock mass. The mining activity could result in a sudden excessive loading on that surface if, during the stress redistribution, the normal pressure is reduced abruptly to a very low level, consequently causing sudden reduction of the resistance on that surface.

8.4. OCCURRENCE OF VIOLENT FAILURE IN COMPRESSIVE TEST

To apply above results, the violent failure of rock specimens is considered here. Violence is a commonly observed in the conventional compressive test of rock specimens. From this research it has been found that the compressive and shear tests have a close relationship and that they both exhibit similar physical reactions such as noise and fracturing at failure. The occurrence of violence during compressive testing can be interpreted in the same way as for the violent shear failure discussed before.

If a weakness exists in a rock specimen, it is very possible for failure to take place along that weakness if the direction of loading is not perpendicular to the weakness plane. The failure may be gradual or violent. The closer this weakness is to the failure surface as determined in figure 3.4, the less the possibility of violence exists. This is because if the weakness coincides with the

predicted surface, the whole process may be controlled by the shear mechanism at static loading on that weakness. In this case, as the load increases from zero, the failure may take place as a smooth sliding or small stick-slip.

If the rock specimen does not contain any major weakness, or if the existing weakness plane is perpendicular to the loading direction, the result will be different. At the beginning of loading, stress will build up uniformly within the specimen. When the stress reaches some level, fracturing initiates, which is accompanied by acoustic emission. As loading continues, a fracturing zone will be formed. Once a macrofracture surface is formed in the fractured zone, shear process occurs and the failure mechanism discussed before will apply. On this newly fractured surface, the shear stress is close to the maximum shear stress, figure 3.4 and makes an acute angle of $\beta = \pm(45° - \phi/2)$, equation (3.1), with the major principal stress σ_1. Because the rock specimen is not perfectly intact, this angle actually would vary somewhat from the theorectically predicted value of β.

Upon the formation of the fracturing surface, the instantaneous normal and shear stresses acting on it can be estimated by these two equations [26]:

$$\begin{cases} \sigma = \sigma_1 \cos^2 a + \sigma_3 \sin^2 a \\ \tau = -\frac{1}{2}(\sigma_1 - \sigma_3)\sin 2a \end{cases} \quad \text{..... (8.2)}$$

At the very moment when the failure surface is formed, σ_1 equals to the peak compressive strength.

This shear stress τ can be much higher than the shear strength τ_s on the fractured surface at this moment. It is the excessive shear stress which

introduces the effect of dynamic loading. Violent failure takes place if this excessive stress is not extracted quickly enough at that moment. The mode III violence of failure defined in chapter 7 refers specifically to this type of failure.

As an example of above statement, the testing results to be presented in chapter 10 are used in the following. The mechanical properties and the actual breakage angle for each specimen are given in table 10.1. Among the three cylindrical specimens, #2 and #3 specimens had some tiny microcracks which possibly caused the disparity of the compressive strength σ_c and changed the breakage angle of the failure surface. It is very difficult to determine the real frictional coefficient μ_s on the failure surfaces of those specimens. However, these surfaces are similar to the chisel-cut surface. Then the results from direct shear test of breakage surface given in table 10.2 can be used, where the empirical formula for the shear strength of the natural breakage surface is

$$\tau_s = 0.0144 + 0.58323\sigma \quad \text{..... (8.3)}$$

During the uniaxial compressive test, $\sigma_3 = 0$ and by figure 3.4, $\alpha + \beta = 90°$. Using the data in table 10.1, the instantaneous normal stress σ and shear stress τ on the failure surface can be calculated by equation (8.2). The shear strength of the failure surface can be estimated by equation (8.3). The final results for the three specimens are listed in table 8.2.

As can be seen, all ratios of τ/τ_s are above one. Apparently, the higher this ratio, the more violent the failure. Because the specimen #1 is almost intact, it has the highest compressive strength. Its real shear stress is as high

Table 8.2 stress estimation on failure surface of rock specimen in compression

specimen No.	β deg.	α deg.	σ_1 ksi	σ_3 ksi	σ ksi	$\lvert\tau\rvert$ ksi	τ_s ksi	τ/τ_s
1	25.756	64.244	18.459	0	3.4855	7.2242	2.0329	3.5540
2	46.057	43.943	11.320	0	5.8688	5.6561	3.4228	1.6525
3	39.508	50.492	9.44	0	6.006	4.6335	3.5029	1.323

as 3.55 times the estimated shear strength on the failure surface, which have definitely made the failure violent. In fact, a big bang was heard at the failure of this specimen. Even for the specimen #2 and #3, which are not very intact, the ratio τ/τ_s is also above one, which can still increase the violence at failure. However, their failure was much less strong than the specimen #1. These phenomena are clearly indicated by the acoustic emission shown in figures 10.2 and 10.3, where both event rate and energy rate are much higher from specimen #1 than from specimen #2.

8.5. SUMMARY

This chapter specifically deals with the problem of sudden/excessive loading. It is found from above analysis that:

1. Violence always occurs at failure of rock if a large shear force is applied to the shear surface suddenly.
2. The effects of sudden loading on the shear behavior during each slip are extensively studied using a computer program. In all cases, the change of slip behavior is much greater than the change of ratio of shear force over the strength.

3. The conditions which are likely to give rise to sudden loading in laboratory tests and in situ are discussed and a typical example of a compressive test is given to show the violent failure due to sudden loading.

CHAPTER 9. THE NATURE OF ROCKBURSTING

9.1. GENERAL

In the previous chapters, a mechanism of rock failure is postulated and the conditions which may give rise to violent failure are obtained. In this chapter, above results will be used to interpret the violence of rock failure occurring in field. From previous analysis, it has been found that violent rock failure can happen under three modes, each of which occurs in certain conditions. These conditions consist of rock properties, loading speed and stress state and vary with them. Violent rock failure may therefore happen in any mine rock as long as the critical conditions are present.

The most important factors contributing to the critical conditions are the normal pressure on the rock surface, the loading speed and the elasticity of the rock. The previous modelling results indicate that the possibility of violent failure increases when the normal stress goes up (Mode I violence), when the loading speed becomes very high (Mode II violence) or when sudden loading occurs (Mode III violence). Therefore violent rock failure would be more likely to happen in the stress concentration zone, such as a pillar, the corner of an opening, the excavation face or any irregularity where stress concentration exists. Similarly, this problem is expected in places close to geological structures, such as a natural fault, dyke, intrusion, etc. At the same time, rapid stress change brought about, for example, by blasting and sudden change of stress state induced, such as, on a fault will also increase the incidence of violence. In the following, the issue of how violent rock failure occurs in given conditions is discussed.

9.2. VIOLENT ROCK FAILURE ALONG A NATURAL FAULT

When a major geological discontinuity exists in the rock mass, the stability of the rock mass will be completely controlled by it. The geological discontinuity can be a big natural fault, or a small joint, even a bedding or foliation.

A big natural fault can be considered as a shear model. In this case, the loading condition is very similar to that of shear test. The three-dimensional stress components can always be resolved into the normal stress σ and shear stress τ on the fault plane no matter what the orientation of this plane is, as indicated in figure 9.1. These stresses may be very high due to the gravity of overburden, the residual stress from tectonic movement or mining induced stress concentration.

As an opening is excavated in the rock mass, according to the theory of elasticity and rock mechanics [47], the virgin stress field is disturbed and a new state of stress will be created. This new stress field can be divided into three zones, figure 9.2, i.e. the stress relaxing zone I, the stress concentration zone II and the undisturbed zone III. In zone I, the stress decreases due to removal of the supporting force on the opening face. In zone II, the stress becomes much higher than the virgin stress and is possibly above the strength of the rock mass.

Any mining activity close to the fault will probably increase the normal and shear stresses due to the stress concentration. Figure 9.3 shows a typical case of stress change due to mining activity near a natural fault. Because the

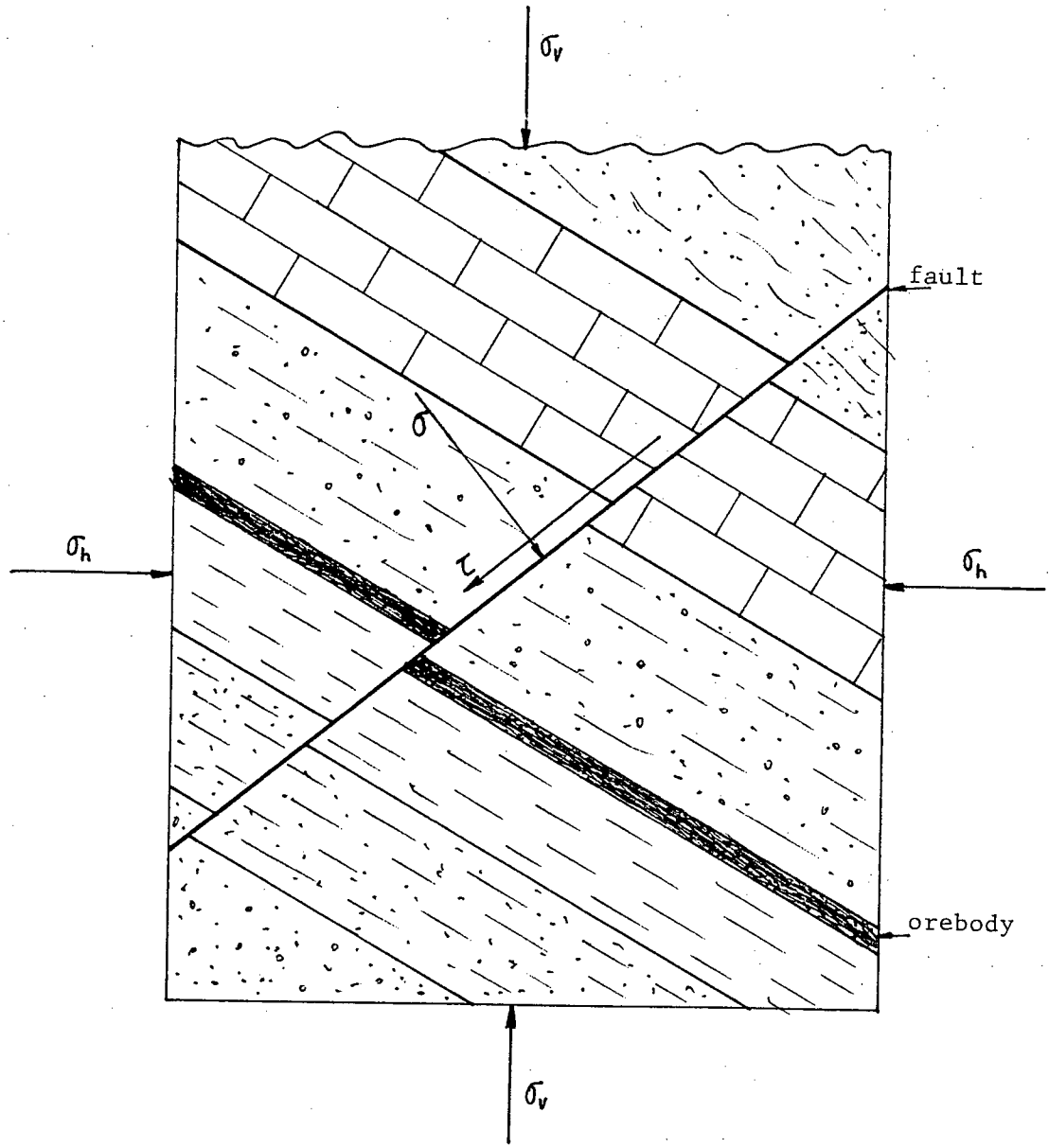

Fig.9.1 Stress components on a natural fault in the rock mass

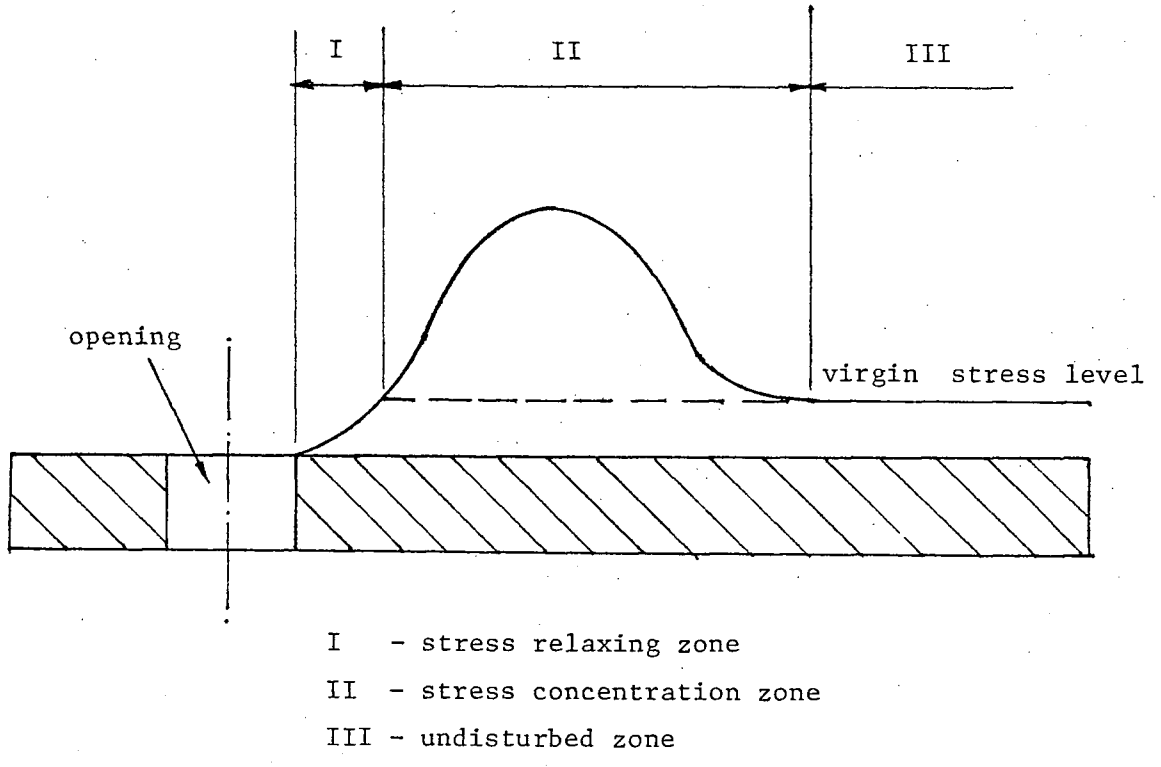

Fig.9.2 Stress redistribution after excavation of an opening in the rock mass

rock mass is usually interrupted and cut into blocks by joints and fractures, the high shear stress may cause shear failure along this fault by pushing the highly stressed block(s) towards a free surface, or towards the low stress direction, figure 9.4. As discussed in chapter 7, when the failure occurs as stick-slip, Mode I violence may occur, because a violent slip can happen under high normal stress. In this case, a single slip may give rise to violence due to the release of energy. Successive slips may result in the complete destruction of underground openings.

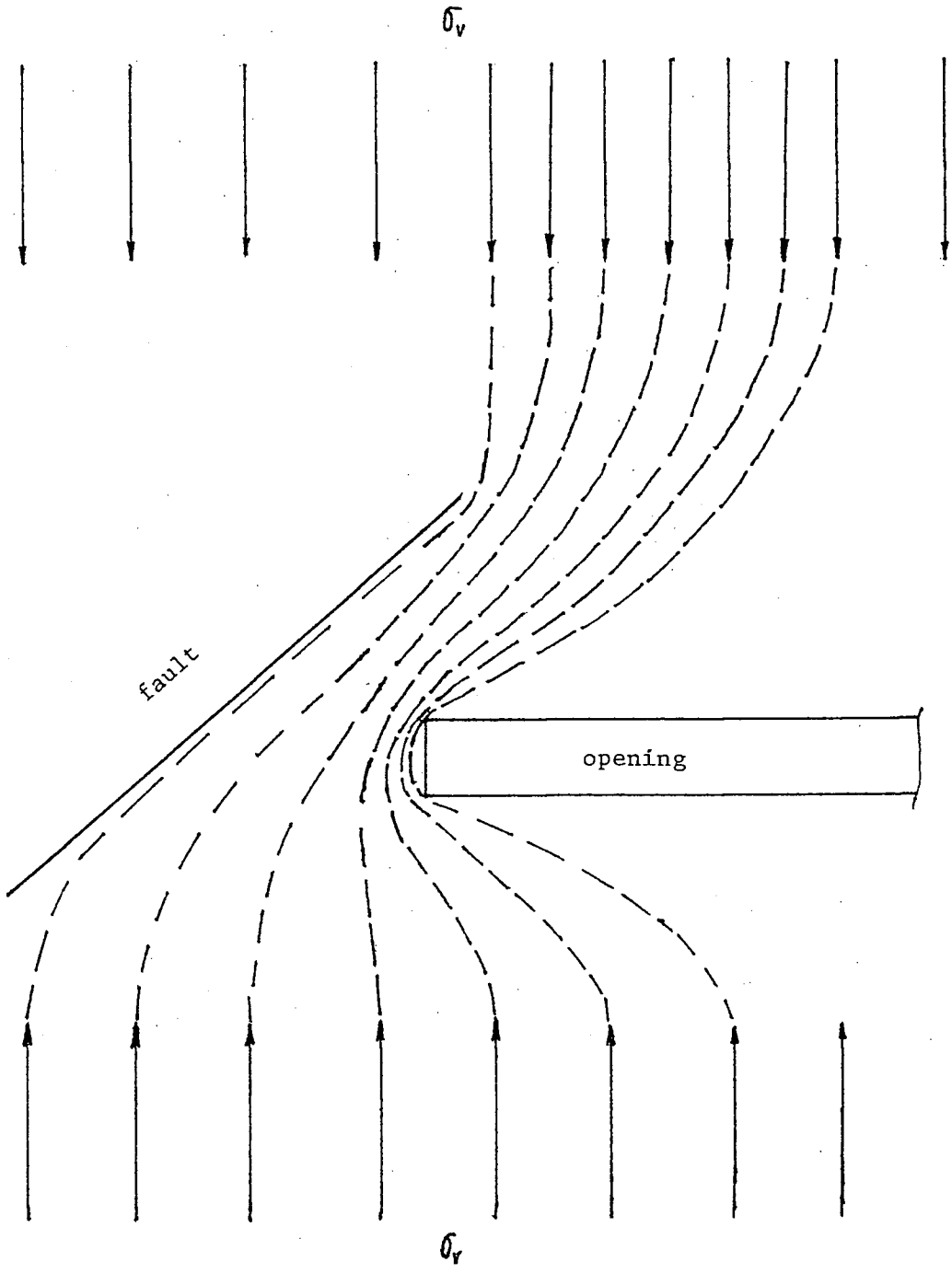

Fig.9.3 Streamline of stress change due to mining activity adjacent to a fault

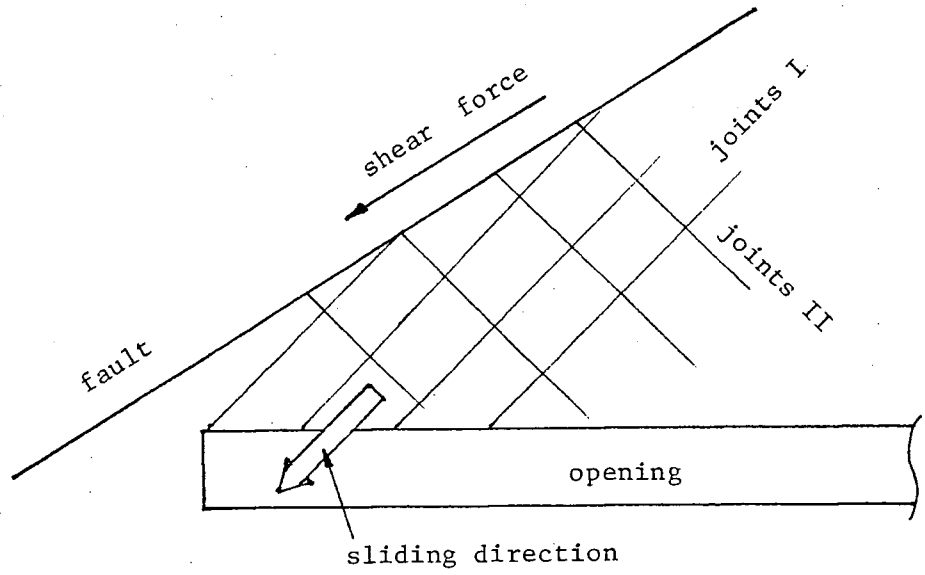

Fig.9.4 Possible sliding of highly stressed blocks

Even if the stress is not high enough to cause failure during the stress concentration, violent failure is still possible at the stress relaxation. When the excavation passes through or is very close to the fault so that the fault is within the stress relaxing zone, the normal stress on the fault plane will decrease and the shear stress may increase at the same time, figure 9.5. Consequently, the shear stress would be relatively high with the normal stress being relatively low, in which case, the frictional resistance would drop. If during the process of stress redistribution, the total shear resistance dropped far below the shear stress, failure would occur. If this drop were big enough to induce the transition from stick-slip to stable sliding as discussed in chapter 7, with excessive shear stress being available to cause a sudden slip, the effect of

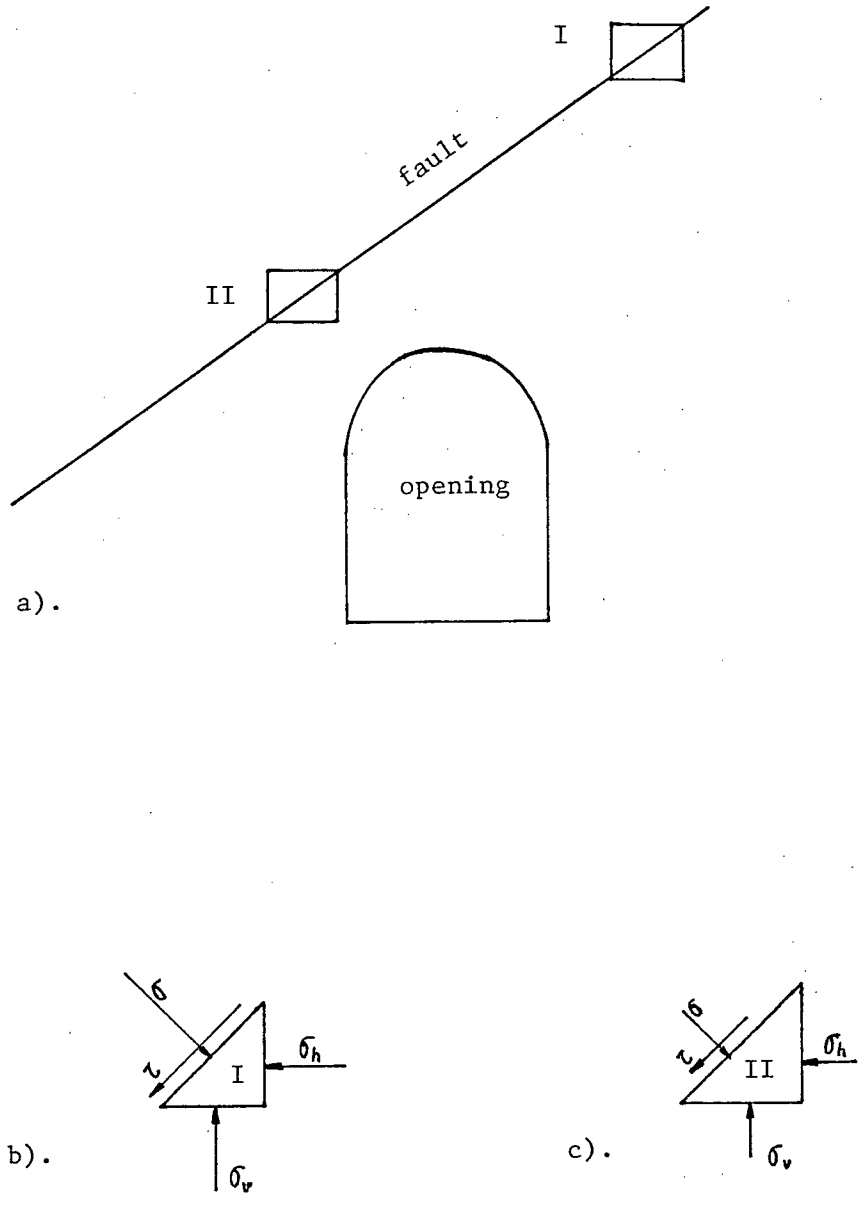

Fig.9.5 Stress change due to the existence of an opening around a fault

dynamic loading appears and the Mode II violence could happen.

9.3. ROCKBURSTING IN A MASSIVE ROCK MASS

If the rock mass does not contain any major weakness, the stability of the rock mass still depends on the rock mass itself. However, due to the minor joints, the strength of the rock mass will be lower or much lower than that of intact rock. For heavily jointed rock mass, the rock mass can be treated similarly as homogeneous isotropic system with much lower strength [42]. For the rock mass containing some joints, its strength will be between that of the intact rock and that of the heavily jointed rock mass.

When the stress in the rock mass has reached the strength of the rock mass, failure will occur along a failure surface, which as discussed in chapter 3, can be a joint or a newly fractured surface. At the initiation of this surface, the failure process is controlled by the shear mechanism. In the case of a massive rock, however, the shear force is usually much higher than the corresponding shear strength on the failure surface. Therefore the Mode III violence is most likely to happen. A typical example is the loading of a rock pillar, figure 9.6, where the loading condition is very similar to that of uniaxial compressive test. The shear stress can be estimated from equation (3.5) and the shear strength from equation (4.6a) if the frictional coefficient for the fracture surface is known. For a hard rock with high elasticity and high compressive strength, the ratio of the shear stress over the shear strength will be far above one. As discussed in chapter 8, the rock specimen #1, which was tested under uniaxial compression and failed violently, has a value of above 3 of this ratio,

table 8.2. In this case, Mode III violence occurs due to the dynamic effect of the excessive shear stress at the initiation of failure. Obviously, the higher the compressive strength and this ratio are, the more violent the failure would be.

The case of a stope face or sidewall of an opening as shown in figure 9.7 can be treated as a semi-infinite pillar. As a result of fracturing development, a pair of conjugate shear surfaces may be developed first, which would make a V-shape in the section view. Under the high internal stress field, this wedge of rock may be suddenly pushed out by a resultant force pointing outwards. As this block of rock moves out, the resistance decreases quickly due to the loosening of contact on the failure surfaces. This would make the failure process very fast and produces violence accordingly. For the more complex geometry, the finite element and boundary element methods will be a big help in estimating the stresses.

9.4. INFLUENCE OF OTHER GEOLOGICAL STRUCTURES

The presence of regional geological structures results in uneven distribution of the stress field. In the vicinity of a fold, an anticline or a syncline, which are the results of tectonic movement, the stress may be higher than in areas far away from them due to the possible residual tectonic stress and some rock mass may be heavily crushed. A zone of crushed rock can act as a weakness. As mining gets close to these areas, the mining openings may undertake a heavy load, which will increase both the difficulty of supporting and the violence of failure along those crushed zones.

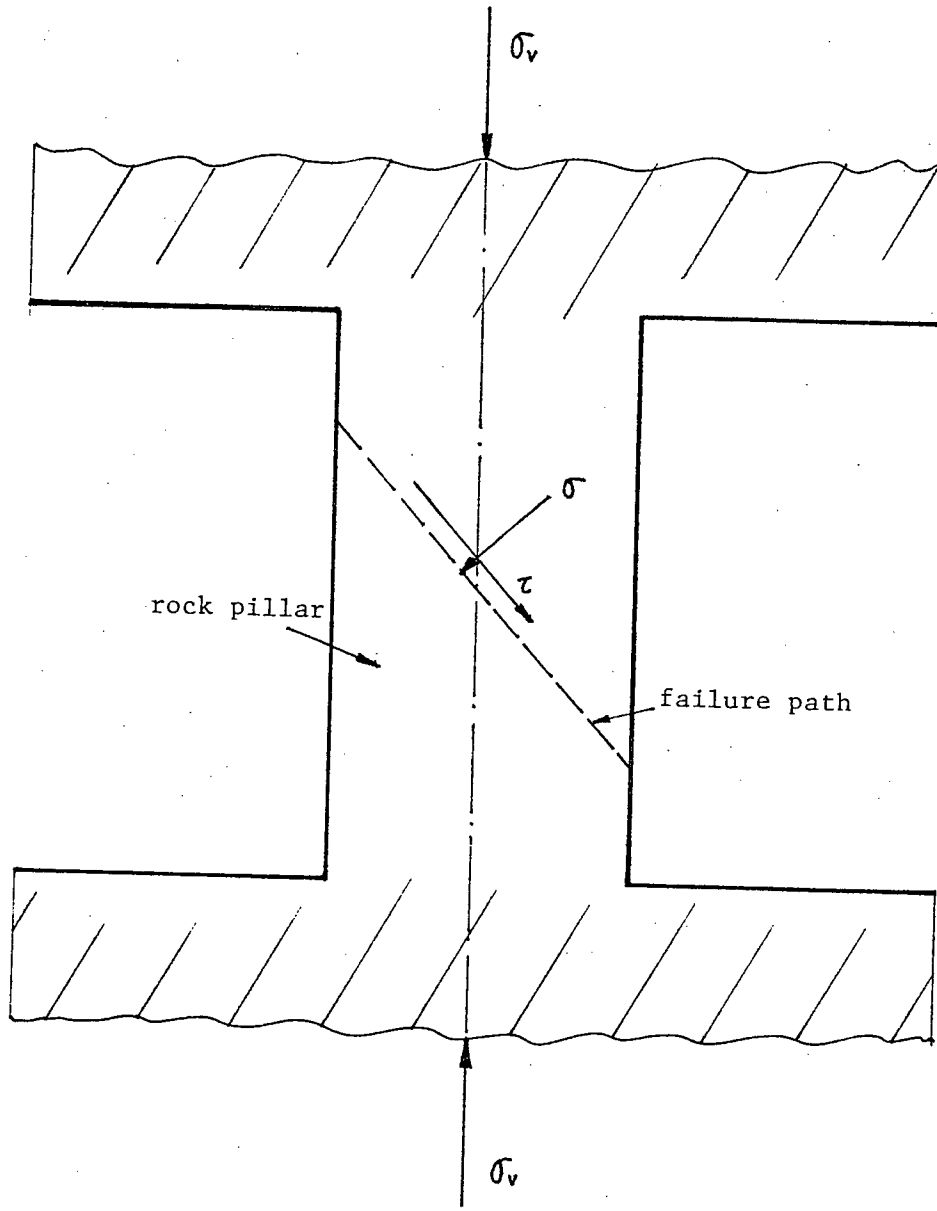

Fig.9.6 The loading and the failure path of rock pillar

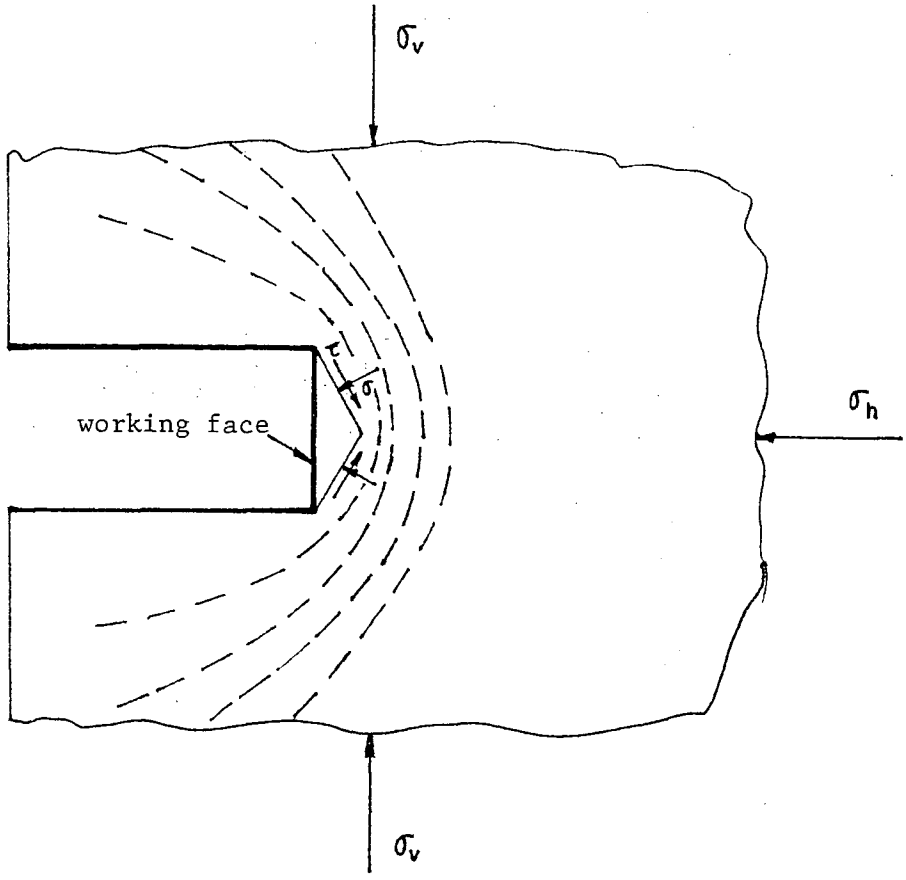

Fig.9.7 The loading and the possible failure path of a working face

On the other hand, if the country rock contains some hard inclusive, such as dyke, sills or any other intrusive, the stress will certainly concentrate around them during the stress redistribution due to mining activity. As in figure 9.8, the intrusive just acts as a "stiff pillar" and undertakes the extra load first from excavation. Therefore even though the average stress estimated is relatively low, violent failure can still happen. In this case, the failure is characterized by

a large number of seismic events [48], which is discussed in more detail in chapter 13. The failure under this condition can happen in two possible ways. The first instance will be the failure of the inclusion itself under extremely high stress. The process of failure will be the same as a rock pillar and Mode III violence is expected when failure occurs. The second case will be the failure of the country rock in a very thin zone around the inclusion. In fact, due to the continuity of the stress field, the country rock which is much weaker than the intrusive will be loaded by a relatively high stress within this thin zone and probably fail near to or at the interface between the country rock and the inclusion. As excavation reaches the inclusion, failure may take place first in this thin zone.

In general, any regional geological structure giving rise to stress concentration will increase the possibility of violence at failure.

9.5. INFLUENCE OF MINING CONDITIONS

As discussed before, the normal pressure on a surface and the loading speed are important factors in violent rock failure. In addition to the geological conditions discussed above, mining conditions can also affect these factors significantly.

9.5.1. The Shape and Size of a Pillar

In mining, pillars are usually used to support the overburden or to protect an opening. In longwall mining, pillars are usually very long, such as the barrier pillar between two longwall faces. In room and pillar mining, they are usually very short, in square or rectangular shape. Because of the variety of geological

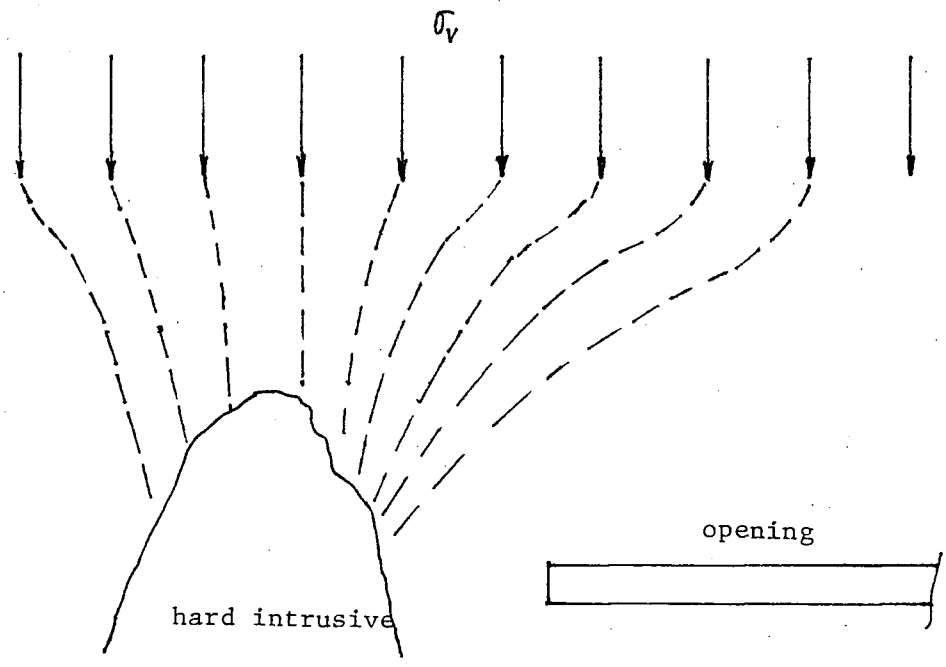

Fig.9.8 Stress redistribution due to mining around a hard intrusive

conditions and rock types, it is difficult to specify the pillar design in terms of reducing the incidence of rockbursting. The rule of thumb is to reduce the unnecessary stress concentration.

If the pillar is so large that its center is not affected by the stress concentration, the matter will not be important. If the pillar size is so small that the stress concentration on both sides overlay each other, the behavior of the entire pillar will be important. Apparently, the pillar with smaller loading area undertakes higher stress and is easier to fail and larger pillar has higher supporting ability and energy storing capacity. When a large pillar fails, the

failure may be more violent than a small pillar because of higher total load, which is completely applied on the failure surface at the initiation of failure. It might be better in this sense to replace a large pillar by two small pillars with the same loading area in designing temporary pillars.

Pillars with same loading areas can also behave differently. A shorter pillar has higher stability than a taller pillar. When the ratio of height over width of a pillar is above some value, say 2, the pillar can behave in a completely different way. In this case, the pillar may act as a bar and is likely to fail in buckling. If a large load is available at buckling, violent failure can also be expected.

9.5.2. Mining Rate

The loading speed is another key factor in violent rock failure. During mining, this loading speed is directly related to the speed of stress change. During continuous excavation, the stress concentration zone ahead will move forward as a result of self-adjustment and the creep effect of the rock mass. If the advance speed of excavation is lower than the stress movement, the stress concentration zone will just move forward smoothly as the excavation continues. Otherwise, stress may become higher and higher as excavation advances and eventually failure takes place. In this case, the higher the excavation speed, the higher the risk of failure. If a large stress is available under the high loading speed, violent failure can arise.

In the case of drilling and blasting, the excavation is discontinuous and

failure usually happens at blasting. Here, each blasting results in instantaneous loading on the adjacent rock mass. If a blasting involves a large amount of rock mass, a very high load will be transferred to adjacent rock mass and the speed of stress change will be very high as well. Then failure can be violent. In order to reduce the risk of rockbursting, it may therefore be better to blast a large area on several separate occasions than in a single large blasting.

Similarly, if two mines have the same daily production but the number of mining faces is different, the mine with less mining faces would have the higher possibility of violent rock failure due to higher advancing speed of mining.

9.6. ESTIMATION OF POSSIBLE VIOLENT FAILURE

In order to prevent and control a rockburst, the possibility of its occurrence should be estimated first. As discussed in chapter 7, the violence comes from three major causes. Therefore the possibility of occurrence can be estimated for each cause respectively.

The Mode I violence is from stick-slip on a major discontinuity under high pressure. If the failure appears as stable sliding, violence will not occur because extra energy cannot be built up. Even if the stick-slip happens, the violence will not necessarily occur under low pressure because the energy released during each slip is relatively small. Only when the pressure is very high, the energy released at a slip can cause violence.

As we can see here, the term "violence" is ambiguous. How high the

pressure is enough to cause violent failure depends on what we think of as violent in the amount of energy released. This energy release is usually closely related to the damage it caused. If the energy release is used as a measurement, a level can be specified from the damage observed. The relationship between the seismic energy release and the normal pressure, figure 6.9 and table 6.5, is given as

$$Wr = C_2 P^2.$$

Therefore, for an amount of energy specified as violent, the corresponding normal pressure can be determined. When this value of normal pressure is applied to the transition chart of figure 7.2, the violence zone can be clearly seen for Mode I violence. For a particular case, the transition chart given in figure 7.2 should be calibrated by the test results of the rock mass concerned.

When the conditions determined from the rock properties, mining conditions and stress state falls in the violence zone of this chart, violent failure is possible. Then above factors should be changed to avoid getting into this violence zone. The stress state can be obtained from in-situ stress measurement or numerical modelling.

Mode II violence occurs when the normal pressure drops quickly to a level low enough or when the loading speed increases fast enough to cause transition from stick-slip to stable sliding. Therefore, when mining is close to a major discontinuity, if the stress redistribution causes this big increase of stress rate or large drop of normal pressure on it, violence will be possible. However, in this

case, the stress change cannot be determined by in-situ stress measurement because by the time the stress is measured the violence would have happened. This stress change after the mining activity can be estimated in advance by the experience of working in similar conditions or more accurately by numerical modelling such as finite element or boundary element method. Thus better mining design should be adopted to avoid the sudden increase of stress rate and large drop of normal pressure.

Mode III violence refers to the failure in a massive rock, caused by a large excessive shear stress on a joint plane or the newly fractured surface. This fracture surface can be determined from the stress state and the shear strength envelope. It is easy to determine the shear stress by Mohr's circle if the stress state is known. Similarly, the shear strength of the fracture surface can be determined if the frictional coefficient is obtained by shear testing on the fresh fracture surface of the rock mass concerned. Again, the stress state for a given mining condition can be estimated by in situ stress measurement or by numerical modelling. A more conservative way to estimate the possible violence under this condition is to use the uniaxial compressive strength to calculate the approximate shear stress on the fracture surface and compare it with its shear strength. An example has been given in chapter 8.

9.7. PREVENTION OF VIOLENT FAILURE

As previously discussed, the violence of failure can occur in three modes, and different methods of prevention should be utilized for each case. From the point of view of mining technology, the preventive methods can be adopted at different

stages of the mining process, such as at mining design, during and after excavation.

9.7.1. Mining Design

The fundamental method of rockburst prevention is to optimize the mine planning so as to reduce the possibility of unnecessary stress concentration to the maximum extent. Good mining design would cause stress change uniformly during the stress redistribution after excavation. This is extremely important in minimizing all the three modes of violence.

Mine planning is a rather complex problem, because many geological, technical and economical factors have to be concerned. However, the preventive methods suggested in this section can be used as a guideline in design. For instance, the corner pillar at the intersection of two openings should be made round as represented by the dot line in figure 9.9. The sharp turning of a roadway should be avoided. In retreat panel mining or in recovering of pillars, the mining sequence can be adjusted to reduce the stress concentration. Leaving larger areas behind at the mined out zone is better than leaving a smaller area, figure 9.10. When mining across a big natural fault, it is better to approach the fault from the upper panel than from the lower panel, figure 9.11 in order to avoid the stress concentration shown in figure 9.3. The best way if possible, is to start mining at and move away from the fault.

However, when excavation is near a fault, whether the advance direction

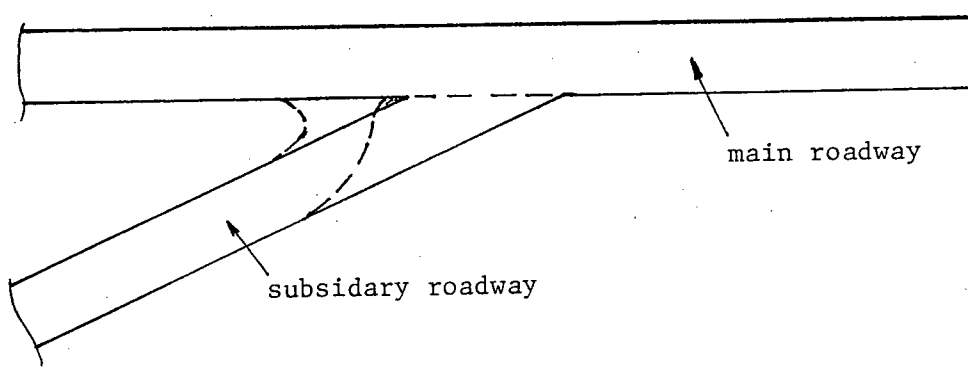

Fig.9.9 The intersection at two roadways should be made round as shown by the dot line in order to reduce stress concentration

of the excavation should be parallel, inclined or perpendicular to the fault depends on whether the normal stress on the fault will be released after the excavation. If the normal stress is released quickly to a low level, Mode II violence would possibly happen. In this case, the advance direction should be adjusted. This stress change due to the mining activity can be estimated well in advance by numerical method, such as finite element modelling and a better design can be chosen accordingly. At the same time, it should be kept in mind that the axis of an opening should be parallel to the direction of the major principal stress in order to minimize the induced stress on the opening.

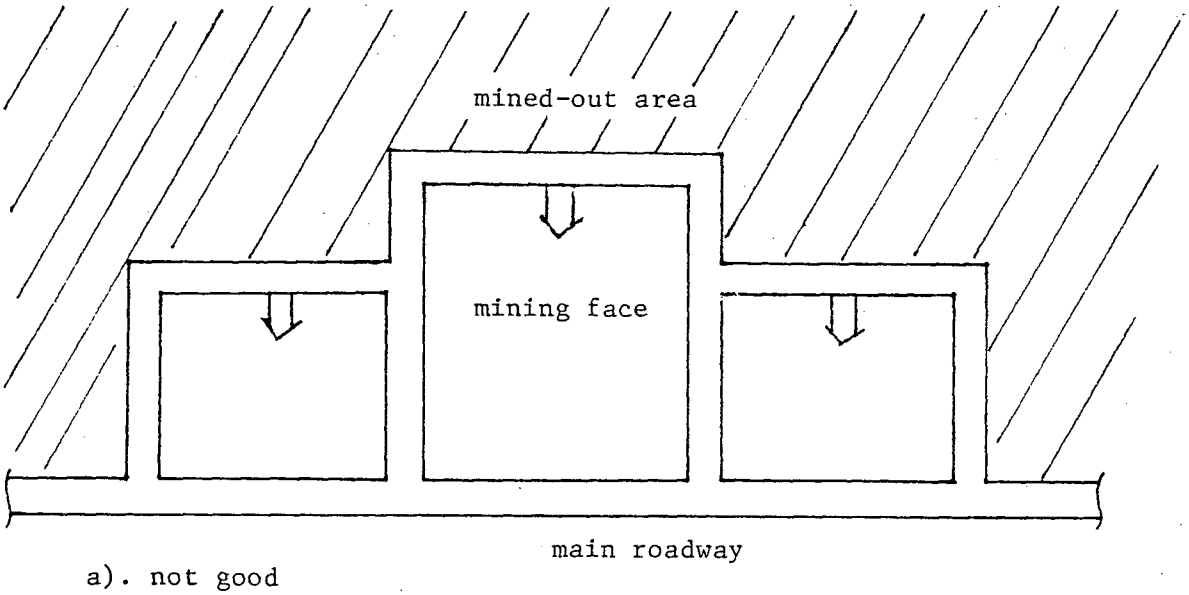

a). not good

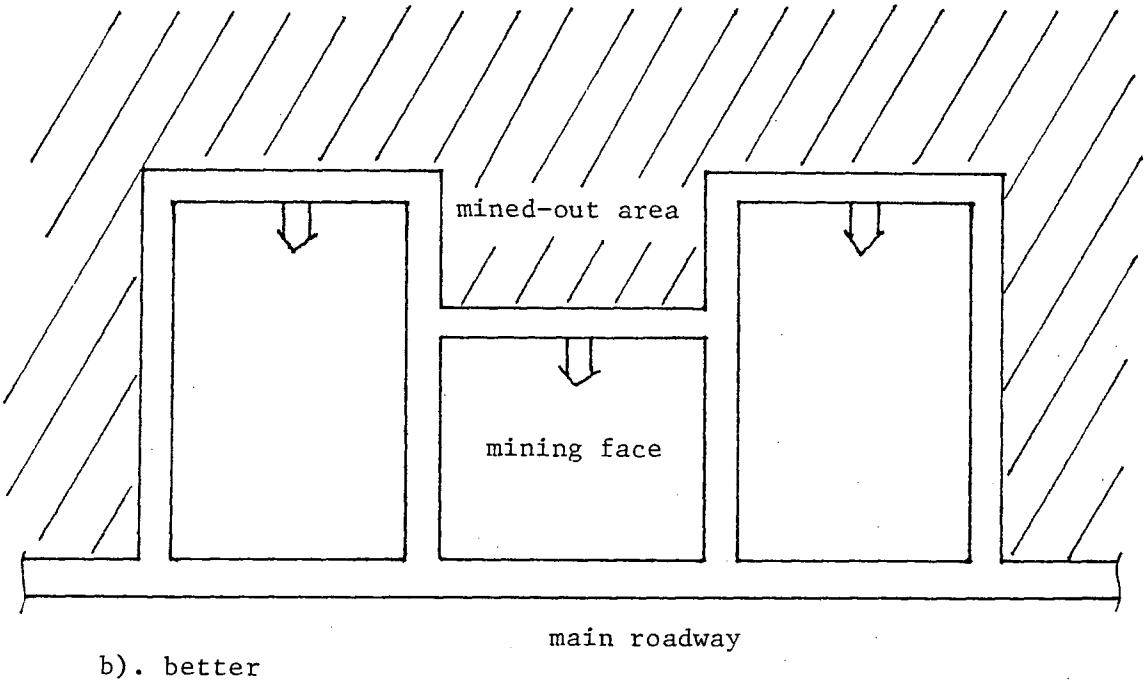

b). better

Fig.9.10 Adjusting mining sequence to achieve better stress condition

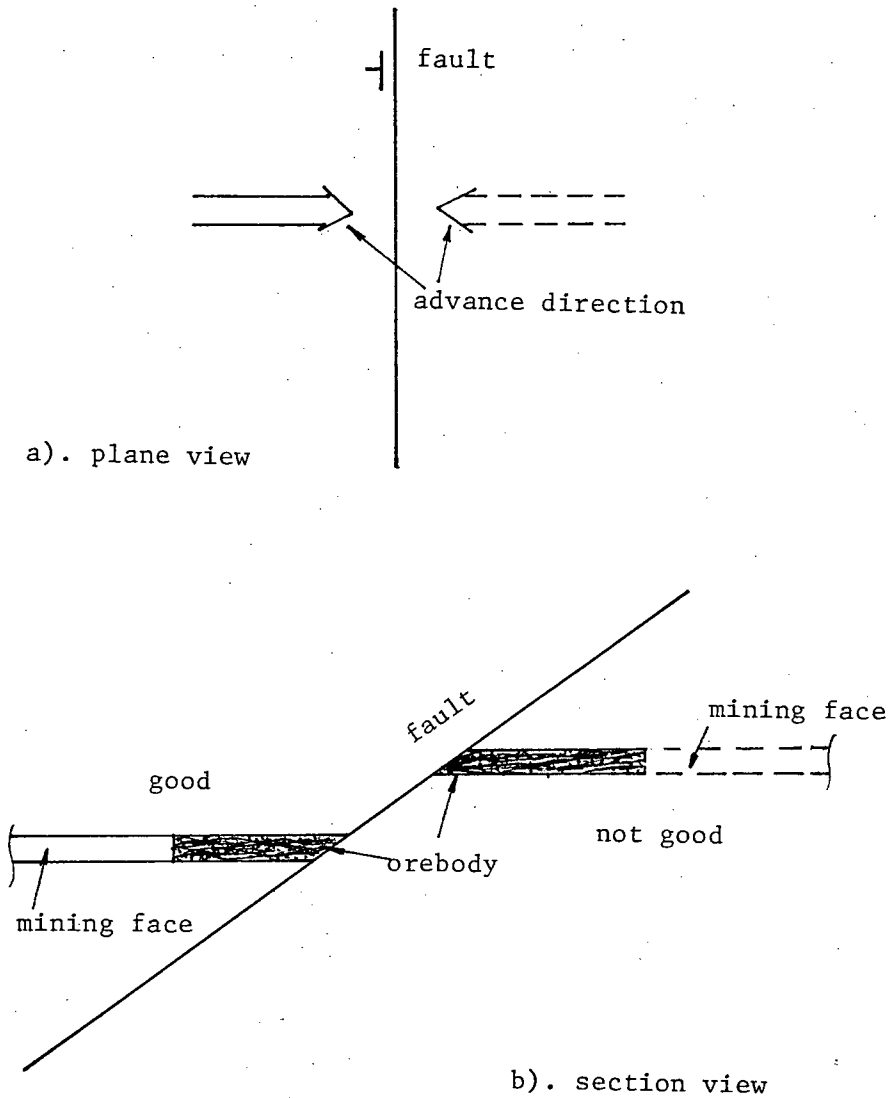

Fig.9.11 When mining across a fault, it is better to approach it from the upper panel in order to reduce unnecessary high stress

9.7.2. Destressing

No matter how good the mining planning is, it is inevitable that stress concentration will occur after excavation, sometimes due to technical problems or other factors. The second method, which can be used during the excavation to prevent violent failure, is to destress an area concerned if stress has been built up, or to pre-destress an area before the possible stress concentration occurs.

The destressing techniques have been widely used in practice, such as pre-conditioning [18], destressing blasting or infusion [19], etc. In pre-conditioning, it is intended to induce some fractures in the rock mass by blasting before the stress concentrates there so as to reduce its strength and its ability to store strain energy. When the destressing blasting is used at the stress concentration zone, the fractured zone is widened and the extra load is distributed over a larger area. At the same time, the stress concentration is moved further into the rock mass, then the possible problem can be reduced. In the use of infusion, high pressure water is supposed to have a purpose similar to blasting. It also reduces the elasticity and the ability of the rock mass to store energy.

There have been many publications about the destressing technique available in the last few years. No attempt is made here to describe them in detail. However, it should be pointed out that when using these techniques, caution should be taken. The over fractured rock mass will cause supporting problems. Especially in the use of infusion, the presence of water will bring in its special effects. Obviously, the water pressure existing on a fault or any other failure surface will reduce the effective normal pressure and then increase the

incidence of Mode II violence. This should not be allowed to happen in rock burst control. Meanwhile, as discussed in chapter 4, the shear strength of the surface of rock mass when wet will either increase or remain unchanged for polished, smooth surface, or decrease for rough natural surface. Therefore, it would be advisable to test the water effect on the rock mass in the laboratory before infusion can be applied for a particular mining condition.

9.7.3. Support

Effective support can reduce the load on the protected structures. This is the most efficient way after excavation is finished. But it seems impossible to eliminate the danger of rock burst by support only, as far as the limited ability of a support and the tremendous energy released from a rock burst are concerned. However, according to the suggested failure hypothesis and the results obtained in this research as given in chapters 6 through 8, the role of a support when it is applied at the right place and right time is more than expected in other occasions. As discussed in chapter 7, Mode II violence is caused by the transition from stick-slip to stable sliding either due to the sudden drop of normal pressure or due to the sudden increase of loading speed. An effective support which increases the normal pressure and/or the shear resistance on a failure surface can certainly at least reduce the violence of any mode of failure. In this sense, the support applied either parallel or perpendicular to the failure surface if it is known is much more effective than applied in other ways, provided this is acceptable for other mining purposes, figure 9.12.

As to the heavily loaded structure, such as a pillar or places close to the

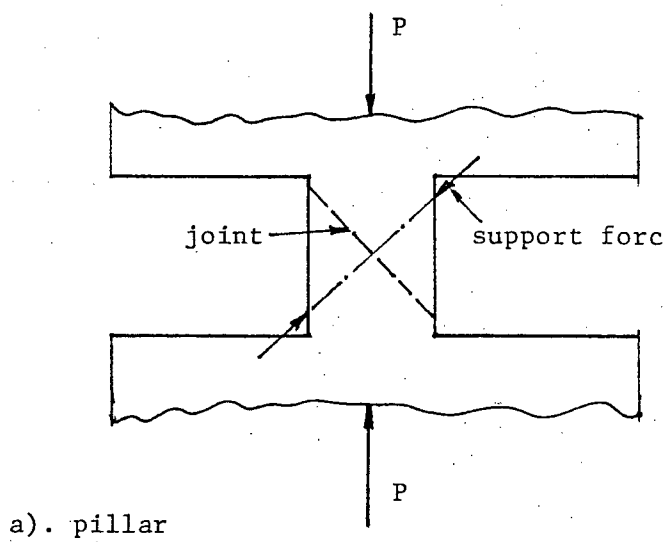

a). pillar

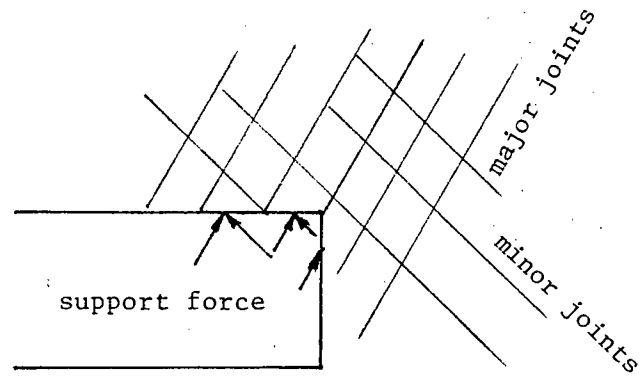

b). working face

Fig.9.12 proper support in advance can reduce the incidence of violent failure

excavation area, an effective support may avoid violent failure. Because in the sudden excavation, such as blasting, the extra load will be suddenly applied to surrounding rock mass, which will be loaded at a high speed. If a support is applied in advance, it can reduce the loading speed as well as the actual load. The reduction of the loading speed is expected here because of the actual yielding effect of the support and the creep effect of the rock mass. This yielding effect prolongs the loading time during which the whole load is applied to the structure and at the same time the load is distributed over a larger part of the rock mass due to the creep of the rock mass. In this case, the support should be designed with its yielding speed less than the creep speed of the structure to be protected. In general, effective supports applied before the stress change takes place will help in the reduction of incidence of violent failure, especially when a critical condition occurs.

9.8. SUMMARY

Based on the numerical analysis of conditions which may cause violent failure obtained in previous chapters, rockbursts occurring in field are adequately interpreted and their possible occurrence is extensively discussed. Specifically,

1. rockbursting on a natural fault is either from a sudden slip or from the transition induced by a sharp increase of stress change rate or a sudden reduction of normal stress on the fault.
2. Rockbursting in a massive rock is similar to violent failure of rock specimen in uniaxial compression and is caused by the excessive shear force available upon the formation of the failure surface.
3. The effects from other geological structures and mining conditions, such as

a hard inclusive, mining speed, etc. are examined.

4. Various measures are suggested to reduce and to eliminate the possibility of violent failure, such as optimizing mining design to avoid unnecessary stress concentration, destressing and providing efficient support to the unstable structure.

CHAPTER 10. LABORATORY STUDY OF ACOUSTIC EMISSION AT ROCK FAILURE

10.1. INTRODUCTION

The second objective of this research is to find precursory signals for violent rock failure in terms of acoustic emission. As stated before, even though millions of dollars has been spent on field research into rockburst prediction, little real progress has been reported. This is because of the difficulty in finding a reliable precursor to violent rock failure. In order to avoid expensive field trials, this research has attempted to identify a reliable precursor to violent faillure from laboratory testing of rock specimens. The obtained results will be compared with field measurements.

As discussed in chapter 3, extensive microfractures are developed prior to the failure of rock. These micro-fractures radiate acoustic energy during their propagation through vibration of rock particles. This process is referred to as "acoustic emission". The more intense the acoustic activity, the more energy is radiated, for as the unstable development of fractures occurs, the acoustic emission will be most active. Detecting these signals with suitable instrumentation provides us with a unique method to study the fracture development process and the rock behavior prior to the failure.

Acoustic emissions have been widely used in many fields to detect a defect of a structure, such as in aircraft frames or an oil tank. In mining engineering and related fields, they are usually used to monitor the stability of

structures of geological materials, such as rock slopes and underground openings. It has been found in the past that violent rock failure was preceded by an abnormal increase of acoustic activity. Similar phenomena were observed in laboratory experiments on acoustic emission of rock specimens in compression. However, the information obtained seems inadequate to interpret the violent rock failure properly and to give a reliable warning. Besides, in previous laboratory experiments, the effect of testing method on acoustic emission was not fully studied.

In order to correlate the acoustic signals with violent rock failure and to examine the effect of shear and compressive loading, further laboratory tests on rock specimens were conducted during this research. An attempt has been made to take full advantage of the available resources. Shearing and compressive loading equipments and an acousti equipment were used. A few specimens were prepared from a hard rock sample for both compression and shear tests. To study the effect of rock type on acoustic emission, one sample of each of coal and potash were tested. It is expected that the testing results can show some precursory signals for violent rock failure.

10.2. TEST PROGRAM

The laboratory tests were mainly designed to study the acoustic emission pattern from specimens of same type of rock under different loading conditions of compression and shear. It was desired to test the rock specimens on an MTS servo-controlled testing machine and a standard shear test equipment, with the acoustic activity being monitored throughout the tests. The acoustic

instrumentation should be able to record the acoustic information as fast as it occurs during the test and to re-process these data in several ways afterwards.

10.2.1. Specimen Preparation

All test specimens were prepared from the same sample of a Metamorphic rock, which consists of Schist, Biotite, Quartz, Chlorite, Actinolite and some submetallic sulphide and oxide. For compressive tests, three 1.58 in. diameter cylindrical specimens were cut with a length/diameter ratio of 2:1. The specimens were prepared by cutting the core in the same direction. The sample ends were then ground parallel to each other and perpendicular to the core axis. For shear tests, four 3 in. diameter specimens were prepared. These specimens were halved and each half was cast in cement with mould formers. Three of them had their shear surfaces created by breaking the specimen with a chisel. The fourth specimen was cut with a diamond saw. Care was taken during casting that the specimens were in alignment and the shear planes horizontal. Access was left in the cement cast for mounting accelerometer, or the acoustic transducer, which is recoverable after each test. The cement was completely dry when the specimens were tested.

10.2.2. Equipment

A servo-controlled MTS hydraulic testing machine was used for compressive tests. This machine can control loading either by loading speed or displacement rate. It is also able to record data of load and displacement on disk and to plot them against testing time throughout the test. Its technical specifications are as follows:

name: MTS 810 hydraulic testing machine
load frame model: 312.41

load frame capacity: 250 KN
cell model: 661.23A-01
cell capacity: 250 KN
control mode: load/stroke

A manual-loading device was used for shearing tests. It consisted of two load gauges, two hand pumps and two mould formers. The technical specifications include:

name: Potable Shear Box
load frame model: EL77-103
load frame size: 460×250×600 mm
hand pump capacity: 50 KN
mould former model: EL77-103/4

In selecting the acoustic equipment, the broad band of frequency and the small amount of energy associated with acoustic events, and the background noise were considered. The frequency of acoustic events from rock falls in the range of 100 Hz to up to 500 KHz [15] with the largest concentration within 16~32 KHz [49]. The energy released in such an event varies from something barely detectable with sensitive geophones to something that can be physically felt and heard. Generally, larger events have lower frequencies [15,23]. The major background noises are due to electricity and the mechanical vibration of various equipment in and around the laboratory. However these noises have very low frequencies compared with the major frequency range of acoustic events. Therefore the desired acoustic equipment should have high sensitivity, wide frequency response and ability to cut off the background noises.

The selected acoustic equipment is the PAC (Physical Acoustics Corporation) system, which has a four-channel data recorder and a processor. The

PAC system can record acoustic signals at very high speeds which can be changed by setting the dead time between signals and eliminate background noises by changing the amplification and the threshold levels. Because the transducer, preamplifier and the processor of this system came as a unit, they are compatible with each other. The PAC equipment had the following technical specifications:

name: PAC 3000 AE system
channels: 4
AE amplifier:
- noise: 4.5 μV RMS RTI
- gain: 0~60 db
- bandwidth: 10 KHz – 1.2 MHz
- threshold: .1~8V
- input impedance: 50Ω @ 120 pf
- AE in: 10μV – 10VAC
- AE out: 0 – 10 VAC into 50Ω and 470pf

AE preamplifier: PAC 1220A
- noise: <2μV RMS RTI
- gain: 40 or 60 db selectable
- bandpass: 10 KHz – 2 MHz selectable
- input impedance: 10KΩ//120pf
- output voltage: 20 Vpp into 50Ω
- input: single or differential selectable
- power: +28 VDC

AE sensor: PAC R15-1123 Piezoelectric Crystal
- sensitivity: voltage 0.06 v/g
- capacitance: 15pf
- resonant frequency: 150 KHz
- frequency response: 10 – 300 KHz

During the tests, signals of acoustic emission were picked up by the AE sensor and cabled to the processor after 40db pre-amplification. These data can be both displayed on the screen and recorded on the disk at the same time. They can also be played back and processed on the micro-processor of the PAC system, which has up to 20 ways of plotting graphs. Hard copies are available at the printer of the PAC system on request.

10.2.3. Test Procedure

Following preparation, an acoustic emission transducer was attached to the specimen by tape. An acoustic couplent was used to make a good contact between the transducer and the specimen surface. The diagram of the testing setup is given in figure 10.1. Before the test of each specimen, the PAC acoustic equipment was calibrated. In particular, the amplification and the threshold were carefully chosen by trials so that as many signals as possible could be picked up and any background noise could be cut off. This came up with a 1~2V threshold and 49~55db in gain. The dead time between events was set to 1ms for the shear tests and 3~6ms for the compressive tests.

During the compressive test, the MTS testing machine was programmed to give a constant rate of displacement. To shorten the testing time, this rate was set to 0.0001 mm/s at the beginning of tests and 0.00001 mm/s when the load reached approximately 40% of the uniaxial compressive strength. Load and displacement data were recorded by the MTS system. The PAC system monitored the acoustic information as well as the load. During the direct shear tests, loading was applied manually. Normal pressure was set to 1, 2, 3 and 4.5 ksi respectively for each specimen. Load and displacement data were taken by hand.

The acoustic signals recorded by the PAC system were both displayed on the screen and stored on disk. These data can be replayed back and plotted in different formats.

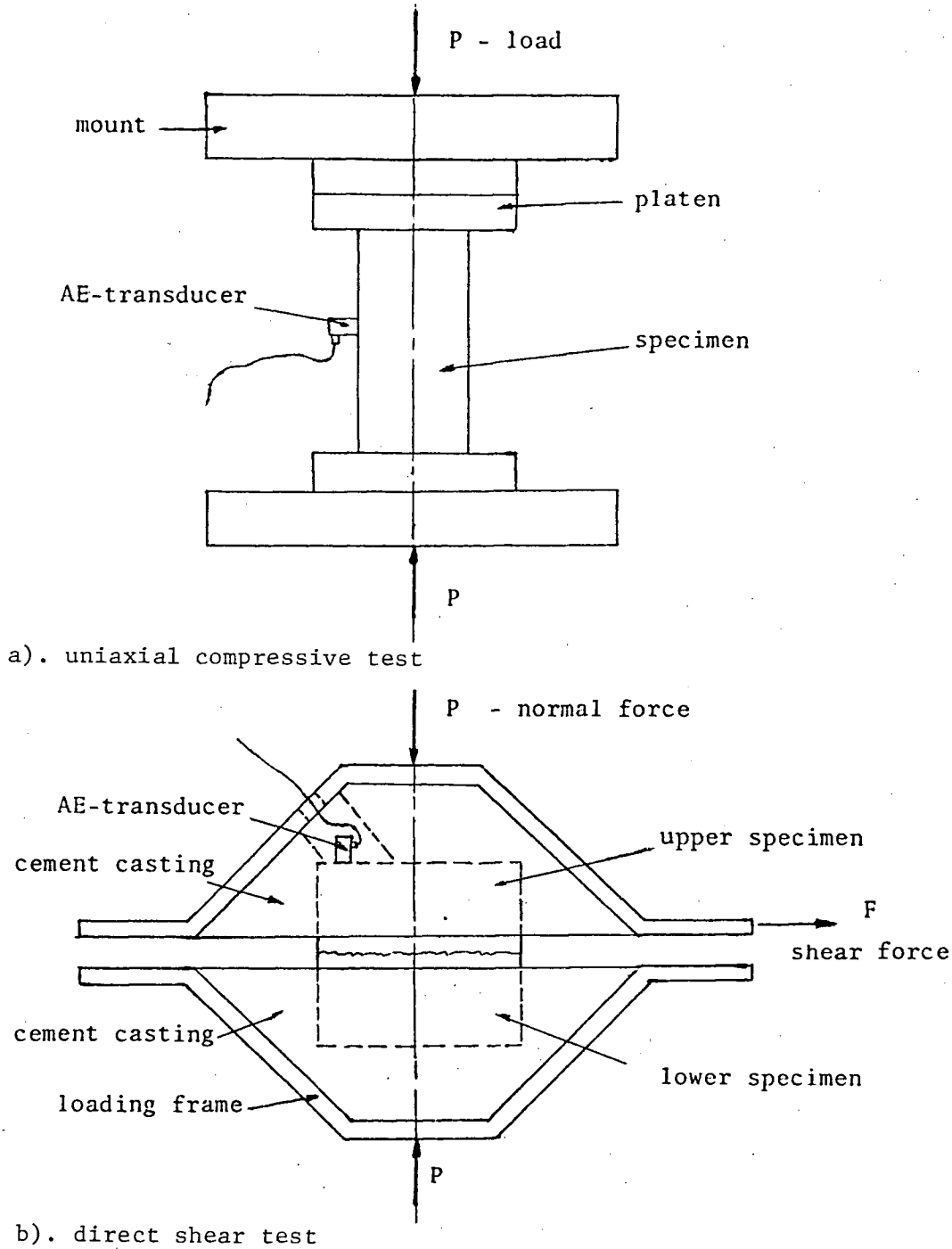

Fig. 10.1 Loading diagram for acoustic emission test

10.3. TEST RESULTS

Results from the uniaxial compressive tests and the direct shear tests are presented below. Despite the limited number of specimens tested, these results provide useful information for analyzing rock behavior before its failure.

10.3.1. Acoustic Emission from Compressive Tests

The identification and mechanical properties of the specimens loaded to failure under uniaxial compression on the MTS testing machine are listed in table 10.1. The disparity of compressive strength is probably due to the fact that the specimen #2 and #3 contained some micro-cracks which initiated the failure. Therefore the actual breakage surfaces are away from as determined by Mohr's circle for intact rock, i.e. away from $\pm(45° - \phi/2)$, equation (3.1).

During the tests, an attempt was made to acquire as much acoustic data as possible. At first, in the test of specimen #1, the dead time between adjacent events was set to 3ms, which resulted in use of six disks for the single

Table 10.1 Identification and mechanical properties of compressive specimens

specimen No.	length L_0 (in)	diameter D (in)	area A in^2	strength σ_c 10^3psi	modulus E 10^6psi	failure strain ϵ_0	breakage angle $\beta°$ *
1	3.2835	1.5842	1.9711	18.459	1.955	.00947	25.756
2	3.0041	1.5845	1.9718	11.32	2.426	.00636	46.057
3	3.1272	1.5858	1.9752	9.44	2.045	.00548	39.508
average				13.073	2.142	.00710	

* not: the breakage angle β is definedd in figure 3.4a)

specimen. In order to cut off some data without losing the basic characteristics, the dead time was changed to 6ms instead of changing the gain and the threshold. Then, two disks were enough for each specimen.

The acoustic emission information is presented here as event rate, energy release rate and energy release ratio against loading time and axial load. They are plotted in figures 10.2 through 10.5 together with the load-displacement curves for specimen #1 and #2 only. Due to technical problems during the test, data for specimen #3 are not complete and therefore have not been analyzed.

Figures 10.2 and 10.3 show that at the start of the test, there was little acoustic activity. As loading continued, acoustic emission increased slowly. However, this activity was minimal until the specimen was close to failure and was most intense during a period immediately preceding the failure. The length of this high emission period is likely to vary with the mechanical properties of the specimen and with the loading speed.

During this active period, the event rate increases rapidly at first, then dies down just before the failure. At the same time, the energy release rate keeps going up and shows a peak at the failure. The tendency of the energy release ratio, or the average energy released per event is similar to that of the energy release rate. It shows a sharp increase before the failure.

The quiet period of emission corresponds to the perfect elastic phase up to

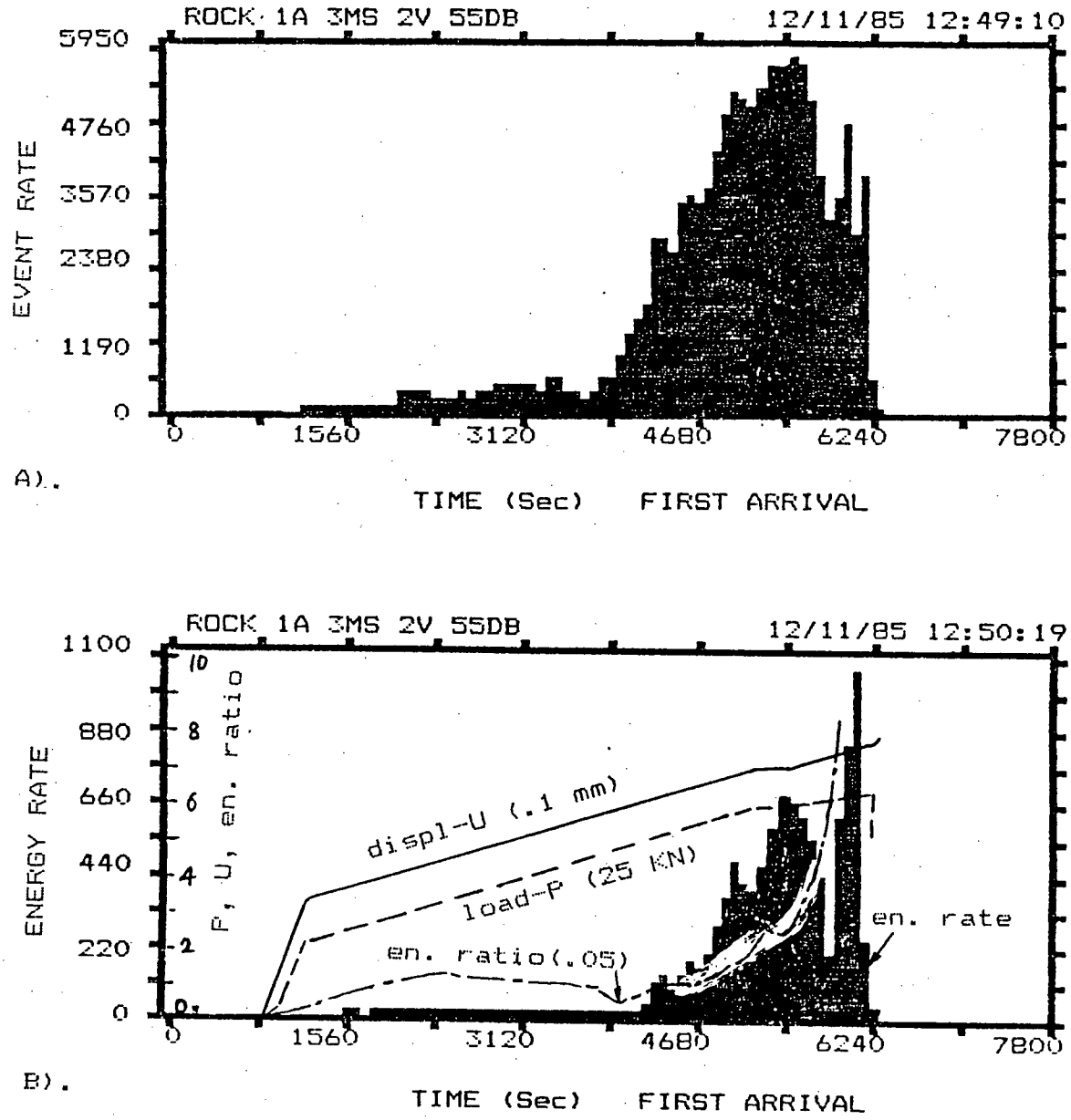

Fig.10.2 Acoustic emission from uniaxial compressive test for specimen #1

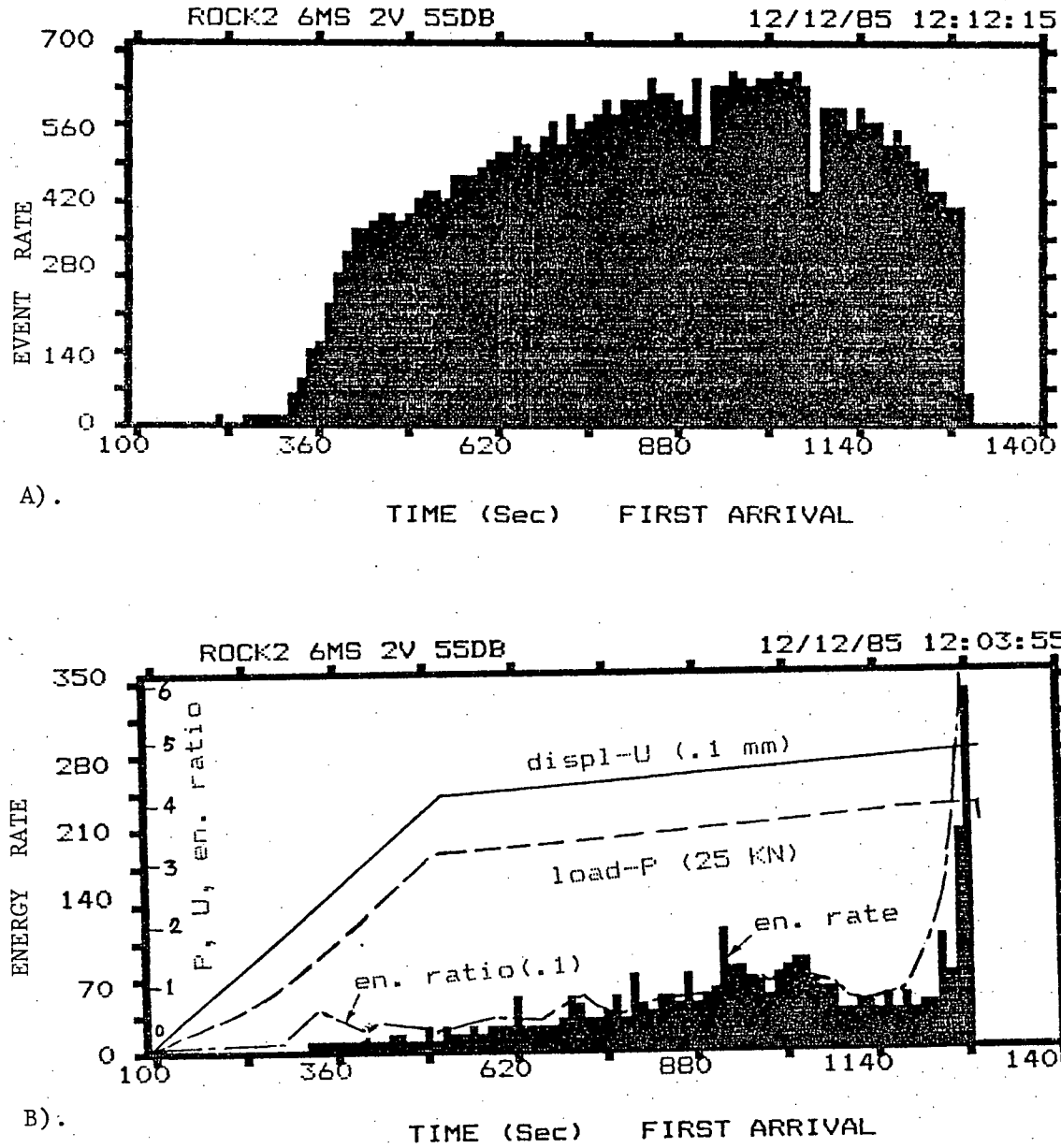

Fig.10.3 Acoustic emission from uniaxial compressive test for specimen #2

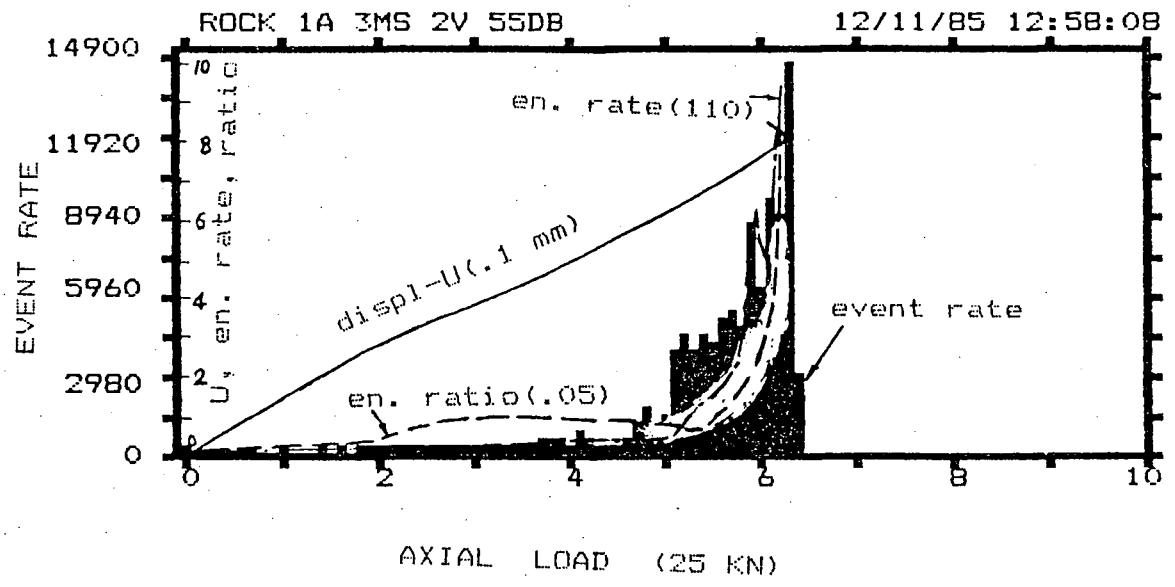

Fig.10.4 Acoustic emission vs axial load for specimen #1

fracture initiation. As fracturing propagates further, acoustic activity becomes more intense. The event number of emission increases accordingly. However, the increase of acoustic energy is not significant because the fracturing is still in micro scale and the vibration of rock particles remains on the low level. When the transition, or crack forking occurs within the unstable fracture propagation, coalescence of micro-fractures leads to the formation of macro-fractures, which join together to form a failure surface, culminating in complete failure of the specimen. During this period, the event number of acoustic emission will decrease due to the coalescence of micro-fractures. But the acoustic energy will increase dramatically because macro-fractures release more energy than micro-fractures. From above results, it may be suggested that prior to rock failure, there is a buildup of acoustic emission and that immediately preceding the failure, the event

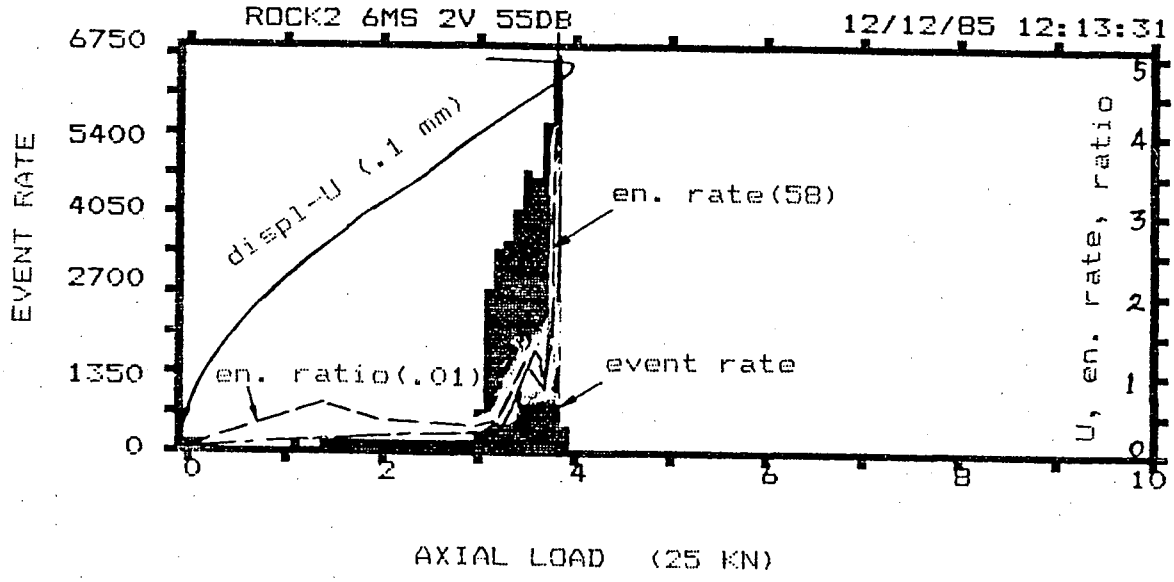

Fig.10.5 Acoustic emission vs axial load for specimen #2

number drops after a sharp increase and the acoustic energy increases suddenly.

Graphs of acoustic emission versus the axial load, figures 10.4 and 10.5, give further indication of the failure process. This data correspond very well to the fracturing mechanism discussed in chapter 3. In these tests, the emissions are negligible when the load is low and increases as loading continues. The acoustic emission increased suddenly at about 71% and 78% of the compressive strength for samples #1 and #2 respectively. At this point, event rate, energy rate and energy ratio all showed a sharp increase. This point may correspond to the beginning of unstable fracturing development. It is interesting to notice that there is a delay between the peaks of the acoustic parameters. The event number shows a peak before the energy release. This may correspond to the

fact that at the fracture initiation, micro-fractures of low energy are formed and as the fracture propagation reaches the unstable stage, the acoustic activity is greatly intensified first by number and then by energy when macrofractures are formed. This phenomenon may provide significant information in analyzing rock noise data measured in field.

During the tests, some peaks of acoustic emission were observed before the failure. False warning evidenced by a buildup of rock noise in field monitoring may be due to this kind of phenomenon. However if the strength of a rock mass is known, and if only those buildups of rock noises at high stress level are considered as warning signals of an impending failure, the reliability of a monitoring system could be adequately improved.

10.3.2. Acoustic Emission from Direct Shear Tests

Three specimens with breakage surfaces and one with sawcut surface were tested under direct shear and at different normal stress levels. Their mechanical properties are listed in table 10.2. Empirical formulae of the shear strength with respect to the normal stress were obtained statistically for these two types of shear surfaces. For both, there is a good relationship between the shear strength and the normal stress, with linear correlation coefficients above 0.96. The surface roughness is accounted for by the friction angle. The sawcut surface is smoother than the breakage surface and consequently has a lower friction angle, figure 10.6.

The basic information of acoustic emission, i.e. event rate, energy rate and

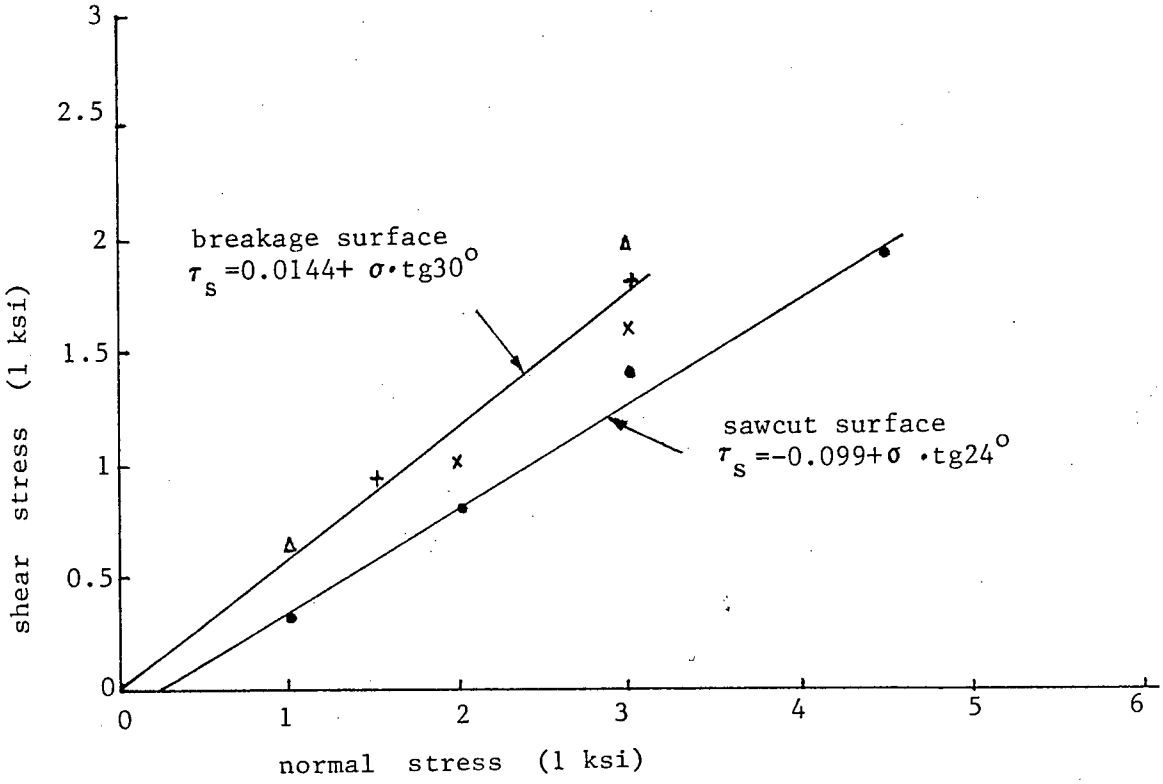

Fig.10.6 Shear strength of sawcut and breakage surfaces

energy ratio, is presented as a function of testing time, figures 10.7 to 10.9 and shear displacement, figures 10.10 through 10.12. Due to problems during the test, information for specimen #6 is not complete and not shown here. Although it was not possible to record the oscillation, the phenomena of stick-slip were observed during the test of the sawcut specimen #4, especially at high normal stress level.

The breakage surfaces were not ideally flat and had some undulations. The shear stress therefore still went up slightly after slip began and the appearance of slip is not very clear, as indicated by arrows in figures 10.7 and 10.8

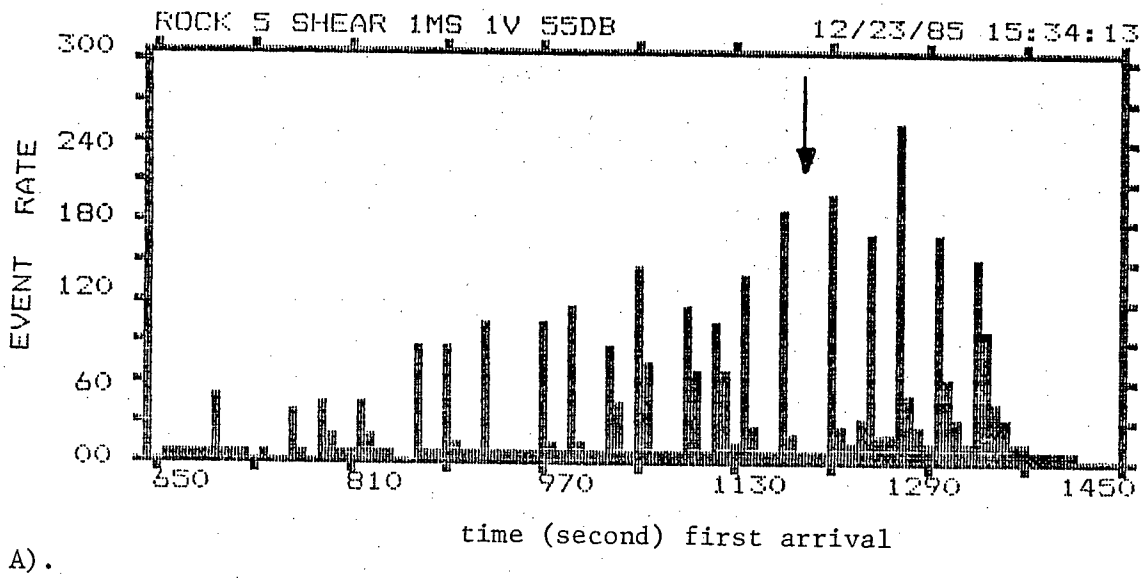

A).

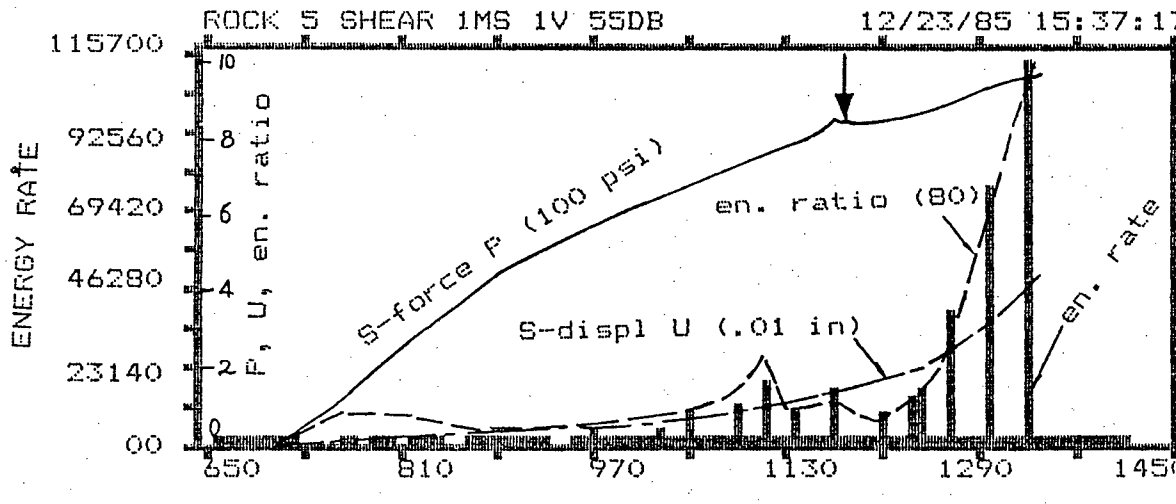

B).

normal pressure 1.5 ksi

Fig.10.7 Acoustic emission from breakage specimen #5 under direct shear test. Arrow indicates the beginning of slip

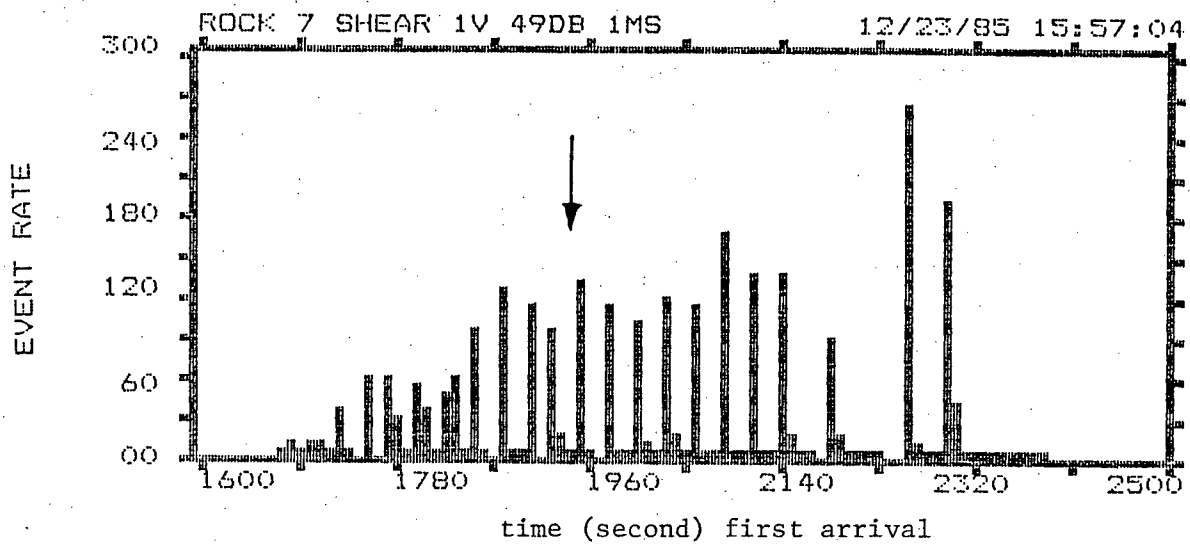

A).

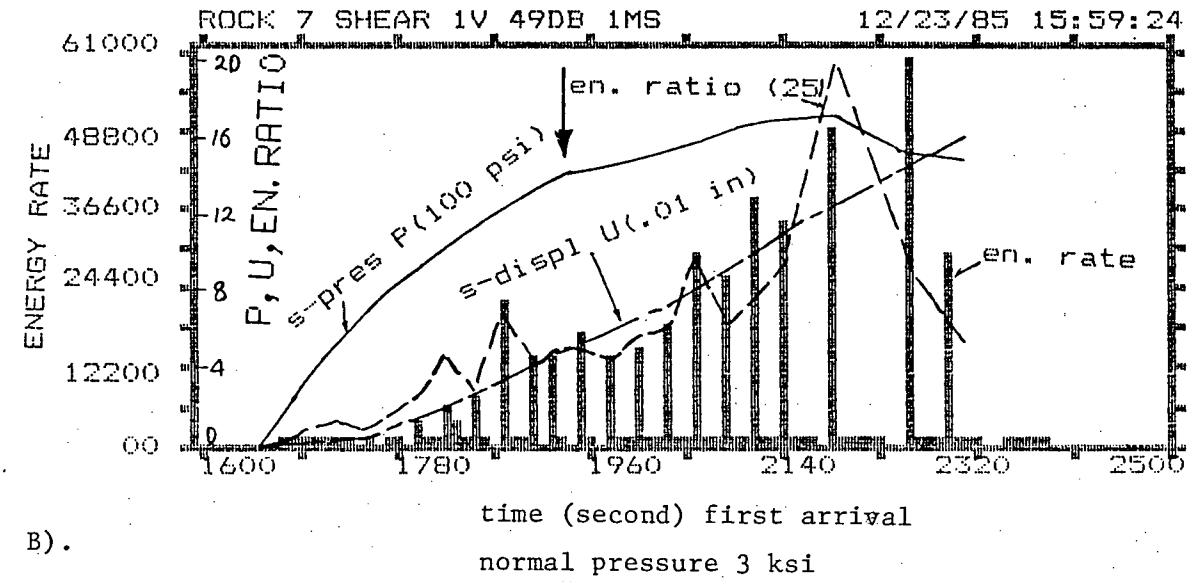

B).

Fig.10.8 Acoustic emission from breakage specimen #7 under direct shear test. Arrow indicates the beginning of slip

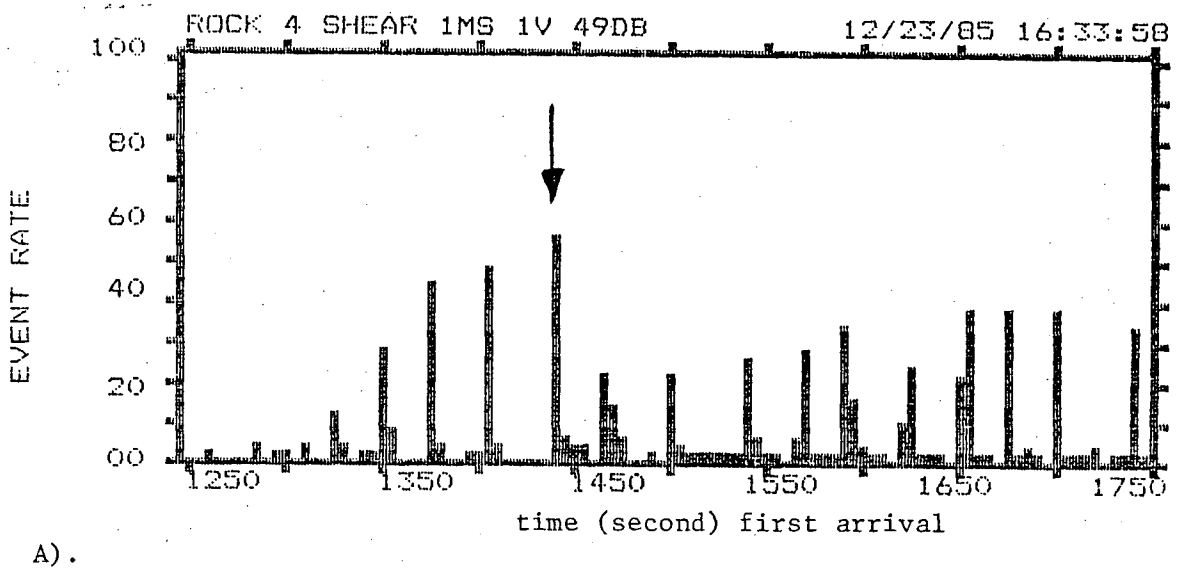

A).

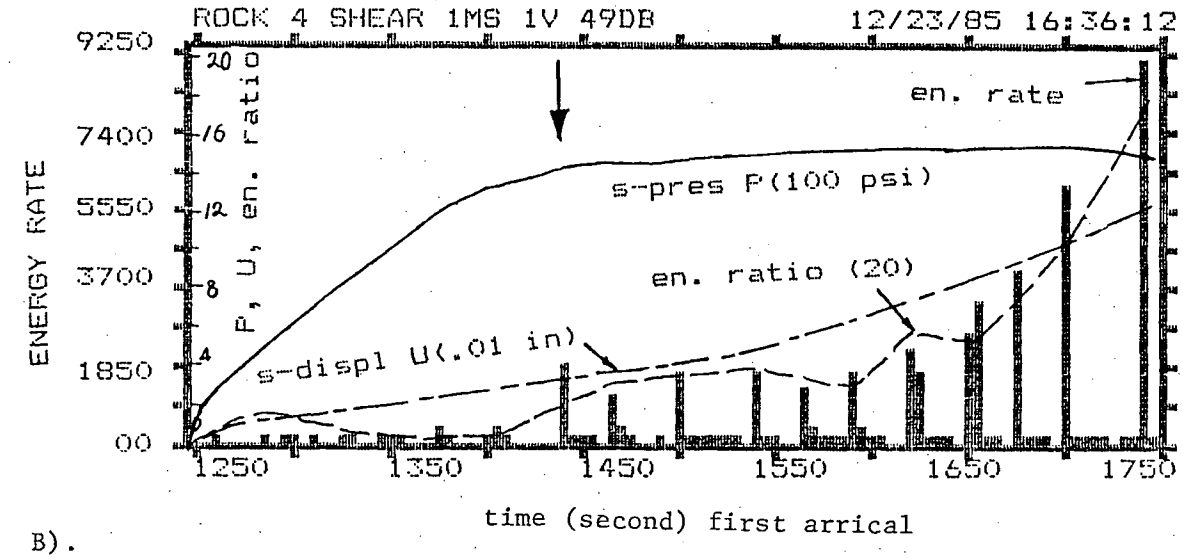

B).

normal pressure 3 ksi

Fig.10.9 Acoustic emission from sawcut specimen #4 under direct shear test. Arrow indicates the beginning of slip

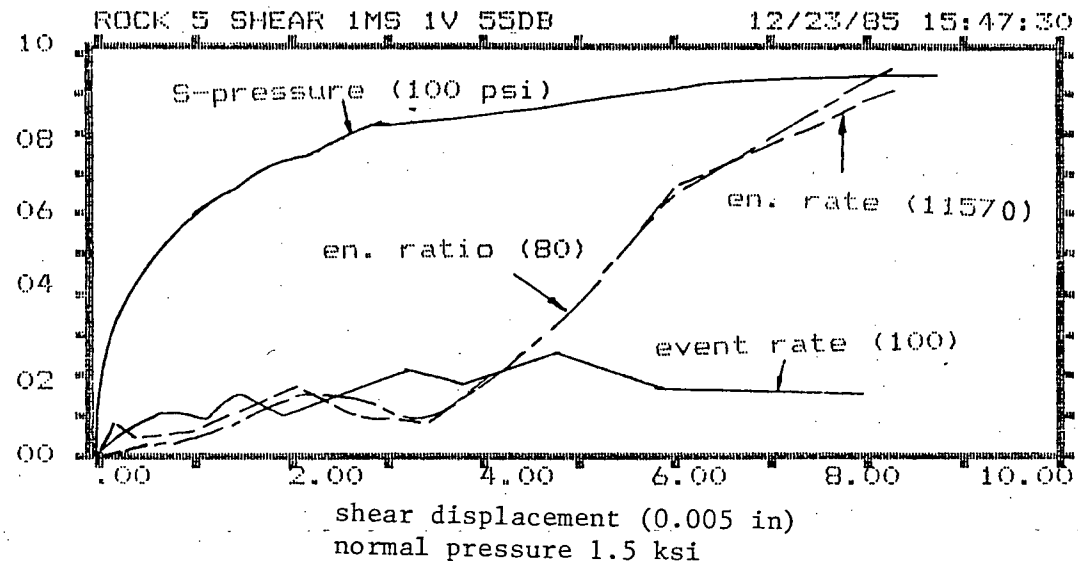

Fig.10.10 Acoustic emission vs shear displacement for specimen #5

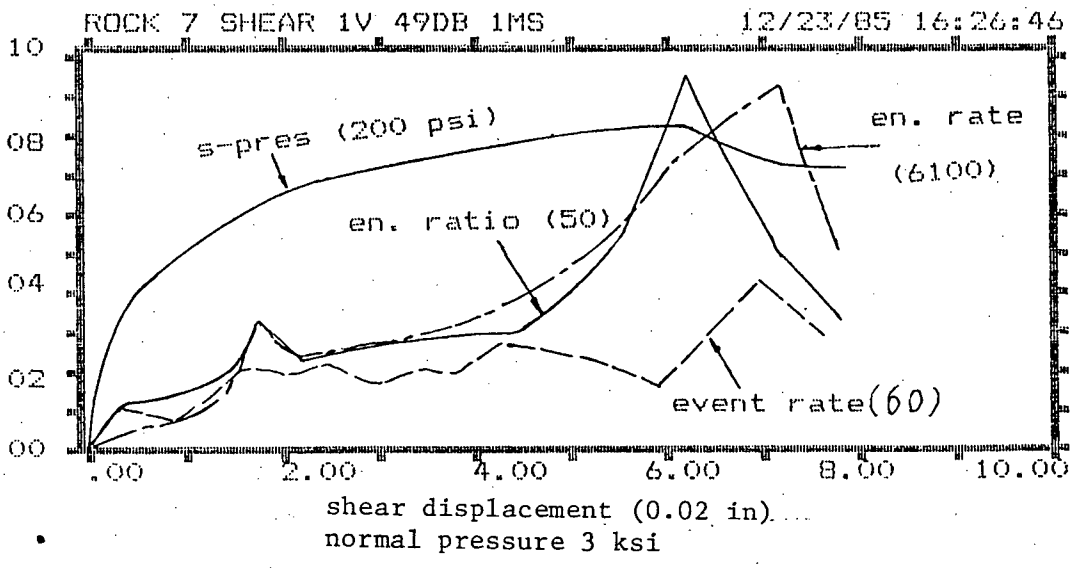

Fig.10.11 Acoustic emission vs shear displacement for specimen #7

At the beginning of testing, there was little acoustic emission. As the test

Table 10.2 Mechanical properties of shear specimens

specimen No.	sawcut surface #4				breakage surface #5		#6		#7	
normal stress σ(ksi)	1	2	3	4.5	1.5	3	1	3	2	3
failure shear stress τ(ksi)	.32	.8	1.4	1.9	.94	1.8	.65	1.97	1	1.6
shear strength τ_s	$\tau_s = -.099 + .45869\sigma$				$\tau_s = .0144 + .58323\sigma$					
friction angle ϕ	24.5°				30°					
standard diviation Sd_{n-1}	$\sigma \pm 1.493$, $\tau_s \pm 0.69$				$\sigma \pm 0.8803$, $\tau_s \pm 0.5342$					
correlation coefficient r	0.99253				0.96117					

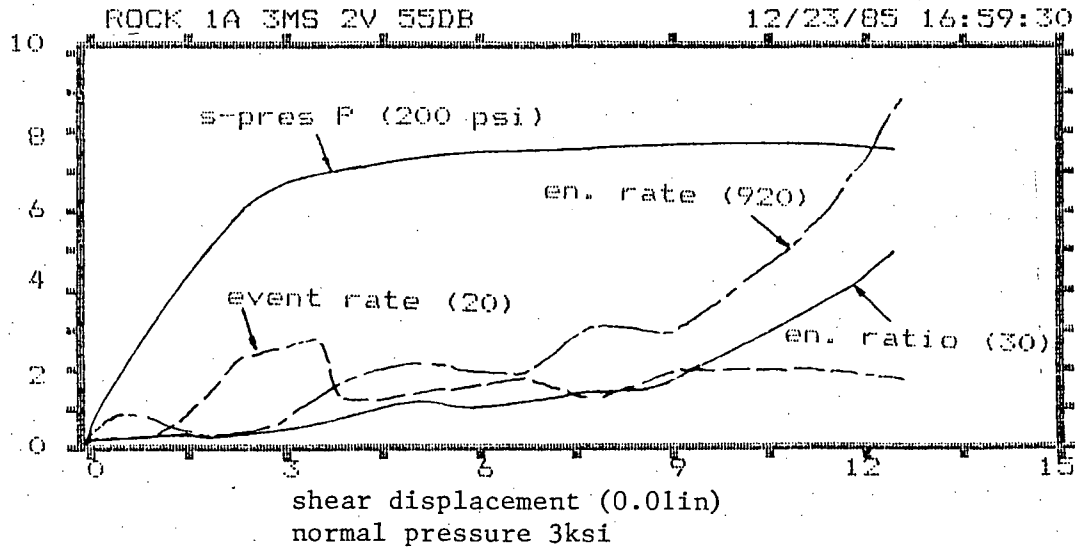

Fig.10.12 Acoustic emission vs shear displacement for specimen #4

continued, event rate began to increase. When slip showed up, event rate reached a maximum value. Then it remained almost constant as sliding went on. However, the energy release rate was very small until slip began and most energy was released during slip as shown in figures 10.7b) and 10.9b). It is interesting to look at the shear displacement and energy release rate. When the rate of displacement, indicated by its slope, increases the energy release rate goes up, especially at the end of each test. This may suggest that acoustic emission is displacement-rate dependent for shear failure as compared with the compressive failure where acoustic emission appears more likely to be stress dependent.

Figures 10.10 to 10.12 show the acoustic emission and shear pressure against shear displacement. Slipping took place when both event rate and energy release reached some critical values. During the slip where shear pressure was almost constant, event rate remained unchanged as for breakage surface, or remained constant at a lower level after a drop as for sawcut surface, and the energy release remained almost constant for a period then went up sharply. This abrupt increase of energy release is due to the increase of displacement rate. This may suggest that if slip rate is constant, the acoustic activity will be unchanged.

The acoustic emission from the sawcut surface is similar to that from the breakage surface. The only difference is that the magnitudes of event rate and energy release for the breakage surface are bigger than the sawcut surface.

During the test, the normal pressure seems to have a significant effect on acoustic emission. As a typical example, the acoustic emission for the sawcut specimen #4 under normal pressure ranging from 1000 to 4500 psi is presented in figures 10.13 and 10.14, which indicate that at low normal pressure, little or even no acoustic activity existed before slip. As the normal pressure increased, acoustic emission in this period became more active. It seems that the normal pressure does not change the profile of event rate very much after slip begins, only the magnitude alters. This can be clearly seen in figures 10.13 and 10.15b).

The normal pressure is also related to the way of slip. A stable sliding at low normal pressure can become stick-slip when normal pressure reaches critical value. Figures 10.14d) and 10.15a) show two significant drops of shear stress at normal pressure of 4500 psi. These drops are accompanied by sharp energy release which are clearly seen in figures 10.14d) and 10.15c).

10.4. DISCUSSIONS

From above results, there seems to be little relationship between acoustic emissions from compressive and shear tests. However, from previous analysis, the failure of intact rock under compression has two stages. The first is a path similar to a conventional compressive test up to the point where a failure surface is first formed. In this path, the failure process is a matter of fracturing development. After this point, the failure path is one similar to that of shear test. Unfortunately, this shear process in the compressive test happens extremely fast and cannot be easily observed. This is because the shear stress

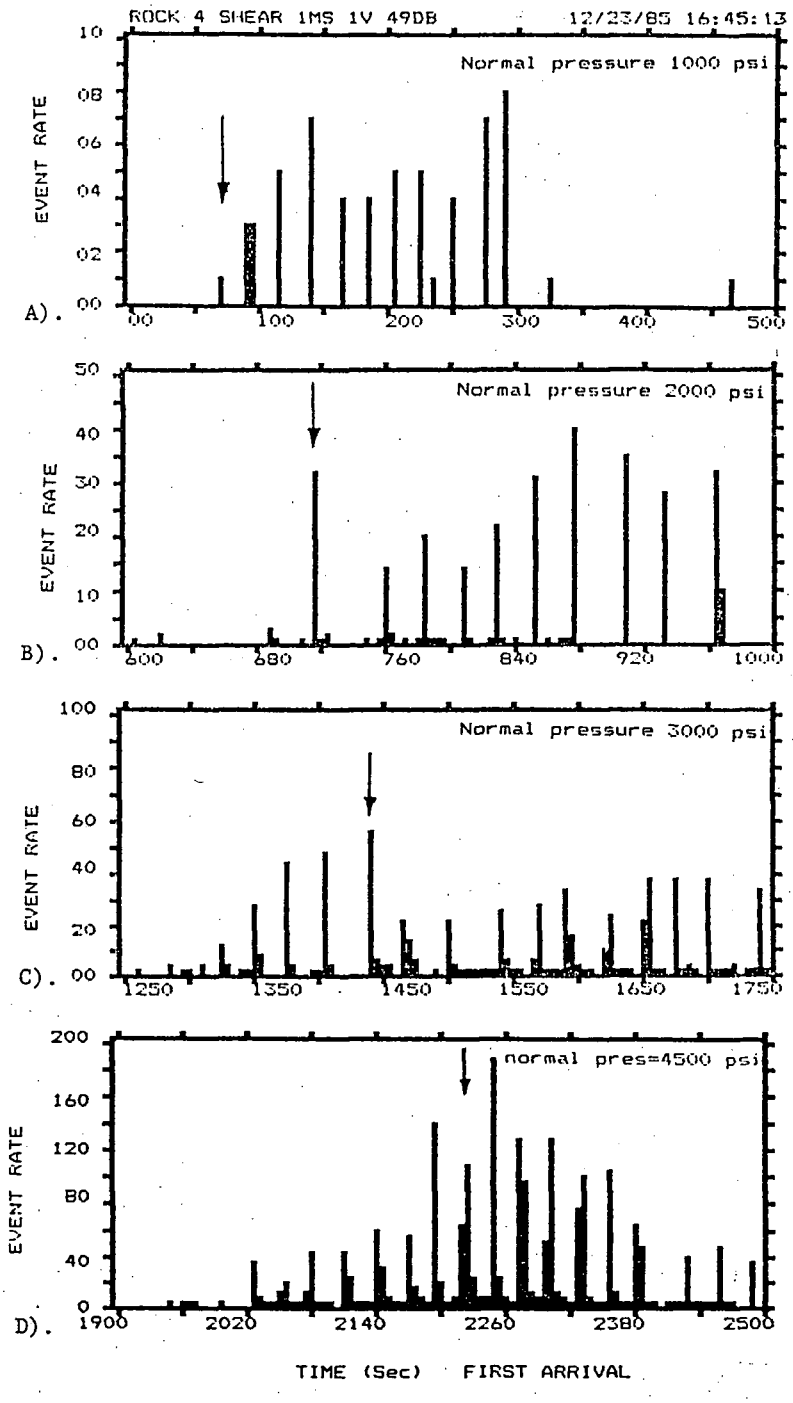

Fig.10.13 Effect of normal pressure on event rate, specimen #4 sawcut surface, arrow indicates the starting of slip

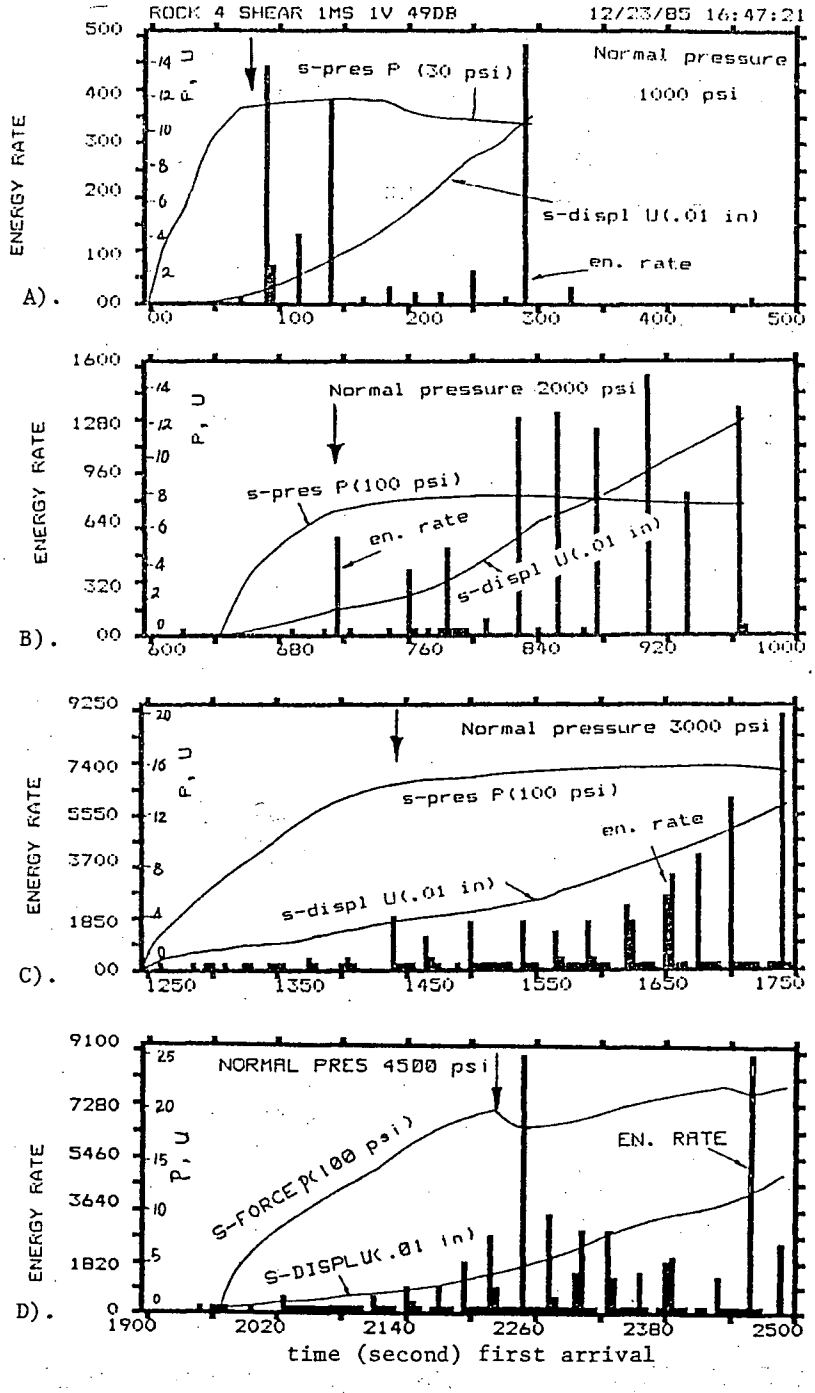

Fig.10.14 Effect of normal pressure on energy release, specimen #4 sawcut surface, arrow indicates the starting of slip

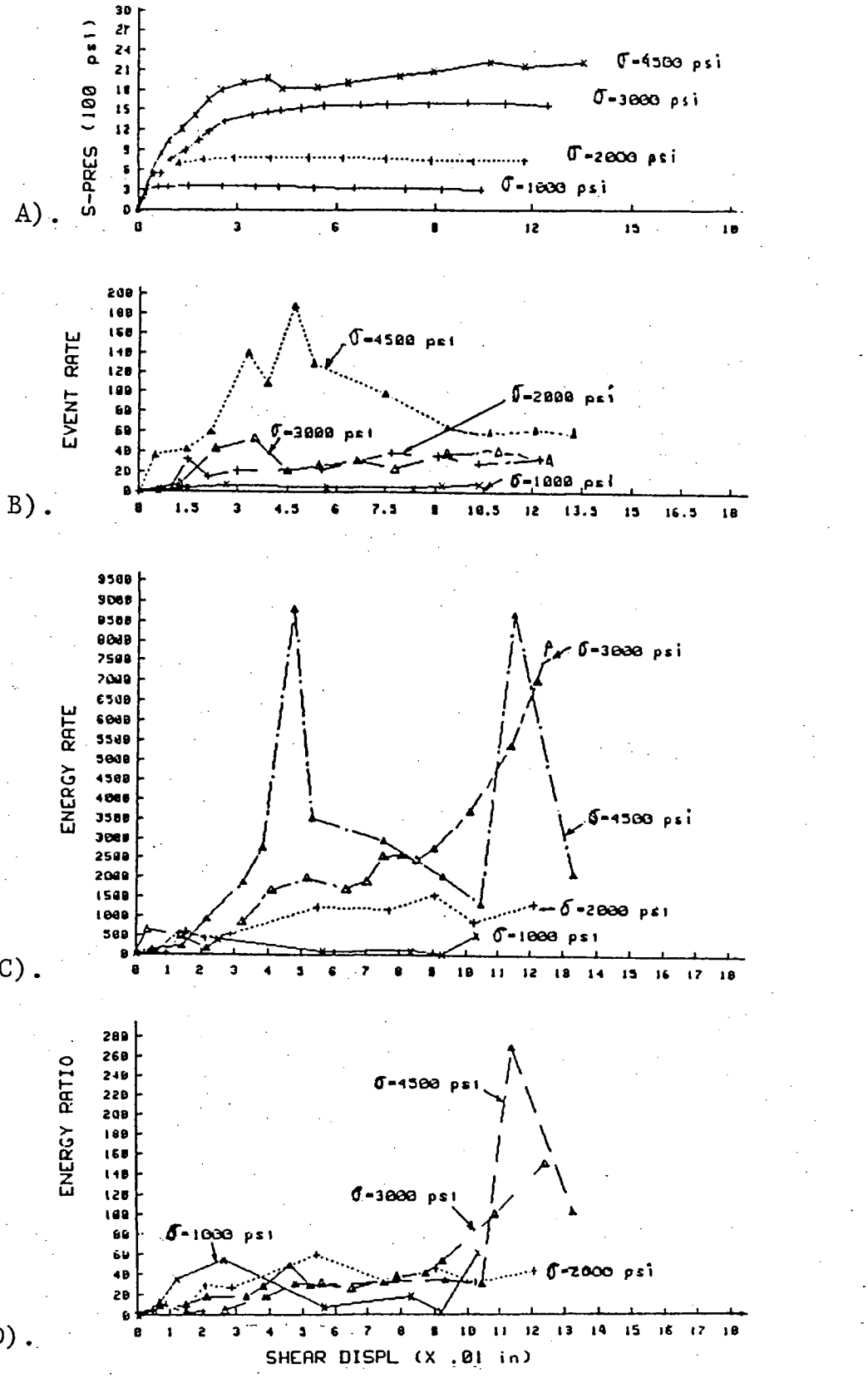

Fig.10.15 Acoustic emission vs shear displacement at various normal pressure, specimen #4

on the newly formed failure surface is much higher than the shear strength. At the same time, the shear strength of the failure surface drops because the normal pressure acting on it may decrease. Therefore, the shear failure occurs immediately once the failure surface is formed.

This means that if a large shear load is suddenly applied to a specimen, the failure will occur extremely rapidly. This has been successfully proven during tests by releasing the normal pressure quickly when the slip began and bursting phenomena were observed. Figures 10.16 and 10.17 illustrate the acoustic emissions for this kind of sudden shear failure. As can be seen, the acoustic emission occurring prior to the slip had been completely shadowed by the peaking up of signals at the instantaneous failure. Because the load is reduced to minima instantly, after shock is hardly observed. Meanwhile, more acoustic activity is expected if the excessive load is higher. From discussions in previous chapters, the acoustic activity is expected to increase with loading speed because high loading speed will accelerate the process of fracture development.

As for the effect of rock type, one specimen of coal and one specimen of potash were tested for comparison. During these tests, load was applied at approximately the same speed. The acoustic results are given in figure 10.18. It can be seen that acoustic emission from the ductile failure of potash is completely different from the brittle failure of coal and granite and it has no evidence of failure at all. Although coal is brittle, its acoustic activity is higher than granite because of more pre-existing cracks. This may suggest that acoustic emission can show clear evidence prior to failure for brittle material but not for

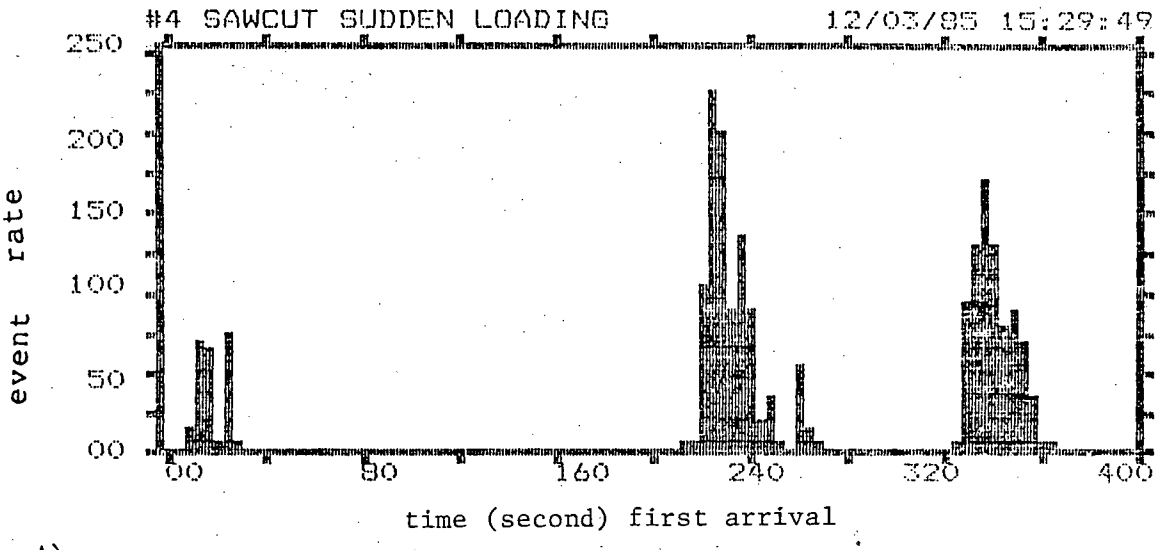

A).

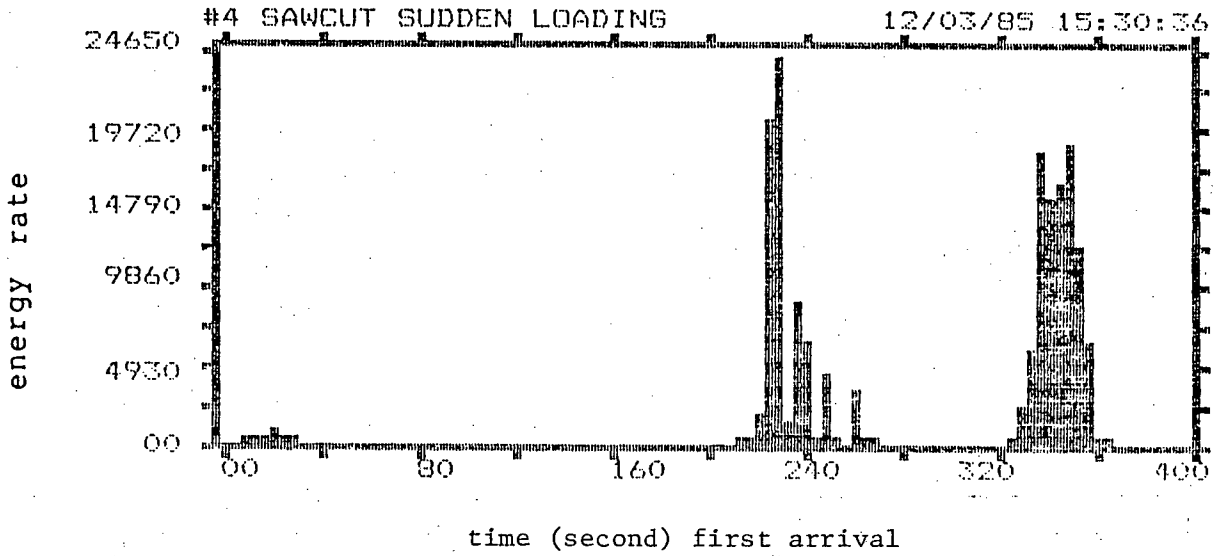

B).

Fig.10.16 Acoustic emission from sawcut specimen at sudden shear loading, by releasing normal pressure at 1, 2.5 and 4.5 ksi level, respectively

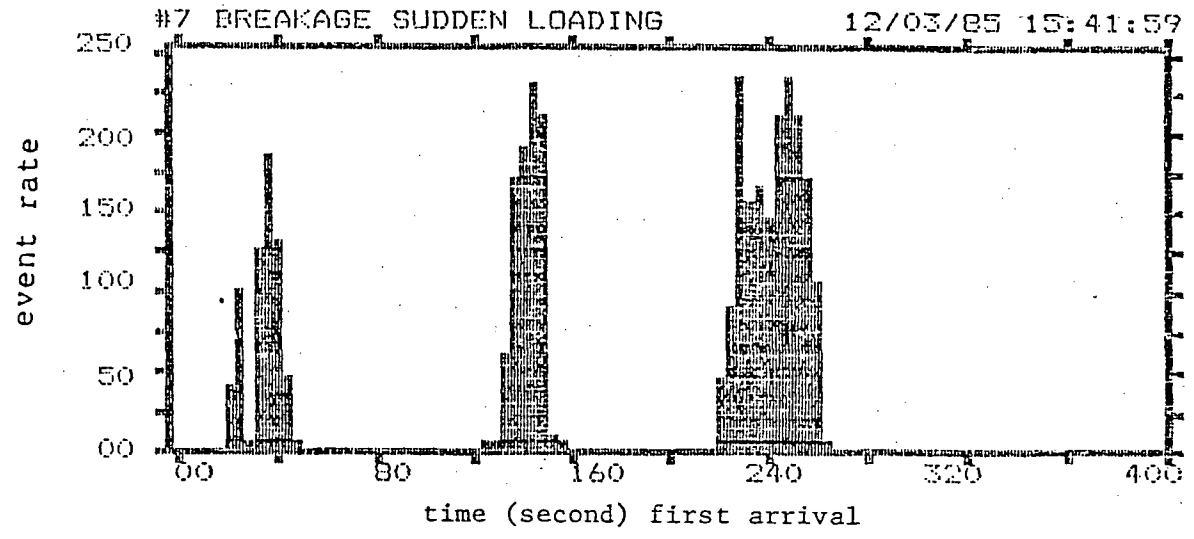

A).

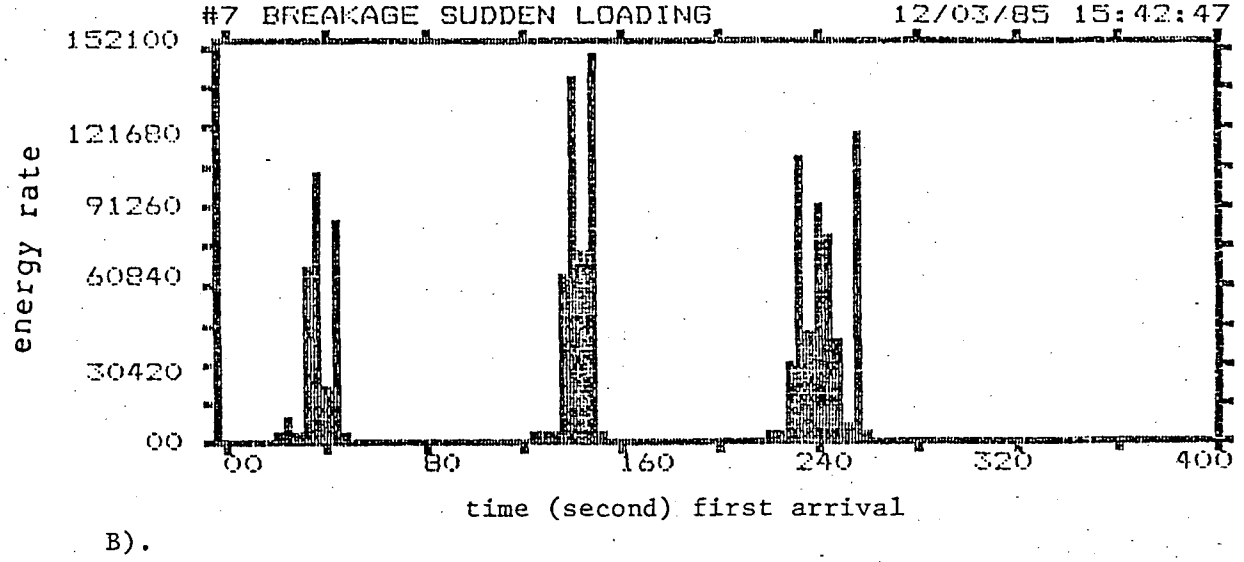

B).

Fig.10.17 Acoustic emission from breakage specimen at sudden shear loading, by releasing normal pressure at 1, 2.5 and 4.5 ksi level, respectively

ductile material.

10.5. SUMMARY

A limited number of rock specimens were tested under the availabl resources. A few important points may be noted from the testing results.

For the uniaxial compressive test:

1. At the beginning of loading, acoustic emission was very low. This corresponds to the period of perfect elasticity during the brittle failure.
2. As load reaches some value, say 71%-78% of the compressive strength for the rock tested, acoustic emission begins to build up quickly, in response to

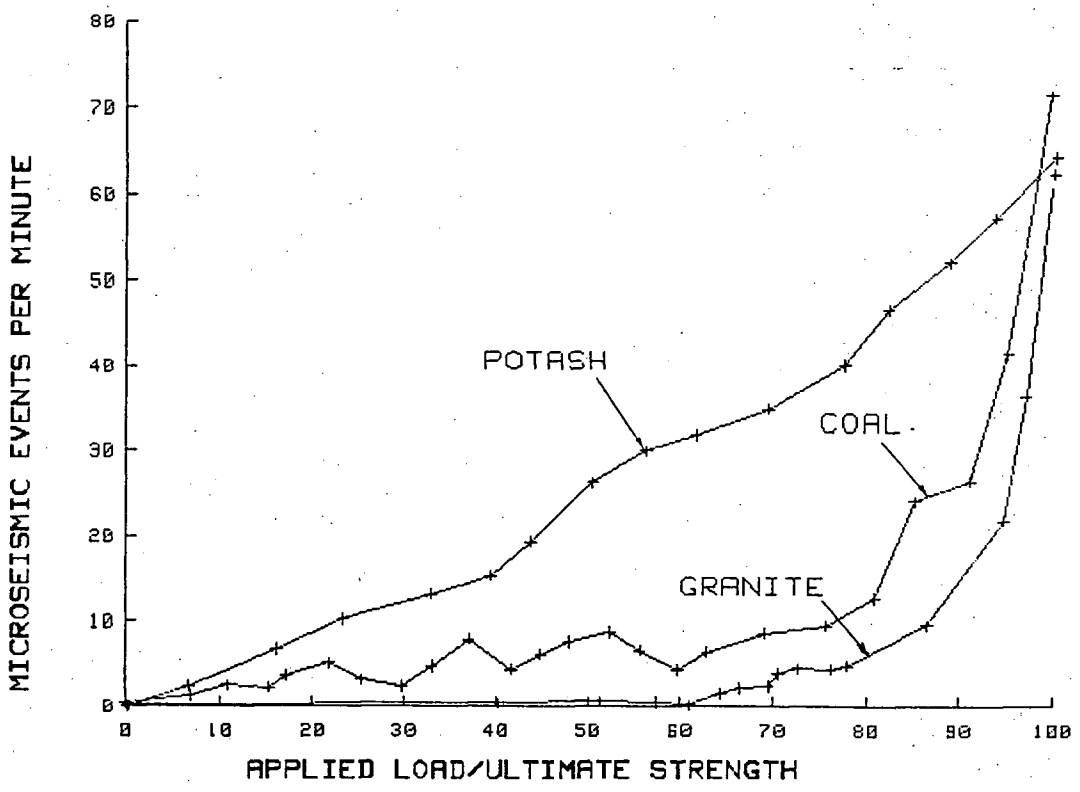

Fig.10.18 Effect of rock type on acoustic emission

the onset of unstable fracture propagation and is most active in a period immediately before the failure, during which fractures develop rapidly.

3. During this active period, if displacement rate is constant, the event rate goes up initially, then drops preceding the failure. However the energy release keeps increasing and shows a peak at failure. This may be due to the fact that as failure is approached, events become bigger in magnitude because of the formation of macro-fractures.
4. There is a short delay between buildups of event rate and energy release, with event rate increasing first. This is probably because microfractures develop first, which then join up to form larger fracture zones.
5. During the ductile failure, acoustic emissions do not show above signals.

For the direct shear test:

6. At low stress level, there is little acoustic emission. When slip begins, acoustic activity reaches a critical level and remains more or less constant.
7. Most energy is released during slip.
8. During slip, the event rate remains constant, but energy release rate rises sharply towards failure, which is accounted for by the increase of shear displacement rate. It may suggest that acoustic emission in shear mode is more displacement-rate dependent than stress dependent.
9. Roughness of shear surface does not change the pattern of acoustic emission very much. However the magnitude of emission for breakage surface is much higher than for the sawcut surface.
10. In stick-slip, each slip is accompanied by a drop of shear stress and an increase of energy release, then followed by a drop of acoustic activity.

Effect of normal pressure on acoustic emission in shear test:

11. At low normal pressure, little acoustic emission exists before the onset of slip. At high normal pressure, emission becomes more active in this period. It is probable that a macro-failure is a combination of many local micro-fractures, each of which initiates at some local point. The higher the normal pressure, the more local micro-fractures initiate.
12. After slip begins, normal pressure seems not to change the pattern of acoustic emission, except for increasing the magnitude.
13. Normal pressure may change the way of slip. A stable sliding at low normal pressure may become stick-slip at higher normal pressure given other conditions. This agrees well with the transition conditions described in chapter 7.

CHAPTER 11. PRECURSORY SIGNALS IN COMPARISON WITH FIELD MEASUREMENTS

11.1. GENERAL

In order to verify the acceptability of acoustic results from laboratory tests, a comparison will be made with some field measurements. In field monitoring, it is well established that a rockburst is usually preceded by a sharp increase of microseismic activity. However, the reliability of prediction of an impending failure based on a sharp increase of either of event rate or energy release rate is poor because few successful predictions have been achieved in the past. In some mines, the introduction of spectrum analysis of seismic waveform has increased the reliability [17]. Unfortunately, seismic data of potential successfully predicted rockbursts are very rare and in fact are only available from some South African mines.

11.2. PRECURSORY SIGNALS IN THE LABORATORY TESTS

During the laboratory tests of this research, a limited number of rock specimens were tested under the available resources. The testing results have shown some ignificant phenomena. The acoustic emission is very low until some time prior to the final failure of the specimens. During the acoustically active period, the event rate increases sharply at first, then decreases immediately preceding the failure. Simultaneously, the energy released increases steadily and peaks abruptly at failure, figures 10.2 to 10.3. The sharp increase of energy released appears to lag the event rate. This has been described in detail in the previous chapter. The most important fact is that a sharp increase of the event number alone can

not indicate an impending failure but the simultaneous peak up of energy rate or energy ratio will be critical for violent rock failure.

11.3. PRECURSORY SIGNALS IN FIELD MONITORING

In microseismic monitoring of rockbursts, precursory signals are also observed. The acoustic signals are recorded as event number and energy release. A single event may mean little, but a number of events occurring successfully can indicate a "hot spot" where violent failure will take place [16]. To predict violent failure, however, the energy released has to be considered and precursory signals are needed.

11.3.1. Precursory Signals prior to Rockbursting

It is found that a sharp increase of the event rate alone is not enough to predict a rockburst [21]. To improve the reliability, better ways of data analysis have to be found and the technique of data acquisition needs to be improved. Seismic events can however be distinguished by their magnitudes [23,25]. At the beginning of fracture development, an event has small magnitude. As failure progresses, the event magnitudes increase due to the formation of macro-fractures. Therefore, in addition to the sharp increase of acoustic events, the event magnitude should also be examined in judging an impending failure.

With the introduction of the technique of recording seismic wave forms, the frequency spectrum of the events has been analyzed in some mines. It is found that the pattern of seismic waves varies at different stress levels and therefore the waveform frequency distribution of the waveform should change as

failure is approached. In some cases, a characteristic parameter---the corner frequency, which will be discussed later in this chapter, is also found to shift to the lower band prior to a rockburst. In laboratory experiments, Scholz [23] and Savage et al [24] observed that microfracture propagation is the mechanism responsible for the high-frequency events and the audible events at failure have lower frequency. When the waveform frequency distribution, the increases of event rate and energy released are all considered, the ability to predict rockbursting has been greatly improved in some cases. In particular, it is found that when the pattern is established where the event energy is increasing and at the same time the corner frequency is shifting downwards, a violent rock failure can beexpected. Experience is still being obtained in interpreting the results in order to predict precisely when a failure will take place. The pattern of the rate at which acoustic events are emitted appears to be irrelevant.

11.3.2. Typical Examples

In a South African mine, some useful precursory signals were recorded prior to rockbursts [17]. Two case examples are copied in the following.

Example 1: rockburst on May 15, 1983

A large rockburst (magnitude 3.4) occurred on 101W1 panel, No.3 shaft, on May 15, 1983, at 03h37. A concentration of microseismic events is apparent. In figure 11.1, the number of microseismic event per hour originating from the panel for the period 8th to 18th May, 1983 is plotted. A steady increase can be seen, from approximately 60 events 6 days before the burst to almost 300 events only 24 hours beforehand. A sharp drop in the rate of microseismic activity was measured immediately before the burst. For in this particular case, the change in the ratio between numbers of larger and smaller events provided the researchers with

additional information to make a reliable prediction.

Example 2: Rockbursts on October. 4 and 10, 1984

On October 4, a 2.6 magnitude rockburst occurred during shift time (10h31) on 110 level. Figure 11.2 shows the event rate, the average corner frequency and average event energy as observed from that area for the time window 22h00 to 04h00 every night. The symbol B indicates a blast during the previous afternoon. On September 27, inference from an external source made the measurement unreliable. On the the basis of event rate alone the rock burst would not have been anticipated on October 4th, as the event rate parameter is very sensitive to the mining activity and no blasting took place in that area the previous afternoon. However the corner frequency showed a steady drop for the preceding 11 days and a further drop to below 600 Hz was indicated a few hours before the burst. This behavior of the corner frequency gave a clear precursory indication of a pending rockburst. The average event energy conformed to what was expected and the rockburst occurred at a relatively high energy level.

5 days later, regular blasting started and was followed by a small rockburst (magnitude 1.4) at 4h39 on October 10th. Again a relative low corner frequency and a relative high event energy preceded the burst. The blasting the previous afternoon made the event rate unusually high.

11.4. COMPARISON

There is a correlation between precursory acoustic signals recorded in laboratory tests and the field monitored data in example 1. In both cases, the event rate increases sharply at first and drops immediately preceding the failure. The abrupt increase of the event energy corresponds with an abrupt increase of the ratio

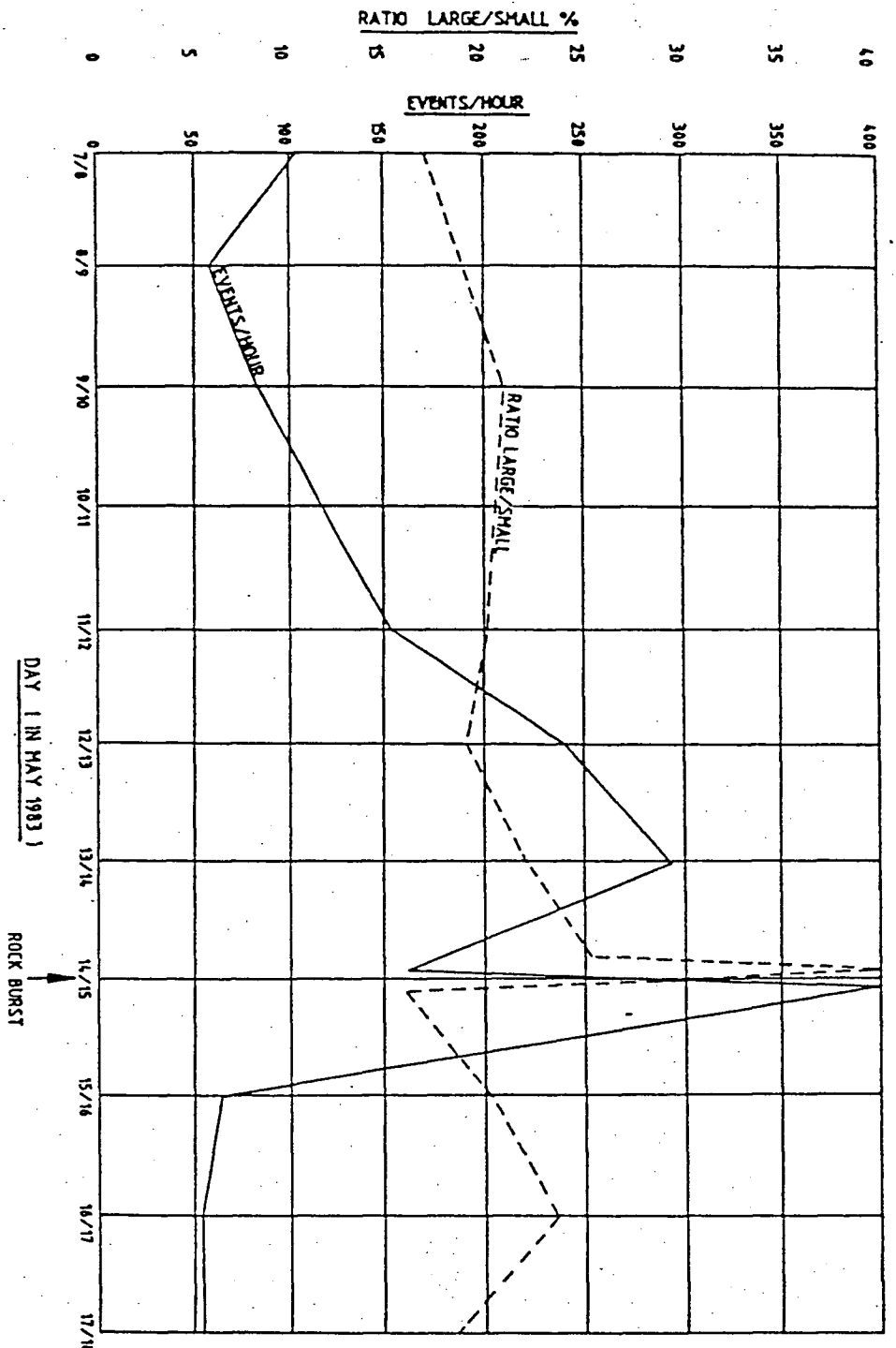

Fig.11.1 Microseismic event rate and relative energy plotted for one week before and three days after the May 15 event (after Brink et al, [17])

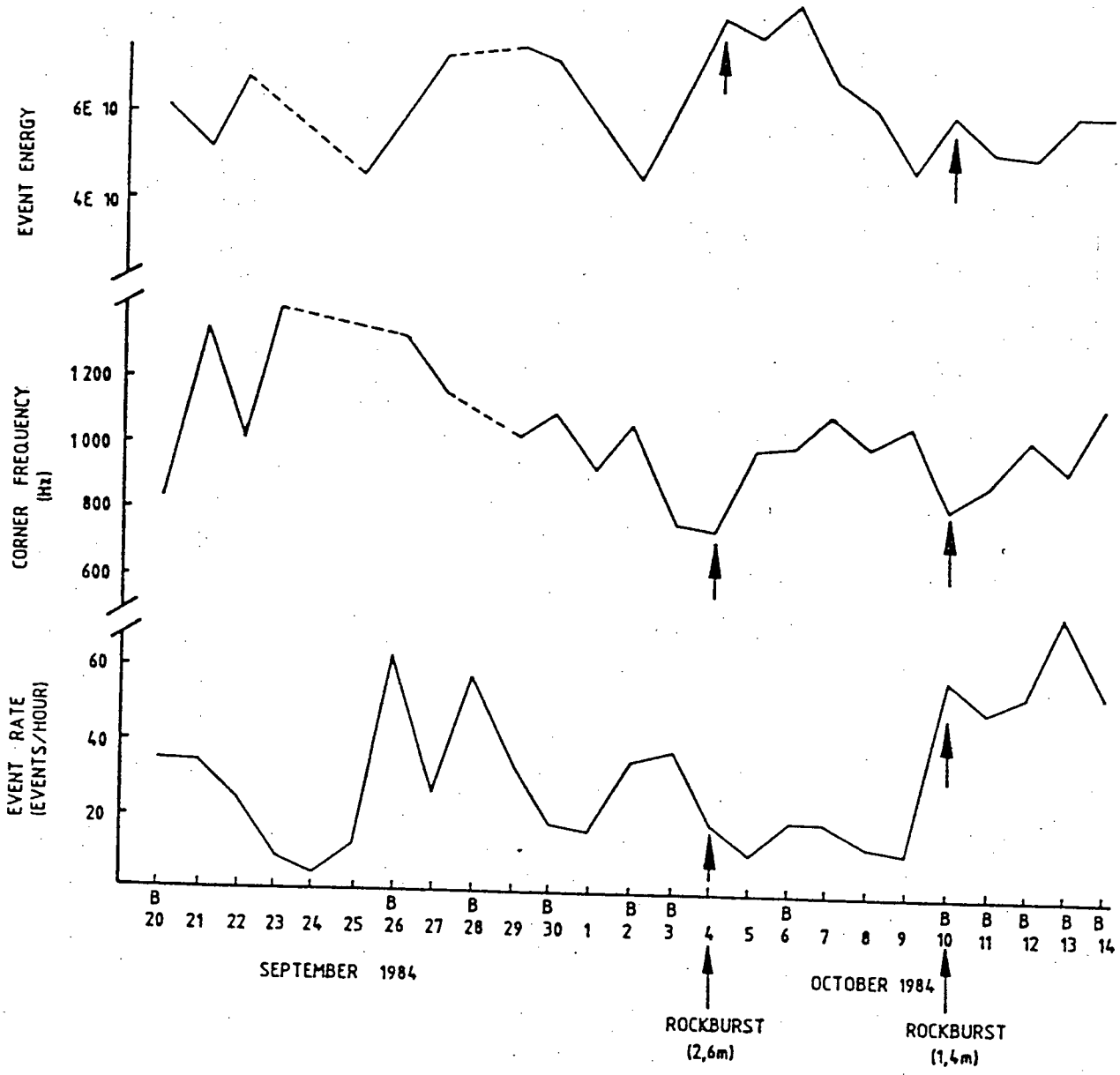

Fig.11.2 Event rate, corner frequency and event energy measured over a period of 25 days, covering two rockbursts (after Brink et al, [17]).

between the numbers of large and small events. This is because, according to the fracturing mechanism discussed in chapter 3, the increase in this ratio is due to both the decrease in smaller events and the increase in larger events. Larger events correspond to the development of macro-fractures, which release more energy.

In example 2, the behavior of event rate and energy release prior to the rockbursts are generally in agreement with laboratory tests prior to the specimen failure. The event rate drops after a sharp increase. The energy release continues to increase and shows a peak value at failure. Exception is the rock burst on October 10th, when the blasting the previous afternoon caused the unusual high event rate.

In the 2nd example, the corner frequency, which is introduced as another precursory parameter, shifts to a low level as a burst occurs. The corner frequency is usually defined as the frequency corresponding to the intersecting point of the two asymptotes on the spectrum diagram [41,50]. Figure 11.3 shows a schematic seismic spectrum [5], f_0 being the corner frequency. It can be seen from the scheme that at low frequency band $f \leq f_0$ the amplitude spectrum is level, and at high frequency band $f > f_0$, the spectrum decays. This means higher frequency corresponds to lower magnitude. Because smaller events have lower magnitudes, figure 11.3 indicates that normally, small events are characterized by high frequency and large events by low frequency [23,24].

When f_0 shifts to the lower band, the high frequency amplitude decays

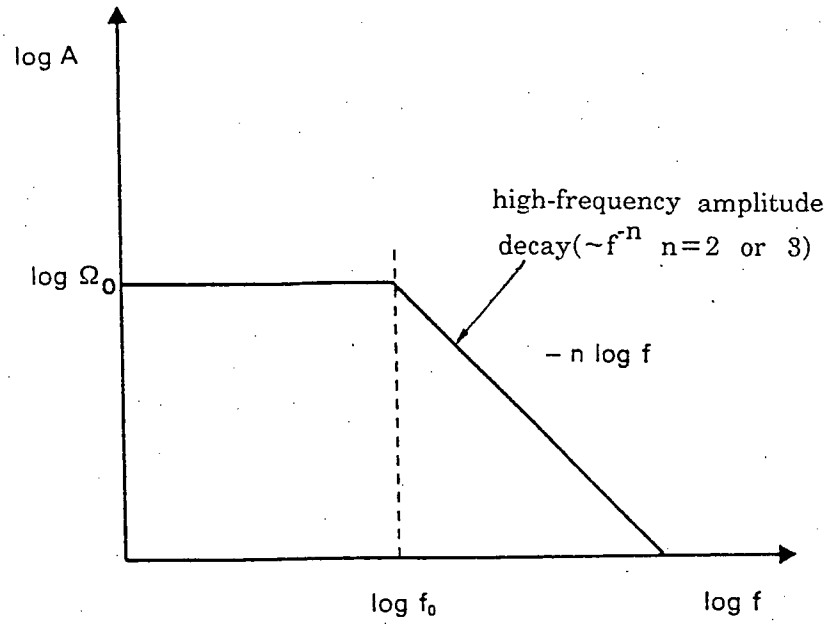

Fig.11.3 Schematic seismic spectrum, clarifying: low-frequency amplitude level, corner frequency (fo), and high-frequency amplitude decay (after Bath, [51])

much more. Thus fewer events occur at the high-frequency band and more events occur at the low-frequency band, which is characterized by large amplitude. Therefore with the decrease in the corner frequency, more energy is released. This is in agreement with the top curve in figure 11.2

Meanwhile, many years of observation of seismic events has found an inverse relation between the number of events and their magnitudes [17,43]:

$$\log N = a - bM \quad \text{..... (11.1)}$$

where N is the number of events of magnitude $\geq$ M,

M is the magnitude of event,

a and b are constants, with $b>0$

This is illustrated in figure 11.4. Notice the difference of the scale on the two axes. A small increase of M can result in a great decrease of N. Therefore when the event amplitude increases, which is accompanied by the down-shift of the corner frequency, the event number during that period decreases sharply. Thus the event rate appearing on the recorded data drops accordingly. This is indicated in the first rockburst at the bottom curve of figure 11.2. The unusual high event rate in the second rockburst is caused by blasting. Therefore the down-shift of the corner frequency agrees with both the decrease of the event rate and the increase of event size or more energy release.

It can be seen from above examples that the laboratory results are generally similar to the measurements made in the field. Violent rock failure is preceded by intense acoustic activity. The event rate will increase sharply and may decrease preceding the failure. Simultaneously, the energy release rate and ratio will increase abruptly at some critical level, indicating an impending failure. In fact, research by Scholz [23] and Mogi [25] have showed that laboratory acoustic emission is similar to earthquakes.

11.5. SUMMARY

In this chapter, the precursive phenomena of acoustic emission observed in laboratory tests are compared with measurements made in the field. From the above discussion, these statements can be made:

1. Acoustic emission can be used as a precursive signal for violent failure of rock mass in laboratory and in field.

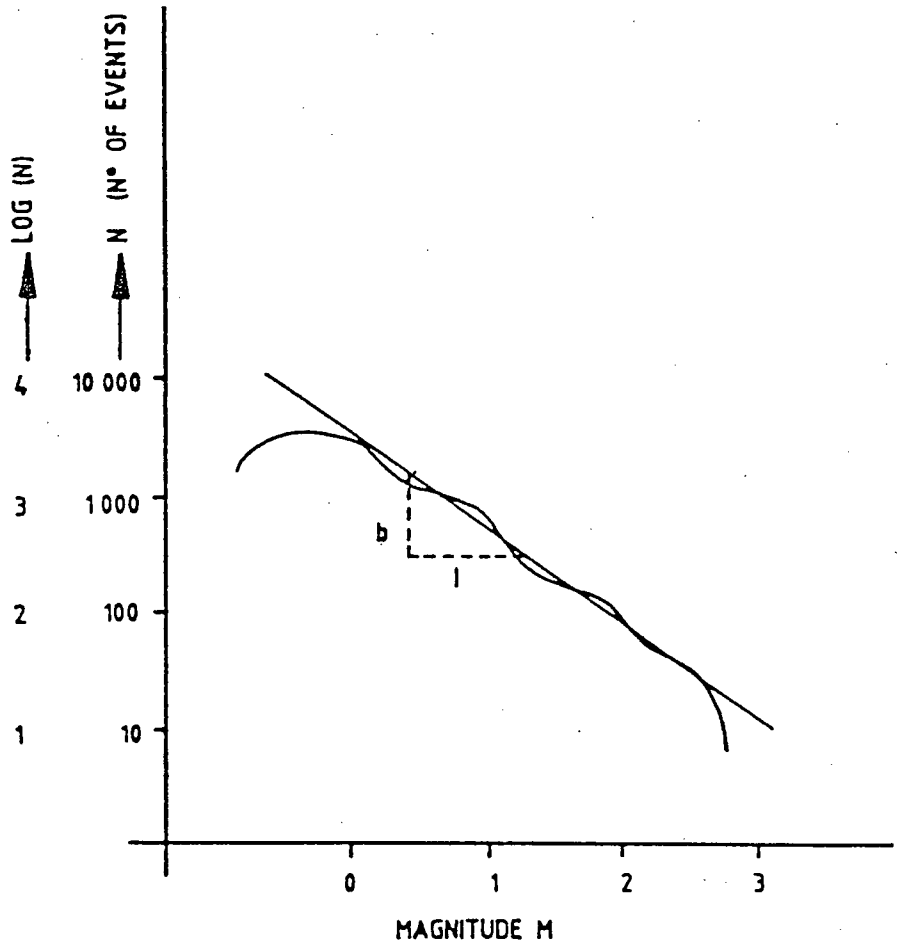

Fig.11.4 The relationship between size and number of seismic events. The wavy line shows measured typical data. The straight line is a best fit of the form $\log N = a - bM$ (after Brink et al, [17])

2. Before the violent failure, the event rate increases sharply, usually followed by a drop immediately preceding the failure, and at the same time, acoustic energy increases steadily and shows a peak at the failure.
3. The most significant effect measured in the field is that the corner frequency usually decreases prior to the failure. This is found to be associated with the previous facts.
4. Precursive signals monitored in the laboratory tests can be related to violent rock failure in the field. When compared with field measurements, a

similar pattern of acoustic emission is observed, and these may be universal phenomena preceding specimen failure and rockbursts.

Most microseismic monitoring systems used in the field today cannot carry out the spectrum analysis. Data is usually displayed as event rate and associated energy release. Reliability in predicting an impending failure can be improved if the phenomena of decreasing corner frequency and increasing emitted energy are taken into consideration.

CHAPTER 12. NUMERICAL SIMULATION OF ACOUSTIC ACTIVITY AT ROCK FAILURE

Because the testing results of acoustic emission were obtained on a limited number of specimens and actual rockbursts predicted are very rare from field studies, the behavior of acoustic emission taking into account other factors that may affect it is still not clear. Therefore it is hard to say if the precursory signals obtained above are universal phenomena. In order to obtain a better understanding of acoustic emission behavior and to verify the acceptability of the above results, a numerical model based on the seismic model by Burridge [43] is developed to simulate acoustic emission under various conditions.

This model is unique and no evidence of similar work has been found. Usually modelling means to simulate a phenomenon or an event according to a given set of relationships of that event. There is however no physical law or empirical formula available for the acoustic emission of rock. This model is entirely based on the proposed stick-slip process.

12.1. MATHEMATICAL MODEL

As described earlier, rockbursting can be considered as a kind of violent failure of the nonhomogeneous anistropic rock mass. Before the strength point, the failure process is a matter of fracture development beginning at some stress level. A macrofailure starts from some local microfractures. At any stage of the fracture process, such as at the beginning, during fracturing, or during slipping, any movement of rock particles at a local area will induce vibration among the surrounding rock particles. It is this vibration which generates acoustic signals

and it is by this means that the seismic energy is radiated.

In the same way as with other numerical methods in stress-strain analysis, the finite element or boundary element method, the rock mass is discretized into individual elements. The continuous system of the rock mass is represented by a discrete system of individual particles.

Because the shear process takes place on the contacting surfaces, the movement occurs only on the failure plane. Besides, two variables are enough to describe an exact location in a plane. This model is not however involved in the exact description of location of an element. Only the behavior of an element during the movement is of interest, so only one degree of freedom is needed for the model.

This model is a multi-particle shear system and is a combination of many simple shear models presented in chapter 6. It consists of a series of particles connected together by weightless springs, figure 12.1. The mass of the material is concentrated on the individual particles and the spring represents the elasticity of the rock mass. The driving force is applied at the end of the last particle from a support which moves at speed V.

Let the mass of particle i be M_i, the stiffness of spring i be λ_i and the distance between adjacent two particles be a. Further assume that at the beginning, all particles are at rest, with particle N at the origin of the coordinate system shown in figure 12.1a) and all springs are unstressed except

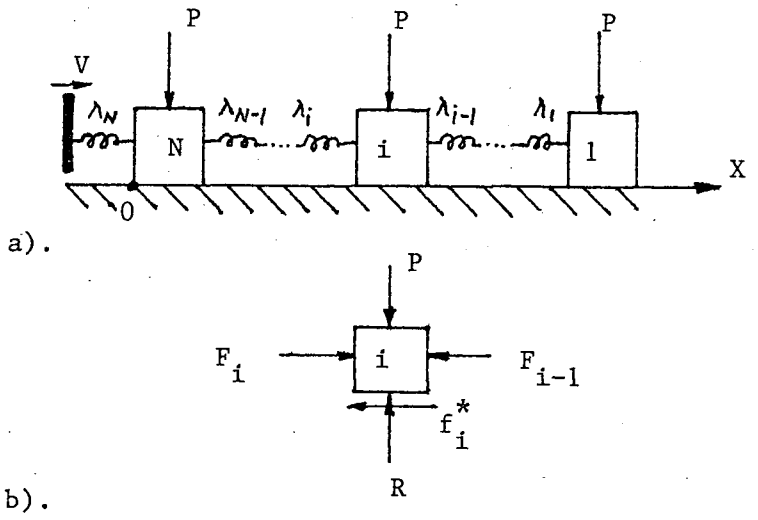

Fig.12.1 Diagram of acoustic activity model

the last spring N. Then the initial conditions of position and speed of each particle are

$$\begin{cases} X_i(0) = (N - i)a \\ \dot{X}_i(0) = 0, \quad i=1, 2, \ldots, N. \end{cases} \qquad (12.1)$$

Because we are interested in the slip behavior of the whole system of the model, we further assume the driving support has moved a distance ξ_0 at t=0, or the driving force in spring N has reached the static friction of particle N:

$$\lambda_N \xi_0 = f_N(0) = C + \mu_s \sigma, \text{ or}$$

$$\xi_0 = (C + \mu_s \sigma)/\lambda_N \qquad (12.2)$$

where f(0) is the static frictional resistance,

μ_s is the coefficient of static friction,

σ is the normal stress.

Therefore at any time t, the motion equation of particle i can be obtained by the equilibrium of forces acted on that particle, as in figure 12.1b), in the horizontal direction.

$$M_i\ddot{X}_i = F_i - F_{i-1} - f_i^* \quad \text{..... (12.3)}$$

$$i = 1, 2, ..., N$$

where M_i is the mass of particle i,

$\ddot{X}_i$ is the acceleration of particle i,

F_i is the driving force from spring λ_i behind,

F_{i-1} is the resistance force from spring λ_{i-1} ahead,

f_i^* is the total resistance force from particle i.

The forces in the vertical direction are in balance. According to the force vectors in figure 12.1b), springs on both sides of particle i are in compression. The distance between two adjacent particles at any time t will be

$$\Delta X_i = X_i - X_{i+1}, \quad i=1, 2, ..., N.$$

Obviously, the compression in spring i is

$$\xi_i = a - \Delta X_i = a + X_{i+1} - X_i.$$

Therefore, the force F_i in spring i is

$$F_i = \lambda_i \xi_i = \lambda_i(a + X_{i+1} - X_i) \quad \text{..... (12.4)}$$

$$i = 1, 2, ..., N-1.$$

Similarly, the force in spring i-1 is

$$F_{i-1} = \lambda_{i-1}(a + X_i - X_{i-1}) \quad \text{..... (12.5)}$$

$$i = 2, 3, ..., N.$$

Note in above two equations, i=1, 2, ..., N can be used by assigning special values to Xo and X_{N+1}, see equations (12.8) and (12.9).

The resistance force f_i^* includes the frictional force $f_i(\dot{X}_i)$ and the component of seismic radiation $Eo\dot{X}_i$ and is a combination function of the two terms. The frictional force $f_i(\dot{X}_i)$ is in turn a combination function of C, σ and μ_s, referring equations (6.16) through (6.20) for detail.

Substituting equations (12.4) and (12.5) into (12.3), the motion equation becomes

$$\ddot{X}_i = [\lambda_i(a+X_{i+1}-X_i) - \lambda_{i-1}(a+X_i-X_{i-1}) - f_i(\dot{X}_i) - Eo\dot{X}_i]/M_i \quad \text{..... (12.6)}$$

$$i = 1, 2, ..., N$$

where Eo is the coefficient of seismic radiation, $Eo=k\sqrt{E}$,

E is the elastic modulus of rock concerned,

k is the material constant.

For the simplicity of programming, equation (12.6) will be left as it is. If all springs have the same stiffness λ and all particles have equal mass M, then equation (12.6) becomes

$$\ddot{X}_i = [\lambda(X_{i-1}-2X_i+X_{i+1}) - f_i(\dot{X}_i) - Eo\dot{X}_i]/M \quad \text{..... (12.7)}$$

$$i = 1, 2, ..., N$$

In order to solve equation (12.6) or (12.7), boundary conditions are required. It can be seen from figure 12.1 that if i=1, Fo=0 and if i=N, $F_N=\lambda_N(\xi_0+Vt-X_N)$. Substitute Fo into equation (12.5),

$$0 = \lambda_0(a + X_1 - Xo).$$

Then either $\lambda_0 = 0$, or $Xo = a + X_1$. In later programming, both λ_0 and Xo have to be assigned values. For convenience, we set

$$\begin{cases} \lambda_0 = 0 \\ Xo = a + X_1. \end{cases} \quad \text{..... (12.8)}$$

Similarly, substituting F_N into equation (12.4) results in

$$\lambda_N(\xi_0 + Vt - X_N) = \lambda_N(a + X_{N+1} - X_N), \text{ or}$$

$$X_{N+1} = \xi_0 + Vt - a \quad \text{..... (12.9)}$$

Obviously, by equations (12.8) and (12.9), we have

$$\begin{cases} \dot{X}_0 = \dot{X}_1 \\ \dot{X}_{N+1} = V. \end{cases} \quad \text{..... (12.10)}$$

Therefore, with equations (12.8) to (12.10), i varies from 1 to N in equations (12.4) and (12.5).

12.2. ENERGY ESTIMATION

The energy changes during slip can be estimated in the same way as for the simple shear model. The basic energy calculation for a single particle model has been achieved in chapter 6. As previously described, this multi-particle model is a combination of many single particle models, and so the energy of the whole system will be the sum of energies stored in all particles and all springs. By equation (6.23a), the energy change rate is given as

$$\frac{d}{dt}(E_k + Ep) = \dot{W}e - \dot{W}_f - \dot{W}r \quad \text{..... (12.11)}$$

where E_k is the total kinetic energy, and

$$E_k = \sum_{i=1}^{N} \tfrac{1}{2} M_i \dot{X}_i^2 \quad \text{..... (12.12)}$$

Ep is the total potential energy stored in all springs, and

$$Ep = \sum_{i=1}^{N} \tfrac{1}{2}\lambda_i(X_i - X_{i+1})^2 \quad \text{..... (12.13)}$$

$\dot{W}e$ is the rate of doing work in moving the support against the spring N, being of order V, and

$$\dot{W}e = F_N \cdot V = \lambda_N(\xi_0 + Vt - X_N)V,$$

$\dot{W}_f$ is the rate at which work is done against friction, positive,

$$\dot{W}_f = -\sum_{i=1}^{N} f_i(\dot{X}_i)\dot{X}_i,$$

$\dot{W}r$ is the power radiated along the semi-infinite string, positive,

$$\dot{W}r = \sum_{i=1}^{N} Eo\dot{X}_i^2.$$

For a time period $\Delta t = t_2 - t_1$, the total energy change in the system would be the integration of both sides in equation (12.11) over Δt. That is

$$\int_{t_1}^{t_2} \frac{d}{dt}(E_k + Ep)dt = \int_{t_1}^{t_2} (\dot{W}e - \dot{W}_f - \dot{W}r)dt, \text{ or}$$

$$\Delta E_k + \Delta Ep = We - W_f - Wr \quad \text{..... (12.14)}$$

where $\Delta E_k = E_k(t_2) - E_k(t_1)$,

$\Delta Ep = Ep(t_2) - Ep(t_1)$,

$$We = \int_{t_1}^{t_2} [\lambda_N V(\xi_0 + Vt - X_N)]dt \quad \text{..... (12.15)}$$

$$W_f = -\int_{t_1}^{t_2} [\sum_{i=1}^{N} \dot{X}_i f_i(\dot{X}_i)]dt$$

$$= -\int_{t_1}^{t_2} \sum_{i=1}^{N} f_i(\dot{X}_i)dX_i$$

$$Wr = \int_{t_1}^{t_2} [\sum_{i=1}^{N} Eo\dot{X}_i^2]dt$$

During the period Δt, the total energy loss is $W_l = W_f + Wr$. Because the dominant function given in equation (12.6) will be solved by the numerical method later, these energies can only be estimated by approximation. In field

microseismic monitoring of rock burst, the recorded energy is the only information available and is just a small part of the total energy loss, which is the energy radiated out to some distance away from a source. Therefore it is significant to estimate the item Wr in this modelling, which represents the seismic energy radiated from the source. Items W_f and E_k will also be computed for comparison. In later programming, according to the numerical integration by rectangle which can be found in mathematics textbook on numerical integration [45], the approximation of these parameters will be :

$$Wr \simeq Eo \sum_{j=1}^{n} \sum_{i=1}^{N} \dot{X}_{ij}^2 \cdot \Delta t_j \quad \text{..... (12.16)}$$

$$W_f \simeq -\sum_{j=1}^{n} \sum_{i=1}^{N} f_i(\dot{X}_{ij}) \cdot \Delta X_{ij} \quad \text{..... (12.17)}$$

where Δt_j is the time increment at step j,

ΔX_{ij} is the movement of particle i at step j,

$\dot{X}_{ij}$ is the slip velocity of particle i at step j,

$n \geq 1$, is the number of sampling points within time window $\Delta t = t_2 - t_1$.

In each succeeding running of the program, the period Δt will be specified. The sampling number n varies and is determined by the program itself, depending on the time step Δt_j, which is in turn controlled by the accuracy ϵ specified to the computer solution of slip velocity $\dot{X}$.

12.3. COUNT OF EVENT

In field seismic monitoring, in addition to the seismic energy released, the seismic event number is another important precursory signal. The event rate indicates the frequency of microseismic activity. In this acoustic activity modelling, both the

energy change will therefore be calculated and the acoustic event will be simulated and counted.

As discussed in previous chapters, the stick-slip is a significant phenomenon in shear failure. The rock mass can be considered to consist of many discrete particles connected together by springs. When a load is applied to the model, some springs are compressed first and a force is induced in each of them. This force can move the relevant particle for some distance if it overcomes the corresponding resistance. When the load is removed, due to the elasticity of the springs, these particles will move back to and probably vibrate around their original positions until the energies stored in the springs damp off. If the load is held at some point, the particle moving will still possibly induce vibration. If the load continues to increase, the compressed springs will transmit the load to adjacent springs and chain reaction takes place. If the load is so high that a shear failure surface is formed as discussed in chapter 4, all particles along this surface will begin to move. At the same time, the vibration becomes intense.

If any slip or any change of moving direction during the vibration of every particle is considered to generate an acoustic event, the history of acoustic activity prior to the failure can be recorded during the program running. As is expected from laboratory tests of acoustic emission, the acoustic event should increase significantly as the failure is approached due to the more intensive vibration. In the following program, a specific register, L, is assigned to count the moving and the change of direction of all particles.

12.4. LIMITS TO THE MODEL

The physical conditions and certain requirements of this model introduce some limits which should be considered in programming. They are the logical position of each particle, the effectiveness of the spring and the stick-slip conditions.

12.4.1. The Logical Position

This model is concerned with the problem of one dimension. All the N particles stand in a line when no shear force is applied to them. Once movement starts due to a shear force, they move one after another along the same axis but not necessarily in the same direction. This can be pictured from the fact that some part may be in compression and some part may be in tension. But they all keep in the original consecutive sequence. In other words, there is no superposition among particles, and so the following conditions must be satisfied all the time,

$$X_{i-1} > X_i > X_{i+1} \quad \text{..... (12.18)}$$

$$i = 1, 2, ..., N.$$

12.4.2. The Physical Condition

The springs connecting adjacent particles are elastic only under normal conditions, i.e., the load is not too high. Once the load reaches the capacity of the spring, the elastic deformation or the compression of the spring reaches its maximum limit. If the load continues to increase, the elasticity disappears and no more compression happens. At this point, the spring would act as a "stiff stick" and the load would be transmitted through it to the next spring with no further deformation, or very little.

This extreme case can occur when the normal load acting on a particle is so high that the frictional resistance is more than the maximum elastic force in the spring. Because the normal load increases the friction force linearly and the elastic force of the spring is linearly proportional to its elastic deformation. In order to avoid this problem during running the program, the normal load should be limited under this maximum value corresponding to a particular spring which is characterized by its stiffness λ_i.

As shown in figure 12.1, at any time the distance between two adjacent particles is

$$\Delta X_i = X_i - X_{i+1}, \quad i=1, 2, \ldots, N.$$

Apparently, if no stress is induced in spring i, $\Delta X_i = a$. As the spring is compressed under load, the deformation will be

$$\xi_i = a - \Delta X_i, \quad (\xi_i < a)$$

and the induced force in spring i is $F_i = \lambda_i \xi_i$. If the normal pressure on the particle i is σ, the static friction would be

$$f_i(0) = C + \mu_s(M_i + \sigma).$$

The maximum elastic force occurs in the spring when $F_i = f_i(0)$, or

$$\lambda_i \xi_{io} = C + \mu_s(M_i + \sigma).$$

Usually, the particle mass M_i is extremely small compared with σ and negligible. Then above equation reduces to

$$\lambda_i \xi_{io} \simeq C + \mu_s \sigma.$$

Therefore, in order for the model to function properly, the normal pressure σ should satisfy the condition:

$$\lambda_i \xi_{io} \geq C + \mu_s \sigma, \text{ or}$$

$$\sigma \leq (\lambda_i \xi_{i0} - C)/\mu_s \quad \text{..... (12.19)}$$

where λ_i is the stiffness of spring i, which is proportional to the elastic modulus,

ξ_{i0} is the allowed maximum deformation of spring i,

C is the cohesion, and

μ_s is the static coefficient of friction.

In running the program later, $\xi_{i0} = 0.2a$ is used for demonstration purpose. Therefore, once $\xi_{i0} \geq 0.2a$, or $\Delta X_i = a - \xi_{i0} \leq 0.8a$ occurs, the corresponding λ_i is increased to a large value to simulate the stiffening. λ_i is reassigned to its normal value when $\Delta X_i > 0.8a$.

12.4.3. Conditions for Stick-slip

This acoustic model is based on the principle of shear process. As we know, when slip begins, either stable sliding or stick-slip will occur. This model works on the assumption of stick-slip of individual particles. The stable sliding, once it occurs, means the movement of all particles and is considered as the final failure of the whole system.

The stick-slip phenomenon only occurs under certain conditions, which have been discussed in chapter 7. These conditions are satisfied if the loading conditions of the model system fall into the lower part of the transition chart in figure 7.2. For a given material, its elasticity is given, and in order for the stick-slip to occur, for each normal pressure there is a maximum loading speed, or for any loading speed there is a minimum normal pressure.

Therefore, in order for this model to function properly, all the above conditions have be to satisfied and must be considered during programming.

12.5. NUMERICAL SOLUTION BY RUNGE-KUTA METHOD

The expression given in equation (12.6) is a set of ordinary multi-variable second order differential equations, with unknown in their denominators. Again, explicit solutions cannot be found due to their complexity and we must look for numerical solution.

An introduction to Runge-Kuta method has been given in chapter 6 and it is applied to the second order differential equation of one variable. By the same principle of extension, it can be applied to equation (12.6) of multi-variables. It will be much more convenient for discussion to express equation (12.6) as an implicit function. Let $\dot{X}^i = Y^i$, then (12.6) becomes:

$$\begin{cases} \dot{Y}^i = f(t,\ X^{i-1},\ X^i,\ X^{i+1},\ Y^i) \\ \dot{X}^i = g(Y^i) = Y^i \end{cases} \quad \text{..... (12.20)}$$

$i = 1,\ 2,\ \ldots,\ N$

Note, the function f represents the right hand side of equation (12.6) and for convenience in the following , all subscripts in (12.6) have been replaced by superscripts here. Then from (12.1) and (12.8) to (12.10), we have initial conditions

$$\begin{cases} Y^i(0) = 0 \\ X^i(0) = (N - i)a \end{cases} \quad \text{..... (12.21)}$$

and boundary conditions

$$\begin{cases} X^0 = X^1 + a \\ X^{N+1} = Vt + \xi_0 - a \end{cases} \quad \text{..... (12.22)}$$

$$\begin{cases} Y^0 = Y^1 \\ Y^{N+1} = V. \end{cases} \quad \text{..... (12.23)}$$

By simple extension of equation (6.29), the solution to (12.20) can be expressed as

$$\begin{cases} X^i_{n+1} = X^i_n + (m^i_1 + 2m^i_2 + 2m^i_3 + m^i_4)/6 \\ Y^i_{n+1} = Y^i_n + (k^i_1 + 2k^i_2 + 2k^i_3 + k^i_4)/6 \end{cases} \quad \text{..... (12.24)}$$

$$i = 1, 2, \ldots, N$$

where X^i_{n+1} and Y^i_{n+1} are new values to be found for particle i,

X^i_n and Y^i_n are known from previous calculation at step n,

each m^i and k^i for particle i are calculated as following:

$$\begin{cases} k^i_1 = h \cdot f(t_n,\ X^{i-1}_n,\ X^i_n,\ X^{i+1}_n,\ Y^i_n) \\ m^i_1 = h \cdot g(Y^i_n) = h \cdot Y^i_n \\ k^i_2 = h \cdot f(t_n + h/2,\ X^{i-1}_n + m^i_1/2,\ X^i_n + m^i_1/2,\ X^{i+1}_n + m^i_1/2,\ Y^i_n + k^i_1/2) \\ m^i_2 = h \cdot (Y^i_n + k^i_1/2) \\ k^i_3 = h \cdot f(t_n + h/2,\ X^{i-1}_n + m^i_2/2,\ X^i_n + m^i_2/2,\ X^{i+1}_n + m^i_2/2,\ Y^i_n + k^i_2/2) \\ m^i_3 = h \cdot (Y^i_n + k^i_2/2) \\ k^i_4 = h \cdot f(t_n + h,\ X^{i-1}_n + m^i_3,\ X^i_n + m^i_3,\ X^{i+1}_n + m^i_3,\ Y^i_n + k^i_3) \\ m^i_4 = h \cdot (Y^i_n + k^i_3). \end{cases} \quad \text{..... (12.25)}$$

Here h is the increment of time t between step n and step n+1 and is determined according to accuracy ϵ for the solution.

12.6. PROGRAMMING

A computer program named MODEL4 for the numerical solution given in equation (12.24) was written in BASIC language for running on the Hewlett-Packard computer. The flow chart of this program is given in figure 12.2 and the program is listed in appendix 4. Some variables used in the program are listed in the following.

To and T_j are start time and instant time,

h is the time step, varies,

X_{ij} and $\dot{X}_{ij}$ are slip distance and velocity of particle i at time T_j,

F_{ij} is the total driving force on particle i at T_j,

F_{fij} is the total resistance from particle i at T_j

L is the event counter, and

T_{int} is the sampling window Δt in which numerical sampling is taken. The sampling number n depends on the window Δt and the time step h.

This program starts counting the event number from the beginning. At the same time, the work against friction W_f, the seismic energy Wr, the energy ratio Wr/L and the total energy loss Wl are calculated. All these results are accumulated for a given time window T_{int} and stored on file. The kinetic energy can also be estimated at any moment.

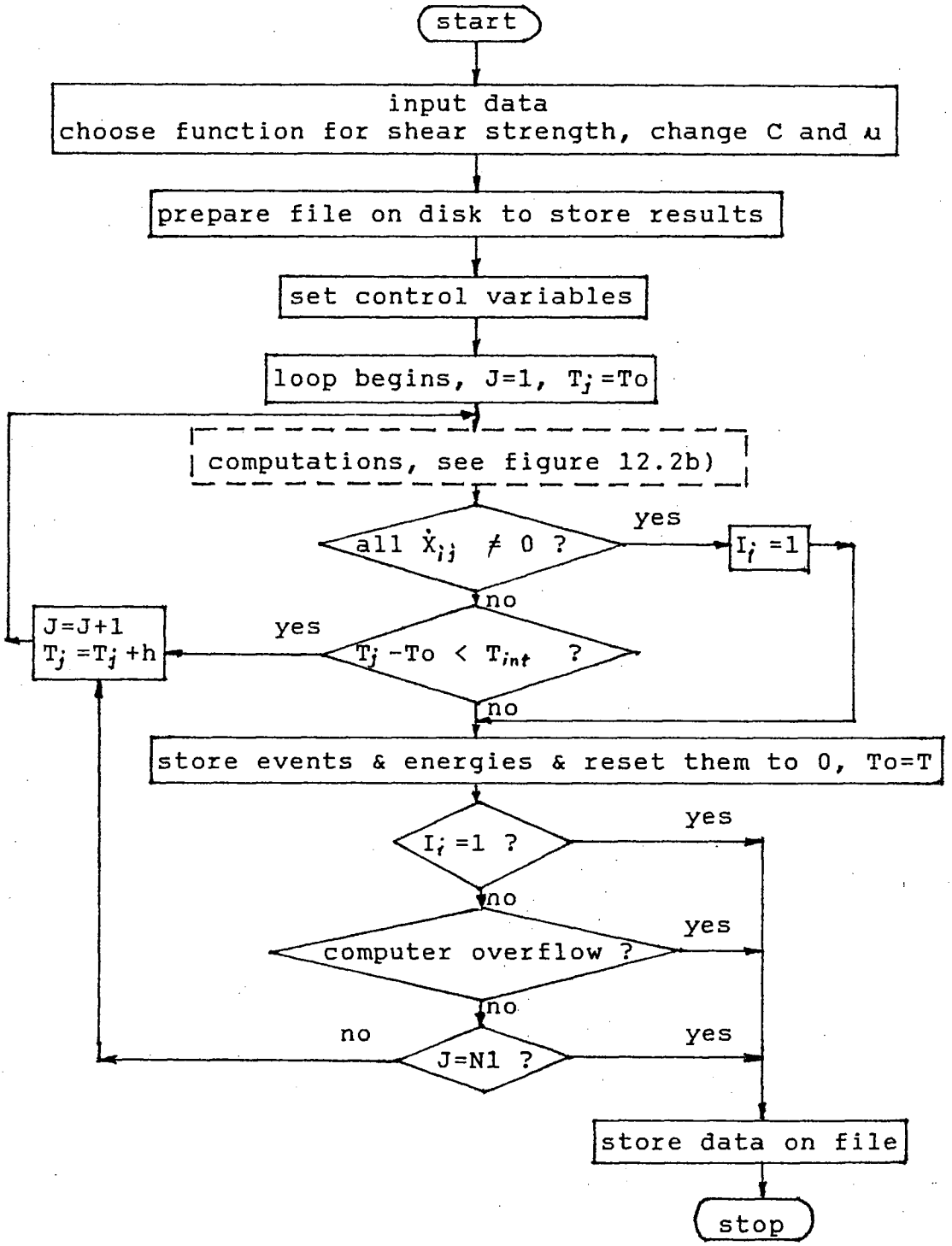

Fig.12.2a) Flow chart for program MODEL4: acoustic simulation

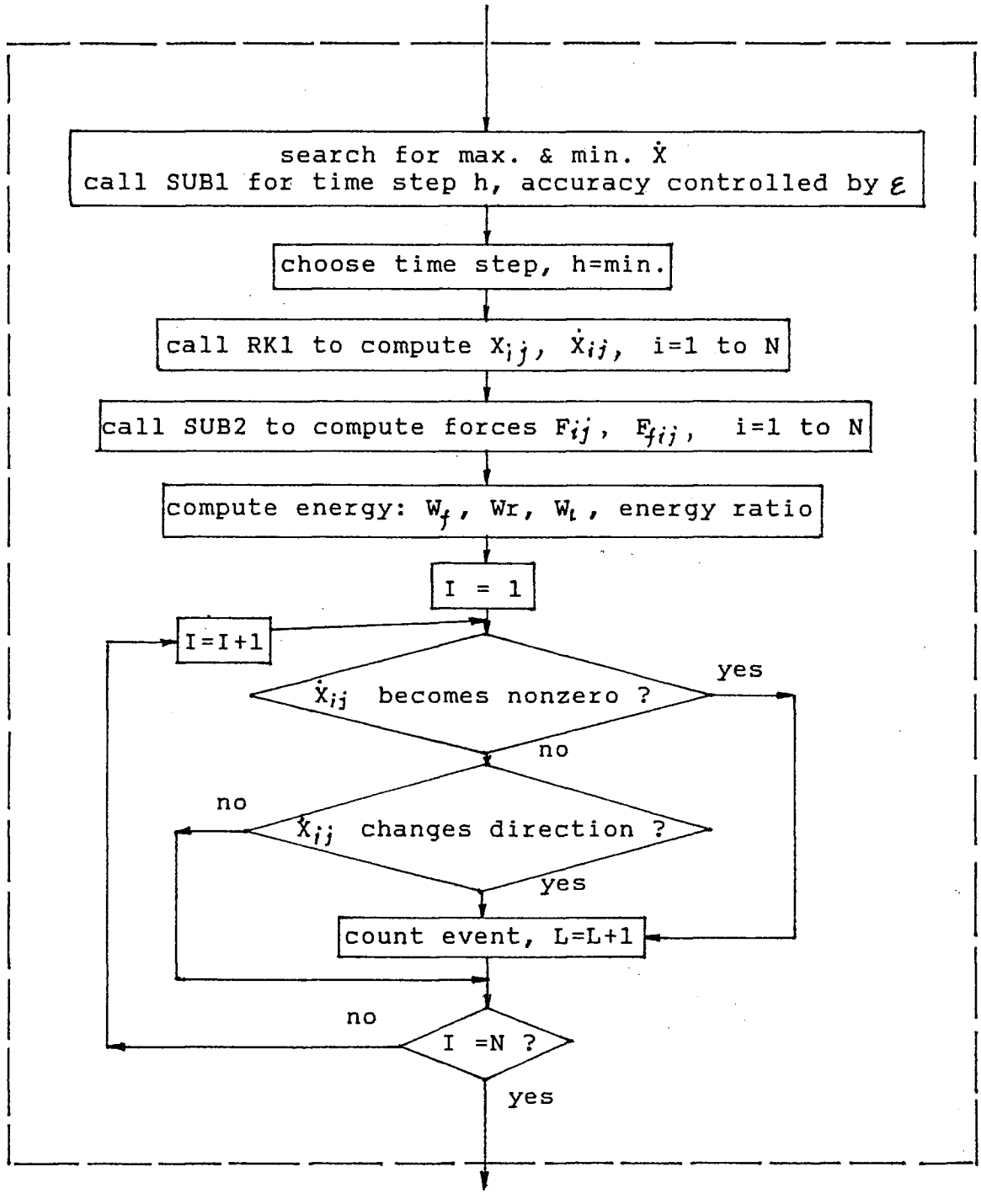

Fig.12.2b) Flow chart of the computation part in program MODEL4

12.7. MODELLING RESULTS

12.7.1. Resemblance to the Testing Results

The acoustic model produced fascinating results, which surprisingly are very similar to those results recorded during acoustic emission tests. Some typical computer results from two runs of program MODEL4 are given in figures 12.3 and 12.4. Before the failure took place as indicated by the arrow, the modelled acoustic activity in terms of event rate and seismic energy, behaves the same way as from tests, figures 10.2 and 10.3. At the beginning, not much signal is generated. As failure is approached, the generated signals are very active, both the event rate and energy release increasing sharply.

In chapter 10, the acoustic emission from experiments was compared with field data and a good agreement was found between them. These precursory signals are realistically simulated again by this numerical model. The event rate increases sharply as failure is approached and then drops to the previous low level immediately preceding the failure. Meanwhile, the seismic energy, both the energy rate and the energy ratio, remains low when the event rate goes up and increases dramatically prior to the failure. The increase in event rate corresponds to fracture propagation. The drop of event rate and the increase of acoustic energy indicate the formation of macrofractures.

Even though the model itself has no direct relation to the acoustic

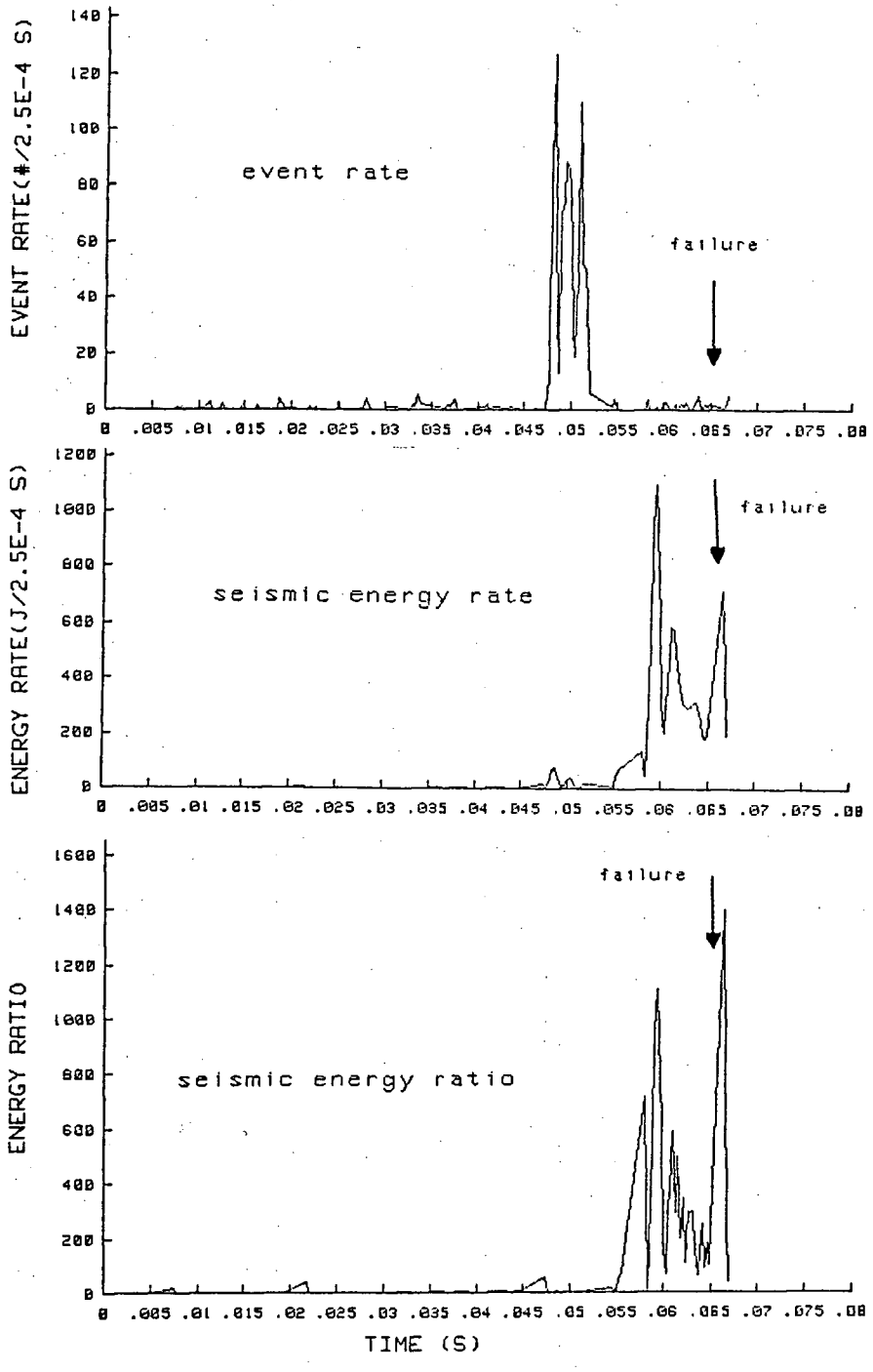

Fig.12.3 Computer results from the numerical acoustic model

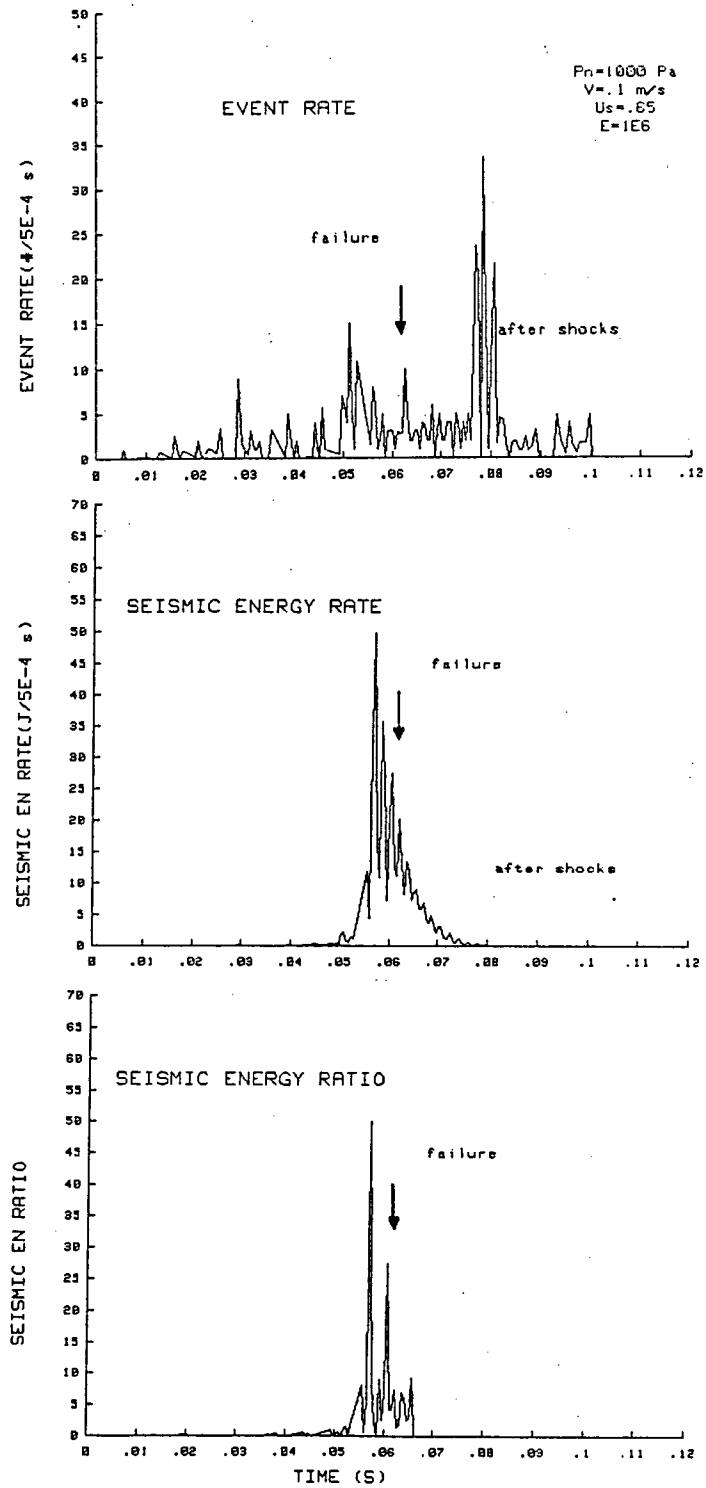

Fig.12.4a) Complete pattern of acoustic activity prior to failure, showing after shocks

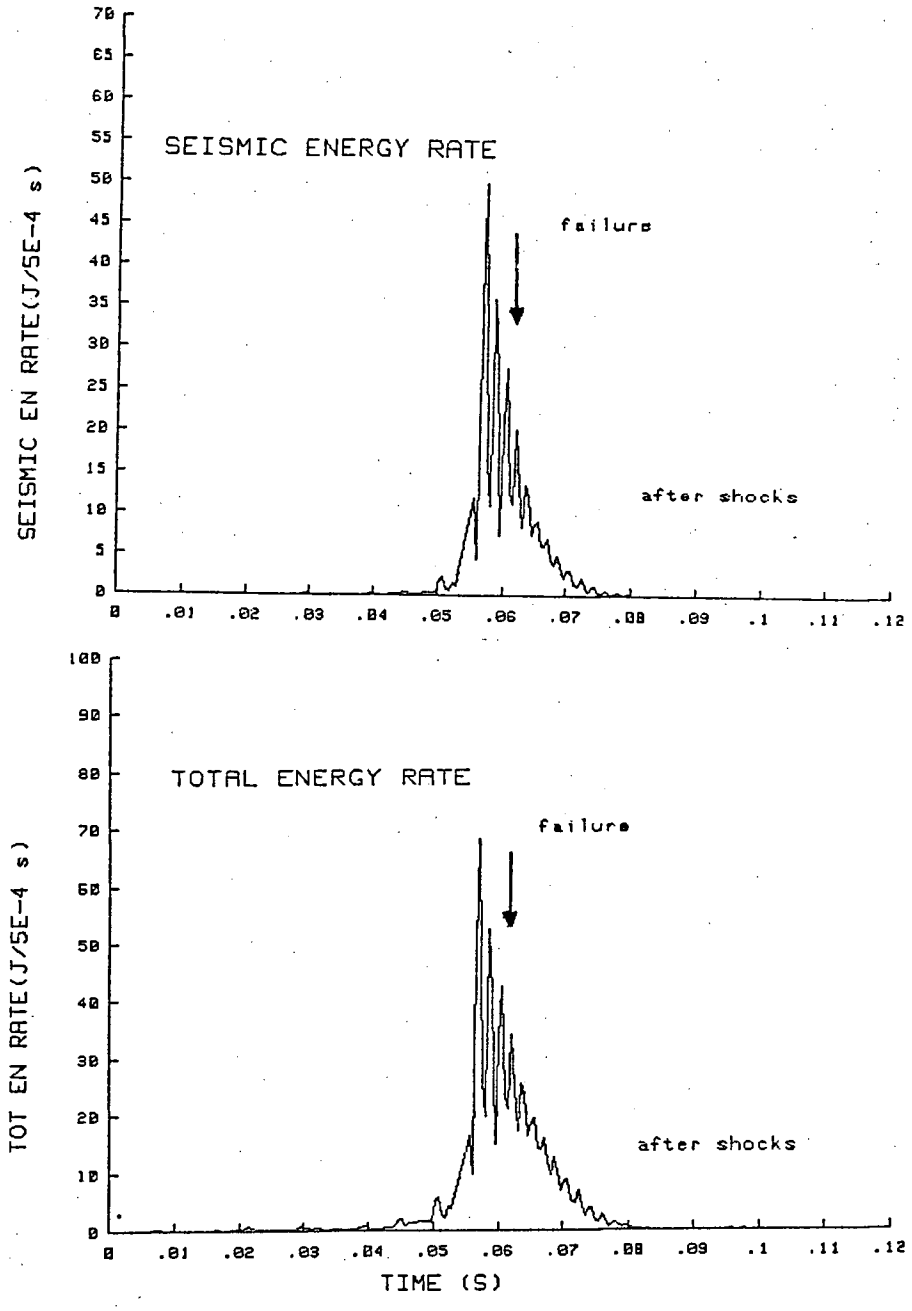

Fig.12.4b) Complete pattern of acoustic activity prior to failure, showing the similarity between total and seismic energy

emission, its results are in good agreement with both the experimental and the field results. This justifies that the postulated shear failure mechanism can be used to interpret violent rock failure. Acoustic emission is indeed a precursory phenomenon for rock failure.

12.7.2. The Total Energy Released versus the Seismic Energy

Energy released during a rockburst is complicated and cannot be calculated precisely. In microseismic monitoring, the monitored energy is only a small part of the total energy released. This part of energy is radiated out as seismic energy and is detectable by special sensor. It is not known what the relationship is between the seismic energy and the total energy released.

It is believed that the major part of the energy released during a burst is consumed against the resistance force including frictional force. In addition to a small part transformed into heat, the rest is almost completely transmitted out as seismic energy. If the seismic energy has not damped off completely when the seismic waves reach the boundary between the rock mass and air, it is transformed into sound energy. If this sound energy is big enough, an air shock can be experienced.

A question arises about how accurate it is to estimate the pattern of the total energy through the detected seismic energy, as is usually done in the field. In other words, it is a question of whether the proportion of these two energy parameters remains the same throughout the failure process. In this numerical modelling, the total energy release is also calculated for comparison. Some typical

results are given in figure 12.4b). These two parameters are alike, for they change in largely the same way throughout the process. This gives us confidence in the use of the seismic energy to estimate the change of total energy release.

The seismic energy is analyzed in this modelling as both energy release rate and energy release ratio, which is the average energy per event during a given time window. In the results from all the runs of the program, these two parameters show a similar behavior, although the energy ratio shows the anomaly more clearly.

12.7.3. After Shocks

The program is usually stopped once the final failure occurs because each run takes hours to finish. In some cases, an attempt was made to run the program until the energy accumulated before the failure has completely damped off. A typical example is given in figure 12.4a). As can be seen, after the failure, many after shocks were generated. But the energy release rate decayed in a lower speed than it built up before the failure. Obviously, more energy is released during the after shocks. This is also clearly shown by the area under the curve of energy rate and above the horizontal axis, because this area represents the total amount of energy released. This is in agreement with the what was observed during the direct shear tests described in chapter 10.

After the failure, the energy ratio drops immediately, and so the anomaly of failure indicated by this parameter is well defined. During the period of after shocks, the event rate seems to build up again when the energy is about to be

finished. These after shocks may be explained in such a way that at the initiation of failure, many microcracks are formed. As slip continues, these cracks are crushed and at the same time new cracks are formed.

According to the fracturing principle, the joining of macro-fractures will lead to the formation of a final failure surface, on which the shear process takes place. During the shear movement, some new micro-fractures are generated and some micro-fractures are crushed. Therefore, the event rate will remain high on some levels but the energy release involved is small. When the energy is consumed, the shear movement ceases. At this moment, the build up of event rate may be confused with the the major failure. This mis-impression of a failure induced from the build up of the event rate can be cleared by looking at the energy release rate simultaneously.

12.8. SUMMARY

1. A numerical acoustic model has been developed based on the stick-slip to simulate the acoustic activity prior to violent rock failure. Events are counted by examining the slip and the change of slip direction and energy release is estimated for each event.
2. The limiting conditions for this model are considered, which are the logical position of each particle in the string, the physical condition for the spring to effect properly and the condition for stick-slip to occur.
3. To do the simulation, a numerical method is used and a computer program has been written, which has reproduced results very similar to the acoustic signals recorded during laboratory tests of rock specimens and measured in

field monitoring.

4. The simulated results show that the total energy release and the seismic energy vary in similar way.
5. After shocks may be generated after the failure due to the new microcracks formed during slip but they have very little energy.
6. These results therefore show that:
   a. The process analogous to shearing can be a fundamental mechanism at the post failure stage of rock,
   b. The acoustic emission is indeed a useful precursory signal for violent rock failure,
   c. This acoustic model is a useful tool to study the acoustic activity prior to the violent rock failure.
   d. More importantly, the precursory signals obtained during this research are probably universally acceptable and the method can be applied to field interpretation of violent rock failure.

CHAPTER 13. ACOUSTIC ACTIVITY UNDER DIFFERENT CONDITIONS

Because the behavior of acoustic emission is not clear for many conditions due to the limited results from laboratory tests and field measurements, acoustic emissions under various conditions are studied in this research using the numerical model developed in the previous chapter. This acoustic model can be used to simulate the acoustic activity prior to violent rock failure because it has allowed violent rock failure and the associated acoustic activity to be simulated realistically. Therefore, it provides us with a method to study the acoustic activity during violent rock failure on computer. Further study was carried out using a computer program MODEL4 to uncover the mystery of acoustic emission under different situations. For each condition to be simulated, this program runs under a given set of parameters and generates the associated acoustic emission.

Conditions are modelled as realistically as possible, but they have to be within the limits of the model given in the previous chapter and the convergence speed of the program should be tolerable. In the following, the most useful parameters or the event rate and the seismic energy are examined as conditions are changed. The main interest is in the pattern of change of each parameter instead of its absolute value. The simulated results are presented in the following.

13.1. ACOUSTIC EMISSION AS NORMAL PRESSURE VARIES

First, the effect of normal pressure on acoustic emission is examined. The normal pressure is set to 500 Pa, 1 KPa and 10 KPa respectively for each run of the program, with other conditions unchanged. The computed results are plotted in

figure 13.1a) to c). The results from the three runs have a similar pattern. Before the failure, a sharp increase of the event rate occurs and is followed by a drop. The increase of energy occurs at a moment prior to failure. The pattern of acoustic emission is the same under all normal pressures considered. The event rates are in the same order of 10^4 per second, although the energy release increases with the normal pressure. The increase of seismic energy is expected because the energy released during each slip increases with the square of the normal pressure, figure 6.9, where a linear increase of stick time with the normal pressure also exists. For a single particle, the event rate is approximately the reciprocal of the stick time. If however more than one particle exists, as in this acoustic model, the event rate is also influenced by other factors, such as the mutual reaction between particles. The vibration effect should also be considered.

This suggests that the pattern of acoustic emission is similar for all pressures if other conditions are the same. The only difference is the magnitude of the energy release. It can be believed that during the fracturing process, a high stress field does not change the process of fracturing propagation, but it will increase the fracturing energy and consequently make the failure more violent. In addition, these results show that the normal pressure has not much effect on the time it takes for the failure to occur from the beginning of loading.

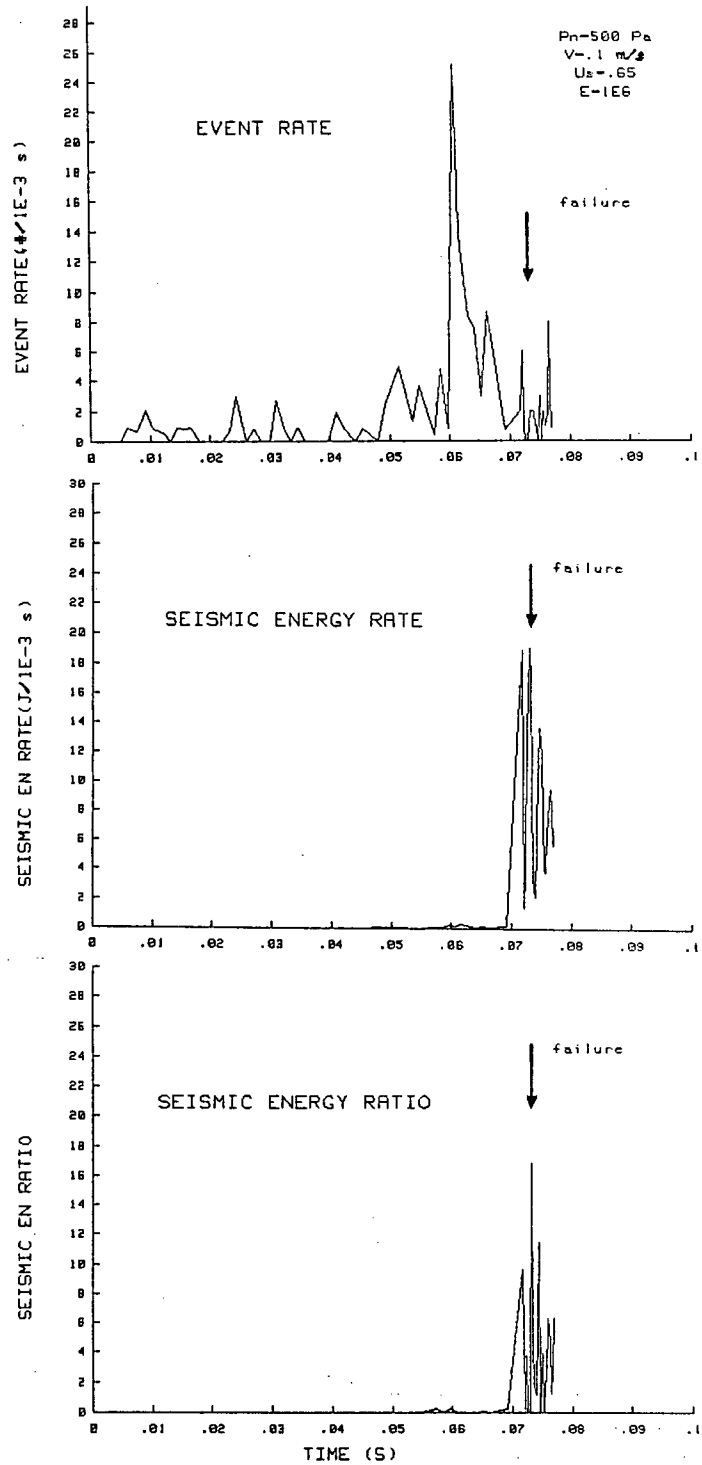

Fig.13.1a) Numerical acoustic emission at normal pressure 500 Pa

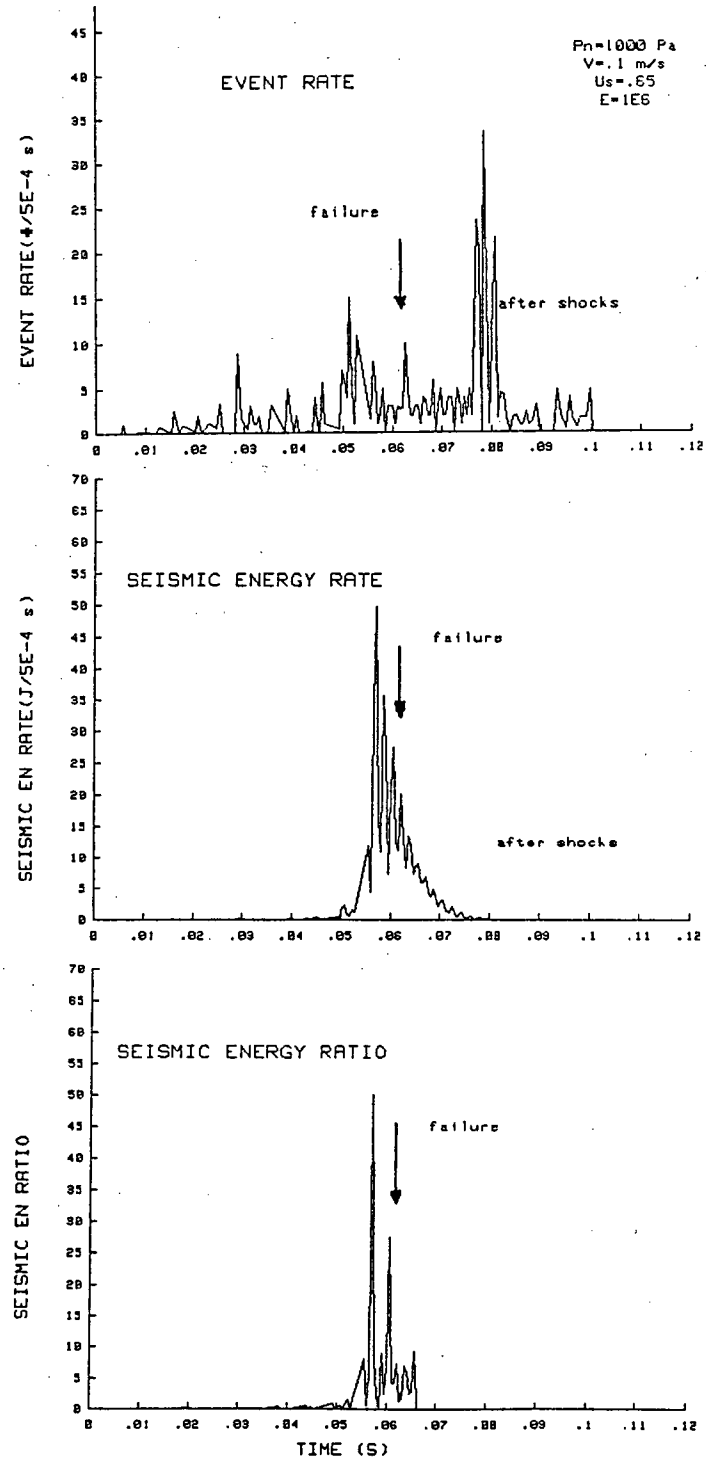

Fig.13.1b) Numerical acoustic emission at normal pressure 1 KPa

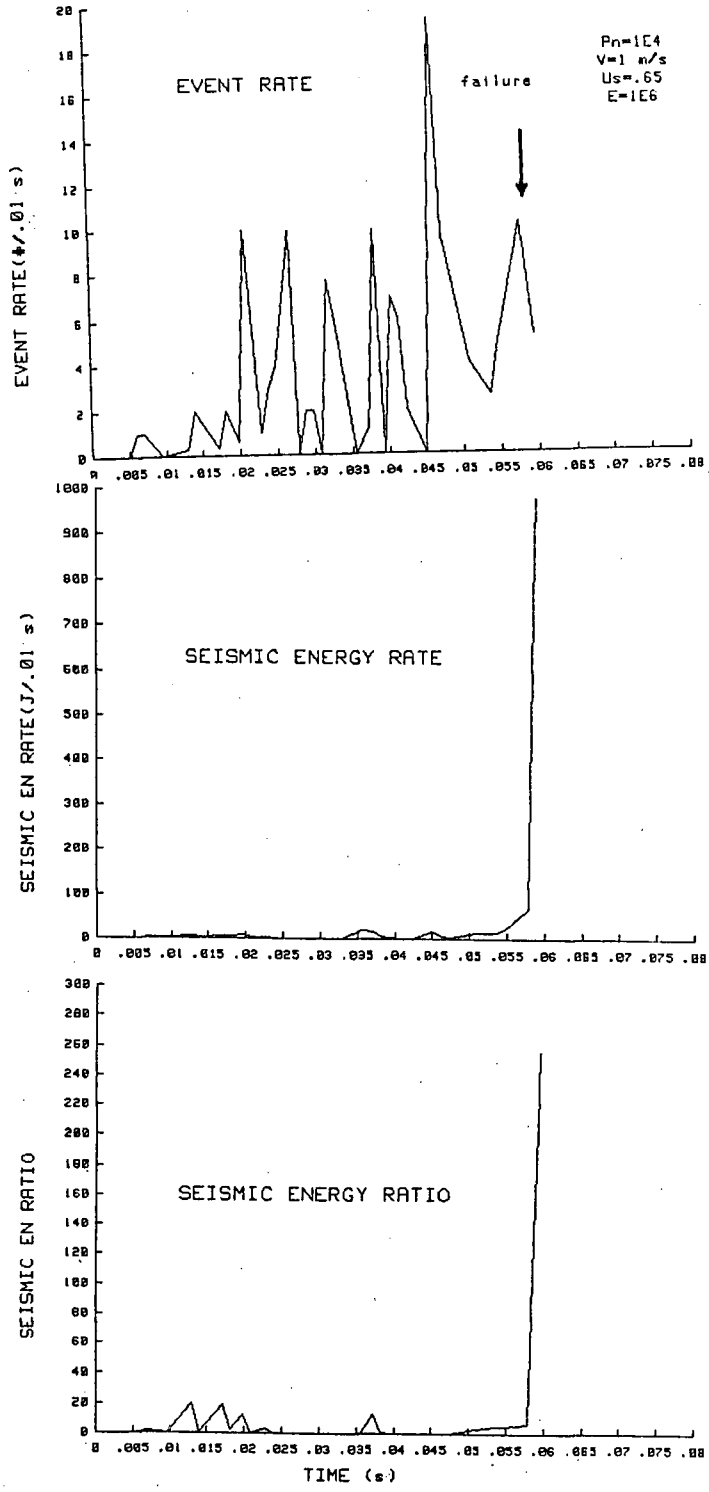

Fig.13.1c) Numerical acoustic emission at normal pressure 10 KPa

13.2. ACOUSTIC EMISSION AS LOADING SPEED VARIES

In chapter 6, the loading speed is found to be another important factor in the slip behavior. When this speed is above a critical level, which is described in chapter 7, the stable sliding will occur. When this speed is less than the critical level, the stick-slip behavior remains the same, but the stick time has an inverse relation with the loading speed $T_2 = c/V$, figure 6.10. The value of the constant c is very small. In fact, if V is much higher than c, the stick time T_2 will be very short. The stable sliding corresponds to a near zero stick time.

During this research, the acoustic emission is modelled for loading speed $V = 0.01$, 0.1, 1.0 m/s respectively. The computed results are plotted in figure 13.2a) to c). When the loading speed is relatively low, or when $V < 1$ m/s for the particular condition modelled, both event rate and seismic energy indicate a clear precursory signal as observed before. The pattern of acoustic activity is not changed by varying loading speed, but the number of events per second increases with the increase of loading speed, although the energy release rate remains relatively unchanged. These are in agreement with the results of single particle model, figure 6.10. This may indicate that during the fracturing process, higher loading speed will increase the fracture propagation, but it has little effect on the energy release from fracturing.

When the loading speed is relatively high, say $V = 1$ m/s, only the energy ratio indicates a clear anomaly. The other two parameters, event rate and energy rate, are ambiguous. This is probably caused by the fact that for the

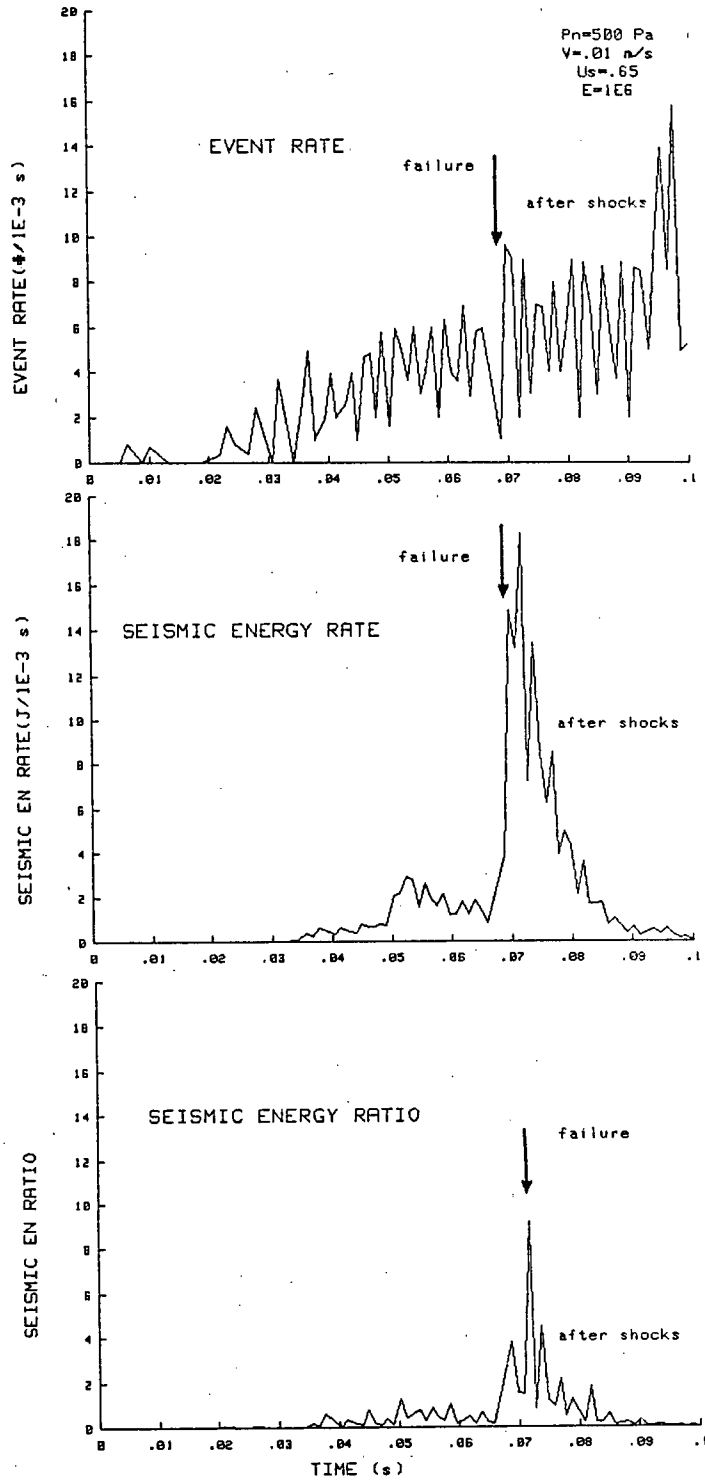

Fig.13.2a) Numerical acoustic emission at loading speed 0.01 m/s

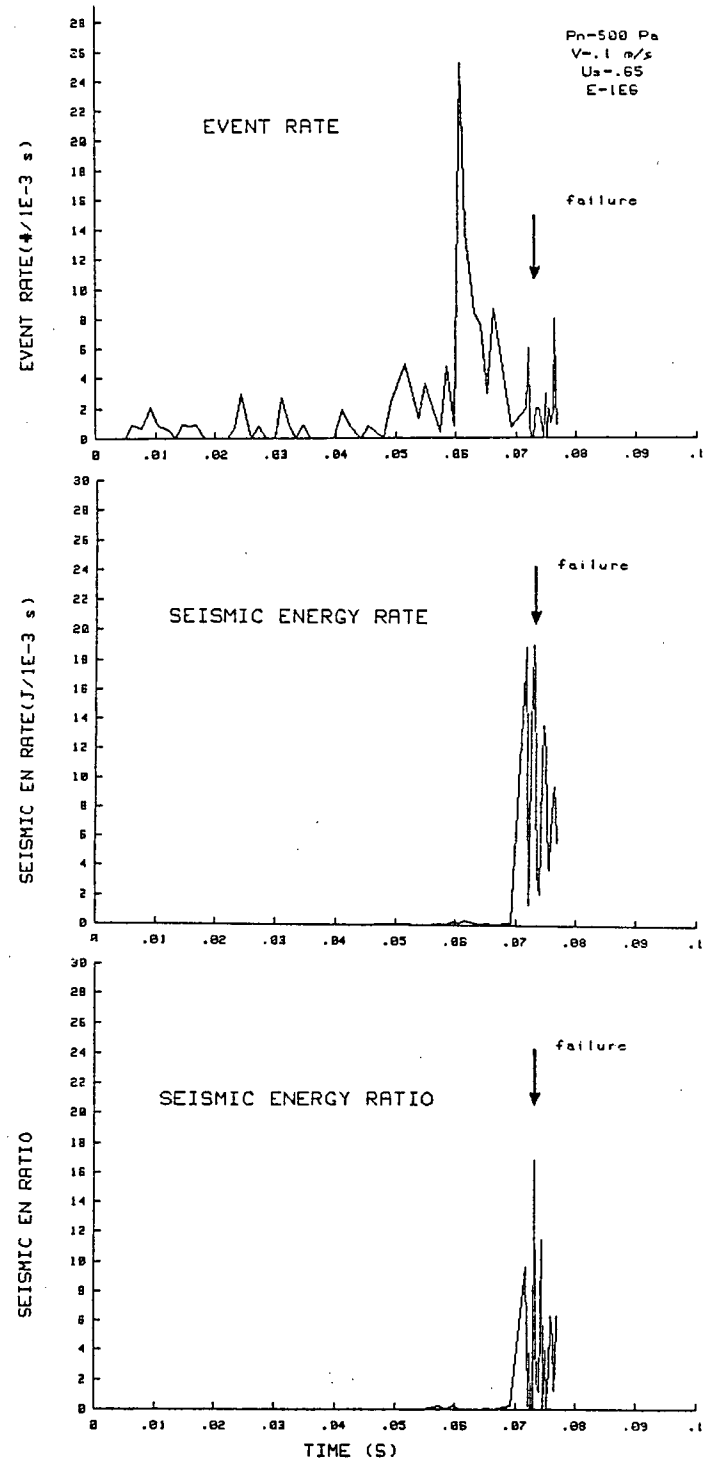

Fig.13.2b) Numerical acoustic emission at loading speed 0.1 m/s

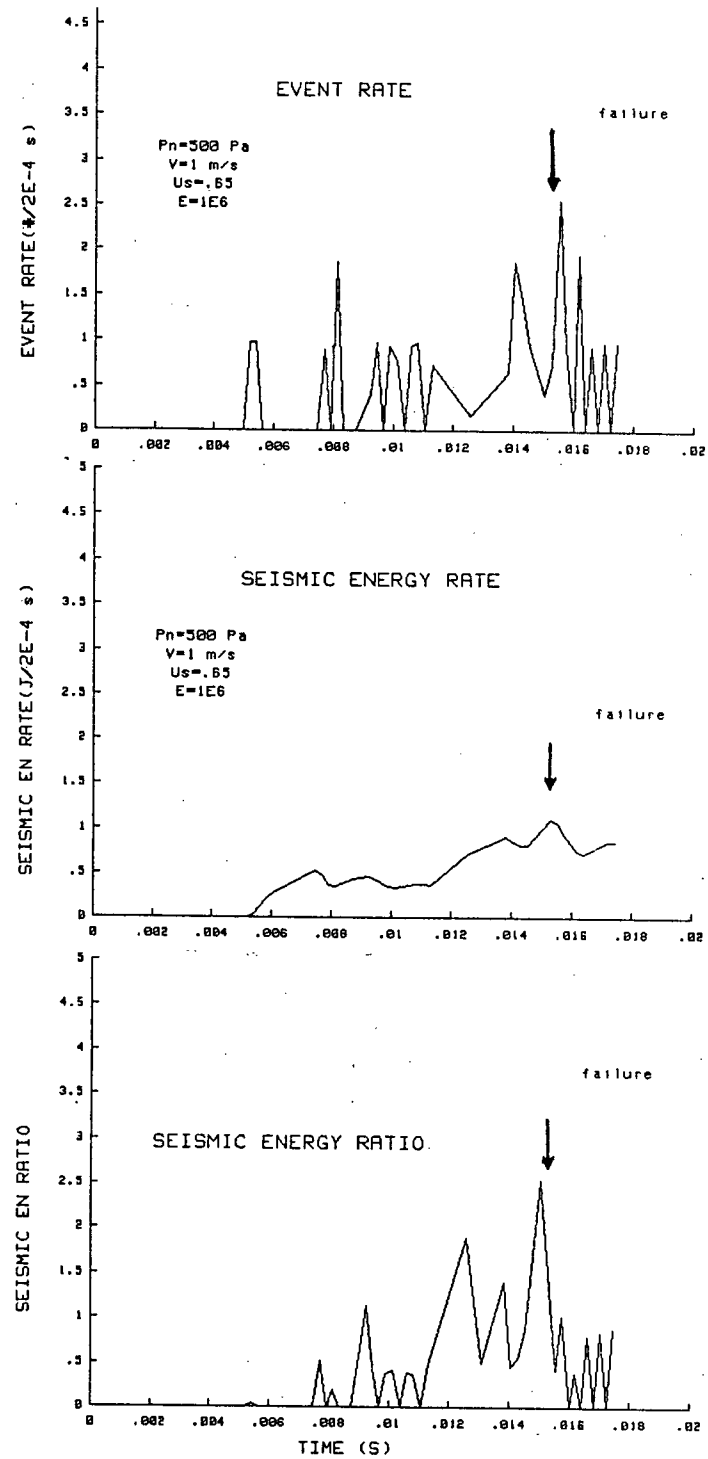

Fig.13.2c) Numerical acoustic emission at loading speed 1.0 m/s

particular condition modelled, this loading speed is close to the limit boundary given in section 12.4. If the loading speed becomes higher, the stable sliding is going to happen instead of stick-slip.

Figure 13.2 also shows the effect of loading speed on the time between the beginning of loading and the failure. At higher loading speed, this time should be shorter. This effect can be clearly seen from the results.

13.3. ACOUSTIC EMISSION AS ELASTICITY VARIES

The elasticity of rock mass has a close relation to its capacity of energy storage and hence directly influences the behavior of failure. Its effects on acoustic emission were studied on the model program under different values of elastic modulus with $E = 10^8$, 10^6, 10^5, 3×10^4 Pa respectively. Some typical results are plotted in figure 13.3a) to d).

When the elasticity is high, the previously described precursive signals are clearly observed, figure 13.3a) and b). Both event rate and seismic energy release indicate a well defined anomaly. It can also be seen that the event rate and energy release rate increase in magnitude with the increase of the elasticity. This increase of energy release may indicate that higher elasticity of the rock mass can make the failure more violent.

However, when the elasticity is low as in figure 13.3c) and d), the precursive phenomena tend to disappear. Both event rate and energy release

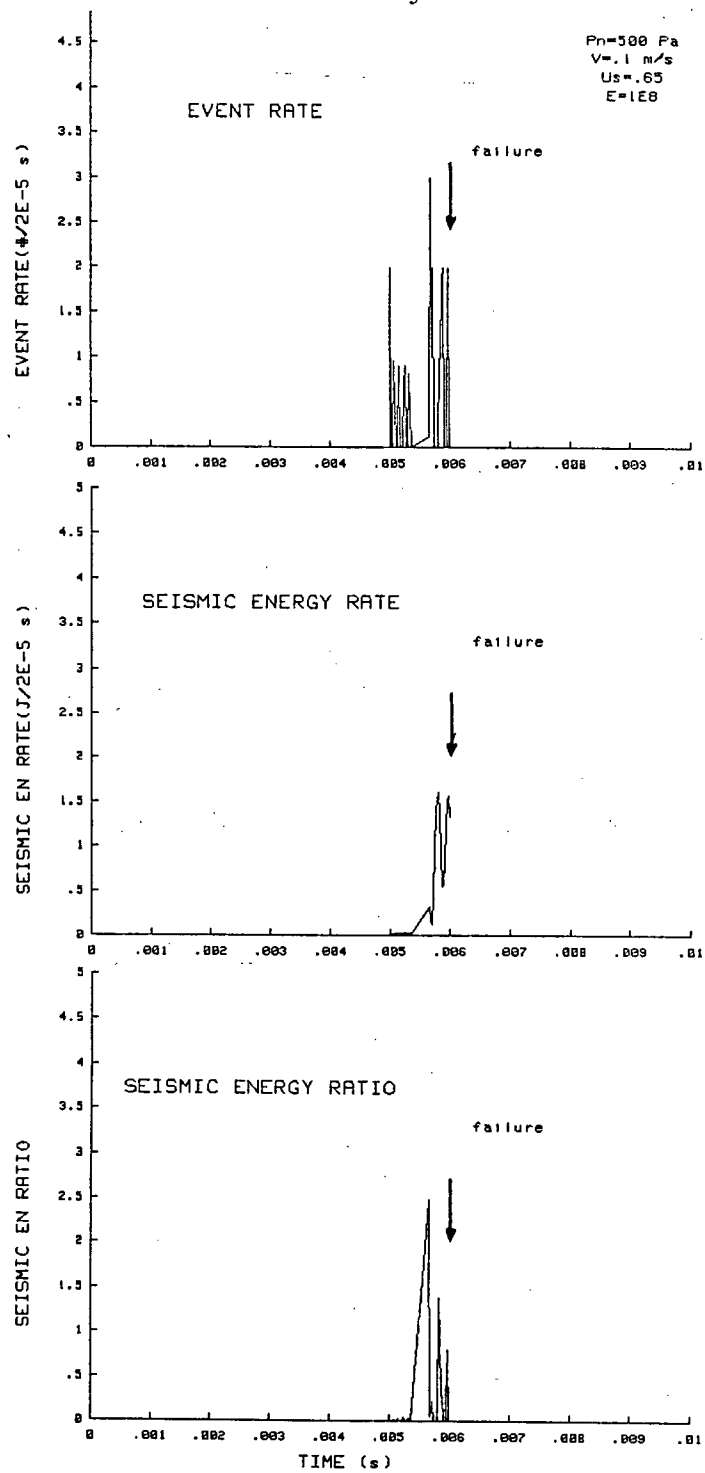

Fig.13.3a) Numerical acoustic emission at elastic modulus 100 MPa

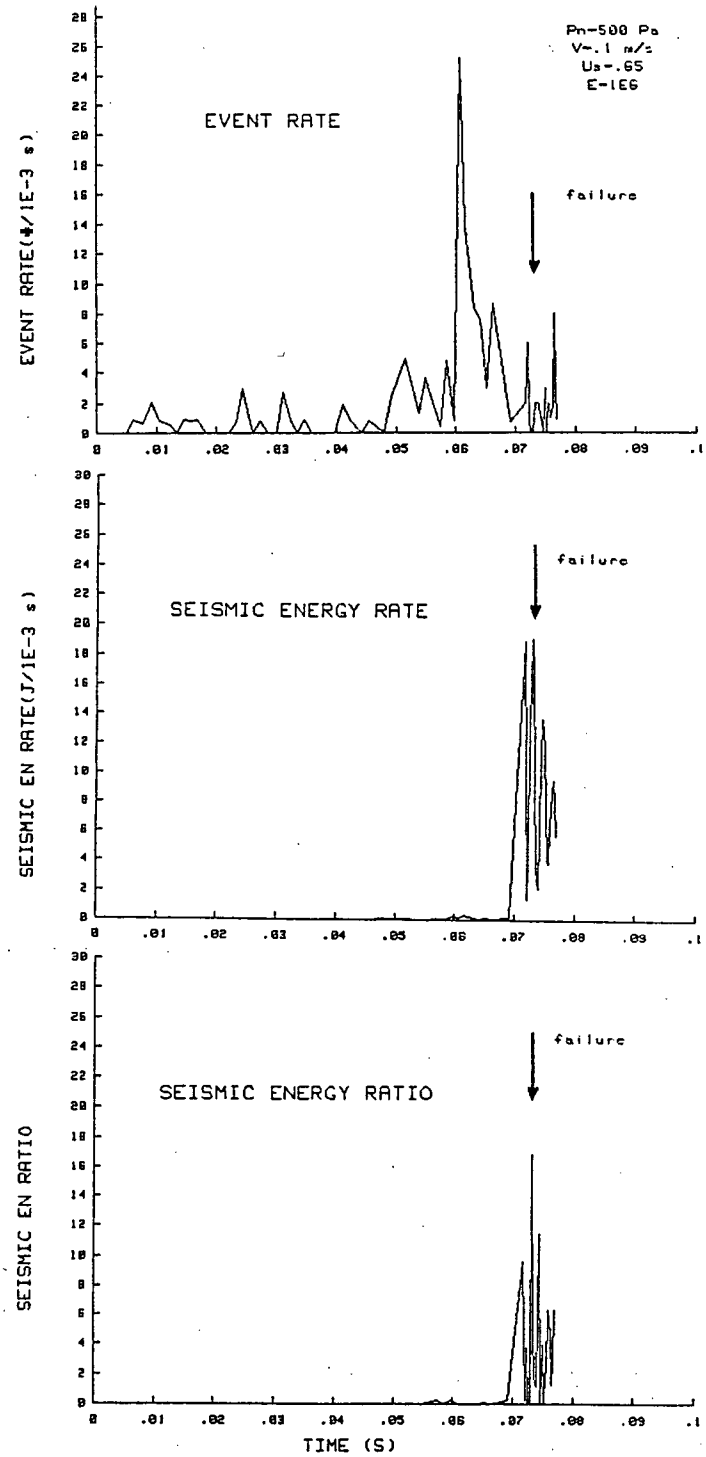

Fig.13.3b) Numerical acoustic emission at elastic modulus 1 MPa

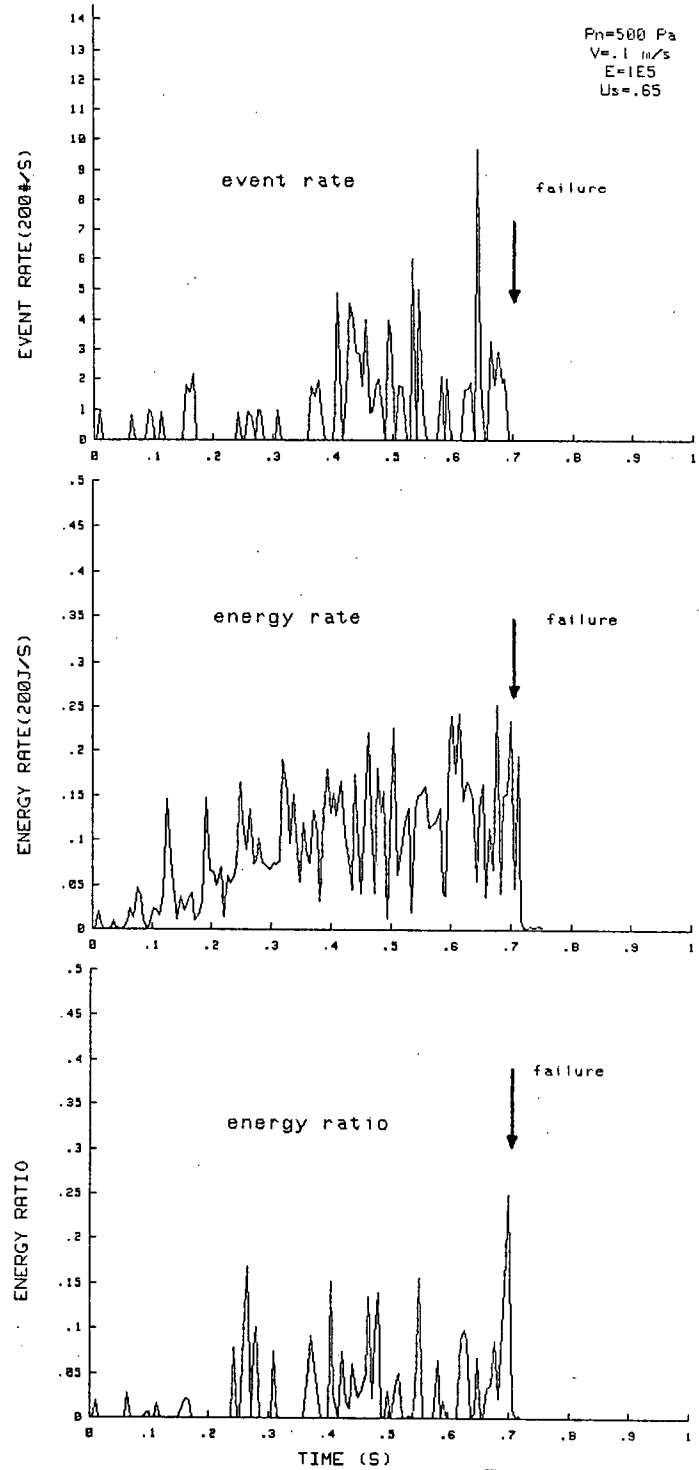

Fig.13.3c) Numerical acoustic emission at elastic modulus 100 KPa

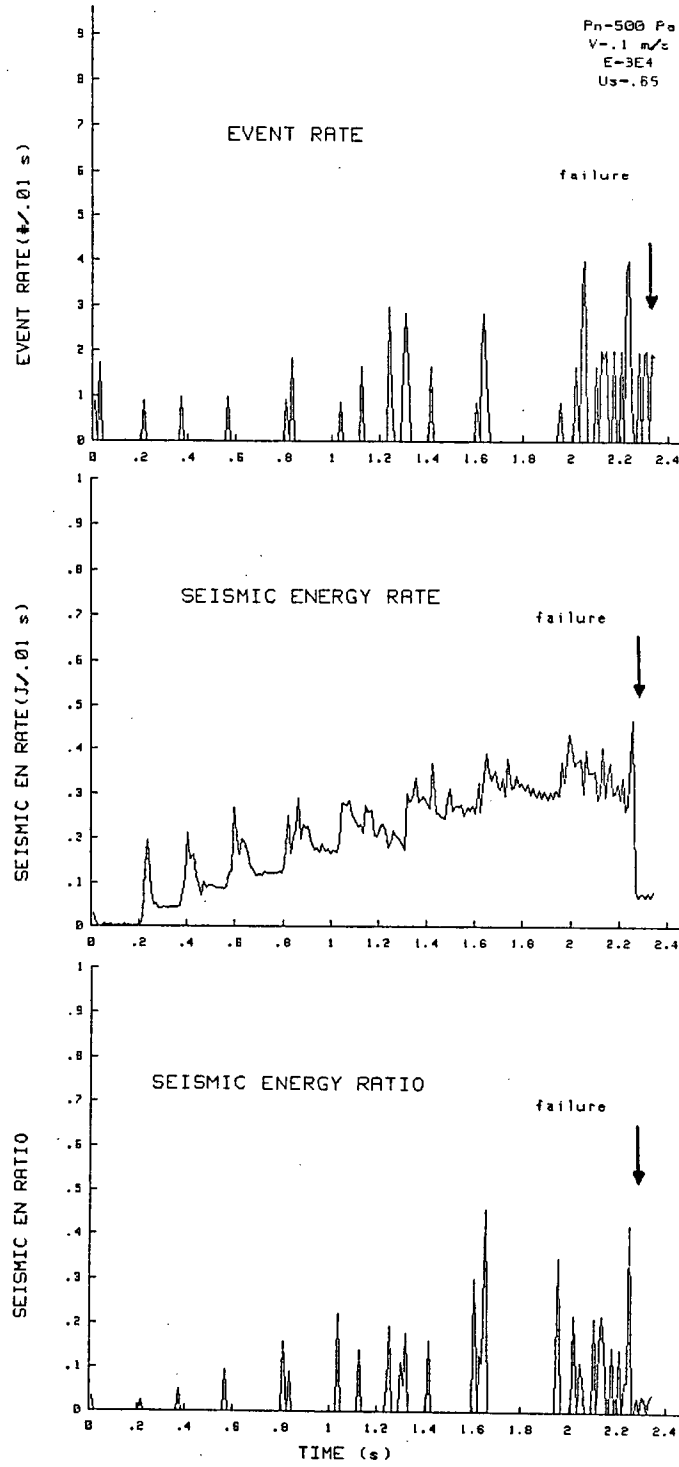

Fig.13.3d) Numerical acoustic emission at elastic modulus 30 KPa

showed broad signals. Even at the moment of failure, the anomaly is not clear. However, all these parameters are characterized by low magnitude. This is probably because the rock mass with very low elasticity possesses higher plasticity. Hence during the failure process, fracturing becomes less intense, the event number consequently decreases. Meanwhile, due to the low elasticity, the capacity of storing strain energy is lowered. Energy released during the failure is small. In this case, when failure occurs, the damage and danger will be little.

From figure 13.3, it can be seen that the time it takes for the failure to occur from the beginning of loading decreases dramatically as the elasticity increases. This may also indicate that fracturing and energy release will be more intense at failure when the elasticity becomes higher.

13.4. ACOUSTIC EMISSION UNDER MULTIPLE ELASTICITY

Rock masses usually consist of different kinds of rocks. Each of them has different mechanical properties. In various conditions, the acoustic activity may be different from that in a massive rock mass consisting of a single layer. In order to study the effect of the anistropy of the rock mass, acoustic emissions were modelled for cases in which a thin harder or softer rock is intercalated in the middle of a massive rock mass. This is done by assigning different elastic values to the springs of the model shown in figure 12.1.

13.4.1. A Hard Intercalation

First, the case of a hard intercalation is modelled. The elastic modulus of this intercalated layer is one order of magnitude higher than the matrix rock. The computed results are given in figure 13.4. Apparently, the acoustic activity is different from that as in the matrix rock alone shown in figure 13.3b). A large number of events are generated before the failure, which surprisingly agrees with observations [40] made in the field because more seismic events were recorded in this condition.

As can be expected, when the shear force is transmitted to the hard layer which seems to behave like a barrier, the acoustic emission begins to build up sharply. From then, the seismic energy rate remains on a level of magnitude equivalent to the maximum value in figure 13.3b), until a dramatic jump at failure. Meanwhile, the event rate varies greatly and shows more than one anomaly. The precursive signal described before, or the up and down of event rate, is not unique, even though one occurs prior to the failure. In this situation, the event rate alone can give a misleading interpretation to the final failure. However, if the seismic energy is examined at the same time, the precursive signals are still observable. A sharp increase followed by a drop of the event rate, and a peaking up of the energy release can be seen prior to the failure. However, the magnitude of the event rate and of the energy release is much higher than in the country rock, figure 13.3b).

The increase of acoustic activity is caused by the presence of the hard layer. As harder rock usually has higher strength and fails at higher level of

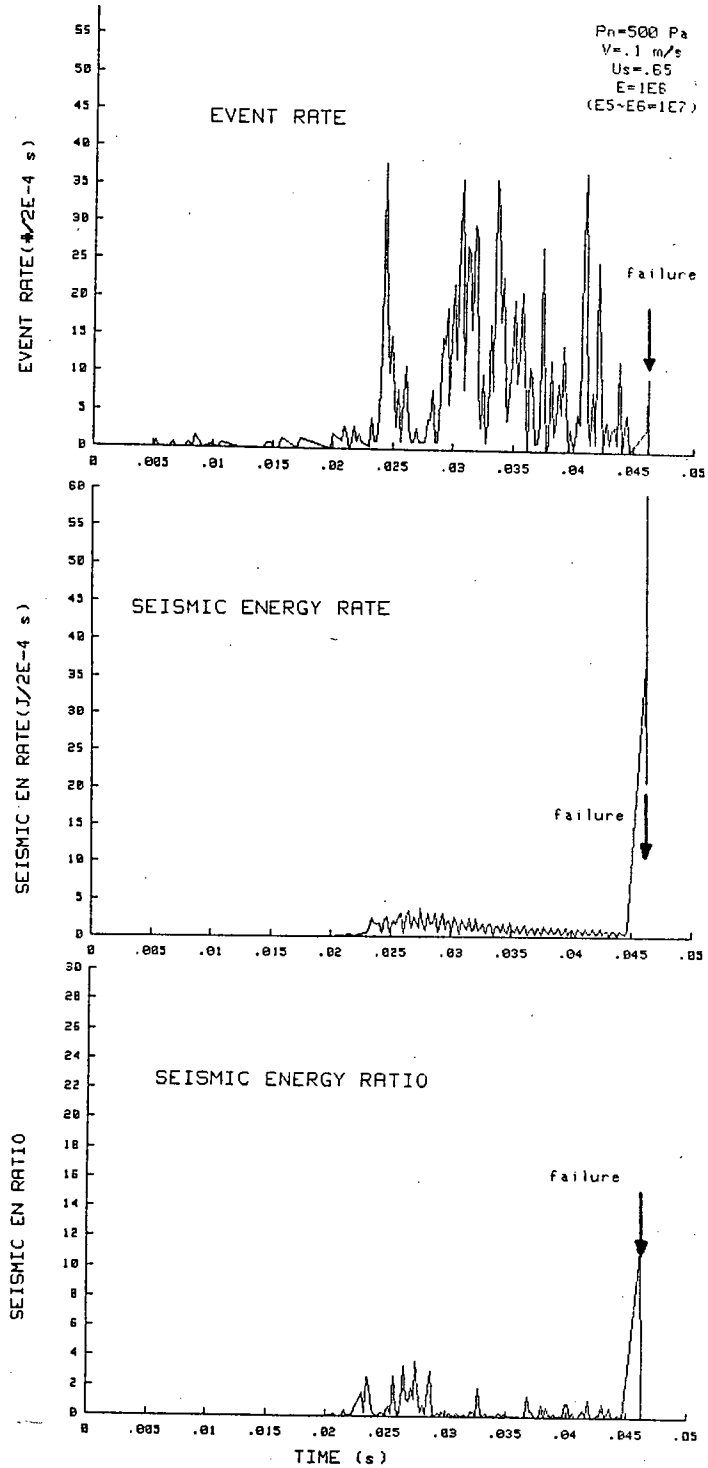

Fig.13.4 Numerical acoustic emission with a hard intercalation

stress. When the stress reaches a certain level, microfractures may well be developed in the matrix rock. But the hard layer may remain intact. By the time microfracturing develops in the hard layer, the stress will have reached a higher level. During this period, the microfracturing in the matrix rock will have become more intense due to the increase of stress. Correspondingly, the event rate increases sharply. But because the fracturing is still in micro scale, the increase of energy may be not significant. As the stress continue to increase, the hard layer may dominate the failure process until it fails. Obviously, the energy released at failure will be much higher because the existence of the hard layer has enabled the stress to reach a higher level.

In addition, due to the existence of the hard intercalation, the time it takes for the failure to occur is decreased as compared with that given in figure 13.3b).

13.4.2. A Soft Intercalation

Similarly, the case of a soft intercalation is modelled. The elastic modulus of this intercalated layer is one order of magnitude lower than the matrix rock mass. The computed results of acoustic emission are plotted in figure 13.5. As can be seen, these results are quite similar to those from the matrix rock shown in figure 13.3b). However the magnitudes of event rate and energy release rate become much higher. The warning time by event rate seems very short. Even though the event rate drops after a sharp increase, it drops not long before the failure. However a precursive signal is well developed by the energy release. The event rate and energy release together can still work to indicate the failure.

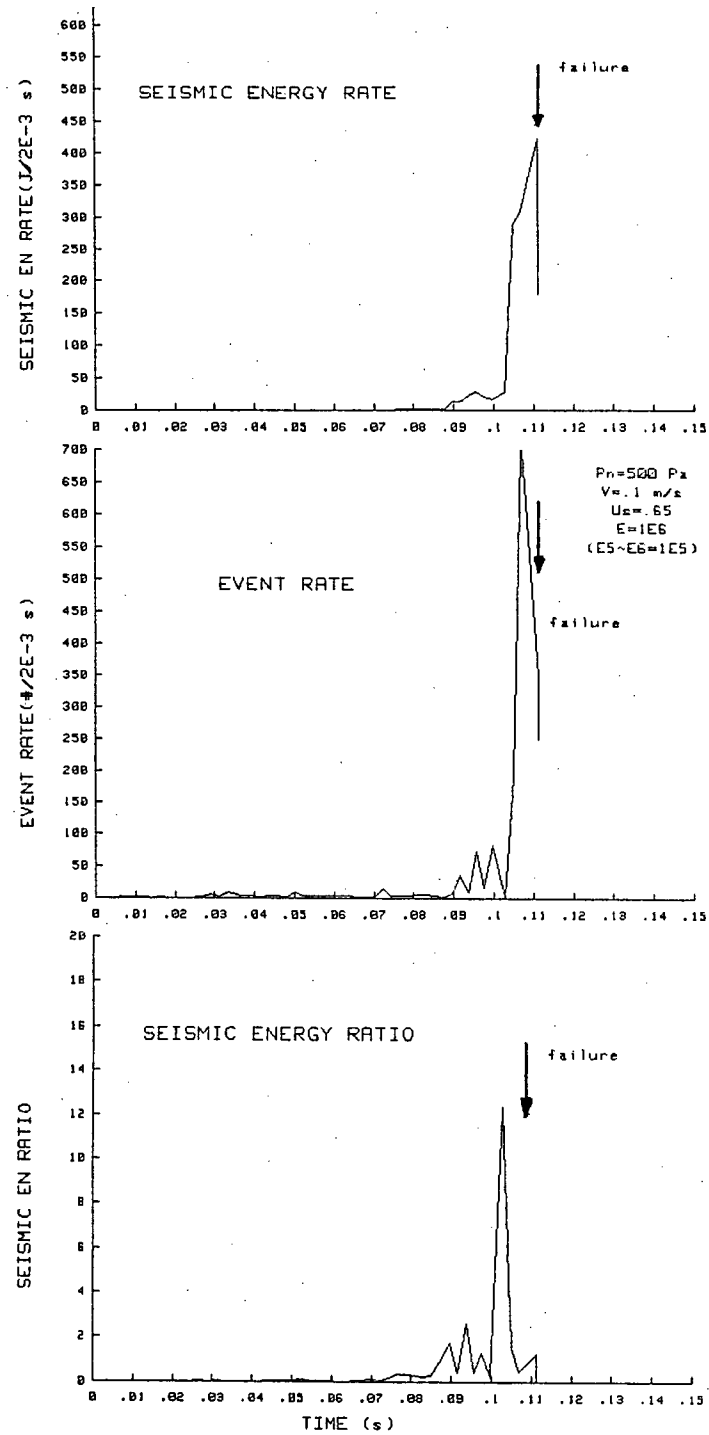

Fig.13.5 Numerical acoustic emission with a soft intercalation

The presence of a soft layer will obviously affect the failure behavior of the rock mass because this layer has lower strength. Its effect is however closely related to its orientation with respect to the loading direction. If this soft layer is parallel to the major shear direction, it will dominate the failure process and the failure behavior will be the same as in the soft layer alone. If it has a maximum angle to the major shear direction, the failure behavior will be different. In this case, microfracturing initiation and deformation may take place in the soft layer first. At this time the acoustic emission is small as shown in figure 13.3c). As loading continues, fracturing will initiate and propagate in the matrix rock until the failure occurs. The soft layer may act as a bumper and delay the failure as can be seen by the failure time in figure 13.5 which is shorter than in figure 13.3b).

13.5. SUMMARY

In this chapter, acoustic emissions under various conditions were studied on the numerical model. The changes of pressure, loading speed, elasticity of the rock mass and the anistropy were introduced. Except in some extreme conditions, the previously described precursive signals obtained from laboratory tests and field measurements exist in all cases. Before the failure, the event rate increases sharply and drops to a low level prior to the failure. At the time the event rate drops the energy release increases dramatically when the failure is approached. While the profile of acoustic emission is not changed, the magnitude does vary with the change of conditions.

As the pressure increases, the magnitude of energy release increases. The number of event rate and the time for failure to take place remain more or

less unchanged. When the loading speed gets higher but below the critical level, the magnitude of event rate becomes higher and the failure time becomes shorter. However the energy release is not affected. In the rock mass with higher elasticity, the magnitude of energy release and the number of events become much higher, and the failure time becomes significantly shorter.

In the case of a hard intercalation, the results show a large number of events which surprisingly agrees with field measurements, and give more than one anomaly in event rate, higher value in energy release and a shorter failure time than in the country rock mass; if a softer layer is intercalated in a massive rock, increases in the event rate and energy release are observed before the failure, which is delayed. Here the precursive signal from the event rate disappears and the time delay between the increases of event rate and energy release can hardly be seen. The simulated acoustic activities under these two conditions may give some explanation of the problems encountered microseismic monitoring in the field, in that sometimes anomaly is not followed by failure and sometimes failure occurs without anomaly [21,52].

Under the extreme conditions, such as a high loading speed above the critical level, or a rock mass with very low elasticity, those precursive signals may not be well developed.

CHAPTER 14. CONCLUSIONS

14.1. CONCLUSIONS

During this project, a basic mechanism of violent rock failure and rockbursting has been postulated. A process analogous to shearing is considered to be the basic mechanism of rock failure under all conditions. Even with massive rock, the shearing process ultimately determines the post-failure behavior because the development of extensive microfracturing will eventually lead to the formation of a fracture surface on which the final failure takes place. This assumption has been used to interpret violent rock failure occurring under any condition and at any location of an underground opening. According to this hypothesis, the normal non-violent rock failure is a gradual process which occurs when a low pushing force as a result of small stress differences at low speed results in smooth sliding. However if large stress differences and therefore a high pushing force is applied suddenly or at high speed, or if a sudden reduction of the shearing resistance makes a sudden slip, the stored energy will be released suddenly and the resulting failure will be violent.

Based on stick-slip that takes place during shearing, a numerical model was developed, by which the effects on the slip behavior from all factors involved were examined. Cohesion has no effect on slip behavior. The effect of the frictional coefficient is negligible. The effect of normal pressure is the most significant factor and all slip parameters increase with the normal pressure. The effect of elasticity is great when it is relatively low but becomes less important when it is high. Loading speed has an inverse relation with the stick time but it hardly changes other slip parameters when it is below the critical transition level.

Transition conditions of slip behavior between stick-slip and stable sliding were obtained and they are combinations of normal pressure, loading speed and elasticity. From the transition conditions, violent failure is expected to occur in the following three cases:

Mode I. Violence is the result of stick-slip under very high normal pressure because of the large amount of energy released at each slip.

Mode II. Violence comes from the transition from stick-slip to stable sliding due to the extra energy available at transition.

Mode III. Violence occurs under sudden loading. Whether the shear behavior is in stable sliding or stick-slip, violent failure is bound to occur if a shear force much higher than the strength is instantly/suddenly applied.

A rockburst along a natural fault or a major discontinuity can be explained by Mode I and II violence. Violent failure during shear testing is an example of Mode II violence. Mode III violence can be used to interpret clearly the violent failure of a rock specimen in conventional compressive testing and the results can also be applied to describe rockbursts occurring in a massive rock.

Acoustic emissions from rock specimens were also studied in laboratory conditions and some important results were obtained. Acoustic emission during the shearing process is considered to be a continuation and an expansion of the acoustic emission in compression after the formation of the failure surface. For warning purposes, the most significant information is the precursive signals before the formation of the failure surface under compression. In this case, after an initial quiet period, which corresponds to the perfect elastic deformation, the event

rate increases rapidly initially when stress has reached a certain level and then may die down immediately preceding the specimen failure. At the same time, the energy released increases steadily and reaches a peak as failure is approached. It is proposed that the increase of acoustic activity corresponds with a process of unstable fracture propagation. If this is so then the drop of event rate and the peak up of the energy release indicate the coalescence of microfractures. These phenomena are in good agreement with the fracture process discussed in chapter 3.

A numerical acoustic model based upon the stick-slip during the shearing process is developed to simulate the acoustic activity prior to violent rock failure. It has realistically simulated the acoustic activity during violent rock failure. The numerical acoustic signals are an accurate reproduction of acoustic signals from laboratory tests and measurements made in the field.

The results from both laboratory tests and numerical modeling are compared with measurements made in a mine and they are largely in agreement. This suggests that the proposed mechanism is valid for interpreting violent rock failure and that acoustic signals obtained in this way in the laboratory indicate a method by which rockbursts can be predicted with satisfactory reliability.

Further research was carried out using the numerical acoustic model to study acoustic emissions under various conditions. The influence of factors such as normal pressure, loading speed, elasticity and anistropy of rock mass were

extensively analyzed. In general, if the loading speed is less than the critical transition value and if the elasticity is not too low, when the above factors change, the pattern of acoustic emission changes little and the precursive signals are observable. Significant signals are obtained when an inclusion exists. A hard intercalation can increase the magnitude of energy release, decrease the time it takes for failure to occur and generate a large number of events and more than one anomaly in event rate. A soft intercalation can increase both event rate and energy release and delay the failure. This information may interpret the problems faced in microseismic monitoring in the field that sometimes violent rock failure occurs without warning and sometimes an anomaly is not followed by failure.

In conclusion, the results of this research show that violent rock failure can occur in any mine rock as long as the conditions for violence are satisfied, and that acoustic emission can provide precursive signals for warning of violent rock failure, in terms of event rate, energy release rate and the down-shift in corner frequency, in particular the latter two factors.

14.2. RECOMMENDATIONS FOR FURTHER RESEARCH

Although this research has achieved satisfactory results, it was limited in the amount of laboratory testing that was possible. In order to apply the principals used and the results obtained in this research to the practice of rockburst control and microseismic monitoring in the field, it is felt that the work should be extended to a burst-prone mine with a microseismic monitoring system that can locate "hot spots" in the mine and then monitor the seismic energy emanating from these potential rockburst sites.

As described in this thesis, precursive signals of acoustic emission from a specific rock mass should be obtained from the laboratory testing of small specimens. After being calibrated with data obtained from monitoring in the same mine, these results should provide a sound method of predicting which rocks in a mine would be likely to burst if the geological conditions, stress state and mining activity are clearly known. It will need experience in assessing the changing pattern of acoustic energy emitted prior to a major event in order to establish limits that will allow reliable prediction.

The length of the period during which the acoustic emission is most active can be obtained statistically from tests or monitoring in a particular mine so that an accurate time of warning for a violent failure can be provided.

In order to give a reliable prediction of rockbursting, the existing microseismic monitoring system needs improving in both data analysis and the technique of its data acquisition. For instance, multi-axial geophones should be used as transducers because the uniaxial geophone in use today is only sensitive to its axial direction and cannot detect signals coming in the plane perpendicular to that direction. Energy should be estimated at the signal source or at some common reference point because the energy attenuation can be significant and varies with distance and properties of the rock. But in monitoring in the field, energy is usually estimated at the location of some geophone which receives signals first, and the data measured for different signals are therefore not accurate for use in comparison. It is essential that spectrum analysis of the waveform should be conducted in order to study the frequency change as failure is approached and to provide another important precursor to violent failure.

BIBLIOGRAPHY

1. Blake, W. "Rockburst mechanism". *Quarterly of the Colorado School of Mines, vol.* 67, 1972, 61 p.

2. Curtis, J. F. "Rockburst phenomena in the Gold Mines of the Witwatersrand: a review". *Trans. Inst. Min. Metall. vol.* 90, Oct. 1981, pp.A163-A176.

3. Mclaughlin, W.C., Waddell G.G. & McCaslin J.G. "Seismic equipment used in the rockburst control in the Coeur d'Alene Mining District, Idaho". *USBM RI*8138, 1976, 29 p.

4. Heunis, R. "Rock bursts and the search for an early warning system". *Mining Magzine, Feb.*, 1977, pp.83-89

5. "An industry guide to the amelioration of the hazards of rockbursts and rockfalls". *Compiled by the high-level committee on Rockbursts & rockfalls. A chamber of mines of S. Afr. Publication, P.R.D. Series* No. 216 1977

6. Salamon, M.D.G. contributions to reference 2, pp.A212-213.

7. Morrison, R.G.K. "Report on the rockburst situation in Ontario mines". *The CIM Transactions*, vol. XLV, 1942, pp.225-272.

8. Wawersik, W. R. & Fairhurst, C. "A study of brittle rock fracture in laboratory compression experiments". *int. J. Rock Mech. Min. Sci.* vol. 7, 1970, pp.561-575.

9. Heard, H. C. "Effect of large changes in strain rate in the experimental deformation of Yule Marble". *J. of Geology*, vol. 71, 1962, pp.162-195

10. Hudson, J. A., Crouch, S. L. & Fairhurst, C. "Soft, stiff and servo-controlled testing machines". *Eng. Geology*, (1972).

11. Brace, W. F. & Byerlee, J. D. "Stick-slip as a mechanism for earthquakes". *Science* 153, p990, 1966

12. Cook, N.G.W. "The basic mechanism of rockbursts". *S. Afr. Inst. Min. Metall. J.*, v. 64, pp.71-81, 1963 b.

13. Cook, N.G.W. "A note on rockbursts considered as a problem of stability". *S. Afr. Inst. Min. Metall. J.*, v 65, pp437-446, 1965.

14. Taylor, J. T. M. "Research on ground control and rockbursts on Kolar Gold Field, India." *Trans. Inst. Min. Metall. vol.* 72, 1962-63, pp.317-338.

15. Blake, W. "Microseismic application for mining --- a practice guide". *Final Report*, US Bureau of Mines, 1982.

16. Zou, Daihua & Miller, H. D. S. "Microseismic source location technique --- literature investigation". *Internal Report*, Dept. of Mining Eng., The University of BC, 1984.

17. Brink, A. V. Z. & Mountfort, P. I. "Rockburst prediction research at Western Deep Levels, ltd." *---A Review Report for the Period 1981 - 1984*, report No. RPP.21, 1985.

18. Blake, W. "Preconditioning an entire stope block for rock burst control". *Final Report*, US Bureau of Mines, 1980.

19. Neyman, B., Zuberek, W. & Szecowka, Z. "Effective methods for fighting rock burst in Polish collieries". *5th int. Strata Control Cong.*, 1972, pp.1-9.

20. Krawiec, A. & Stanislaw, T. "Rock bursting in Polish deep coal mines in light of research and practical observation". *Society of Min. Eng.*, AIME, vol. 262, 1977, pp.30-36.

21. Leighton, F. "Growth and development of microseismics applied to ground control and mine safety". *Mining Engineering, August*, 1983, pp. 1157-1162.

22. Bieniawaski, Z. T. "Mechanism of brittle fracture of rock, Part I-III". *int. J. Rock Mech. Min. Sci.*, vol. 4, pp.395-430, Pergamon Press ltd. 1967.

23. Scholz, C. H. "Experimental study of the fracturing process in brittle rock". *J. of Geophy. Res.* vol. 73, No. 4, 1968, pp.1447-53.

24. Savage, J. C. "Radiation from a tensile fracture". *J. Geophys. Res.* 68(23), 6345, 1963.

25. Mogi, K. "Study of the elastic shocks caused by the fracture of hetero-geneous materials and its relation to earthquake phenomena". *Bull. Earthquake Res. Inst.* Tokyo Univ. 40, 125, 1962.

26. Jaeger, J. C. & Cook, N. G. W. "Fundamentals of rock mechanics". *text book*, 1969

27. Scholz, C. H. & Engelder, J. T. "The role of asperity indentation and ploughing in rock frictions: 1 asperity creep and stick-slip". *Int. J. Rock Mech. Men. and Geomech. abstr.* 13, 149-154, 1976.

28. Pan, W.D. "Statistic method", *text book*, Shanghai Publishing House, 1980

29. Stesky, R. M. "Rock friction effect of confining pressure, temperature, and pore pressure". *Pageoph.* vol. 116, pp.690-703, 1978

30. Barton, N. "Review of a new shear-strength criterion for rock joints". *Eng. Geology*, 7, pp.287-332, 1973

31. Schneider, H. J. "The friction and deformation behavior of rock joints".

Rock Mech. 8, pp.169-184, 1976

32. Barton, N. "The shear strength of rock and rock joints". *Int. J. Rock Mech. Min. Sci.* 13, pp.255-279, 1976

33. Byerlee, J. D. "Brittle-ductile transition in rocks". *J. Geophys. Res.*, 73(14), pp.4741-4750, 1968

34. Vesic. A. S. & Clough, G. W. "Behavior of granular materials under high stresses". *J. Soil Mech. Found. Div.* 94(SM3), 661-688, 1968

35. Stesky R.M., Brace W.F., Riley D.K. & Robin P.Y.F. "Friction in faulted rock at high temperature and pressure". *Tectonophysics* 23, pp.177-203, 1974

36. Drennon, C. B. & Handy, R. L. "Stick-slip of lightly-loaded limestone". *Pnt. J. Rcok Mech. Min. Sci.* 9, pp.603-615, 1972

37. Friedman M., Logan J.M. & Rigert J.A. "Glass-indurated quartz gouge in sliding friction experiments on sandstone". *Bull. Geol. Soc. Amer.* 85, pp.937-942, 1974

38. Engelder, J. T. "The sliding characteristics of sandstone on quartz fault-gouge". *Pure and Appl. Geophys.* 113, pp.69-86, 1975

39. Dieterich, J. H. "Time-dependent friction and the mechanism of stick-slip". *Pageoph.* vol. 116, pp.790-805, 1978

40. Hoskins, E.R., Jaeger J.C. & Rosengren K.T. "A medium-scale direct friction experiment". *Int. J. Rock Mech. Min. Sci.* vol. 5, pp.143-154, 1968

41. Spottiswoode, S. M. "Source mechanisms of mine tremors at Blyvooruitzicht Gold Mine". *Proc. 1st int. cong. on Rockbursts and Seismicity in Mines*, Johannesburg, 1982. pp.29-37. SAIMM No. 6, 1984.

42. Hoek, E. "Strength of jointed rock masses". *Geotechnique 33*, No.3, pp.187-223, 1983

43. Burridge, R. & Knoppoff, L. "Model and theorectical seismicity", *Bull. of the Seism. Soci. of America*, vol. 57, No.3, pp.341-371, 1967.

44. Dobrin, M. B. "Introduction to geophysical prospecting". *text book*, 3rd ed. 1976

45. Nie, T. J. "Engineering mathematics: Numerical method". *text book*, China National Defense Publishing House, 1982

46. Engelder, J. T. and Scholz, C. H. "The role of asperity indentation and ploughing in rock friction: II. Influence of relative hardness and normal load". *Int. J. Rock Mech. Min. Sci. and Geomech. Abstr.* 13, pp.155-163,

1976.

47. Coates, D. F. "Rock mechanics principles", *text book*, Methuen & Co Ltd, 1970

48. Gay N.C., Spencer D., Van Wyyk J.J. & Van Der Heever P.K. "The control of geological and mining parameters in the Klerksdorp gold mining district". *Proc. 1st Int. Cong. on Rockbursts and Seismicity in Mines. Johannesburg*, 1982, SAIMM No.6, pp.107-121, 1984

49. Hardy, Jr. H.R. "Emergence of acoustic emission/microseismic activity as a tool in geomechanics". *Proc. 1st conf. on AE/MA in Geol. Structures & Materials*, 1977, pp13-31.

50. Gibowicz, S. J. "The mechanism of large mine tremors in Poland". *Proc. 1st Int. Cong. on Rockbursts and Seismicity in Mines, Johannesburg, 1982.* pp.17-28, SAIMM No.6, 1984.

51. Bath, M. "Rockburst seismology", *Proc. 1st Int. Cong. on Rockbursts and Seismicity in Mines, Johannesburg, 1982.* pp.7-15, SAIMM No.6, 1984.

52. Leighton, F. "Microseismic activity associated with outbursts in coal mines". (*Report, USBM, Denvor Research Center*, 1981, 11 p.)

53. A'lheid, H. J. and Rummel, F. "Acoustic emission during frictional sliding along shear planes in rock". *Proc. 1st Conf. on AE/MA in Geological Structures and Materials*, 1977, pp.149-155.

54. Holcomb, D. J. and Teufel, L. W. "Acoustic emission during deformation of jointed rock". *Proc. 2nd Conf. on AE/MA in Geological Structures and Materials.* 1984, pp.37-45.

55. Sondergeld, C. H. Granryd, L. and Estey, L. H. "Acoustic emission during compression testing of rock". *Proc. 2nd Conf. on AE/MA in Geological Structures and Materials.* 1984, pp.131-147.

56. Starfield, W.M. & Wawersikk W.R. "Pillars as structural components in room and pillar mine design". *Proc. of 10th Symp. on Rock Mech. University of Texas*, 1968, pp793-809.

57. Christensen R.J. "Torsional shear measurements of the frictional properties of Westerly granite". *Final Report, Dept. Nucl. Agency, Contract* No DNA001-72-C-0026, 1973, 48p.

58. personal contact with Dr. Miller, H.D.S.

APPENDIX I. LIST OF FORTRAN PROGRAM MODEL1 AND SAMPLE RESULTS

```
C   ************************************************************
C   *                                                          *
C   *                      " MODEL1 "                          *
C   *          --- typical shearing analysis ---               *
C   *                 by Daihua Zou, 1985                      *
C   *                                                          *
C   ************************************************************

C           Numerical solution: single block model
C         Slip velocity dependent friction: u=u(X')
C                 Slip back permitted here

C     This program is written for numerical solution to the system
C     of first order defferential equations by Runge-Kutta method

C    ************************************************************

      IMPLICIT REAL*8(A-H,O-Z)
      COMMON /BLK1/A,B,XXI
      COMMON/BLK2/TI,XI,H
      COMMON/BLK3/FM,FLAMD,VO,BTA
      COMMON/BLK4/A1,B1,C1,E1
      DATA U,P,CO,G/0.65DO,10.DO,0.DO,9.806DO/
      DATA TO,XXO,XO, EO,N/0.DO,1D-11,0.DO,0.01DO,2500/

      VO=1.OD-7
      BTA=0.DO
      FM=1.DO
      FLAMD=100.DO
      A1=.528DO*(P/FM+G)
      B1=.1218DO*(P/FM+G)
      C1=CO/FM
      E1=1.DO
      E=EO
      HO=.05DO
      TI=TO
      XXI=XXO
      XI=XO
      II=0
      A=FLAMD/FM
      B=U*(P/FM+G)
      A2=(A1+C1)*FM
      B2=B1*FM
      C2=B*FM
      CALL SUB2(A2,B2,C2,E1,FI,FFI)

      WRITE(6,10)
   10 FORMAT(2X,'solultions by Runge-Kutta method for single block
     1 friction model',/,25X,'unit system: ***M-KG-SECOND***',/)
      WRITE(6,12)FM,P,FLAMD,G,U,VO,BTA
   12 FORMAT(6X,'M=',F10.4, 6X,'P=',F10.4,2X,'LAMDA=',F10.4,6X,
     1 'G=',F10.4,/,6X,'U=',F10.4,5X,'VO=',F10.8,3X,'BETA=',F10.5,/)
      WRITE(6,14)
   14 FORMAT(3X,'N',8X,'T(I)',11X,'X¬(I)',
     1   12X,'X(I)',12X,'F(I)',12X,'FF(I)',/)
      WRITE(6,15) II,TO,XXO,XO,FI,FFI
   15 FORMAT(1X,I4,1X,5F15.8)
      J=0
```

```
      J1=0
      K=0

   40 DO 80 I=1,N
      H=HO
   45 CALL SUB1(E,XX2,X2)

C     CHECK THE SIGN OF VELOCITY AT TWO ADJACENT POINTS
   60 IF(DSIGN(XXI,XXI).EQ.DSIGN(XXI,XX2)) GOTO 65

C     INCREASE THE ACCURACY WHEN THE VELOCITY REACHES O
      IF(J.NE.O) GO TO 63
      E=E/((IDINT(J1/10.DO)+1)*5.DO)
      J=J+1
      J1=J1+1
      GO TO 45
   63 J=O
   65 XXI=XX2
      XI=X2
      TI=TI+H
      CALL SUB2(A2,B2,C2,E1,FI,FFI)

   70 WRITE(6,15)I,TI,XXI,XI,FI,FFI
      IF(DABS(XXI).LT.1D-11)GO TO 100
   80 CONTINUE
      GO TO 150

  100 K=K+1
      IF (K.EQ.2)GO TO 150
      IF (BTA.EQ.O)GO TO 105
      TO=(DSQRT(VO*VO+4*BTA*XI)-VO)/(2*BTA)
      GO TO 107
  105 TO=XI/VO
  107 T1=TO-TI

      WRITE(6,110)TI,XI,T1
  110 FORMAT(/,3X,'THE SLIP TIME       T1=',F15.5,'  SECONDS',
     1  /,3X,'THE SLIP DISTANCE Xmax=',F15.5,'  METRES',
     2  /,3X,'THE STICK TIME      T2=',F15.5,'  SECONDS',/)
      TI=TO
      XXI=XXO
      J=O
      J1=O
      E=EO
      GO TO 40

  150 STOP
      END

      SUBROUTINE SUB1(E,XX2,X2)
      IMPLICIT REAL*8(A-H,O-Z)
      COMMON/BLK1/A,B,XXI
      COMMON/BLK2/TI,XI,H

      CALL RK(TI,XXI,XI,H,XX1,X1)
      H=H/2.DO
    5 CALL RK(TI,XXI,XI,H,XX2,X2)
      D1=XX2-XX1
```

```
117             D1=DABS(D1)
118             IF (D1.LT.E)GO TO 20
119          15 H=H/2.DO
120             XX1=XX2
121             GO TO 5
122          20 RETURN
123             END
124
125             SUBROUTINE SUB2(A2,B2,C2,E1,FI,FFI)
126
127       C     CALCULATE FORCES
128             IMPLICIT REAL*8(A-H,O-Z)
129             COMMON/BLK1/A,B,XXI
130             COMMON/BLK2/TI,XI,H
131             COMMON/BLK3/FM,FLAMD,VO,BTA
132
133             FORS(T,X)=C2+FLAMD*(VO*T+BTA*T*T-X)
134             FI=FORS(TI,XI)
135             FFI=O.DO
136             IF (XXI) 5,30,20
137           5 FFI=FI+A2+B2/(7.DO+DLOG10(-XXI+1D-6))-E1*XXI
138             GO TO 30
139          20 FFI=FI-A2-B2/(7.DO+DLOG10(XXI+1D-6))-E1*XXI
140          30 RETURN
141             END
142
143             SUBROUTINE RK(X,Y,Z,H1,YN,ZN)
144
145             IMPLICIT REAL*8(A-H,O-Z)
146             G(X,Y,Z)=Y
147             H=H1
148           5 F1=H*F(X,Y,Z)
149             G1=H*G(X,Y,Z)
150             IF((Y+F1/2.DO).LT.O.DO)GO TO 10
151             F2=H*F(X+H/2.DO,Y+F1/2.DO,Z+G1/2.DO)
152             G2=H*G(X+H/2.DO,Y+F1/2.DO,Z+G1/2.DO)
153             IF((Y+F2/2.DO).LT.O.DO)GO TO 10
154             F3=H*F(X+H/2.DO,Y+F2/2.DO,Z+G2/2.DO)
155             G3=H*G(X+H/2.DO,Y+F2/2.DO,Z+G2/2.DO)
156             IF((Y+F3).LT.O.DO)GO TO 10
157             F4=H*F(X+H,Y+F3,Z+G3)
158             G4=H*G(X+H,Y+F3,Z+G3)
159             YN=Y+(F1+2.DO*(F2+F3)+F4)/6.DO
160             ZN=Z+(G1+2.DO*(G2+G3)+G4)/6.DO
161             IF(YN.LT.O.DO)GO TO 10
162             RETURN
163          10 H=H/2.DO
164             GO TO 5
165             END
166
167             DOUBLE PRECISION FUNCTION F(X,Y,Z)
168
169             IMPLICIT REAL*8(A-H,O-Z)
170             COMMON/BLK1/A,B,XXI
171             COMMON/BLK3/FM,FLAMD,VO,BTA
172             COMMON/BLK4/A1,B1,C1,E1
173
174             FR(Y)=A1+C1+B1/(7.DO+DLOG10(Y+1D-6))
```

```
175            FRO=FR(O)
176            F=O.DO
177            FD=B+A*(VO*X+BTA*X*X-Z)
178            IF(DABS(Y).LT.1D-13) GO TO 30
179            IF(Y.GT.O.DO) GO TO 20
180            F=FD+FR(-Y)-EO*Y/FM
181            GO TO 50
182         20 F=FD-FR(Y)-EO*Y/FM
183            GOTO 50
184         30 IF(DABS(FD).LT.DABS(FRO)) GOTO 50
185            F=FD-DSIGN(FRO,FD)
186         50 RETURN
187            END
188
```

******* Results of typical shearing analysis *******

solultions by Runge-Kutta method for single block friction model
unit system: ***M-KG-SECOND***

M= 1.0000 P= 10.0000 LAMDA= 100.0000 G= 9.8060
U= 0.6500 VO=0.00000010 BETA= 0.0

N	T(I)	X¬(I)	X(I)	F(I)	FF(I)
0	0.0	0.00000000	0.0	12.87390000	0.00397168
1	0.00625000	0.00863706	0.00002069	12.87183064	1.91693689
2	0.00937500	0.01468679	0.00005712	12.86818780	1.92904871
3	0.01250000	0.02077483	0.00011253	12.86264758	1.93064338
4	0.01562500	0.02687720	0.00018698	12.85520213	1.92644067
5	0.01875000	0.03297882	0.00028051	12.84584948	1.91814024
6	0.02187500	0.03906826	0.00039309	12.83459171	1.90654595
7	0.02500000	0.04513593	0.00052466	12.82143416	1.89210415
8	0.02812500	0.05117330	0.00067515	12.80638498	1.87509176
9	0.03125000	0.05717256	0.00084445	12.78945488	1.85569590
10	0.03437500	0.06312634	0.00103243	12.77065693	1.83405218
11	0.03750000	0.06902764	0.00123894	12.75000644	1.81026494
12	0.04062500	0.07486972	0.00146380	12.72752088	1.78441877
13	0.04375000	0.08064606	0.00170681	12.70321978	1.75658540
14	0.04687500	0.08635033	0.00196776	12.67712467	1.72682806
15	0.05000000	0.09197640	0.00224641	12.64925903	1.69520428
16	0.05312500	0.09751824	0.00254252	12.61964826	1.66176783
17	0.05625000	0.10297000	0.00285581	12.58831958	1.62657001
18	0.05937500	0.10832598	0.00318599	12.55530205	1.58966058
19	0.06562500	0.11872837	0.00389575	12.48432538	1.51090206
20	0.07187500	0.12868237	0.00466916	12.40698516	1.42588055
21	0.07812500	0.13814715	0.00550326	12.32357450	1.33498716
22	0.08437500	0.14708405	0.00639489	12.23441136	1.23862125
23	0.09062500	0.15545674	0.00734064	12.13983714	1.13719324
24	0.09687500	0.16323126	0.00833686	12.04021522	1.03112590
25	0.10312500	0.17037613	0.00937972	11.93592941	0.92085455
26	0.12812500	0.19212046	0.01393437	11.48046382	0.44685849
27	0.15312500	0.20197600	0.01888618	10.98528365	-0.05685437
28	0.16562500	0.20221003	0.02141563	10.73233861	-0.31000292
29	0.17812500	0.19928646	0.02392826	10.48107620	-0.55872587
30	0.19062500	0.19324564	0.02638479	10.23542327	-0.79915236
31	0.19687500	0.18908214	0.02757995	10.11590682	-0.91508365
32	0.20312500	0.18417628	0.02874677	9.99922543	-1.02755954
33	0.20937500	0.17854644	0.02988065	9.88583747	-1.13614803
34	0.21562500	0.17221376	0.03097713	9.77618898	-1.24043428

35	0.22187500	0.16520206	0.03203190	9.67071191	-1.34002273
36	0.22812500	0.15753771	0.03304080	9.56982254	-1.43453927
37	0.23437500	0.14924954	0.03399982	9.47391990	-1.52363357
38	0.24062500	0.14036865	0.03490518	9.38338427	-1.60698179
39	0.24687500	0.13092830	0.03575327	9.29857581	-1.68428967
40	0.25000000	0.12600925	0.03615477	9.25842599	-1.72059557
41	0.25312500	0.12096367	0.03654069	9.21983327	-1.75529650
42	0.25625000	0.11579624	0.03691066	9.18283645	-1.78836599
43	0.25937500	0.11051171	0.03726430	9.14747288	-1.81978046
44	0.26250000	0.10511494	0.03760124	9.11377839	-1.84951956
45	0.26562500	0.09961084	0.03792115	9.08178729	-1.87756657
46	0.26875000	0.09400438	0.03822370	9.05153234	-1.90390897
47	0.29375000	0.04607232	0.03998489	8.87541356	-2.05418108
48	0.31875000	0.02052877	0.04040206	8.83369742	-2.09850258
49	0.34375000	0.00740584	0.04048952	8.82495185	-2.13541266
50	0.36875000	0.00062421	0.04050217	8.82368628	-2.27000465
51	0.39375000	0.00017305	0.04050225	8.82367871	-2.37846812
52	0.41875000	0.00005442	0.04050226	8.82367840	-2.51319770
53	0.44375000	0.00002308	0.04050226	8.82367860	-2.64682012
54	0.46875000	0.00000630	0.04050226	8.82367884	-2.92844294
55	0.49375000	0.00000161	0.04050226	8.82367909	-3.33755117
56	0.51875000	0.00000026	0.04050226	8.82367934	-3.82603928
57	0.54375000	0.00000007	0.04050226	8.82367959	-3.97325889
58	0.56875000	0.00000003	0.04050226	8.82367984	-4.01880088
59	0.59375000	0.00000000	0.04050226	8.82368009	-4.04329277
60	0.61875000	0.00000000	0.04050226	8.82368034	-4.04486476
61	0.64375000	0.00000000	0.04050226	8.82368059	-4.04565252
62	0.66875000	0.00000000	0.04050226	8.82368084	-4.04604674
63	0.69375000	0.00000000	0.04050226	8.82368109	-4.04624385
64	0.71875000	0.00000000	0.04050226	8.82368134	-4.04625594

THE SLIP TIME T1= 0.71875 SECONDS
THE SLIP DISTANCE Xmax= 0.04050 METRES
THE STICK TIME T2= 405021.86582 SECONDS

APPENDIX II. LIST OF FORTRAN PROGRAM MODEL2 AND SAMPLE RESULTS

```
      C   ********************************************************
      C   *                                                      *
      C   *                    " MODEL2 "                        *
      C   *             --- sensitivity analysis ---             *
      C   *                 by Daihua Zou, 1985                  *
      C   *                                                      *
      C   ********************************************************

      C          Numerical solution: single block model
      C        Slip velocity dependent friction: u=u(X')
      C                Slip back permitted here

      C     This program is written for numerical solution to the system
      C     of first order defferential equations by Runge-Kutta method

      C    ********************************************************

            IMPLICIT REAL*8(A-H,O-Z)
            DIMENSION S(5)
            COMMON /BLK1/B,XXI
            COMMON/BLK2/TI,XI,H
            COMMON/BLK3/FM,FLAMD,VO,BTA
            COMMON/BLK4/A2,B2,C2,EO
            DATA U,P,G,CO/0.65DO,3.0D05,9.806DO,0.0DO/
            DATA TO,XXO,XO, ESP,N/0.DO,1D-10,0.DO,0.01DO,2500/

            PC=1.379D8
            VO=1.0D-7
            BTA=0.DO
            FM=1.DO
            FLAMD=5.0D10
            P1=PC/P
            EC=4.264D-04
            IF(P1.LT.150.DO)GO TO 2
            U=150.DO*CO/PC+U
            CO=0.DO
          2 EO=DSQRT(FLAMD)*EC
            E=ESP
            HO=.05DO
            TI=TO
            XXI=XXO
            XI=XO
            II=0
      C     calculating static shear force
            US=U*1.DO
            B=US*(P/FM+G)+CO/FM
      C     estimate constants for friction coefficients
            UO=-.14DO+1.03DO*U
            BO=.133DO-.018DO*U
            P1=UO+BO-U
            IF(P1)6,6,4
          4 UO=UO-P1*3.DO/5.DO
            BO=BO-P1*2.01DO/5.DO
          6 A2=CO+UO*(P+FM*G)
            B2=BO*(P+FM*G)
            C2=B*FM
            CALL SUB2(FI,FFI)
            FO=FI
```

```
      XX=C2/FLAMD
      EP1=XX*XX*FLAMD/2.DO

      WRITE(6,10)
   10 FORMAT(2X,'solultions by Runge-Kutta method for single block
     1friction model',/,25X,'unit system: ***M-KG-SECOND***',/)
      WRITE(6,12)CO,UO,BO,EO,FM,P,FLAMD,U,G,VO,BTA,ESP
   12 FORMAT(2X,'COHSN=',E10.3, 3X,'   UO=',F9.6,4X,'   BO=',
     1 F9.6,4X,'RADIA=',F11.4,/,2X,'     M=',F7.4,6X,'    P=',
     2 E9.2, 4X,'LAMDA=',E9.2,4X,'   Us=',F9.6,/,2X,'    G=',
     3 F7.4,6X,'DRIVO=',E12.5,1X,'DRI.AC',F9.6,4X,'PRECISN',F9.5,/)
      WRITE(6,14)
   14 FORMAT(3X,'N',8X,'T(I)',11X,'X¬(I)',
     1  12X,'X(I)',11X,'F(I)',10X,'FF(I)',/,12X,'sec',12X,'m/sec',
     2 13X,'m',14X,'N',13X,'N')
      WRITE(6,15) II,TO,XXO,XO,FI,FFI
   15 FORMAT(1X,I4,1X,E14.8,1X,2E15.7,2E15.5)
      X1=0.DO
      T1=0.DO
      T2=0.DO
      K=0

   40 J=0
      J1=0
      WF=0.DO
      WR=0.DO
      WE=0.DO
      BUF2=XXI
      BUF1=0.DO
      S(1)=TI
      S(2)=XXI
      S(3)=XI
      S(4)=FI
      S(5)=FFI

      DO 80 I=1,N
      H=HO
   45 CALL SUB1(E,XX2,X2,H3)

C     CHECK THE SIGN OF VELOCITY AT TWO ADJACENT POINTS
   60 IF(DSIGN(XXI,XXI).EQ.DSIGN(XXI,XX2)) GOTO 65

C     INCREASE THE ACCURACY WHEN THE VELOCITY REACHES 0
      IF(J.NE.0) GO TO 63
      E=E/((IDINT(J1/10.DO)+1)*5.DO)
      J=J+1
      J1=J1+1
      GO TO 45
   63 J=0
   65 XXI=XX2
      XI=X2
      TI=TI+H3
      CALL SUB2(FI,FFI)

      WR=WR+XXI*XXI*H3
      WE=WE+FI*H3
      WF=WF+DABS(FFI)*(XI-S(3))
C     WRITE(6,15)I,TI,XXI,XI,FI,FFI
```

```
117           IF(BUF2.LT.BUF1.OR.BUF2.LT.XXI)GO TO 75
118           II=I-1
119        70 WRITE(6,15)II,(S(L),L=1,5)
120           BUF1=BUF2
121           BUF2=XXI
122           S(3)=XI
123           GO TO 80
124        75 BUF1=BUF2
125           BUF2=XXI
126           S(1)=TI
127           S(2)=XXI
128           S(3)=XI
129           S(4)=FI
130           S(5)=FFI
131           IF(DABS(XXI).LT.1D-13)GO TO 100
132        80 CONTINUE
133           WRITE(6,15)I,TI,XXI,XI,FI,FFI
134           WRITE(6,81)I
135        81 FORMAT(2X,I4,' times have been run, not converge')
136           GO TO 150
137
138       100 WRITE(6,15)I,TI,XXI,XI,FI,FFI
139           K=K+1
140           X1=XI-XO
141           T1=TI-TO
142     C     TT=(DSQRT(VO*VO+4*BTA*X1)-VO)/(2*BTA)
143           TT=X1/VO
144           T2=TT-T1
145           DF=FO-FI
146           PCT1=DF/FO*100.DO
147
148           WRITE(6,110)T1,X1,T2,DF
149       110 FORMAT(/,3X,'THE SLIP TIME          T1=',E15.8,'  SECONDS',
150          1  /,3X,'THE SLIP DISTANCE  Xmax=',E15.8,'  METRES',
151          2  /,3X,'THE SLICK TIME       T2=',E15.8,'  SECONDS',
152          3  /,3X,'TOTAL FORCE DROP     DF=',E15.8,'  NEWTONS',/)
153           XX1=XX+VO*TI-XI
154           EP2=XX1*XX1*FLAMD/2.DO
155           EK=FM*XXI*XXI/2.DO
156           WR=EO*WR
157           WE=VO*WE
158           DE=EP1-EP2
159           PCT2=WF/DE*100.DO
160           PCT3=WR/DE*100.DO
161           WRITE(6,121)WE,DE,WF,WR,PCT1,PCT2,PCT3
162       121 FORMAT(3X,'WE=',E15.8,
163          1 2X,'DE=',E15.8,2X,'Wf=',E15.8,2X,'Wr=',E15.8,//,
164          2 3X,'FORCE DROP FRACTION        DF/FO=',F7.3,' %',/,
165          3 3X,'FRICTION CONSUMPTION       Wf/DE=',F7.3,' %',/,
166          4 3X,'RADIATION PORTION          Wr/DE=',F7.3,' %',/)
167           IF(K.EQ.1)GO TO 150
168           TI=TI+T2
169           TO=TI
170           XXI=XXO
171           XO=XI
172           E=ESP
173           WRITE(6,14)
174           GO TO 40
```

```
175
176       150 WRITE(6,151)
177       151 FORMAT(2X,/)
178           STOP
179           END
180
181           SUBROUTINE SUB1(E,XX2,X2,H3)
182           IMPLICIT REAL*8(A-H,O-Z)
183           COMMON/BLK1/B,XXI
184           COMMON/BLK2/TI,XI,H
185
186           CALL RK(TI,XXI,XI,H,H2,XX1,X1)
187           H1=H2/2.DO
188         5 CALL RK(TI,XXI,XI,H1,H3,XX2,X2)
189           D1=XX2-XX1
190           D1=DABS(D1)
191           IF (D1.LT.E)GO TO 20
192        15 H1=H3/2.DO
193           XX1=XX2
194           GO TO 5
195        20 RETURN
196           END
197
198           SUBROUTINE SUB2(FI,FFI)
199
200       C   CALCULATE FORCES
201           IMPLICIT REAL*8(A-H,O-Z)
202           COMMON/BLK1/B,XXI
203           COMMON/BLK2/TI,XI,H
204           COMMON/BLK3/FM,FLAMD,VO,BTA
205           COMMON/BLK4/A2,B2,C2,EO
206
207           FR(Y)=A2+B2/(7.DO+DLOG10(Y+1D-6))
208           FRO=FR(O)
209           FI=C2+FLAMD*(VO*TI+BTA*TI*TI-XI)
210           FFI=-FI
211           IF (DABS(XXI).LT.1D-13) GOTO 30
212           IF (XXI.GT.O.DO) GOTO 20
213         5 FFI=FR(-XXI)
214           GO TO 50
215        20 FFI=-FR(XXI)
216           GOTO 50
217        30 IF (DABS(FI).LT.DABS(FRO)) GOTO 50
218           FFI=-DSIGN(FRO,FI)
219        50 RETURN
220           END
221
222           SUBROUTINE RK(X,Y,Z,H1,H,YN,ZN)
223
224           IMPLICIT REAL*8(A-H,O-Z)
225           G(X,Y,Z)=Y
226           H=H1
227         5 F1=H*F(X,Y,Z)
228           G1=H*G(X,Y,Z)
229           IF((Y+F1/2.DO).LT.O.DO)GO TO 10
230           F2=H*F(X+H/2.DO,Y+F1/2.DO,Z+G1/2.DO)
231           G2=H*G(X+H/2.DO,Y+F1/2.DO,Z+G1/2.DO)
232           IF((Y+F2/2.DO).LT.O.DO)GO TO 10
```

```
      F3=H*F(X+H/2.DO,Y+F2/2.DO,Z+G2/2.DO)
      G3=H*G(X+H/2.DO,Y+F2/2.DO,Z+G2/2.DO)
      IF((Y+F3).LT.0.DO)GO TO 10
      F4=H*F(X+H,Y+F3,Z+G3)
      G4=H*G(X+H,Y+F3,Z+G3)
      YN=Y+(F1+2.DO*(F2+F3)+F4)/6.DO
      ZN=Z+(G1+2.DO*(G2+G3)+G4)/6.DO
      IF(YN.LT.0.DO)GO TO 10
      RETURN
   10 H=H/2.DO
      GO TO 5
      END

      DOUBLE PRECISION FUNCTION F(X,Y,Z)

      IMPLICIT REAL*8(A-H,O-Z)
      COMMON/BLK1/B,XXI
      COMMON/BLK3/FM,FLAMD,VO,BTA
      COMMON/BLK4/A2,B2,C2,EO

      FR(Y)=A2+B2/(7.DO+DLOG10(Y+1D-6))
      FRO=FR(0)
      F=0.DO
      FD=C2+FLAMD*(VO*X+BTA*X*X-Z)
      IF(DABS(Y).LT.1D-13) GO TO 30
      IF(Y.GT.0.DO) GO TO 20
      F=(FD+FR(-Y)-EO*Y)/FM
      GO TO 50
   20 F=(FD-FR(Y)-EO*Y)/FM
      GOTO 50
   30 IF(DABS(FD).LT.DABS(FRO)) GOTO 50
      F=(FD-DSIGN(FRO,FD))/FM
   50 RETURN
      END
```

******* results from sensitivity analysis ********

Solutions by Runge-Kutta method for single block friction model
unit system: ***M-KG-SECOND***

```
COHSN= 0.0          UO= 0.529020      BO= 0.120978    RADIA=    95.3459
   M= 1.0000         P= 0.30E+06   LAMDA= 0.50E+11      Us= 0.650000
   G= 9.8060    DRIVO= 0.10000E-06 DRI.AC 0.0         PRECISN  0.01000

 N       T(I)          X¬(I)           X(I)          F(I)          FF(I)
         sec           m/sec            m            N             N
 0 0.0             0.1000000E-09  0.0             0.19501E+06   -0.19500E+06
 3 0.83923340E-05  0.1306933E+00  0.5719526E-06   0.16641E+06   -0.16465E+06
84 0.15612097E-04  0.9748039E-13  0.1189830E-05   0.13551E+06   -0.13551E+06

THE SLIP TIME        T1= 0.15612097E-04  SECONDS
THE SLIP DISTANCE  Xmax= 0.11898298E-05  METRES
THE SLICK TIME       T2= 0.11898282E+02  SECONDS
TOTAL FORCE DROP     DF= 0.59491410E+05  NEWTONS

We= 0.25432353E-06  DE= 0.19663180E+00  Wf= 0.19601157E+00  Wr= 0.16534965E-04

FORCE DROP FRACTION        DF/FO= 30.507 %
FRICTION CONSUMPTION       Wf/DE= 99.685 %
RADIATION PORTION          Wr/DE=  0.008 %
```

APPENDIX III. LIST OF FORTRAN PROGRAM MODEL3 AND SAMPLE RESULTS

```
1
2       C     ***************************************************
3       C     *                                                 *
4       C     *                    MODEL3                       *
5       C     *           --- transition analysis ---           *
6       C     *               by Daihua Zou, 1985               *
7       C     *                                                 *
8       C     ***************************************************
9
10      C           Numerical solution: single block model
11      C         Slip velocity dependent friction: u=u(X')
12      C             No slip back permitted here
13
14      C     This program is written for numerical solution to the system
15      C     of first order defferential equations by Runge-Kutta method
16
17      C    ***** computing the critical normal pressure at transition *****
18
19            IMPLICIT REAL*8(A-H,O-Z)
20            DIMENSION S(5)
21            COMMON /BLK1/B,XXI
22            COMMON/BLK2/TI,XI,H
23            COMMON/BLK3/FM,FLAMD,VO,BTA
24            COMMON/BLK4/A2,B2,C2,EO
25            DATA U,P,G,CO/0.65DO,0.1D05,9.806DO,0.0DO/
26            DATA TO,XXO,XO, ESP,N/0.DO,1D-10,0.DO,0.01DO,5000/
27
28            PC=1.379D8
29            VO=.10D-4
30            BTA=0.DO
31            FM=1.DO
32            FLAMD=.10D10
33            P1=PC/P
34            EC=4.264D-04
35            IF(P1.LT.150.DO)GO TO 2
36            U=150.DO*CO/PC+U
37            CO=0.DO
38          2 EO=DSQRT(FLAMD)*EC
39            E=ESP
40            HO=.05DO
41            TI=TO
42            XXI=XXO
43            XI=XO
44            II=0
45      C     calculating static shear force
46            US=U*1.DO
47            B=US*(P/FM+G)+CO/FM
48      C     estimate constants for friction coefficients
49            UO=-.14DO+1.03DO*U
50            BO=.133DO-.018DO*U
51            P1=UO+BO-U
52            IF(P1)6,6,4
53          4 UO=UO-P1*3.DO/5.DO
54            BO=BO-P1*2.01DO/5.DO
55          6 A2=CO+UO*(P+FM*G)
56            B2=BO*(P+FM*G)
57            C2=B*FM
58            CALL SUB2(FI,FFI)
```

```
      FO=FI
      FFO=FFI
      XX=C2/FLAMD
      EP1=XX*XX*FLAMD/2.DO

      WRITE(6,10)
   10 FORMAT(2X,'solutions by Runge-Kutta method for single block
     1 friction model',/,25X,'unit system: ***M-KG-SECOND***',/)
   12 FORMAT(2X,'COHSN=',E10.3, 3X,'   UO=',F12.6,1X,'   BO=',
     1 F12.6,1X,'RADIA=',F12.6,/,2X,'    M=',F12.4,1X,'    P=',
     2 E10.2, 3X,'LAMDA=',E10.2,3X,'   Us=',F12.6,/,2X,'    G=',
     3 F12.4,1X,'DRIVO=',E12.5,1X,'DRI.AC',F12.6,1X,'PRECISN',F11.6,/)
   14 FORMAT(3X,'N',8X,'T(I)',11X,'X¬(I)',
     1  12X,'X(I)',11X,'F(I)',10X,'Ft(I)')
   15 FORMAT(1X,I4,1X,E14.8,1X,2E15.7,2E15.5)
   20 J=0
   25 J1=0
      K=0
      IW=0
      I=0

   40 I=I+1
      IF(I-IW.NE.50) GOTO 43
      IW=I
      WRITE(7,42)I,VO,XXI
   42 FORMAT(2X,I5,2(2X,E15.8))
   43 H=HO
   45 CALL SUB1(E,XX2,X2,H3)
      XXW=XXI
      XXI=XX2
      XI=X2
      TI=TI+H3
      IF(DABS(XXI).LT.1D-13)GO TO 100
   80 IF(I.LT.N) GOTO 40
      IF(XXW.GT.XXI) GOTO 40
   82 J=J+1
      VO=VO/2.DO
      IF(J.LT.2) GOTO 108
      IF(J1.EQ.0) GOTO 85
      WRITE(6,83)XW,VW,TW
   83 FORMAT(2X,'in previous run: XXI= ',E15.8,'  VO= ',E15.8,'  T2= '
     1,E15.8,/)
   85 WRITE(6,86)I
   86 FORMAT(2X,'run ',I4,' times already, not converge!')
      WRITE(6,14)
      WRITE(6,15)II,TO,XXO,XO,FO,FFO
      WRITE(6,15)I,TI,XXI,XI
      WRITE(6,90)VO,P
   90 FORMAT(2X,'VO= ',E15.8,3X,'Pn= ',E15.8)
      GO TO 150

  100 TT=XI/VO
      T2=TT-TI
      IF(T2.GT.1D-5.OR.T2.EQ.1D-5)GO TO 105
      WRITE(6,12)CO,UO,BO,EO,FM,P,FLAMD,U,G,VO,BTA,ESP
      WRITE(6,14)
      WRITE(6,15)II,TO,XXO,XO,FO,FFO
      CALL SUB2(FI,FFI)
```

```
117           WRITE(6,15)I,TI,XXI,XI,FI,FFI
118
119           WRITE(6,110)T2
120           GO TO 150
121       105 J1=J1+1
122           XW=XXI
123           VW=VO
124           TW=T2
125           VO=VO*10
126       108 TI=TO
127           XXI=XXO
128           XI=XO
129           IF(J.LT.2) GOTO 25
130           GO TO 20
131        110 FORMAT(/,3X,'THE SLEEP TIME    =',E15.8,'  SECONDS')
132
133        150 WRITE(6,151)
134        151 FORMAT(2X,/)
135           STOP
136           END
137
138           SUBROUTINE SUB1(E,XX2,X2,H3)
139           IMPLICIT REAL*8(A-H,O-Z)
140           COMMON/BLK1/B,XXI
141           COMMON/BLK2/TI,XI,H
142
143           CALL RK(TI,XXI,XI,H,H2,XX1,X1)
144           H1=H2/2.DO
145         5 CALL RK(TI,XXI,XI,H1,H3,XX2,X2)
146           D1=XX2-XX1
147           D1=DABS(D1)
148           IF (D1.LT.E)GO TO 20
149        15 H1=H3/2.DO
150           XX1=XX2
151           GO TO 5
152        20 RETURN
153           END
154
155
156           SUBROUTINE SUB2(FI,FFI)
157
158       C   CALCULATE FORCES
159           IMPLICIT REAL*8(A-H,O-Z)
160           COMMON/BLK1/B,XXI
161           COMMON/BLK2/TI,XI,H
162           COMMON/BLK3/FM,FLAMD,VO,BTA
163           COMMON/BLK4/A2,B2,C2,EO
164
165           FR(Y)=A2+B2/(7.DO+DLOG10(Y+1D-6))
166           FRO=FR(O)
167           FI=C2+FLAMD*(VO*TI+BTA*TI*TI-XI)
168           FFI=O.DO
169           IF (DABS(XXI).LT.1D-13) GOTO 30
170           IF (XXI.GT.O.DO) GOTO 20
171         5 FFI=FI+FR(-XXI)
172           GO TO 50
173        20 FFI=FI-FR(XXI)
174           GOTO 50
```

```
      30  IF (DABS(FI).LT.DABS(FRO)) GOTO 50
          FFI=FI-DSIGN(FRO,FI)
      50  RETURN
          END

          SUBROUTINE RK(X,Y,Z,H1,H,YN,ZN)

          IMPLICIT REAL*8(A-H,O-Z)
          G(X,Y,Z)=Y
          H=H1
      5   F1=H*F(X,Y,Z)
          G1=H*G(X,Y,Z)
          IF((Y+F1/2.DO).LT.O.DO)GO TO 10
          F2=H*F(X+H/2.DO,Y+F1/2.DO,Z+G1/2.DO)
          G2=H*G(X+H/2.DO,Y+F1/2.DO,Z+G1/2.DO)
          IF((Y+F2/2.DO).LT.O.DO)GO TO 10
          F3=H*F(X+H/2.DO,Y+F2/2.DO,Z+G2/2.DO)
          G3=H*G(X+H/2.DO,Y+F2/2.DO,Z+G2/2.DO)
          IF((Y+F3).LT.O.DO)GO TO 10
          F4=H*F(X+H,Y+F3,Z+G3)
          G4=H*G(X+H,Y+F3,Z+G3)
          YN=Y+(F1+2.DO*(F2+F3)+F4)/6.DO
          ZN=Z+(G1+2.DO*(G2+G3)+G4)/6.DO
          IF(YN.LT.O.DO)GO TO 10
          RETURN
      10  H=H/2.DO
          GO TO 5
          END

          DOUBLE PRECISION FUNCTION F(X,Y,Z)

          IMPLICIT REAL*8(A-H,O-Z)
          COMMON/BLK1/B,XXI
          COMMON/BLK3/FM,FLAMD,VO,BTA
          COMMON/BLK4/A2,B2,C2,EO

          FR(Y)=A2+B2/(7.DO+DLOG10(Y+1D-6))
          FRO=FR(O)
          F=O.DO
          FD=C2+FLAMD*(VO*X+BTA*X*X-Z)
          IF(DABS(Y).LT.1D-13) GO TO 30
          IF(Y.GT.O.DO) GO TO 20
          F=(FD+FR(-Y)-EO*Y)/FM
          GO TO 50
      20  F=(FD-FR(Y)-EO*Y)/FM
          GOTO 50
      30  IF(DABS(FD).LT.DABS(FRO)) GOTO 50
          F=(FD-DSIGN(FRO,FD))/FM
      50  RETURN
          END
```

****** results from transition analysis ******

solutions by Runge-Kutta method for single block friction model
unit system: ***M-KG-SECOND***

```
COHSN= O.O          UO=    0.529020    BO=    0.120978 RADIA=   13.483952
   M=      1.0000    P=  0.10E+05   LAMDA=  0.10E+10     Us=    0.650000
   G=      9.8060 DRIVO= 0.10000E+01 DRI.AC    0.0      PRECISN   0.010000

 N       T(I)          X¬(I)          X(I)          F(I)          Ft(I)
  0 0.0              0.1000C00E-09  0.0           0.65064E+04   0.68603E-01
592 0.19634916E-03   0.9375850E-13  0.1987518E-03 0.41037E+04   0.0

 THE SLEEP TIME    = 0.24026417E-05  SECONDS
```

APPENDIX IV. LIST OF BASIC PROGRAM MODEL4 AND SAMPLE RESULTS

```
10    !  RE-STORE "MODEL4:H7,0,0"
20    !
30    !  ********************************************************************
40    !  *                                                                  *
50    !  *                        " MODEL4 "                                *
60    !  *           --- acoustic activity simulation ---                   *
70    !  *                  by Daihua Zou, 1986                             *
80    !  *                                                                  *
90    !  *     numerical solution: multi-particle friction model            *
100   !  *         slip velocity dependent friction: U=U(X')                *
110   !  *                  slip back permitted here                        *
120   !  *                                                                  *
130   !  *   Driving force is applied at the end of the last particle       *
140   !  *                                                                  *
150   !  *  This program is written for numerical solution to the system    *
160   !  *  of second order differential equations by RUNGE-KUTTA method    *
170   !  *                                                                  *
180   !  ********************************************************************
190   !
200     OPTION BASE 1
210     INTEGER L,N,I,J,Cno,Cct,N(10),Symbolno(10),Errcode(10),Lct,Lineno(10)
220     SHORT Symbolsize(10),Linesize(10)
230   !
240     DIM S(2,12),Wok(2,12),Wok1(2,12),X(10,400),Y(10,400)
250     DIM Title$[30],Xlabel$[30],Ylabel$[30],A$[1]
260     COM B,Xxi,M
270     COM Ti,Xi1,Xi2,Xi3,H
280     COM Fm,Flamd(11),V0,Bta
290     COM A2,B2,E0,K1,Fa
300     DATA .650,5E2,9.80,0.0
310     DATA 0.0,.050,20000,10
320     READ U,P,G,C0,T0,E,N,M
330   !
340     Bta=0
350     Tint0=2E-2
360     Flamd0=3E4
370     Pc=1.379E8
380     V0=1E-1
390     Fa=1E-1         !  spacing between particles
400     Fm=1E0
410     P1=Pc/P
420     IF P1<1.50E2 THEN L2
430     U=1.50E2*C0/Pc+U
440     C0=0
450   L2: E0=4.264*Sqrt(Flamd0)
460     C1=C0/Fm
470     H0=5E-3
480   !
490     FOR I=1E0 TO 2
500       FOR J=1E0 TO 12
510         S(I,J)=0
520         Wok(I,J)=0
530         Wok1(I,J)=0
540       NEXT J
550     NEXT I
560   !
570     FOR K=1E0 TO M
580       K1=K+1E0
590       Flamd(K1)=Flamd0  !  *(K*1E-1)
600     NEXT K
610     Flamd(1E0)=0    ! set lamda0=0
620   !  calculating static shear force
630     Us=U*1E0
640     B=Us*(P/Fm+G)+C1    !  .99997662
```

```
650   !
660   !  estimate constants for friction coefficients
670     U0=-.14+1.03*U
680     B0=1.33E-1-.018*U
690     P1=U0+B0-U
700     IF P1<=0 THEN L6
710     U0=U0-P1*3/5
720     B0=B0-P1*2/5
730 L6: A2=C0+U0*(P+Fm*G)
740     B2=B0*(P+Fm*G)
750     C2=B*Fm
760   !
770   !  assign initial values for XI(0) AND XI'(0)
780     Ti=T0
790     Cct=5
800     Lct=0
810     FOR K=1E0 TO M
820       K1=K+1E0
830       Wok1(1E0,K1)=(M-K)*Fa
840       Wok1(2,K1)=0
850     NEXT K
860   !
870       Wok1(1E0,1E0)=Wok1(1E0,2)+Fa
880       Wok1(1E0,12)=V0*Ti+C2/Flamd(11)-Fa
890       Wok1(2,1E0)=Wok1(2,2)
900       Wok1(2,12)=V0
910   !
920   !  calculate initial values for fi and fi
930     FOR K=1E0 TO M
940       Km=M-K+1E0
950       K1=Km+1E0
960       K2=Km+2
970       Xi1=Wok1(1E0,Km)
980       Xi2=Wok1(1E0,K1)
990       Xi3=Wok1(1E0,K2)
1000      Xxi=Wok1(2,K1)
1010      CALL Sub2(Fi,Ffi)
1020      S(1E0,K1)=Fi
1030      S(2,K1)=Ffi
1040    NEXT K
1050  !
1060    GOSUB File_data
1070 L10: PRINTER IS 16
1080    PRINT LIN(5),"        EXECUTION BEGINS, PLEASE WAIT !",LIN(3)
1090  !
1100    PRINTER IS 0
1110    PRINT LIN(3)
1120    PRINT "       RESULTS FROM RUNGE-KUTTA METHOD FOR MULTI-PARTICLE SHEAR M
ODEL"
1130    PRINT "                  UNIT SYSTEM : *** M-KG-SECOND *** ",LIN(1E0)
1140    PRINT USING L18;C0,U0,B0,E0,Fm,P,Flamd(11),U
1150 L18: IMAGE 2X,"COHSN=",X,.3DE,4X," U0=",X,.7D,6X," B0=",X,.7D,4X,"SEISM=",4
D.3D/2X," MASS=",X,.3DE,4X," Pn=",X,.3DE,2X,"LAMDA10=",X,.3DE,6X," Us=",X,.6D
1160    PRINT USING L19;G,V0,Bta,E,Fa,Tint0,Flamd(6),Pc
1170 L19:IMAGE 6X,"G=",X,.3DE,2X,"DRIV0=",X,.3DE,3X,"DRI.AC=",X,.3DE,2X,"PRECISN
=",X,.6D,/,6X,"A=",X,.3DE,3X,"TINT=",X,.3DE,3X,"LAMDA5=",X,.3DE,7X,"Pc=",X,.3DE,
1180  !
1190  !  print initial values
1200    I=0
1210    PRINT USING L60;I,Ti
1220    FOR K=1E0 TO M
1230      K1=K+1E0
1240      PRINT USING L66;K,Wok1(2,K1),Wok1(1E0,K1),S(1E0,K1),S(2,K1)
1250    NEXT K
1260    PRINT LIN(1E0)
1270    PRINT USING Ltit
1280 Ltit: IMAGE " II     TI          # RATE      TOT EN      SEISM EN    EN RA
TIO    KINET EN"
```

```
1290  !
1300    Wr=0
1310    Wf=0
1320    L=0  ! counter of first slips
1330    I2=0     ! key to stop program
1340    I0=0
1350    Ii=0
1360    H=H0
1370    Tint=Tint0
1380    Ix=0
1390  !
1400    FOR I=1E0 TO N    ! LOOP FOR TIME INCREMENT BEGINS, ENDS AT L80
1410      I1=0
1420      I3=0
1430      I4=0
1440      I5=0
1450      M0=M+2
1460         FOR K=1E0 TO 2
1470            FOR J=1E0 TO M0
1480  !           Check the logic position
1490              IF K=2 THEN L21
1500              IF (J=1E0) OR (J=12) THEN L21
1510              J1=J+1E0
1520              IF Wok1(1E0,J1)<=Wok1(1E0,J) THEN L21
1530              Wok1(1E0,J)=Wok1(1E0,J1)+8E-1*Fa
1540              IF Wok1(2,J)<Wok1(2,J1) THEN L20
1550              GOTO 1570
1560 L20:         Wok1(2,J)=Wok1(2,J1)
1570              L=L+1E0
1580 L21:         Wok(K,J)=Wok1(K,J)
1590            NEXT J
1600         NEXT K
1610  !
1620  !   search for min & max slip speed
1630 L22: X1=0
1640     X2=0
1650     Kk1=Kk2=1E0
1660         FOR K=1E0 TO M
1670           K1=K+1E0
1680           IF ABS(X1)<ABS(Wok1(2,K1)) THEN Lgo
1690           Kk1=K
1700           X1=Wok1(2,K1)
1710           GOTO 1750
1720 Lgo:      IF ABS(X2)>=ABS(Wok1(2,K1)) THEN 1750
1730           Kk2=K
1740           X2=Wok1(2,K1)
1750         NEXT K
1760  !
1770  !   set up time step by the particle with max or min speed
1780     K1=Kk1+1E0
1790     K2=Kk1+2
1800     Xi1=Wok(1E0,Kk1)
1810     Xi2=Wok(1E0,K1)
1820     Xi3=Wok(1E0,K2)
1830     Xxi=Wok(2,K1)
1840     CALL Sub1(E,X00,Xx0,H3)
1850     K1=Kk2+1E0
1860     K2=Kk2+2
1870     Xi1=Wok(1E0,Kk2)
1880     Xi2=Wok(1E0,K1)
1890     Xi3=Wok(1E0,K2)
1900     Xxi=Wok(2,K1)
1910     CALL Sub1(E,X22,Xx2,Hh)
1920     IF H3<Hh THEN 1960
1930     H3=Hh
1940     Kk=Kk2
1950     GOTO Lcont
```

```
1960      Kk=Kk1
1970      X22=X00
1980      Xx2=Xx0
1990 Lcont: K1=Kk+1E0
2000      Wok1(1E0,K1)=X22
2010      Wok1(2,K1)=Xx2
2020 !
2030  !  solving the differential equation for X and X' for each particle
2040         FOR K=1E0 TO M    ! Loop for each particle begins, ends at L45
2050         Km=M-K+1E0
2060           K1=Km+1E0
2070           K2=Km+2
2080           Kk1=Kk2=0
2090           Xi1=Wok(1E0,Km)
2100           Xi2=Wok(1E0,K1)
2110           Xi3=Wok(1E0,K2)
2120           Xxi=Wok(2,K1)
2130           GOSUB Logic
2140  !
2150  !        time steps are set the same as that determined by max or min spee
d
2160 L30:      CALL Rk1(Ti,Xi1,Xi2,Xi3,Xxi,H3,X22,Xx2)
2170           Wok1(1E0,K1)=X22
2180           Wok1(2,K1)=Xx2
2190           IF Kk2<>0 THEN Flamd(Kk2)=Flamd0
2200           IF Kk1<>0 THEN Flamd(Kk1)=Flamd0
2210 !
2220 L45:    NEXT K
2230 !
2240           Wok1(1E0,1E0)=Wok1(1E0,2)+Fa
2250           Wok1(1E0,12)=V0*Ti+C2/Flamd(11)-Fa
2260           Wok1(2,1E0)=Wok1(2,2)
2270           Wok1(2,12)=V0
2280      Ti=Ti+H3                          !  To increase time step
2290 !
2300 !    calculate forces and energies
2310         FOR K=1E0 TO M
2320         Km=M-K+1E0
2330           K1=Km+1E0
2340           K2=Km+2
2350           Kk1=Kk2=0
2360           Xi1=Wok1(1E0,Km)
2370           Xi2=Wok1(1E0,K1)
2380           Xi3=Wok1(1E0,K2)
2390           Xxi=Wok1(2,K1)
2400           GOSUB Logic
2410           CALL Sub2(Fi,Ffi)
2420           S(1E0,K1)=Fi
2430           S(2,K1)=Ffi
2440           Wf=Wf+ABS(Ffi*(Xi2-Wok(1E0,K1)))
2450           Wr=Wr+Xxi*Xxi*H3
2460 !
2470 !         Count event number for each slip of any particle
2480 L43:      IF (Wok(2,K1)=0) AND (Xxi<>0) THEN L44
2490           IF SGN(Wok(2,K1))<>SGN(Xxi) THEN L44
2500           GOTO L46
2510 L44:      L=L+1E0   ! To count event # for each sampling interval
2520 L46:      IF ABS(Wok1(2,K1))>0 THEN I1=I1+1E0
2530           IF ABS(Wok(2,K1))>0 THEN I5=I5+1E0
2540           IF (ABS(Wok(2,K1))<1E-3) AND (ABS(Wok1(2,K1)))>1E-3) THEN I3=I3+1E
0
2550           IF (ABS(Wok(2,K1))<1.00E2) AND (ABS(Wok1(2,K1)))>1.00E2) THEN I4=I
4+1E0
2560  !
2570           IF Kk2<>0 THEN Flamd(Kk2)=Flamd0
2580           IF Kk1<>0 THEN Flamd(Kk1)=Flamd0
2590         NEXT K
```

```
2600  !
2610        IF I=1E0 THEN L56
2620        IF I-I0<5 THEN L58   ! screen monitoring
2630        I0=I
2640 L56:  PRINTER IS 16
2650        PRINT LIN(13)
2660        PRINT USING "10A,5D,2(2X,M.7DE)";"(I,H,TI)",I,H3,Ti
2670        PRINT USING "/,15A,5(X,M.6DE)";"(X10,X9,X8 etc)",Wok1(1E0,11),Wok1(1E0
,10),Wok1(1E0,9),Wok1(1E0,8),Wok1(1E0,7)
2680        PRINT USING "/,18A,2(1X,M.6DE),3(1X,M.5DE)";"(X10,X9,X8,X7,X6)'",Wok1(
2,11),Wok1(2,10),Wok1(2,9),Wok1(2,8),Wok1(2,7)
2690        PRINT USING "/,17A,3(1X,M.6DE),2(1X,M.5DE)";"(X5,X4,X3,X2,X1)'",Wok1(2
,6),Wok1(2,5),Wok1(2,4),Wok1(2,3),Wok1(2,2)
2700        PRINTER IS 0
2710  !
2720  !   if all particles are moving, stable sliding !
2730 L58:  IF I1=M THEN L55
2740 L59:  IF I3=M THEN L57
2750        IF I4=M THEN L57
2760        GOTO L70                                  !   RIGHT ???
2770 L55:  IF I5=M THEN L59
2780        I2=I2+1E0                          ! Indication of all particles moving
2790 L57:  PRINT USING L60;I,Ti
2800 L60:  IMAGE /,3X,"I =",5D,8X,"time TI =",X,.8DE/2X,"P#",9X,"XXI",14X,"XI",15
X,"Fi",14X,"Fri"
2810           FOR K=1E0 TO M
2820             K1=K+1E0
2830             PRINT USING L66;K,Wok1(2,K1),Wok1(1E0,K1),S(1E0,K1),S(2,K1)
2840           NEXT K
2850        PRINT LIN(1E0)
2860        PRINT USING Ltit
2870 L66:  IMAGE X,3D,X,2(2X,M.8DE),X,3X,M.8DE,3X,M.8DE
2880 !
2890 !     check the pre-set time interval TINT
2900 L70:  Ts=Ti-T0
2910        IF Ts<Tint THEN L80
2920        Ii=Ii+1E0                          ! To count sampling points
2930 !
2940 !     calibrate results for fixed interval TINT
2950        Ts=Tint/Ts
2960        Wr=Wr*E0*Ts
2970        W1=Wf*Ts+Wr
2980        F1=L*Ts
2990        IF F1=0 THEN L73
3000        Ratio=Wr/F1
3010        GOTO L75
3020 L73:  Ratio=0
3030 !
3040 !     compute kinetic energy
3050 L75:  M0=M+1E0
3060        I8=0
3070           FOR K=2 TO M0
3080             D1=ABS(Wok1(2,K))
3090             Ek=D1*D1
3100             IF (ABS(Wok(2,K))>D1) AND (D1<1E-13) THEN Wok1(2,K)=0
3110             IF (ABS(Wok(2,K))<1E-13) AND (D1<1E-13) THEN Wok1(2,K)=0
3120             IF (Wok(2,K)=0) AND (Wok1(2,K)=0) THEN I8=I8+1E0!To count particl
es coming to rest
3130           NEXT K
3140        IF I<10 THEN L76
3150        IF I8<M THEN GOTO L76
3160        H=(C2-S(1E0,11))/Flamd0/V0  ! DX=(C2-Fn)/LAMDA, DT=DX/V0
3170        Tint=H
3180        GOTO L77
3190 L76:  H=H0              ! If all particles stopped moving, change time step
3200        Tint=Tint0
3210 L77:  Ek=Ts*Ek*Fm/2
```

```
3220      PRINT USING L78;Ii,Ti,Fl,W1,Wr,Ratio,Ek
3230 L78: IMAGE 3D,1X,.10DE,5(M.6DE)
3240 !
3250 !    store data for file
3260        FOR K=1E0 TO Cct
3270          X(K,Ii)=Ti
3280        NEXT K
3290      Y(1E0,Ii)=Fl
3300      Y(2,Ii)=W1
3310      Y(3,Ii)=Wr
3320      Y(4,Ii)=Ratio
3330      Y(5,Ii)=Ek
3340 !
3350      IF Ii=400 THEN L85 ! exit 2: computer overflow
3360      IF I2<1E0 THEN L79
3370      Ix=Ix+1E0          ! To count Ii after all particles come to moving
3380      IF Ix=10 THEN L85  ! exit 1: normal exit
3390 L79: L=0
3400      Wr=0
3410      Wf=0
3420      T0=Ti
3430 L80: NEXT I             ! exit 3: abortion due to time limit
3440      I=I-1E0
3450 !
3460 L85: PRINT USING L60;I,Ti
3470        FOR K=1E0 TO M
3480          K1=K+1E0
3490          PRINT USING L66;K,Wok1(2,K1),Wok1(1E0,K1),S(1E0,K1),S(2,K1)
3500        NEXT K
3510      IF Ix=10 THEN L140
3520      IF Ii=400 THEN L130
3530      PRINT USING L95;I
3540 L95: IMAGE 2X,5D," runs, specified cycles not finished yet !",///
3550      GOTO L150
3560 L130:PRINT USING "/,2X,5D,67A,///";I," runs, work is not finished yet! capa
cities of array X & Y exceeded."
3570      GOTO L150
3580 L140: PRINT USING "/,2X,5D,20A,///";I," runs, job is done !"
3590 !
3600 !    store data into file
3610 L150:  PRINTER IS 16
3620      IF B$="N" THEN L160
3630      GOSUB Prep
3640      PRINT LIN(10),"        STORE DATA ON FILE, PLEASE WAIT !",LIN(10)
3650      GOSUB Create
3660      GOSUB En_event
3670      PRINTER IS 0
3680      PRINT USING L155;Filename$
3690 L155: IMAGE /,X,"********  the event rate and energy release are stored in
file: ",5A," *******",////
3700      PRINTER IS 16
3710 L160: PRINT LIN(1E0)
3720      PRINT LIN(5),"                  EXECUTION TERMINATED"
3730      PRINT LIN(7),"                       GOOD-BYE !"
3740 !
3750      STOP
3760      END
3770 !
3780 !   ************************************************************
3790 Logic:       !   Check the logic position: X(i-1)-Xi>0.1A
3800      IF Xi2-Xi3>8E-1*Fa THEN L5
3810      Kk2=K1
3820      Flamd(Kk2)=1E13
3830 L5: IF Xi1-Xi2>1E-1*Fa THEN Soirt
3840      Kk1=Km
3850      Flamd(Kk1)=1E13
3860 Soirt: RETURN
```

```
3870 !
3880 !   ************************************************************
3890 !   preparing file data
3900 Prep:  !
3910     Title$="NUMERICAL RESULTS OF RB MODEL"
3920     Xlabel$="TIME "
3930     Ylabel$="EVENT & ENERGIES"
3940     Xorigen=0
3950     Yorigen=0
3960 !
3970 !   search for Xmax & Ymax
3980     Xextreme=1.0E-7
3990     Yextreme=1E-2
4000        FOR K=1E0 TO Ii
4010            FOR Cno=1E0 TO Cct
4020              IF Y(Cno,K)<=Yextreme THEN Lc
4030              Yextreme=Y(Cno,K)
4040 Lc:          NEXT Cno
4050            IF X(2,K)<=Xextreme THEN Lk
4060            Xextreme=X(1E0,K)
4070 Lk:    NEXT K
4080     Xdelta=(Xextreme-Xorigen)/20
4090     IF Xdelta>1E0 THEN Xdelta=INT(Xdelta)
4100     Ydelta=(Yextreme-Yorigen)/20
4110     IF Ydelta>1E0 THEN Ydelta=INT(Ydelta)
4120        FOR Cno=1E0 TO Cct
4130          Symbolno(Cno)=0
4140          Symbolsize(Cno)=3
4150          Lineno(Cno)=Cno
4160          Linesize(Cno)=4
4170          Errcode(Cno)=0
4180          N(Cno)=Ii
4190        NEXT Cno
4200          Lineno(2)=Cct+1E0
4210     RETURN
4220 !
4230 !    ************************************************************
4240 !
4250 File_data: ! create data file on disk
4260     GCLEAR
4270     B$="Y"
4280     INPUT "DO UOU WANT TO STORE RESULTS ON FILE Y/N ?",B$
4290     IF B$="N" THEN Exit
4300     Device$=":H7,0,0"
4310     INPUT "ENTER DATA STORAGE DIVECE :H7,0,0 ?",Device$
4320     Filename$=" "
4330     INPUT "ENTER FILE NAME ?",Filename$
4340     IF Filename$=" " THEN File_data
4350     File$=Filename$&Device$
4360     ON ERROR GOTO Error1  !to file purging routine
4370     GOTO Try
4380 Error1: IF ERRN=54 THEN Error2
4390     CALL Mess(ERRM$)
4400     GOTO File_data
4410 Error2:  BEEP
4420     DISP "FILE "&CHR$(129)&File$&CHR$(128)&" already exists: do you want it
 be deleted  y/N ?";
4430     A$="N"
4440     INPUT A$
4450     IF A$="Y" THEN GOTO Purge
4460     GOTO File_data
4470 Purge: PURGE File$
4480     GOTO Exit
4490 Try: CREATE File$,1E0,10
4500     PURGE File$
4510 Exit: RETURN
4520 !
```

```
4530 !  ************************************************************
4540 !
4550     GCLEAR
4560 Create:    ! STORE DATA ON FILE
4570     Bytetot=200+28*Cct+80*Lct+16*Ii*Cct
4580     IF Ii>385 THEN 4610
4590     CREATE File$,1E0,Bytetot*1.05 !IF Cct=5,Ii>385 USE:File$,2,Bytetot*1.1/
2
4600     GOTO 4620
4610     CREATE File$,2,Bytetot*1.1/2
4620     ASSIGN File$ TO #1E0          !------------------------------
4630     OFF ERROR
4640     PRINT #1E0;Title$,Xlabel$,Ylabel$,Xorigen,Xextreme,Xdelta,Yorigen,Yextr
eme,Ydelta,Cct,Lct
4650        FOR Cno=1E0 TO Cct
4660         PRINT #1E0;Symbolno(Cno),Symbolsize(Cno),Errcode(Cno),N(Cno),Lineno
(Cno),Linesize(Cno)
4670            FOR K=1E0 TO N(Cno)
4680              IF Errcode(Cno)=0 THEN PRINT #1E0;X(Cno,K),Y(Cno,K)
4690              IF Errcode(Cno)=1E0 THEN PRINT #1E0;X(Cno,K),Y(Cno,K),Yerr(Cno
,K)
4700              IF Errcode(Cno)=2 THEN PRINT #1E0;X(Cno,K),Xerr(Cno,K),Y(Cno,K
)
4710              IF Errcode(Cno)=3 THEN PRINT #1E0;X(Cno,K),Xerr(Cno,K),Y(Cno,K
),Yerr(Cno,K)
4720            NEXT K
4730        NEXT Cno
4740        FOR Lno=1E0 TO Lct
4750          PRINT #1E0;Label$(Lno),Langle(Lno),Lsize(Lno),Lorg(Lno),Lx(Lno),Ly
(Ln0)
4760        NEXT Lno
4770     ASSIGN #1E0 TO *! close file
4780     RETURN
4790  !
4800 En_event:  ! ************************************************
4810     N1=50       ! Count the event # according to energy magnitude
4820     Cct1=Cct+1E0
4830     Xmax=0
4840        FOR K=1E0 TO Ii
4850          IF Xmax>=Y(4,K) THEN Lext1
4860          Xmax=Y(4,K)
4870 Lext1: NEXT K
4880     Xd=Xmax/N1
4890        FOR J=1E0 TO N1+1E0
4900          X(Cct1,J)=(J-1E0)*Xd
4910          Y(Cct1,J)=0
4920        NEXT J
4930     X(Cct1,N1+1E0)=Xmax
4940        FOR K=1E0 TO Ii
4950          FOR J=1E0 TO N1+1E0
4960            IF Y(4,K)>X(Cct1,J) THEN Lext2
4970            Y(Cct1,J)=Y(Cct1,J)+Y(1E0,K)
4980            GOTO Lext3
4990 Lext2:   NEXT J
5000 Lext3: NEXT K
5010     Ymax=0
5020       FOR J=1E0 TO N1+1E0
5030         IF Ymax>=Y(Cct1,J) THEN Lext4
5040         Ymax=Y(Cct1,J)
5050 Lext4:NEXT J
5060 !
5070    Cct=1E0
5080    Xlabel$="AVERAGE ENERGY/EVENT"
5090    Ylabel$="FREQUENCY"
5100    Xdelta=INT(Xmax/20)
5110    Ydelta=INT(Ymax/20)
5120    N(1E0)=N1+1E0
```

```
5130     Filename$=Filename$&"0"
5140     File$=Filename$&Device$
5150     CREATE File$,1E0,(200+28*Cct+16*51*Cct)*1.1
5160     ASSIGN File$ TO #1E0
5170     OFF ERROR
5180     PRINT #1E0;Title$,Xlabel$,Ylabel$,Xorigen,Xmax,Xdelta,Yorigen,Ymax,Ydelt
a,Cct,Lct
5190     PRINT #1E0;Symbolno(1E0),Symbolsize(1E0),Errcode(1E0),N(1E0),Lineno(1E0)
,Linesize(1E0)
5200        FOR K=1E0 TO N(1E0)
5210          PRINT #1E0;X(Cct1,K),Y(Cct1,K)
5220        NEXT K
5230     ASSIGN #1E0 TO *
5240     RETURN
5250   !
5260   ! ============================================================
5270   !
5280     SUB Rk1(T,X1,X2,X3,Y,H,X2n,Y2n)
5290   !
5300     F1=H*FNF(T,X1,X2,X3,Y)
5310     G1=H*Y
5320     F2=H*FNF(T+H/2,X1+G1/2,X2+G1/2,X3+G1/2,Y+F1/2)
5330     G2=H*(Y+F1/2)
5340     F3=H*FNF(T+H/2,X1+G2/2,X2+G2/2,X3+G2/2,Y+F2/2)
5350     G3=H*(Y+F2/2)
5360     F4=H*FNF(T+H,X1+G3,X2+G3,X3+G3,Y+F3)
5370     G4=H*(Y+F3)
5380     X2n=X2+(G1+2*(G2+G3)+G4)/6.0
5390     Y2n=Y+(F1+2*(F2+F3)+F4)/6.0
5400     SUBEND
5410   !
5420   ! ============================================================
5430   !
5440     SUB Sub1(E,X22,Y22,H3)
5450   !
5460     COM B,Xxi,M
5470     COM Ti,Xi1,Xi2,Xi3,H
5480   !
5490     CALL Rk(Ti,Xi1,Xi2,Xi3,Xxi,H,H1,X21,Y21)
5500     H2=H1/2.0
5510 L5: CALL Rk(Ti,Xi1,Xi2,Xi3,Xxi,H2,H3,X22,Y22)
5520     D1=ABS(Y22-Y21)
5530     IF D1<E THEN L20
5540     H2=H3/2.0
5550     Y21=Y22
5560     GOTO L5
5570 L20: SUBEXIT
5580     SUBEND
5590   !
5600   ! ============================================================
5610   !
5620     SUB Sub2(Fi,Ffi)
5630   !
5640   ! calculate forces
5650     COM B,Xxi,M
5660     COM Ti,Xi1,Xi2,Xi3,H
5670     COM Fm,Flamd(*),V0,Bta
5680     COM A2,B2,E0,K1,Fa
5690   !
5700     DEF FNFr(Y)=A2+B2/(7.0+LGT(Y+1E-6))
5710     Fr0=FNFr(0)
5720     Fi=Flamd(K1)*(Fa+Xi3-Xi2)-Flamd(K1-1)*(Fa+Xi2-Xi1)
5730 L15:Ffi=-Fi
5740     IF ABS(Xxi)<1E-13 THEN L30
5750     IF Xxi>0 THEN L20
5760     Ffi=FNFr(-Xxi)
5770     GOTO L50
```

```
5780 L20: Ffi=-FNFr(Xxi)
5790      GOTO L50
5800 L30:IF ABS(Fi)<ABS(Fr0) THEN L50
5810      Ffi=-Fr0*SGN(Fi)
5820 L50: SUBEXIT
5830      SUBEND
5840  !
5850  !  ================================================================
5860  !
5870      SUB Rk(T,X1,X2,X3,Y,H1,H,X2n,Y2n)
5880  !
5890      H=H1
5900 L5: F1=H*FNF(T,X1,X2,X3,Y)
5910      G1=H*Y
5920 !    IF Y+F1/2<0 THEN L10
5930      F2=H*FNF(T+H/2,X1+G1/2,X2+G1/2,X3+G1/2,Y+F1/2)
5940      G2=H*(Y+F1/2)
5950 !    IF Y+F2/2<0 THEN L10
5960      F3=H*FNF(T+H/2,X1+G2/2,X2+G2/2,X3+G2/2,Y+F2/2)
5970      G3=H*(Y+F2/2)
5980 !    IF Y+F3<0 THEN L10
5990      F4=H*FNF(T+H,X1+G3,X2+G3,X3+G3,Y+F3)
6000      G4=H*(Y+F3)
6010      X2n=X2+(G1+2*(G2+G3)+G4)/6.0
6020      Y2n=Y+(F1+2*(F2+F3)+F4)/6.0
6030 !    IF Y2n<0 THEN L10
6040      SUBEXIT
6050 L10: H=H/2
6060      GOTO L5
6070      SUBEND
6080  !
6090  !  ================================================================
6100  !
6110      DEF FNF(T,X1,X2,X3,Y)
6120  !
6130      COM B,Xxi,M
6140      COM Ti,Xi1,Xi2,Xi3,H
6150      COM Fm,Flamd(*),V0,Bta
6160      COM A2,B2,E0,K1,Fa
6170  !
6180      DEF FNFr(Y)=A2+B2/(7.0+LGT(Y+1E-6))
6190      F=0
6200      Fd=Flamd(K1)*(Fa+X3-X2)-Flamd(K1-1)*(Fa+X2-X1)
6210 L15:Fr0=FNFr(0)
6220      IF ABS(Y)<1E-13 THEN L30
6230      IF Y>0 THEN L20
6240      F=(Fd+FNFr(-Y)-E0*Y)/Fm
6250      GOTO L50
6260 L20: F=(Fd-FNFr(Y)-E0*Y)/Fm
6270      GOTO L50
6280 L30:IF ABS(Fd)<ABS(Fr0) THEN L50
6290      F=(Fd-Fr0*SGN(Fd))/Fm
6300 L50: RETURN F
6310      FNEND
6320  !
6330  ! ================================================================
6340  !
6350      SUB Mess(M$)
6360  !
6370  !  display message M$,beep and pauses
6380         FOR K=1 TO 2
6390           DISP CHR$(129)&" "&M$&CHR$(128)&"  CONT"
6400           BEEP
6410           WAIT 200
6420         NEXT K
6430         PAUSE
6440         DISP " "
6450      SUBEND
```

RESULTS FROM RUNGE-KUTTA METHOD FOR MULTI-PARTICLE SHEAR MODEL
UNIT SYSTEM : *** M-KG-SECOND ***

COHSN= .000E+01	U0= .5290200	B0= .1209800	SEISM= 100.000		
MASS= .100E+01	Pn= .500E+03	LAMDA10= .100E+07	Us= .650000		
G= .980E+01	DRIV0= .100E+01	DRI.AC= .000E+01	PRECISN= .050000		
A= .100E+00	TINT= .200E-03	LAMDA5= .100E+07	Pc= .138E+09		

I = 0 time TI = .00000000E+01

P#	XXI	XI	Fi	Fri
1	.00000000E+01	.90000000E+00	.00000000E+01	.00000000E+01
2	.00000000E+01	.80000000E+00	.00000000E+01	.00000000E+01
3	.00000000E+01	.70000000E+00	.00000000E+01	.00000000E+01
4	.00000000E+01	.60000000E+00	.00000000E+01	.00000000E+01
5	.00000000E+01	.50000000E+00	.00000000E+01	.00000000E+01
6	.00000000E+01	.40000000E+00	.00000000E+01	.00000000E+01
7	.00000000E+01	.30000000E+00	.00000000E+01	.00000000E+01
8	.00000000E+01	.20000000E+00	.00000000E+01	.00000000E+01
9	.00000000E+01	.10000000E+00	.00000000E+01	.00000000E+01
10	.00000000E+01	.00000000E+01	.33137000E+03	-.33137000E+03

II	TI	# RATE	TOT EN	SEISM EN	EN RATIO	KINET EN
1	.2500000000E-02	.000000E+01	.000000E+01	.000000E+01	.000000E+01	.000000E+01
2	.5000000000E-02	.000000E+01	.000000E+01	.000000E+01	.000000E+01	.000000E+01
3	.5205078125E-02	.975238E+00	.329092E-01	.664624E-02	.681499E-02	.471888E+00
4	.5410156250E-02	.975238E+00	.129038E+00	.467106E-01	.478966E-01	.186887E+01
5	.5615234375E-02	.000000E+01	.251831E+00	.117341E+00	.000000E+01	.380543E+01
6	.5830078125E-02	.000000E+01	.384237E+00	.200953E+00	.000000E+01	.554775E+01
7	.6064453125E-02	.000000E+01	.507428E+00	.279191E+00	.000000E+01	.639053E+01
8	.7470703125E-02	.000000E+01	.855710E+00	.522719E+00	.000000E+01	.109948E+01
9	.7695312500E-02	.890435E+00	.863949E+00	.465958E+00	.523293E+00	.294280E+01
10	.7929687500E-02	.000000E+01	.729467E+00	.360139E+00	.000000E+01	.551392E+00
11	.8144531250E-02	.186182E+01	.683037E+00	.346300E+00	.186001E+00	.853240E-03
12	.8359375000E-02	.000000E+01	.729930E+00	.367596E+00	.000000E+01	.339711E+00
13	.8564453125E-02	.000000E+01	.818275E+00	.401239E+00	.000000E+01	.908365E+00
14	.8779296875E-02	.000000E+01	.874542E+00	.428885E+00	.000000E+01	.121787E+01
15	.9287109375E-02	.393846E+00	.889188E+00	.450546E+00	.114396E+01	.406694E+00
16	.9492187500E-02	.975238E+00	.857216E+00	.432640E+00	.443625E+00	.441347E+00
17	.9697265625E-02	.000000E+01	.804863E+00	.384088E+00	.000000E+01	.638557E-01
18	.9912109375E-02	.930909E+00	.743366E+00	.343475E+00	.368967E+00	.256305E-01
19	.1016601563E-01	.787692E+00	.731826E+00	.324521E+00	.411990E+00	.269993E+00
20	.1040039063E-01	.000000E+01	.746937E+00	.342090E+00	.000000E+01	.709617E+00
21	.1061523438E-01	.930909E+00	.779501E+00	.356823E+00	.383306E+00	.119754E+01
22	.1082031250E-01	.975238E+00	.829800E+00	.367966E+00	.377309E+00	.157998E+01
23	.1105468750E-01	.000000E+01	.869750E+00	.367910E+00	.000000E+01	.153760E+01
24	.1132812500E-01	.731429E+00	.870186E+00	.355570E+00	.486131E+00	.126239E+01
25	.1257812500E-01	.160000E+00	.128649E+01	.717787E+00	.448617E+01	.126912E+00
26	.1382812500E-01	.640000E+00	.141981E+01	.899829E+00	.140598E+01	.882280E-01
27	.1404296875E-01	.186182E+01	.167901E+01	.846033E+00	.454412E+00	.104433E+00
28	.1431640625E-01	.146286E+01	.160216E+01	.805825E+00	.550857E+00	.363832E-01
29	.1453125000E-01	.930909E+00	.166460E+01	.810811E+00	.870988E+00	.351452E+00
30	.1503906250E-01	.393846E+00	.189502E+01	.999174E+00	.253696E+01	.727129E+00
31	.1531250000E-01	.731429E+00	.208521E+01	.110111E+01	.150543E+01	.160057E+01

I = 299 time TI = .15390625E-01

P#	XXI	XI	Fi	Fri
1	.75042432E-03	.90000001E+00	.35561871E+03	-.28560705E+03
2	.10884304E+01	.80035562E+00	.27793600E+04	-.27845912E+03
3	.39475155E+01	.70349060E+00	.34526046E+03	-.27781353E+03
4	.99103804E-01	.60697084E+00	-.54023152E+04	-.27998036E+03
5	-.42010099E+01	.50504877E+00	.16359555E+04	.27778475E+03
6	.26953725E+01	.40476265E+00	.44482273E+04	-.27799459E+03
7	.27459989E+01	.30892475E+00	-.34769843E+04	-.27798558E+03
8	-.14235112E+00	.20960988E+00	-.14368452E+03	.27971747E+03
9	.44283326E-01	.11015131E+00	.20676451E+04	-.28061768E+03
10	.20910145E+01	.12760397E-01	.33298382E+03	-.27811961E+03

II	TI	# RATE	TOT EN	SEISM EN	EN RATIO	KINET EN
32	.1554687500E-01	.256000E+01	.201098E+01	.105111E+01	.410589E+00	.176856E+01
33	.1576171875E-01	.930909E+00	.191592E+01	.940139E+00	.100992E+01	.160131E+01
34	.1599609375E-01	.000000E+01	.176381E+01	.822377E+00	.000000E+01	.103826E+01
35	.1620117188E-01	.195048E+01	.161290E+01	.747775E+00	.383381E+00	.781920E+00
36	.1640625000E-01	.000000E+01	.160290E+01	.720753E+00	.000000E+01	.471792E+00
37	.1662109375E-01	.930909E+00	.164895E+01	.737029E+00	.791730E+00	.252368E+00
38	.1682617188E-01	.000000E+01	.174377E+01	.779496E+00	.000000E+01	.162857E+00
39	.1703125000E-01	.975238E+00	.179037E+01	.821210E+00	.842061E+00	.127905E+00
40	.1723632813E-01	.000000E+01	.180131E+01	.848888E+00	.000000E+01	.141631E+00
41	.1744140625E-01	.975238E+00	.178040E+01	.854754E+00	.876457E+00	.202660E+00

I = 428 time TI = .17441406E-01

P#	XXI	XI	Fi	Fri
1	.35310227E+01	.90259088E+00	.28117230E+04	-.27786562E+03
2	.12036699E+01	.80540261E+00	-.35031491E+04	-.27840501E+03
3	-.28254492E+01	.70471118E+00	-.87945211E+03	.27797179E+03
4	.59766717E+00	.60314030E+00	.52222208E+04	-.27879584E+03
5	.36873164E+01	.50679165E+00	-.17434151E+04	-.27784531E+03
6	-.93781994E+00	.40869957E+00	-.15069106E+04	.27854043E+03
7	-.17066348E-01	.30910059E+00	.13771086E+04	.28148217E+03
8	.14304128E+01	.21087872E+00	.79157652E+03	-.27831377E+03
9	.18343676E+01	.11344842E+00	-.93964281E+03	-.27818558E+03
10	.64467934E+00	.15078477E-01	.10447093E+04	-.27875189E+03

428 runs, job is done !

******** the event rate and energy release are stored in file: SYE11 *******